

Nuclear shell-model study around  $^{208}\text{Pb}$  and  
the nuclear Schiff moment of  $^{199}\text{Hg}$

Kota Yanase

*Department of Physics, Saitama University*

Supervised by

Professor Naotaka Yoshinaga

March 20th, 2019



# Contents

Chapter 1	Nuclear shell-model study in the northeast region of $^{208}\text{Pb}$	5
1.1	Introduction . . . . .	5
1.2	Theoretical framework . . . . .	6
1.3	Numerical results . . . . .	9
1.4	Discussion . . . . .	29
1.5	Summary . . . . .	34
Chapter 2	One octupole-phonon model in the proton-rich region of $^{208}\text{Pb}$	37
2.1	Introduction . . . . .	37
2.2	Theoretical framework . . . . .	38
2.3	Numerical results . . . . .	40
2.4	Summary . . . . .	47
Chapter 3	Shell-model study in the southwest region of $^{208}\text{Pb}$	49
3.1	Introduction . . . . .	49
3.2	Theoretical framework . . . . .	50
3.3	Numerical results . . . . .	52
3.4	Summary . . . . .	63
Chapter 4	Nuclear Schiff moment of $^{199}\text{Hg}$	65
4.1	Introduction . . . . .	65
4.2	Nuclear Schiff moment . . . . .	66
4.3	Numerical results . . . . .	67
Appendix A	Racah algebra	73
A.1	Orthogonal functions . . . . .	73
A.2	Recoupling Coefficients . . . . .	78
A.3	Representations of Rotations . . . . .	82
A.4	Tensor Operators . . . . .	86
A.5	Matrix elements of tensor operators . . . . .	94

---

Appendix B	Nuclear effective interactions	99
B.1	Pairing interactions . . . . .	99
B.2	Monopole-pairing Interaction . . . . .	103
B.3	Quadrupole-Quadrupole interactions . . . . .	104
B.4	Neutron-proton monopole-pairing interactions . . . . .	107
B.5	Particle-Hole transformation for P+QQ interaction . . . . .	114
B.6	Two-body matrix elements . . . . .	120
Appendix C	<i>CP</i> -odd nuclear moments	129
C.1	Schiff's theorem . . . . .	129
C.2	Nuclear Schiff moment . . . . .	131
C.3	Schiff moment calculations in the shell-model framework . . . . .	138
C.4	Valence excitations . . . . .	141
C.5	Core excitations . . . . .	149
C.6	Over-shell excitations . . . . .	155
References		157

# Chapter 1

## Nuclear shell-model study in the northeast region of $^{208}\text{Pb}$

### 1.1 Introduction

In the first chapter, twenty three nuclei in the neutron-rich ( $N \geq 126$ ) and proton-rich ( $Z \geq 82$ ) region of a doubly magic core of  $^{208}\text{Pb}$  are studied. Each nucleus has up to four valence neutrons and up to five valence protons. These numbers are limited by the power of a private shell-model code and computational resources that we can utilize. As described below, some nuclei in this region have been analyzed theoretically. However, in most of studies only a few nuclei are considered and there were no systematic shell-model calculations in this mass region. We construct an effective Hamiltonian that systematically reproduce low-energy spectra,  $E2$  transition strengths, and electromagnetic moments of all the nuclei considered. Nuclear structures especially of isomeric states, long-lived excited states, are analyzed in terms of the shell-model wavefunctions. This work is based on Ref. [1].

Structure of heavy nuclei has not been studied enough compared to that of light nuclei. Recent experimental situation on some of heavy nuclei ( $Z \geq 82$ ,  $N > 126$ ) is as follows. The  $^{212}\text{Bi}$  nucleus was studied using a  $^{238}\text{U}$  beam, and two isomers with long half-lives of 25 min and 7.0 min were confirmed [2]. However, the number of observed states in this nucleus is limited so that the spins and parities of only a few states are assigned. The level structure of  $^{213}\text{Po}$  was studied through the  $^{18}\text{O}+^{208}\text{Pb}$  reaction using the  $\gamma$  multidetector array [3]. The level scheme was built up to about 2.0 MeV of excitation energy and spins were assigned up to 25/2 using the triple  $\gamma$  coincidence data. The constructed level scheme was compared with an empirical shell-model calculation. The  $^{211}\text{Pb}$  nucleus was studied through the deep-inelastic reactions between a beam of  $^{208}\text{Pb}$  ions and a  $^{238}\text{U}$  target [4]. Spins and parities of high-spin states including three high-spin isomers were identified. Configurations of several states were assigned by comparing them with a shell model calculation using empirical interactions. High-spin states of  $^{210}\text{Pb}$  and  $^{211}\text{Bi}$  were studied using deep-inelastic collisions of a pulsed beam of  $^{208}\text{Pb}$  ions on a  $^{238}\text{U}$  target [5]. Configurations of some isomers were discussed and analyzed.

Nuclei with a few valence nucleons have been studied theoretically using the shell model approach. The  $^{210}\text{Bi}$  nucleus is a system with one valence neutron and one valence proton outside the doubly magic core  $^{208}\text{Pb}$  and it is relatively easy to analyze theoretically [6–10]. It is an intriguing nucleus to study the interaction between a neutron and a proton. One of the theoretical problems on this nucleus is associated with the fact that the spin-parity of the experimental ground state is  $1^-$  with the  $(\nu g_{9/2} \otimes \pi h_{9/2})$  configuration. The  $0^-$ ,  $1^-$ ,  $\dots$ ,  $9^-$  states with the  $(\nu g_{9/2} \otimes \pi h_{9/2})$  configuration are observed in this nucleus. From the Nordheim strong coupling rule [10, 11], the  $0^-$  state should be the lowest among the states with the  $(\nu g_{9/2} \otimes \pi h_{9/2})$  configuration. However, as mentioned, the experimental observation is different from this theoretical prediction. It was concluded in theoretical studies using empirical two-body interactions that tensor-force components are necessary to reproduce the ground state [6–8].

Recently, precise calculations employing the interaction delivered from the  $NN$  potential were performed and good agreements with the experimental data were obtained [10]. The  $(\pi h_{9/2} \otimes \nu g_{9/2})$ ,  $(\pi f_{7/2} \otimes \nu i_{11/2})$ ,  $(\pi h_{9/2} \otimes \nu i_{11/2})$ ,  $(\pi f_{7/2} \otimes \nu g_{9/2})$ , and  $(\pi h_{9/2} \otimes \nu j_{15/2})$  configurations in the low-lying states of  $^{210}\text{Bi}$ ,  $^{212}\text{Bi}$ ,  $^{212}\text{At}$ ,  $^{216}\text{At}$ , and  $^{216}\text{Fr}$  were compared with the experimental results [12]. The structure of the low-lying states and transition rates of  $^{210}\text{Pb}$  and  $^{210}\text{Bi}$  were calculated using a conventional shell-model approach with a central Gaussian-shaped interaction [13]. Although orders of energy levels of several states were reversely predicted, transition rates and  $M1$ - $E2$  branching ratios were well reproduced.

## 1.2 Theoretical framework

Systematic studies are carried out for even-even, odd-mass, and doubly-odd nuclei around the double magic  $^{208}\text{Pb}$  nucleus using a shell-model framework. For neutron single-particle levels, seven orbitals above the magic number 126, the  $1g_{9/2}$ ,  $0i_{11/2}$ ,  $0j_{15/2}$ ,  $2d_{5/2}$ ,  $3s_{1/2}$ ,  $1g_{7/2}$ , and  $2d_{3/2}$  orbitals, are taken into account. For proton single-particle levels, all the six orbitals in the major shell between the magic numbers 82 and 126,  $0h_{9/2}$ ,  $1f_{7/2}$ ,  $0i_{13/2}$ ,  $2p_{3/2}$ ,  $1f_{5/2}$ , and  $2p_{1/2}$  orbitals, are taken into account.

The single-particle energies  $\varepsilon_\tau$  ( $\tau = \nu$  or  $\pi$ ) employed in the present calculations are listed in Table 3.1, which are extracted from the experimental energy levels of  $^{209}\text{Bi}$  (for proton single-particle energies) and  $^{209}\text{Pb}$  (for neutron single-particle energies). As for the neutron  $0j_{15/2}$  and  $0i_{11/2}$  orbitals and the proton  $0i_{13/2}$  and  $1f_{7/2}$  orbitals, the single-particle energies are assumed to be changed linearly with the numbers of valence neutrons and protons. They are determined in units of MeV as follows:

$$\varepsilon_\nu(j_{15/2}) = -0.050N_\nu - 0.160N_\pi + 1.473, \quad (2.1)$$

$$\varepsilon_\nu(i_{11/2}) = -0.070N_\nu - 0.050N_\pi + 0.849, \quad (2.2)$$

$$\varepsilon_\pi(i_{13/2}) = -0.050N_\pi + 1.659, \quad (2.3)$$

$$\varepsilon_\pi(f_{7/2}) = -0.170N_\nu + 0.050N_\pi + 0.846, \quad (2.4)$$

Table 1.1: Adopted single-particle energies  $\varepsilon_\tau$  for neutrons ( $\tau = \nu$ ) and protons ( $\tau = \pi$ ) in units of MeV. The single-particle energies for the neutron  $0j_{15/2}$  and  $0i_{11/2}$  orbitals and the proton  $0i_{13/2}$  and  $1f_{7/2}$  orbitals are changed linearly with the numbers of valence neutrons ( $N_\nu$ ) and valence protons ( $N_\pi$ ). Definitions of  $\varepsilon_\nu(j_{15/2})$ ,  $\varepsilon_\nu(i_{11/2})$ ,  $\varepsilon_\pi(i_{13/2})$ , and  $\varepsilon_\pi(f_{7/2})$  are given in the text.

$j$	$1g_{9/2}$	$0i_{11/2}$	$0j_{15/2}$	$2d_{5/2}$	$3s_{1/2}$	$1g_{7/2}$	$2d_{3/2}$
$\varepsilon_\nu$	0.000	$\varepsilon_\nu(i_{11/2})$	$\varepsilon_\nu(j_{15/2})$	1.567	2.032	2.491	2.538
$j$	$0h_{9/2}$	$1f_{7/2}$	$0i_{13/2}$	$2p_{3/2}$	$1f_{5/2}$	$2p_{1/2}$	
$\varepsilon_\pi$	0.000	$\varepsilon_\pi(f_{7/2})$	$\varepsilon_\pi(i_{13/2})$	3.119	2.826	3.634	

where  $N_\nu$  and  $N_\pi$  represent the numbers of valence neutrons and valence protons, respectively. The number dependence is introduced for a better reproduction of the low-lying states of odd-mass nuclei.

As an effective interaction, an extended pairing plus quadrupole-quadrupole interaction is employed. The effective shell-model Hamiltonian is given by

$$\hat{H} = \hat{H}_\nu + \hat{H}_\pi + \hat{H}_{\nu\pi}, \quad (2.5)$$

where  $\hat{H}_\nu$ ,  $\hat{H}_\pi$ , and  $\hat{H}_{\nu\pi}$  represent neutron, proton, and neutron-proton interactions, respectively. The interactions among like nucleons are expressed as

$$\hat{H}_\tau = \hat{H}_{c\tau} + \hat{H}_{h\tau}. \quad (2.6)$$

The first term  $\hat{H}_{c\tau}$  ( $\tau = \nu$  or  $\pi$ ) represents the conventional pairing interactions, which consist of spherical single-particle energies, the monopole-pairing ( $MP$ ) interaction, and the quadrupole-pairing ( $QP$ ) interaction,

$$\hat{H}_{c\tau} = \sum_{jm} \varepsilon_{j\tau} c_{jm\tau}^\dagger c_{jm\tau} - G_{0\tau} \hat{P}_\tau^{\dagger(0)} \hat{P}_\tau^{(0)} - G_{2\tau} \hat{P}_\tau^{\dagger(2)} \cdot \hat{P}_\tau^{(2)}. \quad (2.7)$$

The second term  $\hat{H}_{h\tau}$  in Eq. (2.6) represents higher-order interactions, which consist of higher multipole-pairing ( $HMP$ ) interactions,

$$\hat{H}_{h\tau} = - \sum_{L=4,6,8,10} G_{L\tau} \hat{P}_\tau^{\dagger(L)} \cdot \hat{P}_\tau^{(L)}. \quad (2.8)$$

The adopted two-body interaction strengths are listed in Table 3.2. Only one set of strengths is adopted for all the nuclei considered. Detailed definitions of the interactions are given in Ref. [14].

Only for the proton part, an additional pairing interaction with spin 8 between two protons in the  $0h_{9/2}$  and  $1f_{7/2}$  orbitals ( $MP$ -8) is added to Eq. (2.6). It is explicitly defined as

$$\hat{H}^{(8)}(\pi h_{9/2} f_{7/2}) = -G_{\pi h_{9/2} f_{7/2}}^{(8)} \hat{P}_\pi^{\dagger(8)}(h_{9/2} f_{7/2}) \cdot \hat{P}_\pi^{(8)}(h_{9/2} f_{7/2}), \quad (2.9)$$

with

$$\hat{P}_{M\pi}^{\dagger(8)}(h_{9/2} f_{7/2}) = \left[ c_{h_{9/2}}^\dagger c_{f_{7/2}}^\dagger \right]_M^{(8)}, \quad (2.10)$$

Table 1.2: Strengths of adopted two-body interactions between neutrons ( $\nu$ - $\nu$ ) and those between protons ( $\pi$ - $\pi$ ).  $G_0$  and  $G_2$  indicate the strengths of the monopole ( $MP$ ) and quadrupole-pairing ( $QP$ ) interactions, respectively.  $G_L$  ( $L = 4, 6, 8, 10$ ) denote the strengths for higher multipole-pairing ( $HMP$ ) interactions. The strengths of the  $MP$  and  $HMP$  interactions are given in units of MeV. The strengths of the  $QP$  interactions are given in units of  $\text{MeV}/b^4$ , where  $b$  is the oscillator parameter.

	$G_0$	$G_2$	$G_4$	$G_6$	$G_8$	$G_{10}$
$\nu$ - $\nu$	0.102	0.008	0.425	0.500	0.500	0.450
$\pi$ - $\pi$	0.145	0.013	0.400	0.400	-0.600	0.000

and the strength is taken as  $G_{\pi h_{9/2} f_{7/2}}^{(8)} = 0.50$  MeV. Here, two protons in the  $0h_{9/2}$  and  $1f_{7/2}$  orbitals are coupled with spin 8, which is the maximum spin available between these two orbitals, and positive parity.  $c_j^\dagger$  is the nucleon creation operator in the orbital  $j$ . The necessity of this interaction was discussed and its effects were analyzed in Ref. [15].

The interaction between neutrons and protons  $\hat{H}_{\nu\pi}$  consists of the quadrupole-quadrupole ( $QQ$ ) interaction, which is given as

$$\hat{H}_{\nu\pi} = -\kappa_{\nu\pi} \hat{Q}_\nu \cdot \hat{Q}_\pi, \quad (2.11)$$

where the strength is taken as  $\kappa_{\nu\pi} = 0.080$  MeV/ $b^4$ . Here harmonic-oscillator states are used as the single-particle basis states with the oscillator parameter  $b = \sqrt{\hbar/M\omega}$ .

The number occupancy  $v_j^2$  is defined as

$$v_j^2 \equiv \langle \Psi(I_i^\pi) | \hat{n}_j | \Psi(I_i^\pi) \rangle, \quad (2.12)$$

where  $\hat{n}_j$  is the number operator in the orbital  $j$  and  $|\Psi(I_i^\pi)\rangle$  is the  $i$ -th eigenstate of the Hamiltonian in Eq.(5) for a specific nucleus.

In this mass region, shell-model dimensions for diagonalization are too large to perform full calculations without truncation. Thus it is necessary to truncate the shell-model dimensions. In this study, the same truncation scheme adopted in Sec. IIB of Ref. [14] is taken for all the nuclei. All calculations are performed with the truncation of  $L_c = 500$ . Here the definition of  $L_c$  is the same as given in Sec. IIB in Ref. [14]. This truncation is found to be sufficient for reproducing low-lying energy levels and electromagnetic transitions among low-lying states after checking the effect of truncation by increasing  $L_c = 500$  to  $L_c = 1000$ .

In this paper,  $E2$  transition rates, magnetic moments, and quadrupole moments are also calculated. For  $E2$  transition rates and quadrupole moments, the effective charges are taken as  $e_\nu = 1.00e$  for neutrons and  $e_\pi = 1.50e$  for protons. For magnetic moments, the gyromagnetic ratios of orbital angular momentum are taken as  $g_{l\nu} = 0.00$  and  $g_{l\pi} = 1.00$ , and the gyromagnetic ratios of spin are taken as  $g_{s\nu} = -2.87$  and  $g_{s\pi} = 2.79$ . These effective charges and gyromagnetic ratios are adjusted

to reproduce the experimental data for single-closed nuclei on the whole. Further details of the electromagnetic transition operators are presented in Ref. [14].

## 1.3 Numerical results

In this section, the results are given for each nucleus. Energy spectra,  $E2$  transition rates, magnetic moments, and quadrupole moments are calculated. For energy spectra, up to four observed energy levels from the yrast state are shown for each spin-parity. As for the theoretical states, the two lowest energy levels are shown for each spin-parity in general.

### 1.3.1 Pb isotopes

Here  $^{210-212}\text{Pb}$  isotopes are discussed. Figure 1.1 shows the theoretical energy spectrum of  $^{210}\text{Pb}$  in comparison with the experimental data [16, 17]. The  $^{210}\text{Pb}$  nucleus is a system with two valence neutrons outside the doubly magic core  $^{208}\text{Pb}$ . This nucleus tells us information about the interactions between two neutrons. The calculation reproduces the yrast band well. In particular the narrow energy gap between the  $4^+$  and  $6^+$  states and that between the  $6^+$  and  $8^+$  states are well reproduced. The  $6^+$  and  $8^+$  states are isomers with half-lives of 49 ns and 201 ns, respectively [16]. The  $2_1^+$ ,  $4_1^+$ ,  $6_1^+$ , and  $8_1^+$  states mainly consist of the  $(\nu g_{9/2}^2)$  configuration, although the structure of the ground ( $0_1^+$ ) state is not simple. In the ground state the occupation numbers  $(v_j^2)$  are 1.28, 0.35, and 0.21 for the neutron  $1g_{9/2}$ ,  $0i_{11/2}$ , and  $0j_{15/2}$  orbitals, respectively. The  $10_1^+$  state consists of the  $(\nu g_{9/2}i_{11/2})$  configuration, which explains the large energy gap between the  $8_1^+$  and  $10_1^+$  states. The  $12_1^+$  and  $14_1^+$  states consist of the  $(\nu j_{15/2}^2)$  configuration.

Figure 1.1 shows the theoretical energy spectrum of  $^{212}\text{Pb}$  in comparison with the experimental data [16, 19]. In  $^{212}\text{Pb}$  the spins and parities of only several states are assigned in experiment. The yrast band up to spin 8 is well reproduced and the unobserved  $10_1^+$  state is calculated at 1.633 MeV. In  $^{210}\text{Pb}$  and  $^{212}\text{Pb}$  the almost degenerate  $3_1^-$ ,  $4_1^-$ ,  $\dots$ ,  $12_1^-$  states are predicted at 2.682 MeV and around 2.69 MeV, respectively in theory. However, the experimental  $3_1^-$  states are located at 1.870 MeV and 1.820 MeV, respectively. These octupole one-phonon states are constructed by the particle-hole excitations [20, 21], which are beyond the present shell-model framework. The low-lying  $3^-$  states made by core excitations are also seen in Pb isotopes in the mass 210 region as discussed in Ref. [15].

Figure 1.1 shows the theoretical energy spectrum of  $^{211}\text{Pb}$  in comparison with the experimental data [16, 18]. Low-lying states are well reproduced. A  $(27/2^+)$  state is observed at  $1.679+x$  MeV with  $x$  unknown and its half-life is 159 ns [16]. The  $27/2_1^+$  state is calculated at 1.554 MeV and consists of the  $(\nu g_{9/2}^2i_{11/2})$  configuration, which is consistent with the result in Ref [4]. The  $(21/2^+)$  state observed at 1.193 MeV is also an isomer with a half-life of 42(7) ns and decays to the  $(17/2^+)$  state observed at 1.056 MeV [16]. Both the initial and the final states consist of the  $(\nu g_{9/2}^3)$  configuration

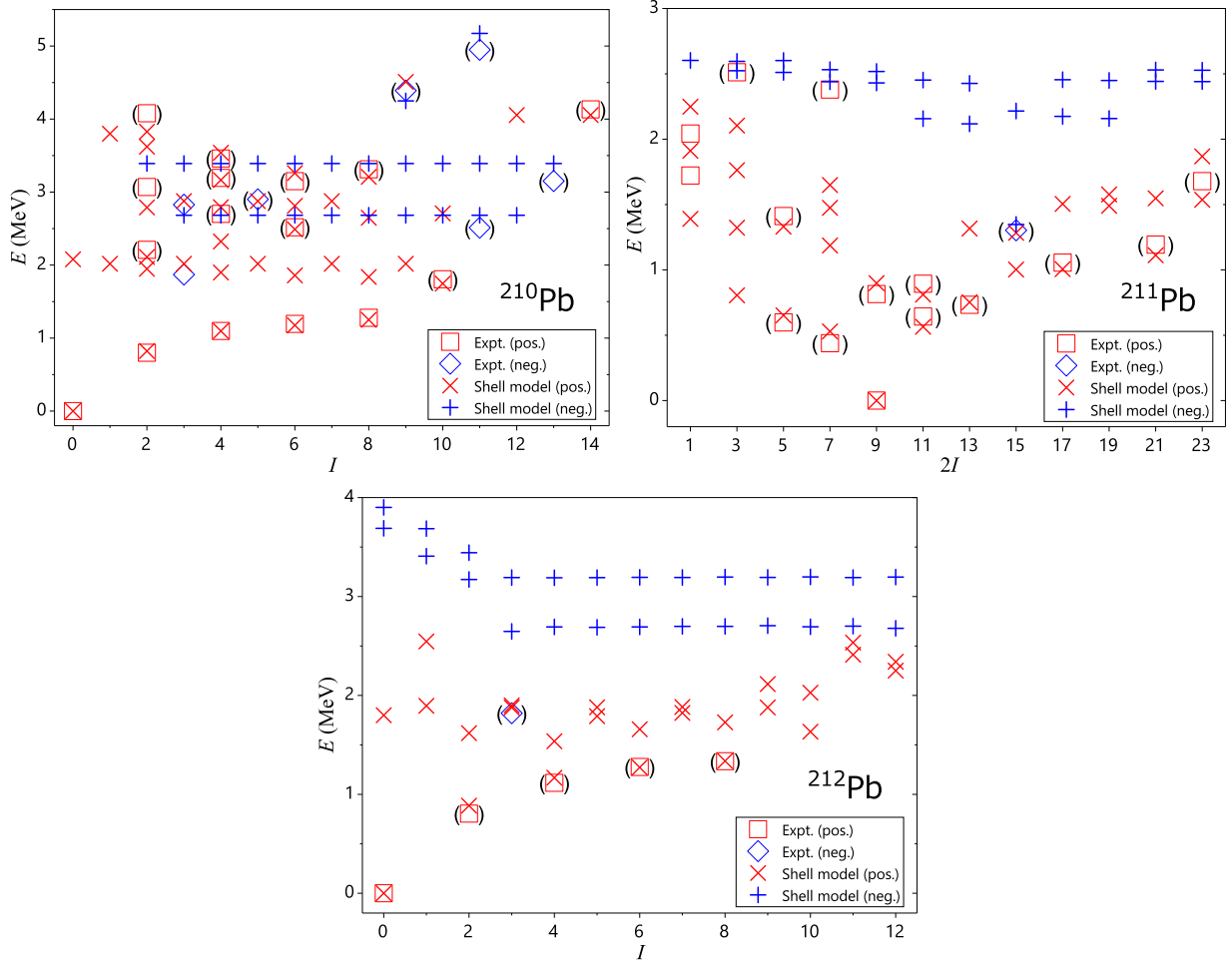


Figure 1.1: The theoretical energy spectrum of Pb isotopes (Shell model) in comparison with experimental data (Expt.). The experimental data are taken from Refs. [16–19]. The squares and diamonds represent experimental positive and negative parity states, respectively. The x marks and pluses represent theoretical positive and negative parity states, respectively.

in theory.

Calculated results for  $B(E2)$  values and electromagnetic moments of Pb isotopes are given in Tables 1.3 and 1.4 in comparison with the experimental data [4, 16–19]. Most of the  $B(E2)$  values are well reproduced in the calculation. The largest discrepancy between the experimental value and the theoretical one is seen in the  $B(E2; 2_1^+ \rightarrow 0_1^+)$  value of  $^{210}\text{Pb}$ . The calculated result is 2.2 times larger than the experimental one. The calculated  $B(E2; 10_1^+ \rightarrow 8_1^+)$  values of  $^{210}\text{Pb}$  and  $^{212}\text{Pb}$  are much smaller than the other transition rates among the yrast states. The  $8_1^+$  state consists of two neutrons in the  $1g_{9/2}$  orbital. However, one neutron needs to be excited to the  $0i_{11/2}$  orbital to make the  $10_1^+$  state and the configuration is changed from the  $8_1^+$  state to the  $10_1^+$  state. The  $E2$  transition rate from the isomeric  $21/2_1^+$  state to the  $17/2_1^+$  state,  $B(E2; 21/2_1^+ \rightarrow 17/2_1^+)$ , is well reproduced.

Table 1.3: The calculated  $B(E2)$  values in units of W.u. for Pb isotopes (Calc.) in comparison with the experimental data (Expt.) [4, 16–19]. \*Using theoretical transition energy of 29 keV [4].

	$B(E2)$	
	Expt.	Calc.
$^{210}\text{Pb}$		
$2_1^+ \rightarrow 0_1^+$	1.4(4)	3.130
$4_1^+ \rightarrow 2_1^+$	4.8(9)	3.435
$6_1^+ \rightarrow 4_1^+$	2.1(8)	2.450
$8_1^+ \rightarrow 6_1^+$	0.7(3)	1.056
$10_1^+ \rightarrow 8_1^+$		0.154
$^{212}\text{Pb}$		
$2_1^+ \rightarrow 0_1^+$		5.535
$4_1^+ \rightarrow 2_1^+$		1.353
$6_1^+ \rightarrow 4_1^+$		0.766
$8_1^+ \rightarrow 6_1^+$		0.303
$10_1^+ \rightarrow 8_1^+$		0.186
$^{211}\text{Pb}$		
$5/2_1^+ \rightarrow 9/2_1^+$		2.870
$7/2_1^+ \rightarrow 9/2_1^+$		4.924
$11/2_1^+ \rightarrow 9/2_1^+$		0.052
$13/2_1^+ \rightarrow 9/2_1^+$		3.125
$21/2_1^+ \rightarrow 17/2_1^+$	1.36(23)	2.290
$27/2_1^+ \rightarrow 23/2_1^+$	$1.0_{-3}^{+2}$ *	1.583

For the quadrupole moment of the  $9/2_1^+$  state in  $^{211}\text{Pb}$ , the experimental value (0.087) has a large error (0.062). So at the moment we cannot have any definite conclusion about the discrepancy between the theoretical value and the experimental one.

### 1.3.2 Bi isotopes

Here  $^{210-213}\text{Bi}$  isotopes are discussed. Figure 1.2 shows the theoretical energy spectrum of  $^{211}\text{Bi}$  in comparison with the experimental data [16, 18]. Low-lying negative parity states are well reproduced. The  $(25/2^-)$  state observed at 1.257 MeV is an isomer with a half-life of 1.4  $\mu\text{s}$  and decays to the  $(21/2^-)$  state at 1.227 MeV by the  $E2$  transition [16]. Both the  $25/2_1^-$  and  $21/2_1^-$  states consist of the  $(\nu g_{9/2}^2 \otimes \pi h_{9/2})$  configuration. In the  $25/2_1^-$  state, two neutrons in the  $1g_{9/2}$  orbital are stretched to have spin 8. The maximum spin in the  $(\nu g_{9/2}^2 \otimes \pi h_{9/2})$  configuration is 25/2. The spin-parity of the state observed at 0.767 MeV is assigned as  $(9/2, 11/2)^-$ . The theoretical  $9/2_2^-$  and  $11/2_1^-$  states are predicted at 0.944 MeV and 0.799 MeV, respectively. Thus the spin-parity of this ambiguous

Table 1.4: The results of magnetic dipole moments  $\mu$  in units of  $\mu_N$  and electric quadrupole moments  $Q$  in units of  $eb$  for Pb isotopes (Calc.) in comparison with the experimental data (Expt.) [16–19].

	$\mu$		$Q$	
	Expt.	Calc.	Expt.	Calc.
$^{210}\text{Pb}$				
$2_1^+$		-0.343		+0.016
$4_1^+$		-0.969		+0.015
$6_1^+$	-1.872(90)	-1.602		-0.137
$8_1^+$	-2.496(64)	-2.360		-0.433
$10_1^+$		-0.207		-0.677
$^{212}\text{Pb}$				
$2_1^+$		-0.316		-0.123
$4_1^+$		-0.894		-0.086
$6_1^+$		-1.469		-0.093
$8_1^+$		-2.182		-0.176
$10_1^+$		-0.187		-0.511
$^{211}\text{Pb}$				
$5/2_1^+$		-0.842		-0.040
$7/2_1^+$		-1.095		-0.332
$9/2_1^+$	-1.4037(8)	-1.380	+0.087(62)	-0.177
$11/2_1^+$		+1.167		-0.338
$13/2_1^+$		-1.658		-0.228

state is suggested to be  $11/2^-$ .

Figure 1.2 shows the theoretical energy spectrum of  $^{213}\text{Bi}$  in comparison with the experimental data [16, 22]. In  $^{213}\text{Bi}$ , only the  $9/2_1^-$  and  $7/2_1^-$  states are definitely assigned in experiment. The states observed at 0.593 MeV and 0.759 MeV are assigned as  $(5/2, 7/2, 9/2)^-$  and  $(5/2^-, 13/2^-)$ , respectively. The  $5/2_1^-$  and  $13/2_1^-$  states are calculated at 0.682 and 0.818 MeV, respectively. Thus it is inferred that the states at 0.593 MeV and 0.759 MeV are spin-parity  $5/2^-$  and  $13/2^-$ , respectively.

Figure 1.2 shows the theoretical energy spectrum of  $^{210}\text{Bi}$  in comparison with the experimental data [16, 17]. The  $^{210}\text{Bi}$  nucleus is a system with one neutron and one proton outside the doubly magic core  $^{208}\text{Pb}$ . This nucleus tells us information on the interactions between neutrons and protons. The value of the strength parameter  $\kappa_{\nu\pi} = 0.08 \text{ MeV}/b^4$  adopted in the present study is slightly larger in magnitude than  $\kappa_{\nu\pi} = -0.06 \text{ MeV}/b^4$ , which had been throughout used for nuclei with neutrons less than 126 and protons more than 82 [15]. The energy spectra for low-lying states of  $^{210}\text{Bi}$  are compared with two choices of  $\kappa_{\nu\pi}$  in Fig. 1.3. As seen in the figure, the experimental spectra are better reproduced with the strength of  $\kappa_{\nu\pi} = 0.08 \text{ MeV}/b^4$ .

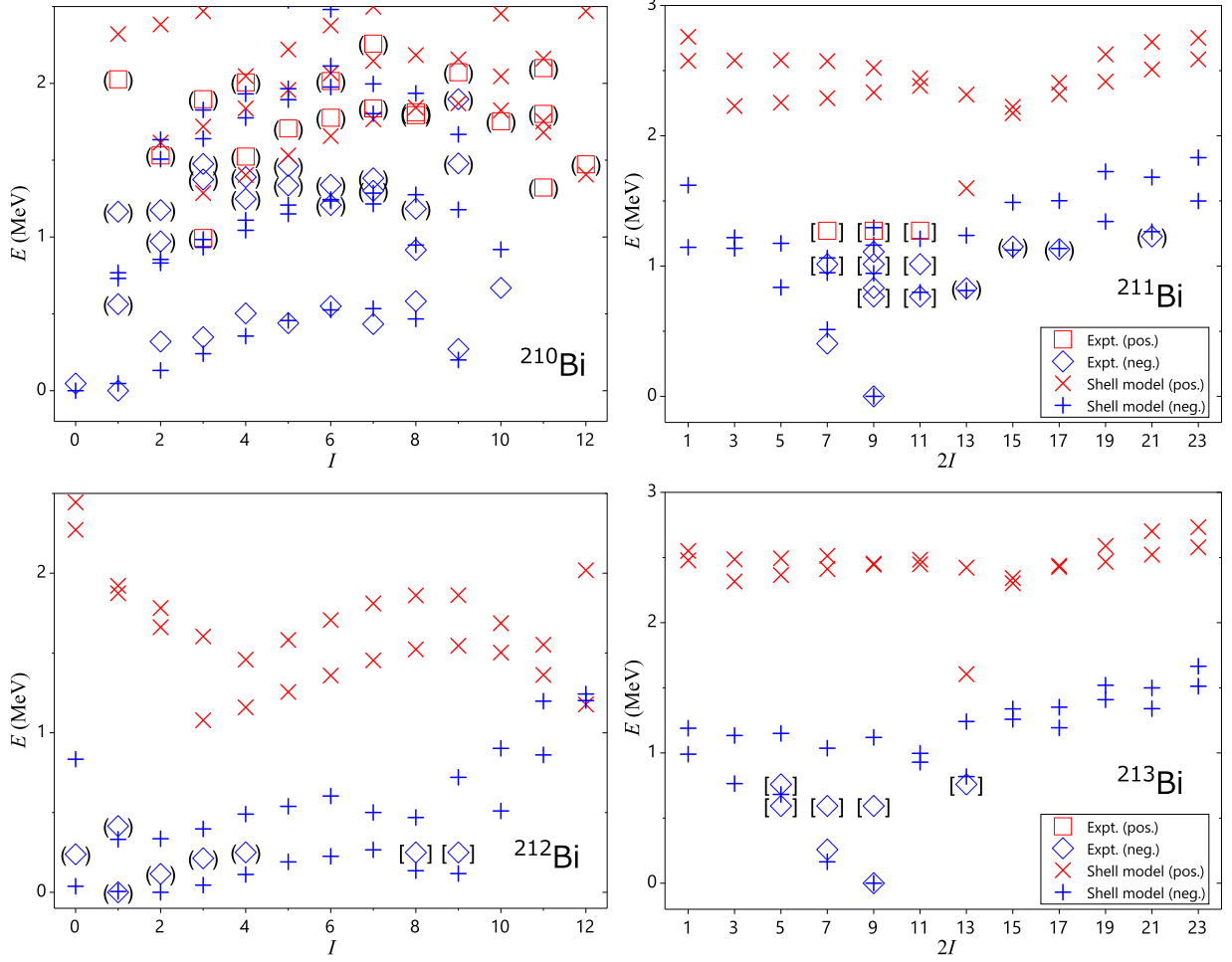


Figure 1.2: Same as Fig. 1.1, but for Bi isotopes. The experimental data are taken from Refs. [16–19, 22]. Each ambiguous state with only one possible set of spin-parity in experiment is shown with parenthesis, while each ambiguous state with more than two possible sets of spin-parity is shown separately with square bracket.

The spin-parity of the ground state is  $1^-$  in experiment. From the Nordheim strong coupling rule [10, 11], the  $0^-$  state should be the lowest among the states with the  $(\nu g_{9/2} \otimes \pi h_{9/2})$  configuration. However the  $0_1^-, 1_1^-, \dots, 8_1^-$  states with the  $(\nu g_{9/2} \otimes \pi h_{9/2})$  configuration are as a whole well described in our calculation. Thus it is suggested that the quadrupole-quadrupole interaction between the neutron and the proton is the main part of the interaction, although some tensor-force components might be necessary to reproduce the ground state. In our calculation the  $1_2^-, 2_3^-, 3_3^-, 4_3^-, 5_3^-, 6_3^-, 7_2^-,$  and  $8_2^-$  states consist of the  $(\nu g_{9/2} \otimes \pi f_{7/2})$  configuration, whereas the  $1_3^-, 2_2^-, 3_2^-, 4_2^-, 5_2^-, 6_2^-, 7_3^-, 8_3^-, 9_2^-,$  and  $10_1^-$  states consist of the  $(\nu i_{11/2} \otimes \pi h_{9/2})$  configuration.

Figure 1.2 shows the theoretical energy spectrum of  $^{212}\text{Bi}$  in comparison with the experimental data [16, 19]. In  $^{212}\text{Bi}$  negative parity states are densely observed and calculated below 0.5 MeV.

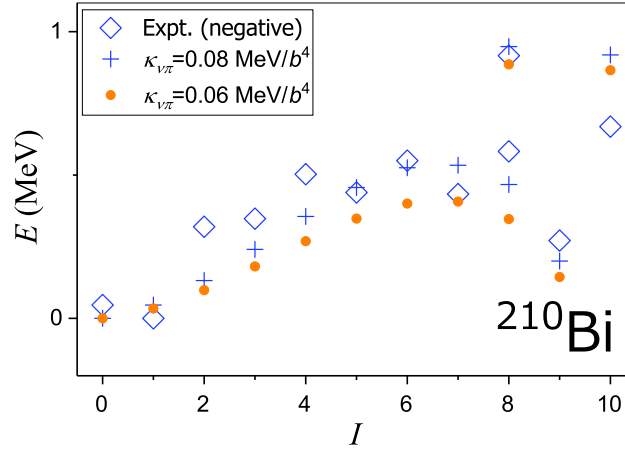


Figure 1.3: Comparison of the low-lying energy levels of  $^{210}\text{Bi}$  with those by the strength parameter  $\kappa_{\nu\pi} = 0.06 \text{ MeV}/b^4$ , which are indicated by the filled circles. This value of  $\kappa_{\nu\pi} = 0.06 \text{ MeV}/b^4$  is the same in magnitude as used in Ref. [15].

In theory the spin-parity of the ground state is  $2^-$ . The lowest members of the  $0_1^-, 1_1^-, \dots, 9_1^-$  states mainly consist of the  $(\nu g_{9/2}^2 i_{11/2} \otimes \pi h_{9/2})$  configuration in our calculation, whereas the second lowest members of the  $1_2^-, 2_2^-, \dots, 8_2^-$  states mainly consist of the  $(\nu g_{9/2}^2 i_{11/2} \otimes \pi f_{7/2})$  configuration. Positive parity states are calculated above 1.0 MeV.

Calculated results for  $B(E2)$  values and electromagnetic moments of Bi isotopes are given in Tables 1.5 and 1.6 in comparison with the experimental data [16–19, 22]. As for  $B(E2)$  transition rates, experimental data are given only for  $^{211}\text{Bi}$ . The calculated  $B(E2)$  value from the isomeric  $25/2_1^-$  state to the  $21/2_1^-$  state,  $B(E2; 25/2_1^- \rightarrow 21/2_1^-)$ , is 2.533 W.u. Most of experimental values for the electromagnetic moments are well reproduced. However, the small experimental value of the magnetic moment for the  $1_1^-$  state of  $^{210}\text{Bi}$  is hardly reproduced without precisely adjusting the gyromagnetic ratios.

### 1.3.3 Po isotopes

Here  $^{211-214}\text{Po}$  isotopes are discussed. Figure 1.4 shows the theoretical energy spectrum of  $^{212}\text{Po}$  in comparison with the experimental data [16, 19]. The  $^{212}\text{Po}$  nucleus is a system with two valence neutrons and two valence protons. The narrow energy gap between the yrast  $6^+$  and  $8^+$  states is well reproduced. The  $0_1^+, 2_1^+, \dots, 8_1^+$  states mainly consist of the  $(\nu g_{9/2}^2 \otimes \pi (h_{9/2}^2)_{0+})$  configuration. In contrast, the  $10_1^+$  state consists of the  $(\nu g_{9/2}^2 i_{11/2} \otimes \pi (h_{9/2}^2)_{0+})$  configuration. The  $12_1^+$  and  $14_1^+$  states consist of the  $(\nu g_{9/2}^2 \otimes \pi (h_{9/2}^2)_{L+})$  configuration with  $L$  greater than zero. These structures are analyzed in Sec. 1.4.

In recent years, negative parity states have been experimentally observed below 2.5 MeV [23, 24]. The observed  $4^-, 6^-,$  and  $8^-$  states are strongly connected to the yrast  $4^+, 6^+,$  and  $8^+$  states by

Table 1.5: Same as table 1.3, but for Bi isotopes. The experimental data are taken from Refs. [16–19, 22].

	$B(E2)$	
	Expt.	Calc.
$^{211}\text{Bi}$		
$7/2_1^- \rightarrow 9/2_1^-$	1.07(10)	0.624
$9/2_2^- \rightarrow 7/2_1^-$	>0.00015	0.392
$9/2_2^- \rightarrow 9/2_1^-$	>0.0031	0.747
$11/2_1^- \rightarrow 9/2_1^-$		3.405
$13/2_1^- \rightarrow 9/2_1^-$		3.984
$21/2_1^- \rightarrow 17/2_1^-$	1.44(11)	4.682
$25/2_1^- \rightarrow 21/2_1^-$		2.533
$^{213}\text{Bi}$		
$7/2_1^- \rightarrow 9/2_1^-$		0.857
$9/2_2^- \rightarrow 7/2_1^-$		4.276
$9/2_2^- \rightarrow 9/2_1^-$		0.807
$11/2_1^- \rightarrow 9/2_1^-$		3.417
$13/2_1^- \rightarrow 9/2_1^-$		8.816
$^{210}\text{Bi}$		
$3_1^- \rightarrow 1_1^-$		3.489
$3_1^- \rightarrow 2_1^-$		0.015
$0_1^- \rightarrow 2_1^-$		14.438
$^{212}\text{Bi}$		
$3_1^- \rightarrow 2_1^-$		1.905
$0_1^- \rightarrow 2_1^-$		7.964

the  $E1$  transitions, respectively. In Ref. [27], it was suggested that these negative parity states are constructed by the  $\alpha$ -particle coupled to  $3^-$  states of  $^{208}\text{Pb}$  (the coupled-channels of  $\alpha + ^{208}\text{Pb}(3_1^-)$ ). Another description of these states was suggested in Ref. [28]. They pointed out a possibility that these negative parity states consist of two-neutron excitations in  $^{210}\text{Pb}$  coupled to the collective  $3^-$  state in  $^{208}\text{Pb}$  times  $^{210}\text{Po}(\text{g.s.})$  ( $[(^{210}\text{Pb}(J^+) \otimes ^{210}\text{Pb}(3^-)]_{I^-} \otimes ^{210}\text{Po}(\text{g.s.})$ ), where  $J$  and  $I$  represent angular momenta of states in  $^{210}\text{Pb}$  and  $^{212}\text{Po}$ , respectively. These negative parity states are out of the present shell-model framework.

The experimental ( $18^+$ ) state at 2.922 MeV is an isomer with a half-life of 45.1(6) s [16], which mainly decays to the ground state,  $3^-$  and  $5^-$  states in  $^{208}\text{Pb}$  by the  $\alpha$  decay and partially decays to the ( $14^+$ ) state at 2.885 MeV in  $^{212}\text{Po}$  by the  $E4$  transition. The configuration of the  $18_1^+$  state is  $(\nu g_{9/2} i_{11/2} \otimes \pi h_{9/2}^2)$ , which is in contrast with the  $(\nu g_{9/2}^2 \otimes \pi h_{9/2}^2)$  configuration of the  $14_1^+$  and the

Table 1.6: Same as table 1.4, but for Bi isotopes. The experimental data are taken from Refs. [16–19, 22].

	$\mu$		$Q$	
	Expt.	Calc.	Expt.	Calc.
$^{211}\text{Bi}$				
$7/2_1^-$	+4.5(7)	+4.147		-0.623
$9/2_1^-$	(+)3.79(7)	+3.647		-0.687
$11/2_1^-$		+2.698		-0.463
$13/2_1^-$		+2.978		-0.559
$^{213}\text{Bi}$				
$7/2_1^-$		+4.095		-0.778
$9/2_1^-$	+3.717(13)	+3.584	-0.60(5)	-0.853
$11/2_1^-$		+3.325		-0.775
$13/2_1^-$		+3.218		-0.880
$^{210}\text{Bi}$				
$1_1^-$	-0.04451(6)	+0.218	+0.136(1)	+0.199
$5_1^-$	+1.530(45)	+1.286		-0.034
$7_1^-$	+2.114(49)	+1.834		-0.349
$9_1^-$	2.728(42)	+2.336	-0.471(59)	-0.754
$^{212}\text{Bi}$				
$1_1^-$	0.41(5)	+0.457	0.1(3)	+0.144
$2_1^-$		+0.734		+0.253
$3_1^-$		+0.880		+0.261
$5_1^-$		+1.276		-0.025
$7_1^-$		+1.792		-0.440
$9_1^-$		+2.286		-0.796

$16_1^+$  states. The theoretical energy of the  $16_1^+$  state is lower than the energy of the  $18_1^+$  state so that the  $18_1^+$  state can easily decay to the  $16_1^+$  state by the  $E2$  transition. Therefore we cannot explain the long half-life of the ( $18^+$ ) state. In order to achieve the situation that the  $18_1^+$  state decays to the  $14_1^+$  state rather than the  $16_1^+$  state, we artificially lower the single-particle energy of the neutron  $0i_{11/2}$  orbital as  $\varepsilon_\nu(i_{11/2}) = 0.1$  MeV, and also reduce the strength of the monopole-pairing interaction between neutrons as  $G_{0\nu} = 0.095$  MeV. The result is shown in Fig. 1.5. The spin-parity of the state observed at 1.249 MeV is not assigned, but theoretically it is suggested to have a spin-parity of  $10^+$ . The calculation suggests that the ( $18^+$ ) state at 2.922 MeV corresponds to the theoretical  $18_1^+$  state, while the unassigned state at 1.249 MeV and the  $10^+$  state at 1.833 MeV each corresponds to the  $10_1^+$  and the  $10_2^+$  states, respectively. We do not pursue this problem further, but the choice of the

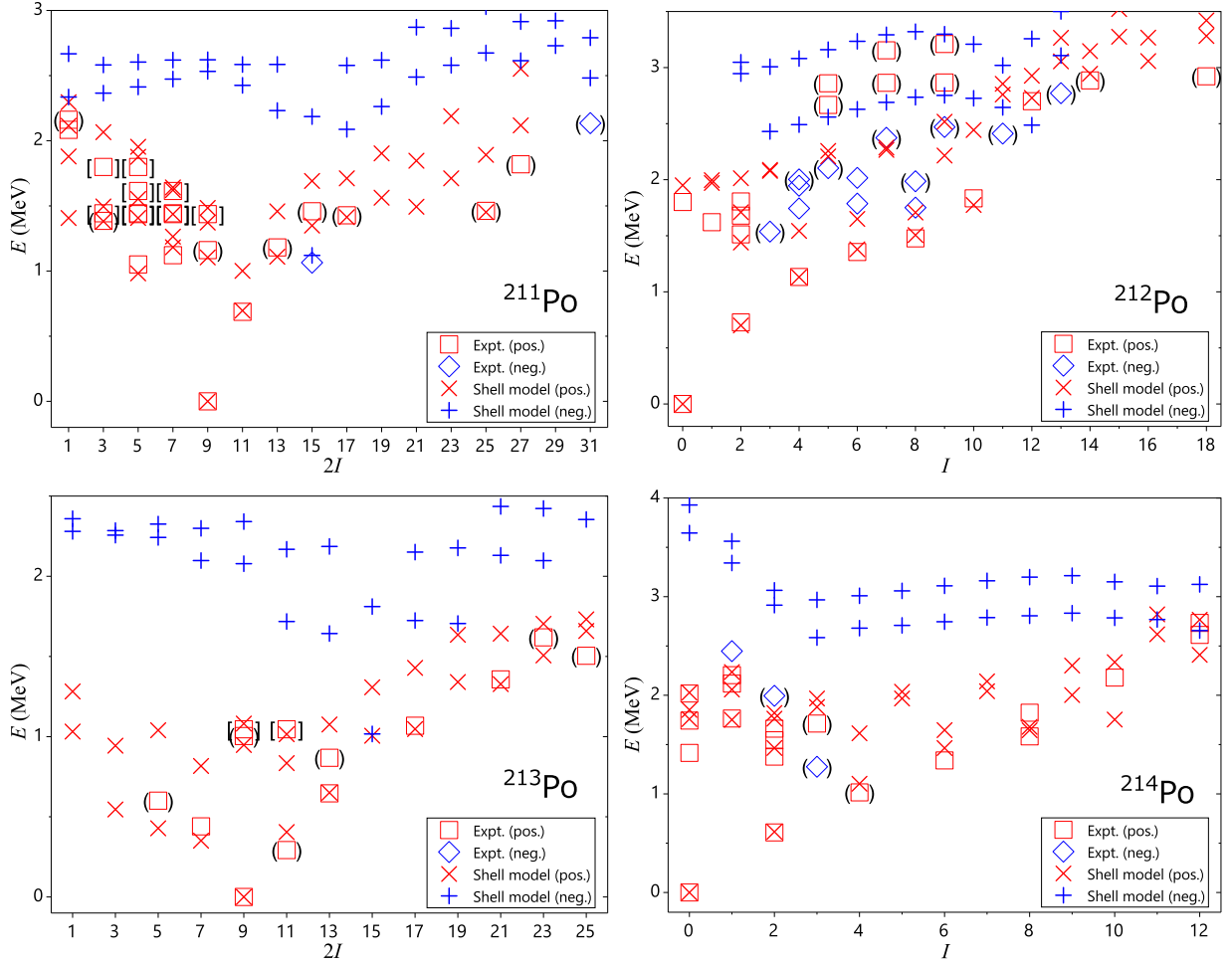


Figure 1.4: Same as Fig. 1.1, but for Po isotopes. The state at 1.249 MeV is not shown in the figure since the spin-parity is not assigned in experiment. The experimental data are taken from Refs. [16, 19, 22–26].

strengths of the interactions certainly affects the spectra of the neighboring nuclei and we need to investigate their effects on those nuclei. This is a future problem.

Figure 1.4 shows the theoretical energy spectrum of  $^{214}\text{Po}$  in comparison with the experimental data [16, 26]. In  $^{214}\text{Po}$ , only the  $0^+$ ,  $2^+$ , and  $4^+$  states are observed in the yrast band. The  $6_1^+$ ,  $8_1^+$ , and  $10_1^+$  states are calculated at 1.465, 1.645, and 1.754 MeV, respectively. The state observed at 1.275 MeV is assigned as  $(3^-)$  [29]. The theoretical first  $3_1^-$  state is calculated at 2.584 MeV. The experimental  $(3^-)$  state is supposed to be an octupole one-phonon state by the core excitation [29]. It is known in this mass region that the octupole correlation is crucial. The  $(2^-)$  state observed at 1.995 MeV is also considered to be a coupled state with the octupole and quadrupole phonon states. In our model space, all the negative parity states are calculated above 2.5 MeV.

Figure 1.4 shows the theoretical energy spectrum of  $^{211}\text{Po}$  in comparison with the experimental

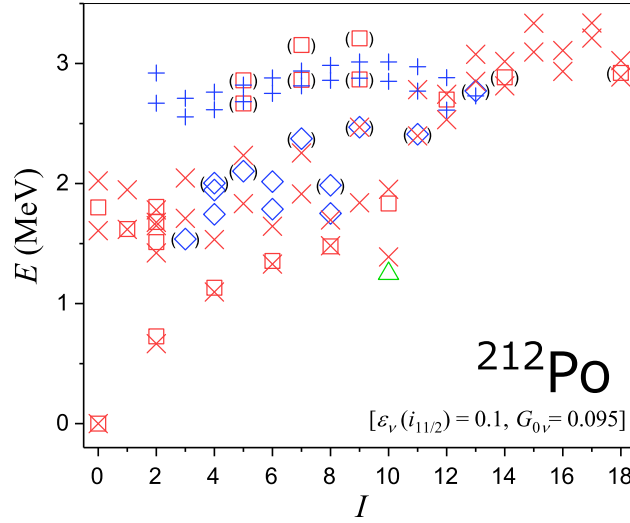


Figure 1.5: Same as Fig. 1.4, but with  $\varepsilon_\nu(i_{11/2}) = 0.1$  MeV and  $G_{0\nu} = 0.095$  MeV. The spin-parity of the state at 1.249 MeV indicated by a triangle is not assigned in experiment, but it is suggested to have a spin-parity of  $10^+$  in this calculation.

data [16, 18]. Low-lying states are well reproduced. The  $25/2^+$  state observed at 1.462 MeV in  $^{211}\text{Po}$  is an isomer with a half-life of 25.2(6) s [18]. This state decays to the  $17/2^+$  state at 1.428 MeV by the  $E4$  transition. The  $25/2_1^+$  and  $17/2^+$  states consist of the same configuration of  $(\nu g_{9/2} \otimes \pi(h_{9/2}^2)_{L+})$  with  $L = 8$  and  $L = 4$ , respectively. The  $21/2_1^+$  and  $23/2_1^+$  states, which are connected to the  $25/2^+$  state by  $E2$  or  $M1$  transitions, are not observed. These states are calculated higher than the  $25/2_1^+$  state. This isomer is classified as a spin-gap isomer.

Figure 1.4 shows the theoretical energy spectrum of  $^{213}\text{Po}$  in comparison with the experimental data [3, 16, 22]. In  $^{213}\text{Po}$ , only positive parity states are observed and well reproduced in our calculation. The lowest negative parity state, the  $15/2_1^-$  state, is calculated at 1.017 MeV.

Calculated results for  $B(E2)$  values and electromagnetic moments of Po isotopes are given in Tables 1.7 and 1.8 in comparison with the experimental data [16, 18, 19, 22, 26, 30, 31]. In  $^{212}\text{Po}$ , the calculated  $B(E2; 2_1^+ \rightarrow 0_1^+)$  and  $B(E2; 6_1^+ \rightarrow 4_1^+)$  values are much larger than the experimental data. In  $^{213}\text{Po}$ , the theoretical calculation predicts large transition rates to the ground ( $9/2_1^+$ ) state from the  $5/2_1^+$ ,  $7/2_1^+$ , and  $13/2_1^+$  states. In  $^{211}\text{Po}$ , the magnetic moment of the  $15/2_1^-$  state is largely predicted in magnitude by a factor of 3.6 compared with the experimental data, whereas the magnetic moment and the quadrupole moment of the ground ( $9/2_1^+$ ) state are well reproduced. This discrepancy suggests that the  $15/2_1^-$  state might be affected by the octupole excitation, namely the coupling the ground ( $9/2_1^+$ ) state with the octupole phonon state.

Table 1.7: Same as table 1.3, but for Po isotopes. The experimental data are taken from Refs. [16, 18, 19, 22, 26, 30].

	$B(E2)$	
	Expt.	Calc.
$^{212}\text{Po}$		
$2_1^+ \rightarrow 0_1^+$	2.6(3)	10.921
$2_2^+ \rightarrow 0_1^+$	0.4(1)	0.246
$2_2^+ \rightarrow 2_1^+$	0.3(2)	1.843
$4_1^+ \rightarrow 2_1^+$		13.462
$6_1^+ \rightarrow 4_1^+$	3.9(11)	11.047
$8_1^+ \rightarrow 6_1^+$	2.30(9)	5.820
$10_1^+ \rightarrow 8_1^+$	2.2(6)	1.280
$^{214}\text{Po}$		
$2_1^+ \rightarrow 0_1^+$		18.451
$4_1^+ \rightarrow 2_1^+$		25.205
$6_1^+ \rightarrow 4_1^+$		20.832
$8_1^+ \rightarrow 6_1^+$		5.445
$10_1^+ \rightarrow 8_1^+$		0.000
$0_2^+ \rightarrow 2_1^+$	0.159(10)	0.352
$^{211}\text{Po}$		
$5/2_1^+ \rightarrow 9/2_1^+$		10.189
$7/2_1^+ \rightarrow 9/2_1^+$		2.321
$9/2_2^+ \rightarrow 9/2_1^+$		2.306
$11/2_1^+ \rightarrow 9/2_1^+$		0.403
$13/2_1^+ \rightarrow 9/2_1^+$		3.752
$^{213}\text{Po}$		
$5/2_1^+ \rightarrow 9/2_1^+$		14.717
$7/2_1^+ \rightarrow 9/2_1^+$		13.168
$7/2_1^+ \rightarrow 11/2_1^+$		0.004
$11/2_1^+ \rightarrow 9/2_1^+$		0.282
$13/2_1^+ \rightarrow 9/2_1^+$		12.848

Table 1.8: Same as table 1.4, but for Po isotopes. The experimental data are taken from Refs. [16, 18, 19, 22, 26, 31].

	$\mu$		$Q$	
	Expt.	Calc.	Expt.	Calc.
$^{212}\text{Po}$				
$2_1^+$		+0.362		-0.070
$4_1^+$		+0.131		-0.198
$6_1^+$		-0.685		-0.423
$8_1^+$		-1.853		-0.769
$10_1^+$		-0.023		-1.141
$^{214}\text{Po}$	Expt.	Calc.	Expt.	Calc.
$2_1^+$		+0.454		-0.399
$4_1^+$		+0.751		-0.682
$6_1^+$		+0.753		-0.853
$8_1^+$		+7.319		-1.441
$10_1^+$		+0.049		-1.005
$^{211}\text{Po}$	Expt.	Calc.	Expt.	Calc.
$7/2_1^+$		-0.916		-0.501
$9/2_1^+$	-1.197(85)	-1.343	-0.77(8)	-0.591
$11/2_1^+$		+1.248		-0.623
$13/2_1^+$		+0.909		-0.357
$15/2_1^-$	-0.38(15)	-1.382		-0.764
$^{213}\text{Po}$	Expt.	Calc.	Expt.	Calc.
$7/2_1^+$		-0.936		-0.535
$9/2_1^+$		-1.251		-0.449
$11/2_1^+$		+1.230		-0.828
$13/2_1^+$		-0.856		-0.503

### 1.3.4 At isotopes

Here  $^{212-215}\text{At}$  isotopes are discussed. Figure 1.6 shows the theoretical energy spectrum of  $^{213}\text{At}$  in comparison with the experimental data [16, 22]. The spin-parity of the state observed at 0.341 MeV in  $^{213}\text{At}$  is assigned as  $(7/2^-, 9/2^-)$ . The  $7/2_1^-$  and  $9/2_2^-$  states are calculated at 0.348 and 0.958 MeV, respectively. Thus our calculation suggests that the spin-parity of this state is  $7/2^-$ .

Figure 1.6 shows the theoretical energy spectrum of  $^{215}\text{At}$  in comparison with the experimental data [16, 32]. The spin-parity of the state at 0.364 MeV in  $^{215}\text{At}$  is assigned as  $(13/2_1^+)$  [33]. However, the  $13/2_1^+$  state is calculated at 1.332 MeV. Our calculation suggests that the spin-parity of the

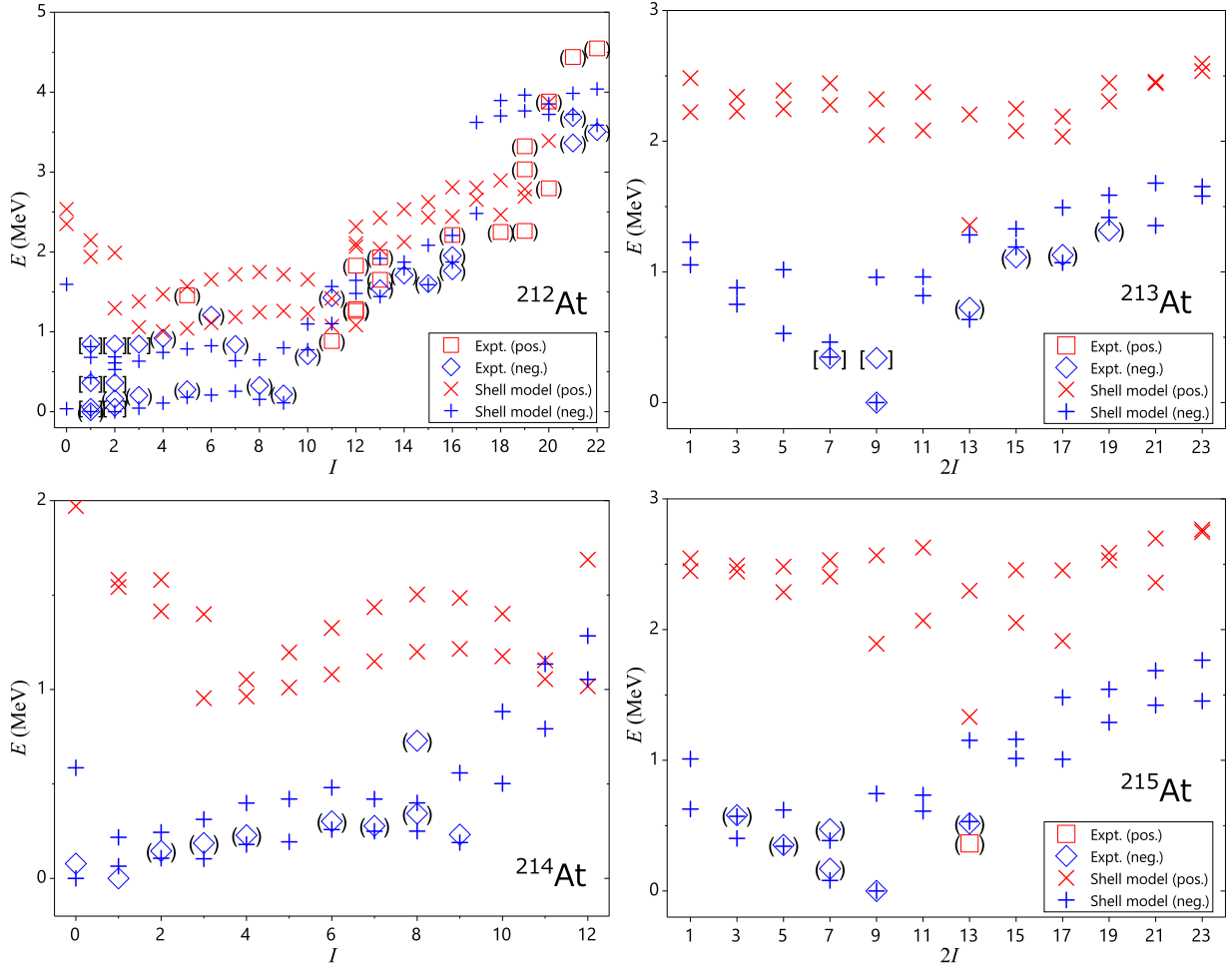


Figure 1.6: Same as Fig. 1.2, but for At isotopes. The experimental data are taken from Refs. [16, 19, 22, 26, 32].

Table 1.9: Occupation numbers in some low-lying states of  $^{215}\text{At}$ .

$\nu$	$1g_{9/2}$	$0i_{11/2}$	$0j_{15/2}$	$2d_{5/2}$	$3s_{1/2}$	$1g_{7/2}$	$2d_{3/2}$
$9/2_1^-$	2.06	0.99	0.61	0.16	0.03	0.09	0.05
$5/2_1^-$	2.17	0.95	0.52	0.18	0.03	0.09	0.05
$7/2_1^-$	2.08	0.98	0.60	0.16	0.03	0.09	0.05
$13/2_1^+$	2.21	0.94	0.50	0.18	0.03	0.09	0.05
$\pi$	$0h_{9/2}$	$1f_{7/2}$	$0i_{13/2}$	$2p_{3/2}$	$1f_{5/2}$	$2p_{1/2}$	
$9/2_1^-$	2.11	0.59	0.18	0.08	0.03	0.01	
$5/2_1^-$	2.10	0.55	0.16	0.13	0.05	0.01	
$7/2_1^-$	1.50	1.20	0.17	0.07	0.05	0.01	
$13/2_1^+$	2.12	0.58	0.16	0.09	0.04	0.01	

state is  $3/2_1^-$  with the excitation energy of 0.402 MeV. A shell model study by Liang and others suggested that the low-lying  $9/2_1^-$ ,  $5/2_1^-$ ,  $7/2_2^-$ ,  $13/2_1^-$ , and  $3/2_1^-$  states have the  $(\nu g_{9/2}^4 \otimes \pi h_{9/2}^3)$  configuration [33]. However, it is shown in Table 1.9 that these states consist of not only the neutron  $1g_{9/2}$  and the proton  $0h_{9/2}$  orbitals.

Figure 1.6 shows the theoretical energy spectrum of  $^{212}\text{At}$  in comparison with the experimental data [16, 19]. The  $(9^-)$  state at 0.223 MeV is an isomer with a half-life of 0.119(3) s [16]. The  $0_1^-$ ,  $1_1^-$ ,  $\dots$ ,  $9_1^-$  states are members of the  $(\nu g_{9/2} \otimes \pi h_{9/2}^3)$  configuration. The calculation reproduces the experimental situation such that the energy of the  $9_1^-$  state is lower than that of the  $8_1^-$  state. The members of the second negative parity band, the  $1_2^-$ ,  $2_2^-$ ,  $\dots$ ,  $8_2^-$  states, consist of the  $(\nu g_{9/2} \otimes \pi h_{9/2}^2 f_{7/2})$  configuration. The  $11^+$  state at 0.885 MeV is an isomer with a half-life of 18.7(7) ns and decays to the  $(10^-)$  state at 0.702 MeV by the  $E1$  transition and the  $(9^-)$  state at 0.223 MeV by the  $M2$  transition [16]. The  $11_1^+$  state mainly consists of the  $(\nu j_{15/2} \otimes \pi h_{9/2}^3)$  configuration. The  $6_1^+$ ,  $7_1^+$ ,  $\dots$ ,  $18_1^+$  states mainly consisting of the same configuration as the  $11_1^+$  state are located energetically higher than the  $11_1^+$  state.

Figure 1.6 shows the theoretical energy spectrum of  $^{214}\text{At}$  in comparison with the experimental data [16, 26]. In  $^{214}\text{At}$ , only negative parity states are observed and densely located below 0.5 MeV. The  $0_1^-$ ,  $1_1^-$ ,  $\dots$ ,  $9_1^-$  states consist of the  $(\nu g_{9/2}^2 i_{11/2} \otimes \pi h_{9/2}^2 f_{7/2})$  configuration.

Calculated results for  $B(E2)$  values and electromagnetic moments of At isotopes are given in Tables 1.10 and 1.11 in comparison with the experimental data [16, 19, 22, 26, 32]. As for the  $E2$  transitions, only two transition rates are measured in At isotopes. In  $^{212}\text{At}$ , the experimental values of  $B(E2; 5_1^- \rightarrow 3_1^-) = 3.3(3)$  W.u. and  $B(E2; 15_1^- \rightarrow 13_1^-) = 3.1(3)$  W.u. are calculated as 4.715 W.u. and 4.295 W.u., respectively. As for electromagnetic moments, only the magnetic moments of the  $15_1^-$  and  $11_1^+$  states in  $^{212}\text{At}$  are observed. The magnetic moment of the  $15_1^-$  state is  $9.46(8) \mu_N$  in experiment and the theoretical result is  $+7.367 \mu_N$ , which is a reasonable value. The magnetic moment of the  $11_1^+$  state is  $5.94(11) \mu_N$  in experiment and the theoretical result is  $+1.874 \mu_N$ , which is 3.2 times smaller than the experimental data. The magnetic moment of the  $11_2^+$  state calculated at 1.417 MeV is  $+6.071 \mu_N$ , which is very close to the experimental value. Thus the  $11_1^+$  and  $11_2^+$  states might be reversely calculated compared to the experimentally observed states. In our calculation, the  $11_2^+$  state, which consists of the  $(\nu g_{9/2} \otimes \pi h_{9/2}^2 i_{13/2})$  configuration, is located 0.344 MeV higher than the  $11_1^+$  state.

### 1.3.5 Rn isotopes

Here  $^{213-216}\text{Rn}$  isotopes are discussed. Figure 1.7 shows the theoretical energy spectrum of  $^{214}\text{Rn}$  in comparison with the experimental data [16, 26]. The yrast band is well reproduced in our calculation. The spin-parity of the state observed at 1.332 MeV is not assigned (not shown in this figure). This state decays to the  $2^+$  state at 0.695 MeV. In our calculation, the  $2_2^+$  state is calculated at 1.626 MeV. Considering this result and the comparison with neighboring nuclei such as  $^{212}\text{Po}$  and  $^{216}\text{Rn}$ , the

Table 1.10: Same as table 1.3, but for At isotopes. The experimental data are taken from Refs. [16, 19, 22, 26, 32].

	$B(E2)$	
	Expt.	Calc.
$^{213}\text{At}$		
$5/2_1^- \rightarrow 9/2_1^-$		16.792
$7/2_1^- \rightarrow 9/2_1^-$		4.474
$7/2_2^- \rightarrow 9/2_1^-$		10.880
$13/2_1^- \rightarrow 9/2_1^-$		14.392
$15/2_1^- \rightarrow 13/2_1^-$		2.913
$17/2_1^- \rightarrow 13/2_1^-$		18.147
$19/2_1^- \rightarrow 17/2_1^-$		1.069
$^{215}\text{At}$		
$5/2_1^- \rightarrow 9/2_1^-$		33.195
$7/2_1^- \rightarrow 9/2_1^-$		0.003
$7/2_2^- \rightarrow 9/2_1^-$		18.121
$13/2_1^- \rightarrow 9/2_1^-$		26.498
$^{212}\text{At}$		
$5_1^- \rightarrow 3_1^-$	3.3(3)	4.715
$8_1^- \rightarrow 9_1^-$		2.079
$15_1^- \rightarrow 13_1^-$	3.1(3)	4.295
$^{214}\text{At}$		
$3_1^- \rightarrow 1_1^-$		2.598
$5_1^- \rightarrow 3_1^-$		8.861

spin-parity of the experimental state at 1.332 MeV is inferred to be  $2^+$ .

Figure 1.7 shows the theoretical energy spectrum of  $^{216}\text{Rn}$  in comparison with the experimental data [16, 34]. In  $^{216}\text{Rn}$  the spin-parity of the state at 1.838 MeV is assigned as  $(8^+, 9^+, 10^+)$ . The  $8_2^+$ ,  $9_1^+$ , and  $10_2^+$  states are calculated at 1.872, 2.217, and 2.369 MeV, respectively. Thus our calculation suggests that the spin-parity of the state at 1.838 MeV is  $8^+$ . One of the peculiar features of even-even nuclei in this region is the narrow energy gap between the  $6^+$  and  $8^+$  states in the yrast band. In  $^{216}\text{Rn}$ , however, the narrow energy gap between the  $6^+$  and  $8^+$  states is not seen anymore in experiment due to the evolution of quadrupole collectivity and the calculation reproduces this feature. Some characteristic features of  $^{214}\text{Rn}$  and  $^{216}\text{Rn}$  are analyzed and discussed in Sec. 1.4.

Figure 1.7 shows the theoretical energy spectrum of  $^{213}\text{Rn}$  in comparison with the experimental data [16, 22]. All the identified states are well reproduced. In  $^{213}\text{Rn}$ , the  $(25/2^+)$  state is observed at  $1.664 + x$  MeV with  $x$  unknown. The  $25/2_1^+$  state is calculated at 1.670 MeV. Our calculation

Table 1.11: Same as table 1.4, but for At isotopes. The experimental data are taken from Refs. [16, 19, 22, 26, 32].

	$\mu$		$Q$	
	Expt.	Calc.	Expt.	Calc.
$^{213}\text{At}$				
$5/2_1^-$		+2.584		-0.131
$7/2_1^-$		+3.708		-0.777
$9/2_1^-$		+3.669		-0.480
$11/2_1^-$		+3.397		-0.354
$13/2_1^-$		+4.099		-0.533
$15/2_1^-$		+2.592		-0.595
$17/2_1^-$		+3.993		-0.625
$19/2_1^-$		+2.169		-0.786
$^{215}\text{At}$				
$5/2_1^-$		2.484		-0.413
$7/2_1^-$		4.019		-1.026
$9/2_1^-$		3.555		-0.850
$11/2_1^-$		4.441		-1.019
$13/2_1^-$		4.040		-0.994
$^{212}\text{At}$				
$1_1^-$		+0.121		+0.121
$2_1^-$		+0.376		+0.226
$3_1^-$		+0.726		+0.195
$15_1^-$	9.46(8)	+7.367		-0.837
$11_1^+$	5.94(11)	+1.874		-0.971
$11_2^+$		+6.071		-1.081
$^{214}\text{At}$				
$1_1^-$		+0.261		+0.120
$2_1^-$		+0.513		+0.186
$3_1^-$		+0.825		+0.344

shows that the ground  $9/2_1^+$  state, the  $11/2_1^+$  state at 0.622 MeV, and the  $15/2_1^-$  state at 0.837 MeV, mainly consist of the  $(\nu g_{9/2} \otimes \pi h_{9/2}^3 f_{7/2})$ ,  $(\nu i_{11/2} \otimes \pi h_{9/2}^3 f_{7/2})$ , and  $(\nu j_{15/2} \otimes \pi h_{9/2}^3 f_{7/2})$  configurations, respectively. These energies are very close to the single-particle energies for the neutron  $1g_{9/2}$ ,  $0i_{11/2}$ , and  $0j_{15/2}$  orbitals, which are given as 0.0 MeV, 0.579 MeV, and 0.783 MeV, respectively. This indicates that one valence neutron in the specific single-particle orbital determines nature of each state, namely, its spin and parity.

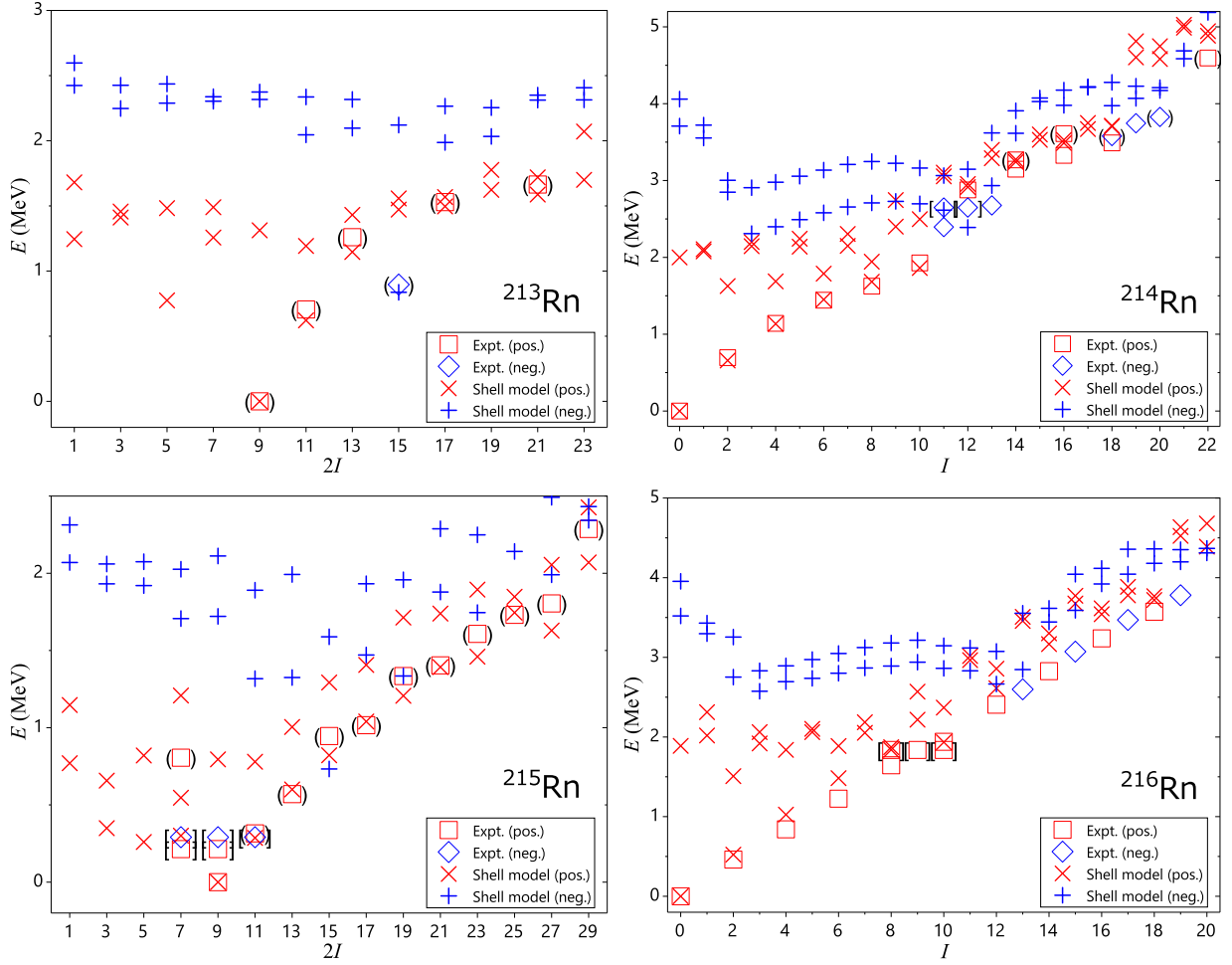


Figure 1.7: Same as Fig. 1.2, but for Rn isotopes. The experimental data are taken from Refs. [16, 22, 26, 32, 34].

Figure 1.7 shows the theoretical energy spectrum of  $^{215}\text{Rn}$  in comparison with the experimental data [16, 32]. In  $^{215}\text{Rn}$ , the spin of the positive parity state observed at 0.214 MeV is assigned as  $(7/2, 9/2)^+$ . The  $7/2_1^+$  and  $9/2_2^+$  states are calculated at 0.301 MeV and 0.795 MeV, respectively. Thus the spin of the state observed at 0.214 MeV is suggested as 7/2. The spin of the negative parity state observed at 0.291 MeV is assigned as  $(7/2, 9/2, 11/2)^-$ . However, the calculation predicts no negative parity states below 0.7 MeV. The  $15/2_1^-$  state, which is not observed in experiment, is calculated at 0.733 MeV.

Calculated results for  $B(E2)$  values and electromagnetic moments of Rn isotopes are given in Tables 1.12 and 1.13 in comparison with the experimental data [16, 22, 26, 32, 34]. In  $^{214}\text{Rn}$ , the observed  $B(E2; 6_1^+ \rightarrow 4_1^+)$  and  $B(E2; 8_1^+ \rightarrow 6_1^+)$  values are much smaller, whereas the calculation predicts large  $B(E2)$  values. The magnetic moments of  $^{213}\text{Rn}$  are well reproduced.

Table 1.12: Same as table 1.3, but for Rn isotopes. The experimental data are taken from Refs. [16, 22, 26, 32, 34].

$^{214}\text{Rn}$	$B(E2)$	
	Expt.	Calc.
$2_1^+ \rightarrow 0_1^+$	$>0.032$	17.380
$4_1^+ \rightarrow 2_1^+$	$>0.28$	23.101
$6_1^+ \rightarrow 4_1^+$	$3.8_{-9}^{+17}$	21.614
$8_1^+ \rightarrow 6_1^+$	$3.3_{-1}^{+3}$	15.905
$10_1^+ \rightarrow 8_1^+$	2.9(7)	5.921
$12_1^+ \rightarrow 10_1^+$	$>0.0064$	4.820
$14_1^+ \rightarrow 12_1^+$		15.829
$16_1^+ \rightarrow 14_1^+$	$\leq 4.4(3)$	11.260
$18_1^+ \rightarrow 16_1^+$	0.71(5)	0.722
$13_1^- \rightarrow 11_1^-$	0.93(8)	0.099
$^{216}\text{Rn}$	Expt.	Calc.
$2_1^+ \rightarrow 0_1^+$		28.567
$4_1^+ \rightarrow 2_1^+$		40.613
$6_1^+ \rightarrow 4_1^+$		40.704
$8_1^+ \rightarrow 6_1^+$		9.671
$10_1^+ \rightarrow 8_1^+$		3.111
$^{213}\text{Rn}$	Expt.	Calc.
$7/2_1^+ \rightarrow 9/2_1^+$		3.676
$11/2_1^+ \rightarrow 9/2_1^+$		0.415
$13/2_1^+ \rightarrow 9/2_1^+$		8.619
$17/2_1^+ \rightarrow 13/2_1^+$		4.536
$21/2_1^+ \rightarrow 17/2_1^+$	1.68(16)	2.287
$^{215}\text{Rn}$	Expt.	Calc.
$7/2_1^+ \rightarrow 9/2_1^+$		18.315
$11/2_1^+ \rightarrow 9/2_1^+$		0.467
$13/2_1^+ \rightarrow 9/2_1^+$		22.646

Table 1.13: Same as table 1.4, but for Rn isotopes. The experimental data are taken from Refs. [16, 22, 26, 32, 34].

	$\mu$		$Q$	
	Expt.	Calc.	Expt.	Calc.
$^{214}\text{Rn}$				
$2_1^+$		+0.449		-0.370
$4_1^+$		+0.378		-0.601
$6_1^+$		-0.248		-0.772
$8_1^+$		-0.969		-0.992
$10_1^+$		+0.135		-1.364
$^{216}\text{Rn}$				
$2_1^+$		+0.612		-0.629
$4_1^+$		+1.021		-0.890
$6_1^+$		+1.138		-1.046
$8_1^+$		+5.923		-1.135
$10_1^+$		+0.236		-1.298
$^{213}\text{Rn}$				
$5/2_1^+$		-1.955		-0.526
$7/2_1^+$		-0.892		-0.427
$9/2_1^+$		-1.293		-0.718
$11/2_1^+$		+1.285		-0.756
$21/2_1^+$	4.73(11)	+3.797		-0.880
$25/2_1^+$	7.63(25)	+5.367		-0.660
$15/2_1^-$		-1.373		-0.909
$31/2_1^-$	9.90(8)	+5.313		-0.796
$^{215}\text{Rn}$				
$7/2_1^+$		-0.725		-0.636
$9/2_1^+$		-1.130		-0.700
$11/2_1^+$		+1.294		-1.136
$13/2_1^+$		-0.489		-0.820

### 1.3.6 Fr isotopes

Here  $^{214-217}\text{Fr}$  isotopes are discussed. Figure 1.8 shows the theoretical energy spectrum of  $^{215}\text{Fr}$  in comparison with the experimental data [16, 32]. In  $^{215}\text{Fr}$ , energy levels of low-lying negative parity states are well reproduced. A  $(13/2^+)$  state is observed at 0.835 MeV in experiment. However, the  $13/2_1^+$  state is calculated at 1.224 MeV, which is 0.409 MeV higher than the experimental one.

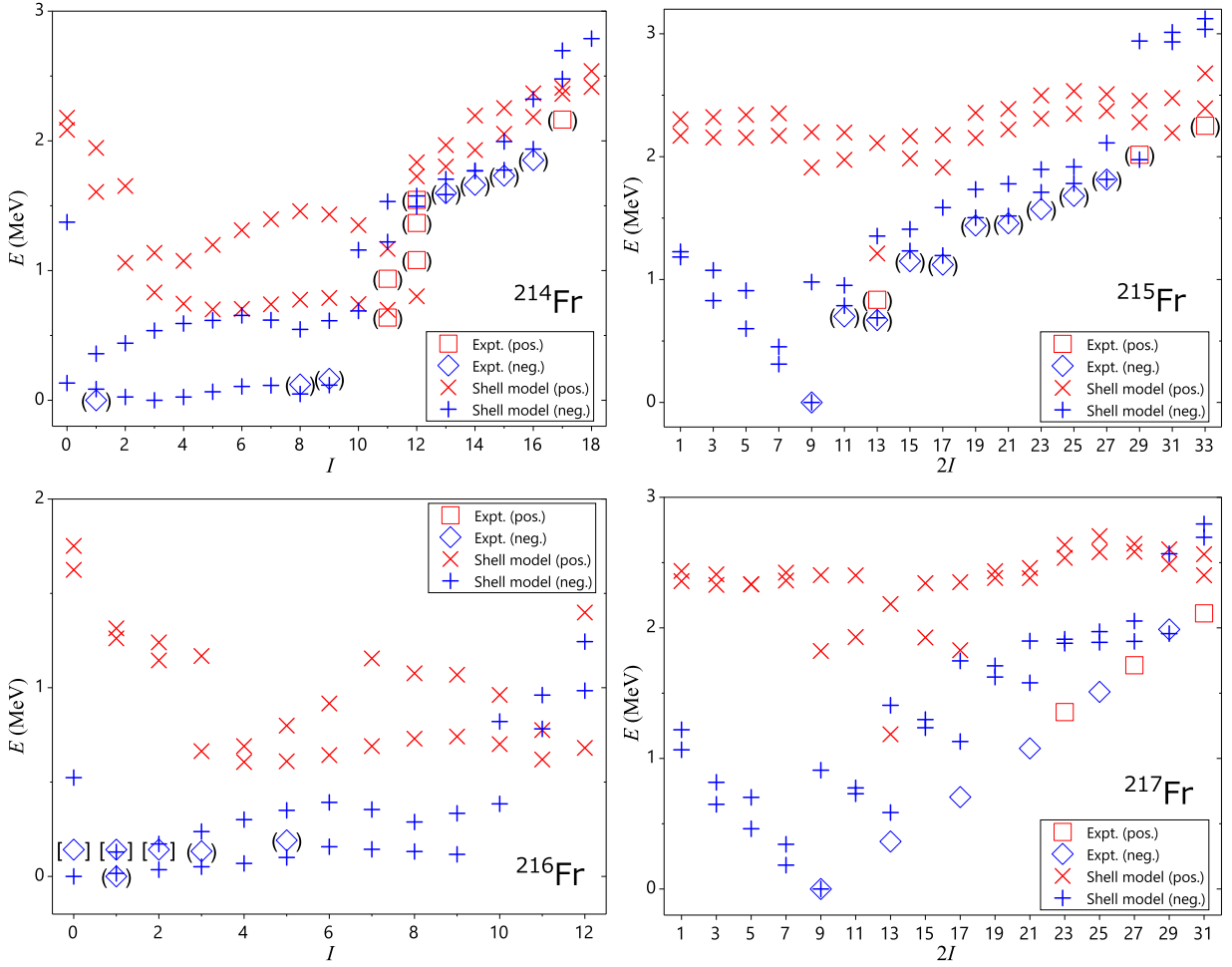


Figure 1.8: Same as Fig. 1.1, but for Fr isotopes. The experimental data are taken from Refs. [16, 26, 32, 34, 35].

Figure 1.8 shows the theoretical energy spectrum of  $^{217}\text{Fr}$  in comparison with the experimental data [16, 35]. In  $^{217}\text{Fr}$ , the spins and parities of the states observed at 0.209 and 0.275 MeV are not assigned (not shown in this figure). The  $7/2_1^-$ ,  $7/2_2^-$ , and  $5/2_1^-$  states are calculated at 0.182, 0.342, and 0.462 MeV. Thus it is suggested that two of these states correspond to the experimental states at 0.209 and 0.275 MeV. The experimental energy levels of high-spin states,  $13/2_1^-$ ,  $15/2_1^-$ ,  $17/2_1^-$ ,  $21/2_1^-$ , and  $25/2_1^-$  states, are not reproduced well in comparison to other Fr isotopes. These states look like members of a quadrupole vibrational band on the ground  $9_1^-$  state. In the present analysis of adjusting the two-body effective interactions, we have not included  $^{217}\text{Fr}$  since it is a complicated system with five valence protons and two neutrons. The quadrupole-quadrupole interactions between like particles and/or the hexadecapole-hexadecapole interactions between a neutron and a proton might be necessary for a better reproduction.

Figure 1.8 shows the theoretical energy spectrum of  $^{214}\text{Fr}$  in comparison with the experimental

data [16, 26]. In  $^{214}\text{Fr}$ , low-lying negative parity states are well reproduced. The  $(8^-)$  state observed at 0.122 MeV is a spin-gap isomer with a half-life of 3.35(5) ms [16]. This state disintegrates only by the  $\alpha$ -decay. The  $0_1^-, 1_1^-, \dots, 9_1^-$  states mainly consist of the  $(\nu g_{9/2} \otimes \pi h_{9/2}^4 f_{7/2})$  configuration. The  $6_1^-, 7_1^-$ , and  $9_1^-$  states, which are connected to the  $8_1^-$  state by  $E2$  or  $M1$  transitions, are calculated higher than the  $8_1^-$  state. As mentioned above, the calculation reproduces the situation that the  $9_1^-$  state is slightly higher than the  $8_1^-$  state. The  $9_1^-$  state is indeed unfavored in the  $(\nu g_{9/2} \otimes \pi h_{9/2}^4 f_{7/2})$  configuration, in which at least one proton pair with angular momentum 0 have to be broken in the  $0h_{9/2}$  orbital. The  $10_2^-, 11_1^-, 12_1^-, \dots, 15_1^-$  states are admixtures of the  $(\nu g_{9/2} \otimes \pi h_{9/2}^5)$  and  $(\nu g_{9/2} \otimes \pi h_{9/2}^4 f_{7/2})$  configurations.

Figure 1.8 shows the theoretical energy spectrum of  $^{216}\text{Fr}$  in comparison with the experimental data [16, 34]. In  $^{216}\text{Fr}$ , the spin-parity of the state observed at 0.142 MeV is assigned as  $(0^-, 1^-, 2^-)$ . The  $0_1^-, 1_2^-,$  and  $2_2^-$  states are calculated at 0, 0.129, and 0.172 MeV, respectively. Thus it is inferred that the spin-parity of the state at 0.142 MeV is  $1^-$  or  $2^-$ . The experimentally observed  $(9^-)$  state with an unknown energy is calculated at 0.117 MeV.

Calculated results for  $B(E2)$  values and electromagnetic moments of Fr isotopes are given in Tables 1.14 and 1.15 in comparison with the experimental data [16, 26, 32]. The experimental  $B(E2; 19/2_1^- \rightarrow 15/2_1^-)$  value of  $^{215}\text{Fr}$  is 0.6(4) W.u. The calculated  $B(E2)$  value of the same transition is 17.221 W.u., which is much larger than the experimental one. The  $15/2_2^-$  state is calculated 0.181 MeV higher than the  $15/2_1^-$  state. The  $B(E2)$  value from the  $19/2_1^-$  state to the  $15/2_2^-$  state is calculated as 0.015 W.u. Therefore the calculated  $15/2_1^-$  and  $15/2_2^-$  states might be largely admixed. The electromagnetic moments are well reproduced except for the magnetic moment of the  $11_1^+$  state in  $^{214}\text{Fr}$ . The magnetic moment of the  $11_2^+$  state is calculated as  $2.982 \mu_N$ . It is thus difficult to resolve the discrepancy even if the  $11_1^+$  and  $11_2^+$  states are reversely predicted in our calculation. However, it should be noted that the experimental  $11^+$  state is ambiguous with respect to spin and parity.

## 1.4 Discussion

In this section, structure of some even-even nuclei is investigated. The expectation numbers of pairs for the yrast states are calculated using the pair-truncated shell model (PTSM) [36–38]. In the present scheme, the building blocks are angular momenta zero ( $S$ ), two ( $D$ ), and four ( $G$ ) collective pairs, and also non-collective ( $H$ ) pairs. The  $S$ ,  $D$ , and  $G$  pair-creation operators are defined as

$$S^\dagger = \sum_j \alpha_j A_0^{\dagger(0)}(jj), \quad (4.1)$$

$$D_M^\dagger = \sum_{j_1 j_2} \beta_{j_1 j_2} A_M^{\dagger(2)}(j_1 j_2), \quad (4.2)$$

$$G_M^\dagger = \sum_{j_1 j_2} \gamma_{j_1 j_2} A_M^{\dagger(4)}(j_1 j_2), \quad (4.3)$$

Table 1.14: Same as table 1.3, but for Fr isotopes. The experimental data are taken from Refs. [16, 26, 32].

$^{215}\text{Fr}$	$B(E2)$	
	Expt.	Calc.
$5/2_1^- \rightarrow 9/2_1^-$		16.474
$7/2_1^- \rightarrow 9/2_1^-$		3.610
$7/2_2^- \rightarrow 9/2_1^-$		20.475
$13/2_1^- \rightarrow 9/2_1^-$		17.350
$19/2_1^- \rightarrow 15/2_1^-$	0.6(4)	17.221
$19/2_1^- \rightarrow 15/2_2^-$		0.015
$23/2_1^- \rightarrow 19/2_1^-$	12(5)	14.100
$27/2_1^- \rightarrow 23/2_1^-$	1.1(8)	6.365
$27/2_2^- \rightarrow 23/2_1^-$		0.002
$^{217}\text{Fr}$	Expt.	Calc.
$5/2_1^- \rightarrow 9/2_1^-$		28.245
$7/2_1^- \rightarrow 9/2_1^-$		1.883
$7/2_2^- \rightarrow 9/2_1^-$		32.920
$13/2_1^- \rightarrow 9/2_1^-$		28.429
$^{214}\text{Fr}$	Expt.	Calc.
$5_1^- \rightarrow 3_1^-$		3.336
$8_1^- \rightarrow 9_1^-$		4.374
$15_1^- \rightarrow 13_1^-$	0.68(24)	0.221
$^{216}\text{Fr}$	Expt.	Calc.
$3_1^- \rightarrow 1_1^-$		1.372
$5_1^- \rightarrow 3_1^-$		5.789

where the pair creation operator of two nucleons in the orbitals  $j_1$  and  $j_2$  with total angular momentum  $J$  and magnetic quantum number  $M$  is constructed as

$$A_M^{\dagger(J)}(j_1 j_2) = \left[ c_{j_1}^\dagger c_{j_2}^\dagger \right]_M^{(J)}. \quad (4.4)$$

The structure coefficients  $\alpha$ ,  $\beta$ , and  $\gamma$  are determined by variation.

The  $H$  pair creation operators for neutrons are defined as

$$H_{M\nu}^{\dagger(K)} = \begin{cases} \left[ c_{j_{15/2}}^\dagger c_{j_{15/2}}^\dagger \right]_M^{(K)}, & K = 0, 2, 4, \dots, 14, \\ \left[ c_{g_{9/2}}^\dagger c_{g_{9/2}}^\dagger \right]_M^{(K)}, & K = 0, 2, 4, 6, 8, \\ \left[ c_{g_{9/2}}^\dagger c_{i_{11/2}}^\dagger \right]_M^{(K)}, & K = 1, 2, 3, \dots, 10, \end{cases} \quad (4.5)$$

Table 1.15: Same as table 1.4, but for Fr isotopes. The experimental data are taken from Refs. [16, 26, 32].

	$\mu$		$Q$	
	Expt.	Calc.	Expt.	Calc.
<sup>215</sup> Fr				
7/2 <sub>1</sub> <sup>-</sup>		+4.010		-0.664
9/2 <sub>1</sub> <sup>-</sup>		+3.690		-0.183
11/2 <sub>1</sub> <sup>-</sup>		+3.546		-0.329
13/2 <sub>1</sub> <sup>-</sup>		+4.089		-0.366
19/2 <sub>1</sub> <sup>-</sup>	3.1(9)	+2.560		-0.771
23/2 <sub>1</sub> <sup>-</sup>	3.8(12)	+2.211		-1.001
<sup>217</sup> Fr				
7/2 <sub>1</sub> <sup>-</sup>		+4.084		-0.878
9/2 <sub>1</sub> <sup>-</sup>		+3.625		-0.464
11/2 <sub>1</sub> <sup>-</sup>		+3.705		-0.627
13/2 <sub>1</sub> <sup>-</sup>		+4.165		-0.577
<sup>214</sup> Fr				
1 <sub>1</sub> <sup>-</sup>		+0.232		+0.119
8 <sub>1</sub> <sup>-</sup>		+2.145		-0.610
9 <sub>1</sub> <sup>-</sup>		+2.472		-0.608
14 <sub>1</sub> <sup>-</sup>	+8.5(4)	+7.412		-0.318
14 <sub>2</sub> <sup>-</sup>		+6.013		-1.339
11 <sub>1</sub> <sup>+</sup>	+5.62(7)	+1.905	0.82(22)	-0.874
11 <sub>2</sub> <sup>+</sup>		+2.982		-1.217
<sup>216</sup> Fr				
1 <sub>1</sub> <sup>-</sup>		+0.275		+0.138
3 <sub>1</sub> <sup>-</sup>		+0.743		+0.277
5 <sub>1</sub> <sup>-</sup>		+1.414		-0.059

and those for protons are defined as

$$H_{M\pi}^{\dagger(K)} = \begin{cases} \left[ c_{i_{13/2}}^{\dagger} c_{i_{13/2}}^{\dagger} \right]_M^{(K)}, & K = 0, 2, 4, \dots, 12, \\ \left[ c_{h_{9/2}}^{\dagger} c_{h_{9/2}}^{\dagger} \right]_M^{(K)}, & K = 0, 2, 4, 6, 8, \\ \left[ c_{h_{9/2}}^{\dagger} c_{f_{7/2}}^{\dagger} \right]_M^{(K)}, & K = 1, 2, 3, \dots, 8. \end{cases} \quad (4.6)$$

Using the  $S$ ,  $D$ ,  $G$ , and  $H$  pair-creation operators, a many-body wavefunction of like nucleons can

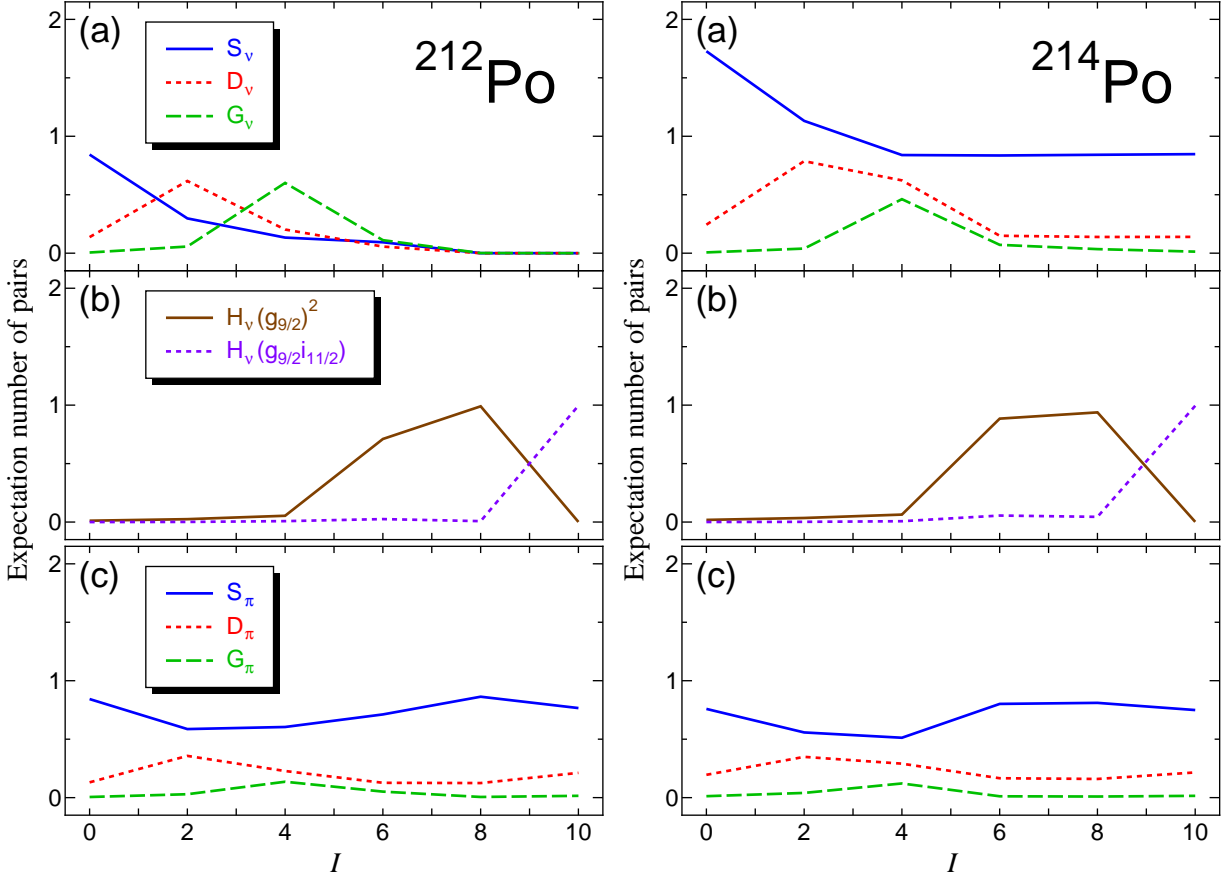


Figure 1.9: (a) The neutron expectation numbers of collective pairs for  $^{212}\text{Po}$  and  $^{214}\text{Po}$ . The S, D, and G indicate  $S$ -pair,  $D$ -pair, and  $G$ -pair, respectively. (b) The neutron expectation numbers of non-collective  $(g_{9/2})^2$ -pair  $[(g_{9/2})^2]$  and  $g_{9/2}i_{11/2}$ -pair  $(g_{9/2}i_{11/2})$ . The definitions of noncollective pairs are given in the text. (c) The proton expectation numbers of collective pairs for  $^{212}\text{Po}$ .

be constructed as

$$|\Psi(I\eta)\rangle = (S^\dagger)^{n_s} (D^\dagger)^{n_d} (G^\dagger)^{n_g} (H^\dagger)^{n_h} |-\rangle. \quad (4.7)$$

The number of valence nucleon pairs,  $n_s+n_d+n_g+n_h$ , is fixed for a specific nucleus. The Hamiltonian for this truncated space (PTSM space) is set identical to the present shell-model Hamiltonian. The consistency between the results with the two methods (SM and PTSM) was discussed concerning the energy levels of the  $^{82}\text{Se}$  nucleus up to 6 MeV in Ref. [39]. In Ref. [40] the energy levels of the  $^{208}\text{Rn}$  nucleus up to 3.5 MeV in the SM are compared with those in the PTSM. The good correspondence between the SM and the PTSM is seen.

Figure 1.9 shows the expectation numbers of pairs for the yrast states up to spin 10 in  $^{212}\text{Po}$ . This nucleus is a system with two neutrons and two protons outside the doubly magic core  $^{208}\text{Pb}$ . It is seen that the proton wavefunction mainly consists of the  $S$ -pair, and the contributions from the

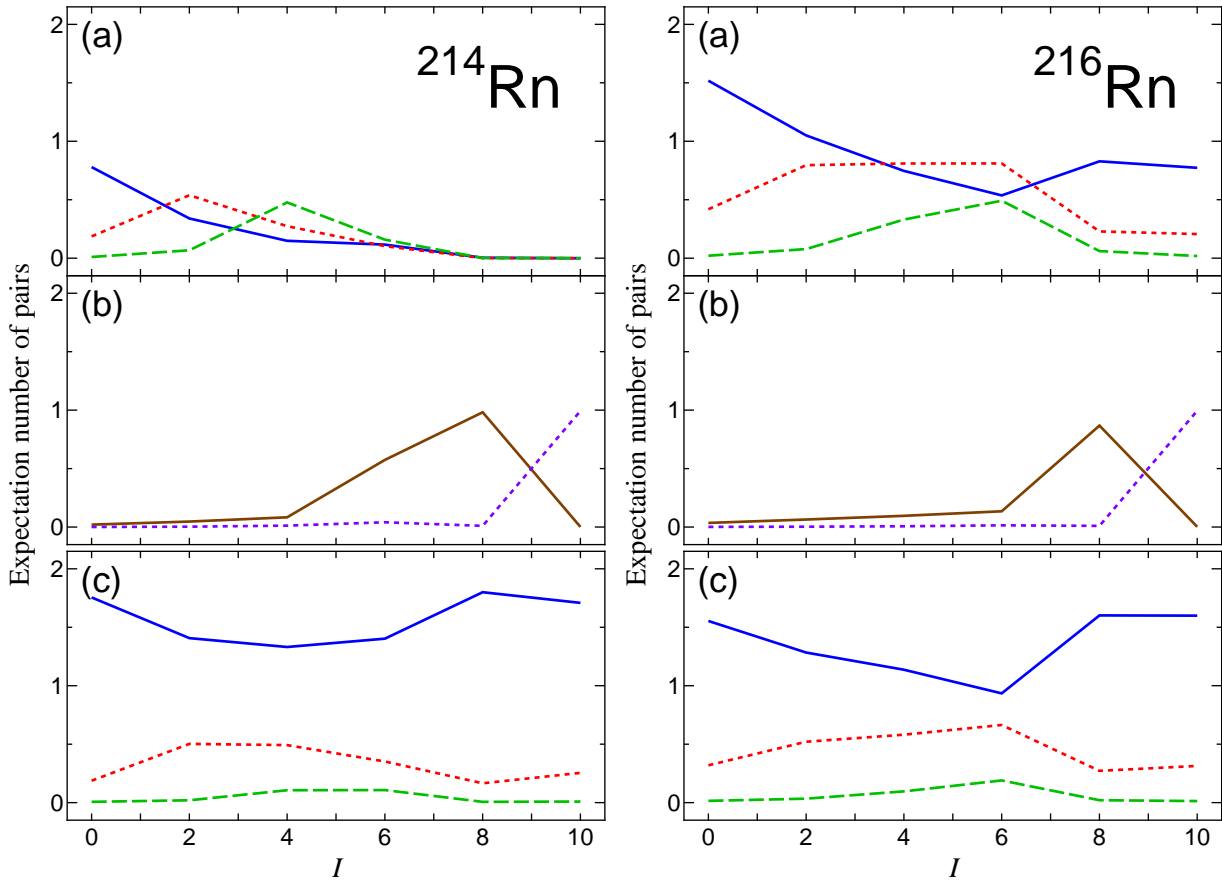


Figure 1.10: The same as Fig. 1.9, but for  $^{214}\text{Rn}$  and  $^{216}\text{Rn}$ .

$D$ -pair and the  $G$ -pair are small for all the spins. The maximum contribution except from the  $S$ -pair is 0.357 pairs of the  $D$ -pair in the  $2_1^+$  state. Thus the total excitation is mainly determined by the neutron part. Up to the  $8_1^+$  state, the states consist of the  $(\nu g_{9/2})_{I^+}^2$  ( $I = 0, 2, \dots, 8$ ) configuration. One neutron needs to be excited to the  $0i_{11/2}$  orbital to make the  $10_1^+$  state since the maximum spin of two neutrons in the  $1g_{9/2}$  orbital is eight. Therefore, the  $10_1^+$  state consists of the  $(\nu g_{9/2} i_{11/2})_{10^+}$  configuration. In this mass region, the strength of the neutron monopole-pairing is smaller than that of protons. Thus the configuration mixing of neutrons is preferred.

Figure 1.9 shows the expectation numbers of pairs for the yrast states up to spin 10 in  $^{214}\text{Po}$ . This nucleus is a system with four neutrons and two protons outside the  $^{208}\text{Pb}$  core. Similar to  $^{212}\text{Po}$ , the proton part mainly consists of the  $S$ -pair for all the spins. For the neutron part, the ground state consists of two neutron  $S$ -pairs. For the  $I^\pi = 2_1^+, 6_1^+, 8_1^+$ , and  $10_1^+$  states, two neutrons are coupled to the  $S$ -pair, and the other two neutrons are coupled to pairs with spin  $I$ . For the  $2_1^+$  state, the expectation numbers of the neutron  $D$ -pair and the proton  $D$ -pair are 0.787 and 0.349, respectively. This result means that the  $2_1^+$  state mainly consists of the neutron  $D$ -pair. For the  $4_1^+$  state, the

expectation numbers of the neutron  $D$ -pair, the neutron  $G$ -pair, and the proton  $D$ -pair are 0.623, 0.462, and 0.291, respectively. Thus it is inferred that the  $4_1^+$  state consists of mixtures of two types of pair structures. The first one consists of one neutron  $S$ -pair, one neutron  $D$ -pair, and one proton  $D$ -pair which are coupled with spin 4 [ $S_\nu(D_\nu D_\pi)_{4+}$ ]. The second one consists of one neutron  $S$ -pair, one neutron  $G$ -pair, and one proton  $S$ -pair ( $S_\nu G_\nu S_\pi$ ).

Figure 1.10 shows the expectation numbers of pairs for the yrast states (except  $6^+$  and  $8^+$ ) in  $^{214}\text{Rn}$ . Those numbers for the  $6_2^+$  and  $8_2^+$  states are shown instead of those for the  $6_1^+$  and  $8_1^+$  states, which are reversely reproduced in order in the PTSM calculations, compared to those in the SM calculations. This nucleus is a system with two neutrons and four protons outside the  $^{208}\text{Pb}$  core. For all the spins, four protons are coupled to the  $S$ -pairs and the spins are mainly determined by the neutron part. Similar to  $^{212}\text{Po}$ , the yrast states up to spin 8 consist of the  $(\nu g_{9/2})_{I^+}^2$  configuration and the  $10_1^+$  state consists of the  $(\nu g_{9/2} i_{11/2})_{10^+}$  configuration.

Figure 1.10 shows the expectation numbers of pairs for the yrast states in  $^{216}\text{Rn}$ . This nucleus is a system with four neutrons and four protons outside the  $^{208}\text{Pb}$  core. Similar to the other three even-even nuclei,  $^{212}\text{Po}$ ,  $^{214}\text{Po}$ , and  $^{214}\text{Rn}$ , the ground state consists of two neutron  $S$ -pairs and two proton  $S$ -pairs, and the  $2_1^+$  state mainly consists of one neutron  $S$ -pair, one neutron  $D$ -pair, and two proton  $S$ -pairs. For the  $4_1^+$  state, the expectation numbers of the neutron  $D$ -pair, the neutron  $G$ -pair, and the proton  $D$ -pair are 0.810, 0.330, and 0.582, respectively. The  $4_1^+$  state has a similar structure with the  $4_1^+$  state in  $^{214}\text{Po}$ . The structure of the  $6_1^+$  state, however, is different from the other three nuclei. The expectation numbers of the neutron  $D$ -pair, the neutron  $G$ -pair, and the neutron  $(g_{9/2})_{6^+}^2$ -pair are 0.811, 0.492, and 0.135, respectively. The expectation number of the neutron  $(g_{9/2})_{6^+}^2$ -pair is small and that of the neutron  $D$ -pair is large compared to the other three nuclei. This indicates that the nucleus shows an aspect of a collective feature.

The low-lying nuclear structures of nuclei with a few valence nucleons outside the doubly magic core  $^{208}\text{Pb}$  are generally determined by the single-particle motion of the valence nucleons. However, as the number of valence nucleons increases, collective features appear. The collectivity of  $^{216}\text{Rn}$  is also seen in the energy spectrum as discussed in Sec. 1.3.5.

A specific feature of even-even nuclei in this mass region is the narrow energy gap between the  $6_1^+$  and  $8_1^+$  states (e.g. see  $^{210}\text{Pb}$  in Fig. 1.1). This small energy gap occurs due to the alignment of two neutrons. In this mass region, the yrast states up to spin 8 in even-even nuclei consist of the two neutrons in the  $1g_{9/2}$  orbital. In the  $8_1^+$  state, the spin of two neutrons in the  $1g_{9/2}$  orbital is stretched and the energy of the  $8_1^+$  state is lowered. However, the narrow energy gap between the  $6_1^+$  and  $8_1^+$  states is not seen in  $^{216}\text{Rn}$  anymore (see Fig. 1.7).

## 1.5 Summary

In the present study, the large-scale shell-model calculations have been carried out for even-even, odd-mass, and doubly odd nuclei of  $_{82}\text{Pb}$ ,  $_{83}\text{Bi}$ ,  $_{84}\text{Po}$ ,  $_{85}\text{At}$ ,  $_{86}\text{Rn}$ , and  $_{87}\text{Fr}$  isotopes in the neutron

rich region around the double magic  $^{208}\text{Pb}$  nucleus.

For neutron single-particle levels, seven orbitals above the magic number 126,  $1g_{9/2}$ ,  $0i_{11/2}$ ,  $0j_{15/2}$ ,  $2d_{5/2}$ ,  $3s_{1/2}$ ,  $1g_{7/2}$ , and  $2d_{3/2}$  orbitals, have been taken into account. For proton single-particle levels, all the six orbitals in the major shell between the magic numbers 82 and 126,  $0h_{9/2}$ ,  $1f_{7/2}$ ,  $0i_{13/2}$ ,  $2p_{3/2}$ ,  $1f_{5/2}$ , and  $2p_{1/2}$  orbitals, have been taken into account. The particle number dependence of the single-particle energies of the neutron  $0j_{15/2}$  and  $0i_{11/2}$  orbitals and the proton  $0i_{13/2}$  and  $1f_{7/2}$  orbitals have been assumed. They are changed linearly so as to reproduce the energy levels of low-lying states of the odd-mass nuclei. As for the effective two-body interaction, higher multipole-pairing interactions among like nucleons and the quadrupole-quadrupole interaction between neutrons and protons are employed in addition to the conventional pairing interactions. Only one set of the strengths of the two-body interactions has been adopted in all the nuclei considered.

Energy spectra,  $E2$  transition rates, magnetic moments, and electric quadrupole moments have been calculated and compared with the experimental data. Good agreements with experimental data have been obtained not only for even-even and odd-mass nuclei, but also for doubly-odd nuclei. Comparing our results and the experimental data, spins and parities of experimentally ambiguous states have been suggested.

Nine isomeric states are analyzed in terms of the shell-model configurations. Four isomeric states appearing in this region are classified as the spin-gap isomers, which do not take gamma transitions with low-spin changes, such as  $E2$  or  $M1$  transitions, because of the large spin difference between initial and final states. The other five states become isomers even if they decay by the  $E2$  transition. They become isomers since the energy gaps between the initial and final states are small.



## Chapter 2

# One octupole-phonon model in the proton-rich region of $^{208}\text{Pb}$

### 2.1 Introduction

Octupole correlations play an important role in determining the low-lying structure of nuclei throughout the periodic table [41, 42]. Nuclei around the double-magic nucleus  $^{208}\text{Pb}$  provides an ideal laboratory to study the concept of octupole-phonon vibrations in nuclear systems because the first excited  $3^-$  states of these nuclei have long been interpreted as collective one-octupole-phonon states. In fact large electric octupole transition probabilities between low-lying  $3^-$  states and the ground  $0^+$  states have been experimentally observed in  $^{208}\text{Pb}$  [43, 44],  $^{206}\text{Pb}$  [45, 46], and  $^{210}\text{Pb}$  [47]. High-spin alternating parity band was also discovered in  $^{216}\text{Rn}$  [48]. Microscopically, they result from the long-range, octupole-octupole interaction between nucleons occupying pairs of orbitals with  $\Delta j = 3$  and  $\Delta l = 3$ . One-octupole-phonon and multi-octupole-phonon excitations around  $^{208}\text{Pb}$  have been studied in theory by many authors [20, 49–56].

The nuclear shell model is one of the most successful models in nuclear structure. In our previous studies [1, 14, 15, 57], low-lying states in the mass number  $A = 130$  and 200 regions were systematically reproduced in the nuclear shell model. The octupole-phonon states which arise from one-particle one-hole excitations across the magic cores were excluded in the previous framework of the nuclear shell model, where the number of the shell-model configurations was limited due to the computational feasibility.

The octupole vibration and deformation are closely related to the parity ( $P$ ) odd nuclear moments. The nuclear Schiff moments and the magnetic quadrupole moments can be largely enhanced in deformed nuclei, for example  $^{225}\text{Ra}$  [58],  $^{161}\text{Dy}$ , and  $^{237}\text{Np}$  [59]. Moreover, an additional enhancement mechanism due to the coexistence of collective quadrupole and octupole modes was suggested, and the effect has been confirmed in RPA-based calculations [60, 61]. Another enhancement mechanism of the  $CP$  violating interactions due to  $\alpha$ -cluster structures is expected in light nuclei [62–64]. In spherical nuclei the nuclear Schiff moment of  $^{129}\text{Xe}$  [65–67] and nuclear dipole moments of

$^{129}\text{Xe}$  [68, 69] and  $^{199}\text{Hg}$  [70] are precisely calculated in the nuclear shell model.

In this paper the shell-model states and one-octupole-phonon states are unified by introducing an octupole phonon, which is helpful to identify the octupole vibrational states based on the shell-model configurations. The model is applied to various nuclei around the  $^{208}\text{Pb}$  nucleus.

This paper is organized as follows. In Sec. 3.2 theoretical framework is given where the collective octupole phonon ( $f$ -boson) is introduced. In Sec. 2.3 numerical results are given. Finally summary is given in Sec. 3.4.

## 2.2 Theoretical framework

A phenomenological model is introduced in this paper to describe collective octupole-phonon excitations based on the shell-model (SM) states. In this model a collective octupole-phonon ( $f$ -boson) weakly couples with each shell-model state. The total Hamiltonian reads

$$\hat{H} = \hat{H}_{\text{SM}} + \hat{H}_f + \hat{H}_{\text{SM}-f}, \quad (2.1)$$

where  $\hat{H}_{\text{SM}}$  is the shell-model Hamiltonian for valence neutrons and protons. The explicit form of the shell-model Hamiltonian and the strengths of the interactions are given in Ref. [15] for the neutron number  $N \leq 126$  and in Ref. [1] for  $N > 126$ . In these works, the shell-model configurations involve all the valence nucleons and all the single-particle orbitals in each one-major shell.

The  $f$ -boson one-body Hamiltonian is given as

$$\hat{H}_f = \varepsilon_f f^\dagger \cdot \tilde{f}, \quad (2.2)$$

where  $f^\dagger$  and  $\tilde{f}_\mu = (-1)^{3-\mu} f_{-\mu}$  are the  $f$ -boson creation and annihilation operators, respectively, with angular momentum 3 and negative parity. As will be discussed in detail, the single  $f$ -boson energy  $\varepsilon_f$  is introduced as a phenomenological parameter.

The interaction between one  $f$ -boson and each shell-model state is simply assumed to be a dipole-type with a coupling constant  $\alpha$ :

$$\hat{H}_{\text{SM}-f} = \alpha \mathbf{I}_{\text{SM}} \cdot \mathbf{L}_f, \quad (2.3)$$

where  $\mathbf{I}_{\text{SM}}$  indicates the angular momentum in the valence space and  $\mathbf{L}_f$  is the angular momentum of the  $f$ -boson that is defined as

$$L_f^{(1)} = \sqrt{14} [f^\dagger \tilde{f}]^{(1)}. \quad (2.4)$$

This dipole-type interaction represents the Coriolis force that does not admix the pure shell-model states with the one-octupole-phonon excited states. Then  $f$ -boson state coupled with each shell-model state is explicitly constructed as

$$|I_k^\pi; J\rangle_f = [|f\rangle \otimes |I_k^\pi\rangle_{\text{SM}}]^{(J)}, \quad (2.5)$$

where  $|I_k^\pi\rangle_{\text{SM}}$  is the  $k$ th eigenstate with spin  $I$  and parity  $\pi$  of the shell-model Hamiltonian within the valence space. Here the shell-model states  $|I_k^\pi\rangle_{\text{SM}}$  are given by diagonalizing the shell-model Hamiltonian as

$$\hat{H}_{\text{SM}} |I_k^\pi\rangle_{\text{SM}} = E_{\text{SM}}(I_k^\pi) |I_k^\pi\rangle_{\text{SM}}. \quad (2.6)$$

The total angular momenta  $J$  of the  $f$ -boson state coupled with the shell-model  $I_k^\pi$  state are given by

$$J = |I - 3|, |I - 3| + 1, \dots, I + 3. \quad (2.7)$$

It should be noted that the  $f$ -boson state coupled with the shell-model  $I_k^\pi$  state has the opposite parity to the corresponding shell-model state. The energy of the  $f$ -boson state coupled with the shell-model  $I_k^\pi$  state is given as

$$E_f(I_k^\pi; J) = E_{\text{SM}}(I_k^\pi) + \varepsilon_f + \frac{1}{2}\alpha [J(J+1) - I(I+1) - 12]. \quad (2.8)$$

As for the single  $f$ -boson energies  $\varepsilon_f$ , the excitation energies of the  $3_1^-$  states are adopted if they are experimentally known. Those values are  $\varepsilon_f = 2.648$  and  $1.870$  MeV for  $^{206,210}\text{Pb}$ , respectively, and  $\varepsilon_f = 2.387$ ,  $1.537$ , and  $1.275$  MeV for  $^{210,212,214}\text{Po}$ , respectively. For other nuclei where any  $3^-$  states are not observed, linearly optimized values with mass number  $A$  given in MeV as

$$\varepsilon_f = -0.121A + 27.3, \quad (2.9)$$

are employed. Here the neutron-closed, proton-closed, and deformed nuclei are excluded in the process of optimization.

Fig. 2.1(a) shows the ratio ( $R_{4/2} = E(4_1^+)/E(2_1^+)$ ) of the excitation energy of the experimental  $4_1^+$  state to that of  $2_1^+$  state. In the lead region the value is in between one and two, indicating that these nuclei are spherical. In heavy Ra and Th isotopes, the ratio changes from two to 3.3, which indicates that these nuclei exhibit vibrational to rotational nature as the valence neutron number increases. Fig. 2.1(b) shows the experimental excitation energies of the  $3_1^-$  states. It is shown in the figure that there is a strong correlation between two quantities ( $R_{4/2}$  and  $E(3_1^-)$ ). The deformation feature appears in the  $A \geq 224$  region, whose nuclei are not treated in the present paper. As for the Coriolis coupling strength, an optimum choice is  $\alpha = -0.02$  MeV throughout all the nuclei considered.

The electric octupole ( $E3$ ) transition operator is simply given as

$$O_\mu = e_f \left( f_\mu^{(3)\dagger} - \tilde{f}_\mu^{(3)} \right), \quad (2.10)$$

where  $e_f$  represents the effective charge of the collective  $f$ -boson. Here it is assumed that the contributions to  $E3$  transition probabilities from valence nucleons are small, compared with the collective contributions. The reduced transition probabilities are then given by

$$B(E3; (I_k; J)_f \rightarrow I_{k'}') = e_f^2 \delta_{I,I'} \delta_{k,k'}. \quad (2.11)$$

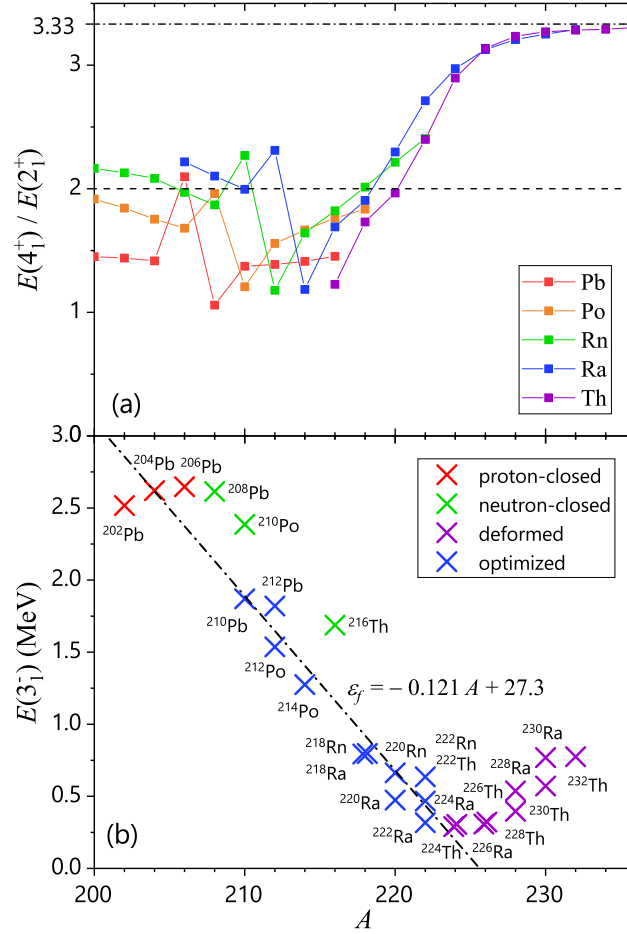


Figure 2.1: (a) Ratio of the excitation energy of the  $4_1^+$  state to that of the  $2_1^+$  state, and (b) Excitation energies of the  $3_1^-$  states for proton-closed (red), neutron-closed (green), deformed (violet), and other open-shell (blue) nuclei. The dot-dash line indicates the single  $f$ -boson energy  $\varepsilon_f$  as a function of mass  $A$ . A more detailed discussion on the optimized parameters of the single  $f$ -boson energy  $\varepsilon_f$  is given in the text.

As shown in Table 2.1, large  $B(E3)$  values of the ground  $0^+$  states to the  $3_1^-$  states are measured with good accuracy for  $^{206}\text{Pb}$  [45, 46],  $^{208}\text{Pb}$  [43, 44], and  $^{210}\text{Pb}$  [47], which demonstrates the collective nature of the  $3_1^-$  states.

## 2.3 Numerical results

As noted in the formalism, the shell-model  $I_k^\pi$  state indicates  $|I_k^\pi\rangle_{\text{SM}}$ , while  $|I_k^\pi; J\rangle_f$  is referred to as the  $f$ -boson  $J^{\pi'}$  state coupled with the shell-model  $I_k^\pi$  state. Here the  $f$ -boson state has the opposite parity  $\pi'$  to the parity  $\pi$  of the corresponding shell-model state.

In the following calculations it should be noted that in the case of  $^{206,210}\text{Pb}$  and  $^{210}\text{Po}$  the shell

Table 2.1: Experimental  $B(E3)$  values in units of W.u. Excitation energies (Exc.) are given in units of MeV. The Weisskopf unit for the electric octupole transition is given as  $B_{\text{sp}}(E3) = 5.940 \times 10^{-2} A^2$  in units of  $e^2\text{fm}^6$  [42]. In the last column type of each electric octupole transition is given. Ambiguous type is enclosed in parentheses.

	$J^\pi$	Exc.	$I^\pi$	Exc.	$B(E3; J^\pi \rightarrow I^\pi)$	Type
$^{206}\text{Pb}$	$3^-$	2.648	$0^+$	0	36 (2) [45, 71]	collective
	$7^-$	2.200	$4^+$	1.998	0.28 (3) [71]	non-collective
	$7^-$	2.200	$4^+$	1.684	0.361 (8) [16]	non-collective
	$12^+$	4.027	$9^-$	2.658	0.137 (12) [71]	non-collective
$^{208}\text{Pb}$	$3^-$	2.615	$0^+$	0	34.0 (5) [43, 44, 72]	collective
$^{210}\text{Pb}$	$3^-$	1.870	$0^+$	0	26 (6) [17, 47]	collective
	$3^-$	2.828	$0^+$	0	14 (4) [17, 47]	(collective)
	$11^-$	2.512	$8^+$	1.278	21 (2) [73]	(collective)
$^{214}\text{Rn}$	$13^-$	2.676	$10^+$	1.928	44 (8) [74]	collective
$^{212}\text{At}$	$18^+$	2.250	$15^-$	1.605	24 (1) [75] *1	collective
	$22^-$	3.506	$19^+$	2.264	29 (9) [19, 75]	collective
	$25^-$	4.772	$22^+$	4.547	26.8 (14) [19, 75, 76]	collective
$^{214}\text{Fr}$	$11^+$	0.638	$8^-$	0.122	10 (4) [26, 77]	(non-collective)
	$14^-$	1.661	$11^+$	0.638	25 (5) [26, 77]	collective

model configuration space involves only two-particle (hole) configurations. However, in the case of  $^{212,214}\text{Po}$  and also Rn, At and Fr isotopes the shell-model configuration space includes all particles in the valence shells.

Figure 2.2 shows the energy spectra of  $_{82}\text{Pb}$  isotopes ( $^{206}, ^{210}\text{Pb}$ ). The  $^{206}\text{Pb}$  nucleus consists of two valence neutron holes out of the doubly magic core of  $^{208}\text{Pb}$ . The valence space consists of six neutron orbitals,  $2p_{1/2}$ ,  $2p_{3/2}$ ,  $1f_{5/2}$ ,  $1f_{7/2}$ ,  $0h_{9/2}$ , and  $0i_{13/2}$ . Thus, the lowest spin among all the negative parity states in the valence space is two, and the  $1^-$  states were out of the shell-model configurations. As shown in Fig. 2.2, the experimental negative-parity states with spin 2 and spin 3 cannot be described in the shell-model framework either. In fact, the shell-model  $2_1^-$  and  $3_1^-$  states are predicted at 5.735 MeV (not shown in the figure) and 4.660 MeV, respectively. Without any kinds of core-excitations, low-spin negative-parity states cannot be reproduced.

In the present framework, where collective octupole-phonon excitations are taken into account, the one-to-one correspondence between theory and experiment for all the negative-parity states with spin  $I \leq 3$  is well retained with the single  $f$ -boson energy as  $\varepsilon_f = 2.648$  MeV. As shown in Table 2.1, the experimental  $B(E3)$  value from the  $7_1^-$  state to the  $4_1^+$  state, and that from the  $12_1^+$  state to the  $9_1^-$  state, are both one order of magnitude smaller than the single-particle estimate. In fact our

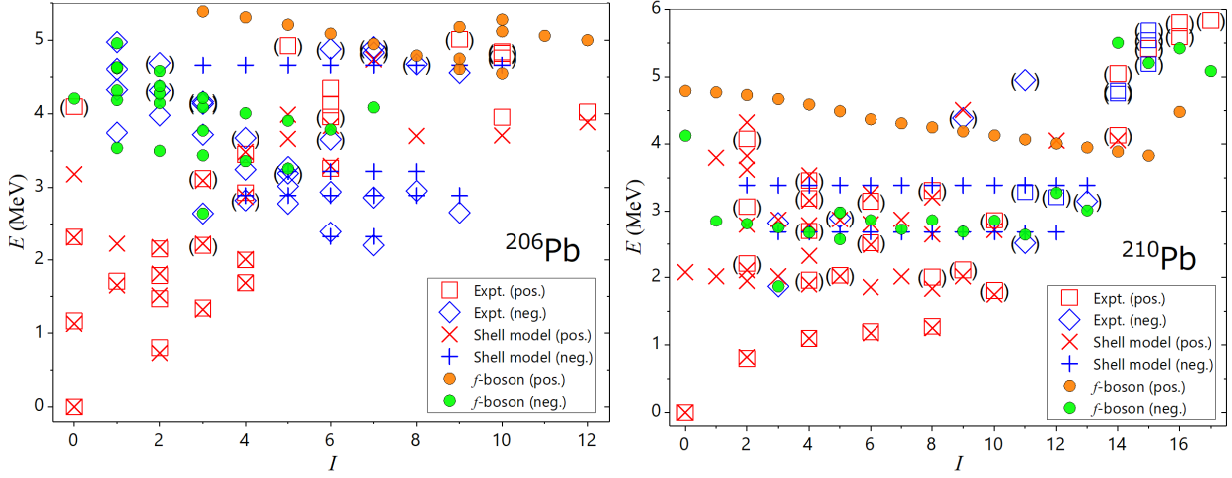


Figure 2.2: Theoretical energy spectra including collective octupole-phonon ( $f$ -boson) excitations for Pb isotopes in comparison with experimental data [16, 17, 71, 73]. As for the  $f$ -boson states indicated with filled circles, only the lowest state for each spin-parity is displayed unless the corresponding state is observed. The  $1^-$ ,  $2^-$ ,  $3^-$ ,  $4^-$ , and  $5^-$  states in  $^{206}\text{Pb}$  and the  $3_2^-$  state and  $5_2^-$  state in  $^{210}\text{Pb}$  are ones of the exceptions.

calculation suggests that the  $7_1^-$  and  $12_1^+$  states correspond to the pure shell-model states, which are not related to the octupole-phonon excitations.

The  $^{210}\text{Pb}$  nucleus consists of two valence neutrons out of the doubly magic core of  $^{208}\text{Pb}$ . Experimental energy levels and electromagnetic properties of low-lying states were well reproduced in the previous shell-model study except for the  $3_1^-$  state observed at 1.870 MeV [1]. The most plausible explanation for the  $3_1^-$  state is that this state is the one-octupole-phonon excitation across the  $^{208}\text{Pb}$  core on top of the ground  $0^+$  state. Recognizing that the  $3_1^-$  state is a collective octupole-phonon excited state ( $f$ -boson state), a number of  $f$ -boson states, not only on top of the ground state, but also on top of other shell-model states such as the  $2_1^+$  and  $4_1^+$  states, should be observed. The energy difference between such kind of an  $f$ -boson state and the corresponding shell-model state should be not so much different from the excitation energy of the  $3_1^-$  state if the  $f$ -boson state and the shell-model state are weakly coupled. It is indeed assumed weak in this work.

In the present framework, there should be an  $f$ -boson  $3^-$  state coupled with the shell-model  $2_1^+$  state, which is predicted at 2.753 MeV with the configuration of  $[[f] \otimes |2_1^+\rangle]^{(3)}$ . In the previous shell-model calculation [1], the  $3_2^-$  was predicted at 2.682 MeV with the configuration of  $(\nu g_{9/2} j_{15/2})$ . The experimental  $B(E3)$  values in Table 2.1, some of which were obtained by Coulomb excitations [17, 47], are helpful to identify the structure of the experimental  $3_2^-$  state. It is shown from Eq. (2.11) that the theoretical  $B(E3)$  value from the  $f$ -boson  $3^-$  state to the shell-model  $0_1^+$  state should be exactly zero if the  $f$ -boson  $3^-$  state is excited from the shell-model  $2_1^+$  state. Taking into account the above,

we have the following assumption for the experimental  $3_1^-$ ,  $3_2^-$  and  $3_3^-$  states as

$$|\widetilde{3}_1^-\rangle = \alpha |f \otimes 0_1^+\rangle + \beta |3_1^-\rangle_{\text{SM}} \quad (3.1)$$

$$|\widetilde{3}_2^-\rangle = \beta |f \otimes 0_1^+\rangle - \alpha |3_1^-\rangle_{\text{SM}} \quad (3.2)$$

$$|\widetilde{3}_3^-\rangle = |f \otimes 2_1^+\rangle \quad (3.3)$$

where  $\alpha^2 + \beta^2 = 1$ . Here the coefficients  $\alpha$  and  $\beta$  may be calculated through the octupole-octupole interaction between the valence nucleons and the octupole phonon. In this case a sum rule is obtained through Eq. (2.11),  $B(E3; 3_1^- \rightarrow 0_1^+) + B(E3; 3_2^- \rightarrow 0_1^+) = e_f^2$ .

Another possibility is that the experimental  $3_1^-$  and  $3_2^-$  states arise from two different kinds of collective-octupole modes with respect to neutron and proton degrees of freedom, namely  $f_\nu$  and  $f_\pi$ . In fact there should be two kinds of excitations expressed as  $|f_1\rangle = \alpha|f_\nu\rangle + \beta|f_\pi\rangle$  and  $|f_2\rangle = \beta|f_\nu\rangle - \alpha|f_\pi\rangle$  where  $\alpha^2 + \beta^2 = 1$ . However, this possibility is low, considering the fact that in  $^{208}\text{Pb}$  the  $3_1^-$  state appears at 2.615 MeV, but the  $3_2^-$  state appears at 4.051 MeV, which is rather high in energy. In order to avoid the complexity, this possibility is not discussed further, but left as a future problem. In this paper only one kind of collective mode characterized by the first  $3^-$  state is assumed.

Figure 2.3 shows the energy spectra of  $_{84}\text{Po}$  isotopes ( $^{210, 212, 214}\text{Po}$ ). The  $^{210}\text{Po}$  nucleus consists of two valence protons in the shell model. In the previous shell-model study [15], the experimental  $3_1^-$ ,  $(11_2^-)$ ,  $(12_1^-)$ ,  $13_1^-$ , and  $14_1^-$  states and some  $5^-$ ,  $6^-$ , and  $7^-$  states were not reproduced. Adopting the excitation energy of the experimental  $3_1^-$  state as the single  $f$ -boson energy  $\varepsilon_f$ , all the experimental  $5^-$ ,  $6^-$ ,  $7^-$ , and  $11^-$  states are well reproduced except for the  $5_1^-$  state. The  $5_1^-$  state is supposed to have nature of a single-particle excitation across the core. Here it should be noted in mind that the experimental  $5_1^-$  state appearing at 3.198 MeV in  $^{208}\text{Pb}$ . In contrast neither of the  $(12_1^-)$ ,  $13_1^-$ , and  $14_1^-$  states are reproduced in the present framework. The  $f$ -boson  $12^-$ ,  $13^-$ , and  $14^-$  states are actually predicted more than 6 MeV higher in energy (not shown in the figure). These high-spin states seemingly have nature of single-particle excitations across the core on top of the pure shell-model states. For example, the  $14_1^-$  state is so constructed that the lowest  $6^-$  particle-hole excitation across the core is coupled to the shell-model  $8_1^+$  state. The excitation energy of  $6^-$  state in  $^{208}\text{Pb}$  is 3.920 MeV. Therefore  $5^-$ ,  $4^-$ , and  $6^-$  one particle-one hole excitations are necessary for the description of the  $(12_1^-)$ ,  $13_1^-$ , and  $14_1^-$  states

For  $^{212}\text{Po}$ , the negative-parity states with spins lower than 11 were reported by the EUROBALL collaboration [23, 24]. The authors assumed that the  $(3_1^-)$ ,  $(5_1^-)$ ,  $(7_1^-)$ , and  $(9_1^-)$  states mainly consist of one-octupole-phonon excitations based on an analogy of the shell-model study in  $^{148}\text{Gd}$  [78]. In the previous shell-model calculations of  $^{212}\text{Po}$  [1], all the negative-parity states were predicted high in energy compared with experiment. The shell-model  $3_1^-$  state was calculated at 2.430 MeV whereas the experimental  $3_1^-$  state is observed at 1.537 MeV. Adopting the excitation energy of the experimental  $3_1^-$  state as the single  $f$ -boson energy  $\varepsilon_f$ , not only the experimental  $(3_1^-)$ ,  $(5_1^-)$ ,  $(7_1^-)$ ,

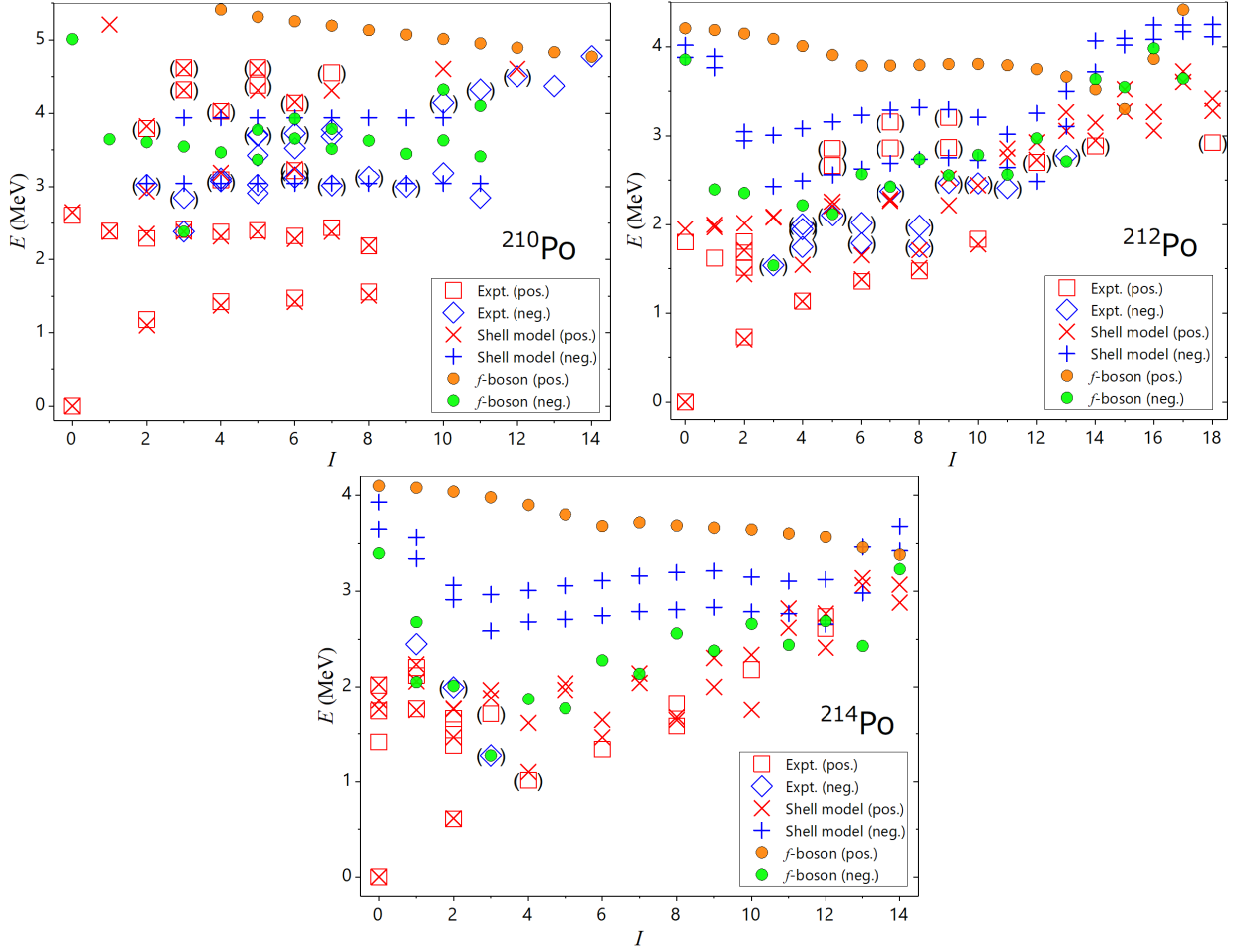


Figure 2.3: The same as Fig. 2.2, but for Po isotopes. The experimental data are taken from Refs. [16, 17, 19, 23–26].

and  $(9_1^-)$  states, but also the  $(11_1^-)$  and  $(13_1^-)$  states are well reproduced.

In contrast it is impossible in the present study to reproduce the low-lying  $(4^-)$ ,  $(6^-)$ , and  $(8^-)$  states just below the excitation of 2 MeV. Based on enhanced  $E1$  transition probabilities, the EUROBALL group pointed out that these states may have  $\alpha + ^{208}\text{Pb}$  cluster structure, which are out of the present framework. A further study is necessary to draw a definite conclusion.

Concerning the  $^{214}\text{Po}$  nucleus in Fig. 2.3, the experimental  $1_1^-$ ,  $(2_1^-)$ , and  $(3_1^-)$  states were out of the shell-model framework [1]. In the present calculation with the  $f$ -boson they are reproduced with the single  $f$ -boson energy as  $\varepsilon_f = 1.275$  MeV, where the excitation energy of the experimental  $3_1^-$  state is adopted. The first  $f$ -boson  $2^-$  and  $1^-$  states, and the second  $1^-$  state are coupled with the shell-model  $2_1^+$ ,  $2_1^+$ , and  $4_1^+$  states, respectively.

Figure 2.4 shows the energy spectra of  $_{86}\text{Rn}$  isotopes ( $^{214}, ^{216}\text{Rn}$ ). In  $^{214}\text{Rn}$  and  $^{216}\text{Rn}$ ,  $3^-$  states have not been observed to date. In  $^{214}\text{Rn}$  a low-lying state with unassigned spin and parity is observed at 1.331 MeV (not shown in the figure), which is rather high in energy for the positive-

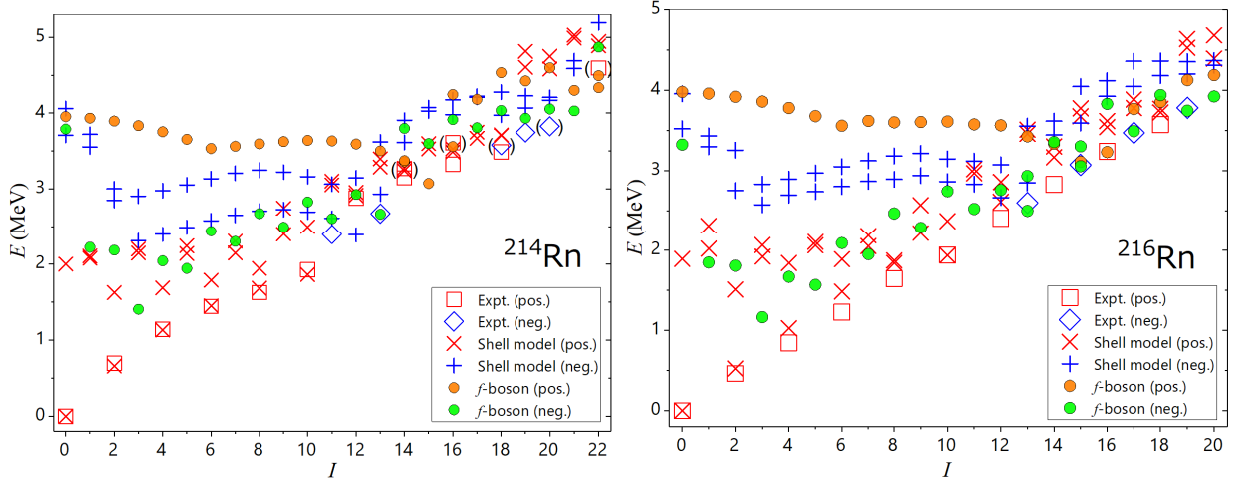


Figure 2.4: The same as Fig. 2.2, but for Rn isotopes. The experimental data are taken from Refs. [16, 26, 34].

parity states predicted in the previous shell-model framework. Thus this state is presumed as the collective octupole-phonon excited state. As for the single  $f$ -boson energies, linearly optimized values of  $\varepsilon_f = 1.406$  MeV and 1.164 MeV in Eq. (2.9) are adopted for  $^{214}\text{Rn}$  and  $^{216}\text{Rn}$ , respectively. The shell-model  $11_1^-$ ,  $13_1^-$ ,  $19_1^-$ ,  $20_1^-$ , and  $22_1^+$  states of  $^{214}\text{Rn}$  were calculated [1] slightly high in energy in comparison with experiment. In the present framework with  $f$ -boson, the experimental  $13_1^-$ ,  $19_1^-$ , ( $20_1^-$ ), and  $22_1^+$  states are preferably reproduced. The experimental  $B(E3; 13_1^- \rightarrow 10_1^+)$  value of 44(8) W.u. shown in Table 2.1 is considerably larger than the single-particle estimate. Therefore it is inferred that the experimental  $13_1^-$  state mainly consists of the  $f$ -boson state,  $[|f\rangle \otimes |10_1^+\rangle]^{(13)}$ .

The experimental  $(18)^-$  state at 3.579 MeV with ambiguity in spin cannot be well reproduced both in the previous shell-model calculation and the present framework with  $f$ -boson. A two-octupole-phonon state on top of the shell-model  $12_1^-$  state at 2.389 MeV may correspond to the  $(18)^-$  state.

In  $^{216}\text{Rn}$ , the  $13_1^-$ ,  $15_1^-$ ,  $17_1^-$ , and  $19_1^-$  states were observed through the  $^{208}\text{Pb}$  ( $^{18}\text{O}$ ,  $2\alpha 2n$ ) reaction [48]. These negative-parity states and the  $16_1^+$  state at 3.238 MeV are well reproduced in the present framework. The first  $f$ -boson  $13^-$ ,  $15^-$ ,  $17^-$ ,  $19^-$ , and  $16^+$  states are so constructed by the octupole-phonon excitation on top of the shell-model  $10_1^+$ ,  $12_1^+$ ,  $14_1^+$ ,  $16_1^+$ , and  $13_1^-$  states, respectively.

Figure 2.5 shows the energy spectrum of  $^{212}_{85}\text{At}$ . One of the almost degenerate ( $12_1^+$ ) and ( $12_2^+$ ) states (at 1.262 MeV and 1.283 MeV), and the ( $13_1^+$ ) state are well reproduced in the present framework. As shown in Table 2.1,  $B(E3)$  values larger than 20 W.u. are measured for the ( $18_1^+$ ), ( $22_1^-$ ), and ( $25_1^-$ ) states, which demonstrates that these states are mainly constructed by the collective octupole-phonon excitations. In the present framework with  $\varepsilon_f = 1.648$  MeV, some  $f$ -boson  $18^+$  and  $22^-$  states appear close to the experimental ( $18_1^+$ ) and ( $22_1^-$ ) states in energy. In contrast, the ( $25_1^-$ ) state cannot be reproduced in the present framework. The ( $25_1^-$ ) state with ambiguity of

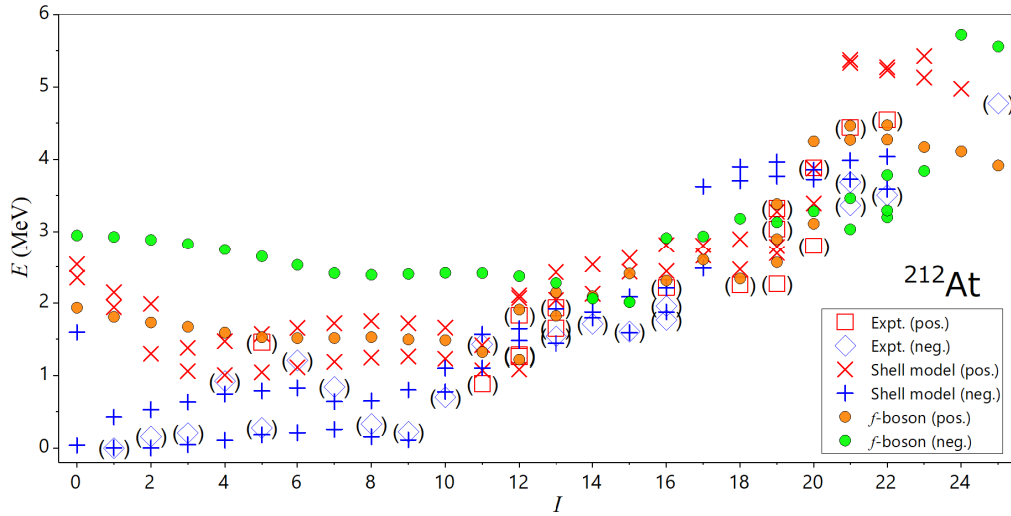


Figure 2.5: The same as Fig. 2.2, but for  $^{212}\text{At}$ . The experimental data are taken from Refs. [16, 19].

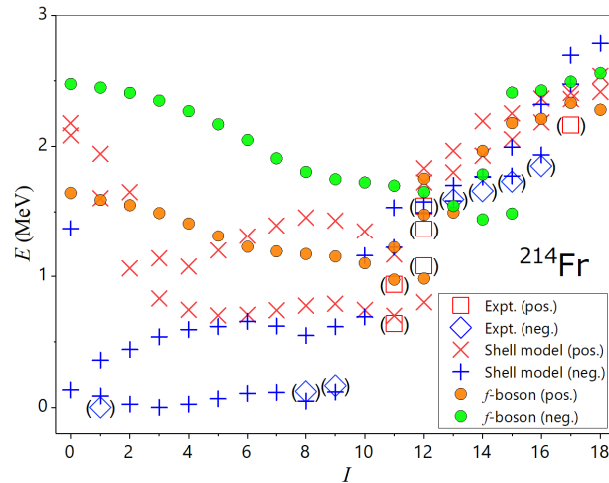


Figure 2.6: The same as Fig. 2.2, but for  $^{214}\text{Fr}$ . The experimental data are taken from Refs. [16, 26].

spin-parity can be thought to be a two-octupole-phonon state on top of the one-octupole-phonon  $22_1^+$  state predicted above 4.273 MeV. Spin and parity of the  $(25_1^-)$  state should be confirmed in experiment.

Figure 2.6 shows the energy spectrum of  $^{214}_{87}\text{Fr}$ . Low-lying  $(11^+)$  and  $(12^+)$  states are well reproduced. In the present framework, the  $(11_1^+)$  state, where  $B(E3; 11^+ \rightarrow 8^-) = 10(4)$  W.u. is observed, preferably corresponds to the shell-model  $11_1^+$  state. The neutron configuration of the shell-model  $11_1^+$  state consists of the  $(\nu j_{15/2})$  orbital while that of  $8_1^-$  state consists of the  $(\nu g_{9/2})$  orbital. The experimental  $B(E3)$  value is not so different from the single-particle estimate of  $B(E3; 0j_{15/2} \rightarrow 1g_{9/2}) = 4.84$  W.u., assuming the neutron effective charge of  $e_\nu = e$ . Another possibility is to assume that the experimental  $11_1^+$  and  $11_2^+$  states are mixtures of the shell-model

$11_1^+$  state and the first  $f$ -boson  $11^+$  state as

$$\left| \widetilde{11_1^+} \right\rangle = \alpha |f \otimes 8_1^- \rangle + \beta |11_1^+ \rangle_{\text{SM}} \quad (3.4)$$

$$\left| \widetilde{11_2^+} \right\rangle = \beta |f \otimes 8_1^- \rangle - \alpha |11_1^+ \rangle_{\text{SM}} \quad (3.5)$$

where  $\alpha^2 + \beta^2 = 1$ .

As shown in Table 2.1, the value of  $B(E3; 14^- \rightarrow 11^+) = 25(5)$  W.u. is reasonably large so that the  $(14_1^-)$  mainly consists of  $f$ -boson states. In the present framework, the lowest two  $f$ -boson  $14^-$  states and the shell-model  $14_1^-$  state are calculated approximately at the same energy of the experimental  $(14_1^-)$  state. However, the higher  $f$ -boson  $14^-$  state is excluded since this state is constructed by an octupole-phonon excitation on top of the shell-model  $12_1^+$  state and then it cannot contribute to the  $E3$  transition (see the discussion on the  $3_2^-$  state of  $^{210}\text{Pb}$ ). In contrast, the lower  $f$ -boson  $14^-$  state is constructed on the shell-model  $11_1^+$  state, and then cause a large  $E3$  transition to the shell-model  $11_1^+$  state. In conclusion, it is inferred that the  $(14_1^-)$  state is a mixture of the  $f$ -boson  $14^-$  state coupled with the shell-model  $11_1^+$ , and the shell-model  $14_1^-$  state.

Through the present study, it is found that, among the experimental states whose  $B(E3)$  values were measured, the  $3_1^-$  state of  $^{206}\text{Pb}$ , the  $3_1^-$  state of  $^{208}\text{Pb}$ , the  $3_1^-$  state of  $^{210}\text{Pb}$ , the  $13_1^-$  state of  $^{214}\text{Rn}$ , the  $18_1^+$ ,  $22_1^-$ , and  $25_1^-$  states of  $^{212}\text{At}$ , and the  $14_1^-$  state of  $^{214}\text{Fr}$  are mainly constructed by the collective octupole-phonon excitations. Using these experimental  $B(E3)$  values, the effective charge of the collective  $f$ -bosons is evaluated as

$$e_f^2 = (8.1 \pm 0.7) \times 10^4 e^2 \text{fm}^6, \quad (3.6)$$

which corresponds to  $31 \pm 2.7$  W.u. for the  $B(E3; 3^- \rightarrow 0^+)$  transition with  $A = 208$ .

## 2.4 Summary

A model is proposed for the octupole vibrational states based on the nuclear shell model. In this model, one-octupole-phonon representing the collective octupole vibration across the magic core is introduced onto the microscopically calculated shell-model states. The model is applied to various nuclei around  $^{208}\text{Pb}$  nucleus. Both pure shell-model states and octupole vibrational states are well reproduced. The type of each electric octupole transition is classified by either collective or non-collective nature. The electric octupole transition probabilities between the octupole vibrational states and the pure shell-model states are consistent with the simple estimate in Eq. (2.11). The effective charge for the  $f$ -boson is obtained in comparison with the experimental data.

In this work we have introduced only one-octupole-phonons. There is some indication of two-octupole-phonon states. For instance in  $^{214}\text{Rn}$ , a two-octupole-phonon state coupled with the shell-model  $12_1^-$  state may correspond to the  $(18)_1^-$  state. Two-phonon states should be included in the future. Also we need to introduce other high angular momentum excitations such as  $5^-$  and  $4^-$ , which have energies of 3.197 and 3.475 MeV in  $^{208}\text{Pb}$ . In this work we have only considered the

Coriolis coupling between the shell-model states and the octupole phonon states. The model needs to be expanded by introducing other effective interactions that couple both the pure shell-model states and the  $f$ -boson states coupled with the shell-model states.

## Chapter 3

# Shell-model study in the southwest region of $^{208}\text{Pb}$

### 3.1 Introduction

Nuclear shell model is one of the most successful models to study the nuclear structure. All the energy levels can be described with reliable effective interactions and enough large model spaces. A nuclear effective interaction for the southwest region of  $^{208}\text{Pb}$  ( $Z < 82$ ,  $N < 126$ ) was developed by Kuo and Herling in the  $G$ -matrix prescription of realistic  $NN$ -interactions (Ref. [8] and references therein). The realistic effective interaction has been modified thanks to the revision of single-particle energies and newly observed levels since the original work in 1971 [79–81].

Experimental energy levels are successfully reproduced in shell-model calculations with the use of revised two-body matrix elements for  $^{202,204,206}\text{Tl}$  [82–84],  $^{202-204,206}\text{Hg}$  [81,82,85,86], and  $^{204}\text{Pt}$  [86]. On the other hand, recent experiment gives new levels and electromagnetic transition strengths also in  $^{201}\text{Hg}$  [87],  $^{201,202}\text{Pt}$  [88], which have not been studied in the nuclear shell model due to a large number of configurations.

The electric dipole moment (EDM) of  $^{199}\text{Hg}$  atom has been explored in the last 30 years [89–94]. The present upper limit updated in 2016 [94] is the most precise experiment among all the atoms. The EDMs of diamagnetic atoms such as  $^{199}\text{Hg}$  are contributed from the nuclear Schiff moment and  $CP$ -odd nucleon-electron interactions through the nucleon spin. The nuclear Schiff moment of the  $^{199}\text{Hg}$  nucleus has been calculated using the simple shell model [95] the random phase approximation (RPA) [96–98] and the quasi-particle RPA (QRPA) [99, 100]. The numerical results of the nuclear Schiff moment of  $^{199}\text{Hg}$  are largely model-dependent. The nucleon spin of the  $^{199}\text{Hg}$  nucleus has been predicted from the experimental value of the magnetic moment [101] and calculated in a pair-truncated shell model (PTSM) [70].

In previous papers [1, 15], we performed large-scale shell-model calculations for even-even, odd-mass, and doubly-odd nuclei in the neutron deficient region of  $^{208}\text{Pb}$  ( $Z \geq 82$ ). In those works, low-lying energy spectra,  $B(E2)$  values, and electromagnetic moments of 56 nuclei were systematically

reproduced.

In this paper, we study the southwest region of  $^{208}\text{Pb}$  ( $Z \leq 82, N \leq 126$ ) with a multipole-pairing plus quadrupole-quadrupole interaction. First we develop a nuclear effective interaction to reproduce the low-lying energy levels of nuclei near the doubly closed shell of  $^{208}\text{Pb}$ . Structure of nuclei in the southwest region are revealed by comparing theoretical energy spectra,  $B(E2)$  values, and electromagnetic moments with the experimental data.

This paper is organized as follows. The general framework of the present shell-model study is given in Sec. 3.2. Energy spectra and electromagnetic properties are presented and compared with the experimental data for each nucleus in Sec. 3.3. Finally this work is summarized in Sec. 3.4.

## 3.2 Theoretical framework

In the present paper large-scale shell-model calculations are performed for even-even, odd-mass, and doubly-odd nuclei in the southwest ( $N < 128$  and  $Z < 82$ ) region of  $^{208}\text{Pb}$ . All the single-particle levels in the one-major shells, neutron  $2p_{1/2}$ ,  $2p_{3/2}$ ,  $1f_{5/2}$ ,  $1f_{7/2}$ ,  $0h_{9/2}$ , and  $0i_{13/2}$  orbitals and proton  $2s_{1/2}$ ,  $1d_{3/2}$ ,  $1d_{5/2}$ ,  $0g_{7/2}$ , and  $0h_{11/2}$  orbitals are taken into account. The single-particle energies  $\epsilon_\tau$  ( $\tau = \nu$  or  $\pi$ ) employed in the present calculations are listed in Table 3.1. These values are extracted from the excitation energies of low-lying states in  $^{207}_{81}\text{Tl}_{126}$  and  $^{207}_{82}\text{Pb}_{125}$ . It is assumed for a better reproduction of the low-lying states in odd-mass nuclei that the single-particle energies of the intruder orbitals,  $\nu i_{13/2}$  and  $\pi h_{11/2}$ , depend on the numbers of valence nucleons. The values are explicitly given in units of MeV as

$$\epsilon_\nu(i_{13/2}) = -0.07\bar{N}_\nu - 0.05\bar{N}_\pi + 1.703, \quad (2.1)$$

$$\epsilon_\pi(h_{11/2}) = 0.03\bar{N}_\pi + 1.318, \quad (2.2)$$

where  $\bar{N}_\nu$  and  $\bar{N}_\pi$  are the numbers of neutron and proton holes, respectively

A multipole-pairing plus quadrupole-quadrupole interaction is employed as an effective interaction. The effective shell-model Hamiltonian is classified as

$$\hat{H} = \hat{H}_\nu + \hat{H}_\pi + \hat{H}_{\nu\pi}, \quad (2.3)$$

where  $\hat{H}_\nu$ ,  $\hat{H}_\pi$ , and  $\hat{H}_{\nu\pi}$  represent neutron, proton, and neutron-proton interactions, respectively. The interactions among like nucleons are expressed as

$$\hat{H}_\tau = \sum_{jm} \epsilon_{j\tau} c_{jm\tau}^\dagger c_{jm\tau} - \sum_{L=0,2,4,6,8,10} G_{L\tau} \hat{P}_\tau^\dagger(L) \cdot \hat{P}_\tau(L) - \kappa_\tau : Q_\tau \cdot Q_\tau : \dots \quad (2.4)$$

Detailed definitions of the interactions are given in Ref. [14].

The interaction between neutrons and protons  $\hat{H}_{\nu\pi}$  consists only of the quadrupole-quadrupole ( $QQ$ ) interaction, which is given as

$$\hat{H}_{\nu\pi} = -\kappa_{\nu\pi} \hat{Q}_\nu \cdot \hat{Q}_\pi, \quad (2.5)$$

Table 3.1: Adopted single-hole energies  $\varepsilon_\tau$  for neutrons ( $\tau = \nu$ ) and protons ( $\tau = \pi$ ) in units of MeV. The single-particle energies for the neutron  $0i_{13/2}$  and the proton  $0h_{11/2}$  orbitals are changed linearly with the numbers of valence neutrons ( $\overline{N}_\nu$ ) and valence protons ( $\overline{N}_\pi$ ). The nucleon number dependence of  $\varepsilon_\nu(i_{13/2})$  and  $\varepsilon_\pi(h_{11/2})$  are given in the text.

$j$	$2p_{1/2}$	$1f_{5/2}$	$2p_{3/2}$	$0i_{13/2}$	$1f_{7/2}$	$0h_{9/2}$
$\varepsilon_\nu$	0.000	0.570	0.898	$\varepsilon_\nu(i_{13/2})$	2.340	3.415
$j$	$2s_{1/2}$	$1d_{3/2}$	$0h_{11/2}$	$1d_{5/2}$	$0g_{7/2}$	
$\varepsilon_\pi$	0.000	0.351	$\varepsilon_\pi(h_{11/2})$	1.683	3.474	

Table 3.2: Strengths of adopted two-body interactions between neutrons ( $\nu$ - $\nu$ ) and those between protons ( $\pi$ - $\pi$ ).  $G_0$  and  $G_2$  indicate the strengths of the monopole ( $MP$ ) and quadrupole-pairing ( $QP$ ) interactions, respectively.  $G_L$  ( $L = 4, 6, 8, 10$ ) denote the strengths for higher multipole-pairing ( $HMP$ ) interactions. The strengths of the  $MP$  and  $HMP$  interactions are given in units of MeV. The strengths of the  $QP$  interactions are given in units of  $\text{MeV}/b^4$ , where  $b$  is the oscillator parameter.

	$G_0$	$G_2$	$G_4$	$G_6$	$G_8$	$G_{10}$	$\kappa$
$\nu$ - $\nu$	0.145	0.013	0.70	0.50	1.10	2.00	
$\pi$ - $\pi$	0.145	0.013	2.00	2.20	4.00	1.00	0.05

where the strength is taken as  $\kappa_{\nu\pi} = 0.07 \text{ MeV}/b^4$ . Here harmonic-oscillator states are used as the single-particle basis states with the oscillator parameter  $b = \sqrt{\hbar/M\omega}$ .

In this mass region, shell-model dimensions for diagonalization are too large to perform full calculations without truncations. Thus it is necessary to truncate the shell-model dimensions. In this study, the same truncation scheme adopted in Sec. IIB of Ref. [14] is taken for all the nuclei. All calculations are performed with the truncation of  $L_c = 500$ . Here the definition of  $L_c$  is the same as given in Sec. IIB in Ref. [14]. This truncation scheme is found to be sufficient for reproducing low-lying energy levels and electromagnetic transitions among low-lying states after checking the effect of truncation by increasing  $L_c = 500$  to  $L_c = 1000$ .

In this paper,  $E2$  transition rates, magnetic moments, and quadrupole moments are also calculated. For  $E2$  transition rates and quadrupole moments, the effective charges are taken as  $e_\nu = -0.85e$  for neutrons and  $e_\pi = -1.50e$  for protons. For magnetic moments, the gyromagnetic ratios of orbital angular momentum are taken as  $g_{\ell\nu} = 0.00$  and  $g_{\ell\pi} = 1.00$ , and the gyromagnetic ratios of spin are taken as  $g_{s\nu} = -1.91$  and  $g_{s\pi} = 2.79$ . These effective charges and gyromagnetic ratios are adjusted to reproduce the experimental data for single-closed nuclei on the whole. Further details of the electromagnetic transition operators are presented in Ref. [14].

Table 3.3: The calculated  $B(E2)$  values in units of W.u. for Tl isotopes (Calc.) in comparison with the experimental data (Expt.) [16, 71, 102–105].

$^{206}\text{Tl}$	$B(E2)$	
	Expt.	Calc.
$2_1^- \rightarrow 0_1^-$	2.22(14)	1.749
$2_2^- \rightarrow 0_1^-$	0.13(4)	0.213
$4_1^- \rightarrow 2_1^-$	1.2(3)	3.586
$(7)_1^+ \rightarrow (5)_1^+$	1.25(8)	0
$^{205}\text{Tl}$	Expt.	Calc.
$3/2_1^+ \rightarrow 1/2_1^+$	6.1(10)	7.187
$5/2_1^+ \rightarrow 1/2_1^+$	2.7(10)	1.805
$5/2_1^+ \rightarrow 3/2_1^+$	5.9(12)	6.545
$^{204}\text{Tl}$	Expt.	Calc.
$(0^-)_1 \rightarrow 2_1^-$	$\sim 0.1$	0.954
$(4^-)_1 \rightarrow 2_1^-$	$> 0.10$	3.290
$^{203}\text{Tl}$	Expt.	Calc.
$3/2_1^+ \rightarrow 1/2_1^+$	7.9(3)	7.927
$5/2_1^+ \rightarrow 3/2_1^+$	0.55(13)	0.691
$5/2_1^+ \rightarrow 1/2_1^+$	9.9(10)	8.060

### 3.3 Numerical results

In this section, energy spectra,  $E2$  transition rates, magnetic moments, and quadrupole moments are given for each nucleus. For energy spectra, up to four observed energy levels from the yrast state are shown in figures for each spin-parity. As for the theoretical states, the two lowest energy levels are shown for each spin-parity in general.

#### 3.3.1 Tl isotopes

Figure 3.1 shows the energy spectra of  $_{81}\text{Tl}$  isotopes with one to five valence neutron holes. The  $^{206}\text{Tl}$  nucleus is a system with one neutron hole and one proton hole outside the doubly closed core of  $^{208}\text{Pb}$ . The strength of the quadrupole-quadrupole interaction  $\kappa_{\nu\pi} = 0.07 \text{ MeV}/b^4$  between neutron and proton is phenomenologically determined to reproduce the energy spectrum of  $^{206}\text{Tl}$ . In the present calculations the  $0_1^-$  state is located slightly higher than the  $1_1^-$  state comprise a degenerate doublet with the  $(\nu p_{1/2} \otimes \pi s_{1/2})$  configuration. In contrast the  $1_1^-$  state is experimentally measured

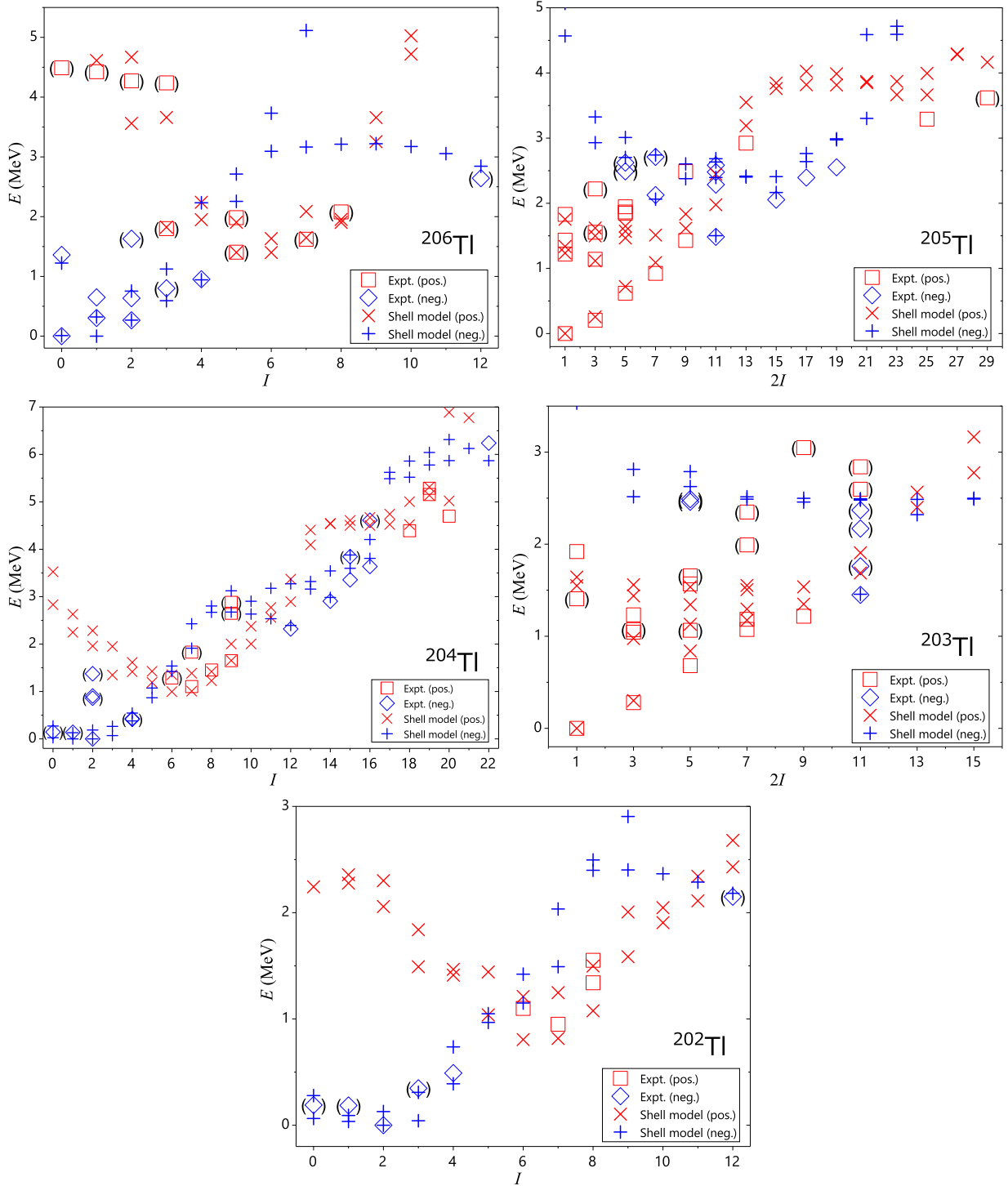


Figure 3.1: The energy spectra of  $_{81}\text{Tl}$  isotopes compared with the experimental data [16, 71, 102–105]. The  $0_2^-$  state in  $^{206}\text{Tl}$ , high-spin states in  $^{204}\text{Tl}$ , and the  $(0_1^-)$ ,  $(1_1^-)$ , and  $(3_1^-)$  states in  $^{202}\text{Tl}$ , were recently reported [83, 84, 106].

Table 3.4: The results of magnetic dipole moments  $\mu$  in units of  $\mu_N$  and electric quadrupole moments  $Q$  in units of  $eb$  for Tl isotopes (Calc.) in comparison with the experimental data (Expt.) [16, 71, 102–105].

$^{206}\text{Tl}$	$\mu$		$Q$	
	Expt.	Calc.	Expt.	Calc.
$(5)_1^+$	4.27(6)	+5.745		+0.519
$(7)_1^+$	<2.45	+0.423		+0.453
$^{205}\text{Tl}$	Expt.	Calc.	Expt.	Calc.
$1/2_1^+$	+1.638	+1.247		
$3/2_1^+$	−0.080(45) +0.02(12) * <sup>1</sup>	+0.387	0.74(15)	+0.326
$5/2_1^+$	+2.2(7)	+1.552		+0.443
$(5/2)_2^-$	0.71(15)	+4.304	−0.54(20)	+0.021
$5/2_{17}^+$		+0.217		−0.072
$25/2_1^+$	+6.80(10)	+5.908		+0.848
$^{204}\text{Tl}$	Expt.	Calc.	Expt.	Calc.
$2_1^-$	0.09(1)	−0.086		+0.173
$7_1^+$	+1.187(6)	+0.239		+0.509
$^{203}\text{Tl}$	Expt.	Calc.	Expt.	Calc.
$1/2_1^+$	+1.622	+1.296		
$3/2_1^+$	+0.16(5)	+0.557		+0.320
$5/2_1^+$	2.6(11)	+1.482		+0.072
$^{202}\text{Tl}$	Expt.	Calc.	Expt.	Calc.
$2_1^-$	0.06(1)	−0.185		+0.032
$7_1^+$	+0.90(4)	+0.297		+0.417

with an excitation energy of 305 keV from the ground  $0_1^-$  state.

Both the  $1_1^-$  and the  $0_1^-$  states mainly consist of the  $(\nu p_{1/2} \otimes \pi s_{1/2})$  configuration with probabilities more than 90%. The structure of other low-lying negative-parity states are classified as follows. The  $1_2^-$  and  $2_1^-$  states, the  $2_2^-$  and  $3_1^-$  states, and the  $3_2^-$  and  $4_1^-$  states mainly consist of the  $(\nu p_{1/2} \otimes \pi d_{3/2})$ ,  $(\nu f_{5/2} \otimes \pi s_{1/2})$ , and  $(\nu f_{5/2} \otimes \pi d_{3/2})$  configurations, respectively.

Theoretical  $B(E2)$  values and electromagnetic moments are compared with the experimental data in Tables 3.3 and 3.4, respectively. The magnetic moments in the  $5_1^+$  and the  $7_1^+$  states are consistent with the experimental data, whereas the  $B(E2; (7)_1^+ \rightarrow (5)_1^+)$  value is not. The  $7_1^+$  and  $5_1^+$  states mainly consist of the  $(\nu i_{13/2} \otimes \pi s_{1/2})$  and  $(\nu p_{1/2} \otimes \pi h_{11/2})$  configurations, respectively. The

configurations,  $(\nu^+ \otimes \pi^+)$  and  $(\nu^- \otimes \pi^-)$ , are never admixed with the effective interactions that are employed in the present study. Thus, the  $7_1^+$  and  $5_1^+$  states are not connected in the  $E2$  channel. Although the present framework has its drawbacks, the dominant configurations are consistent with another shell-model study that successfully represents the  $B(E2; (7)_1^+ \rightarrow (5)_1^+)$  value [?]. It is then concluded that the quadrupole-quadrupole interactions play a major role to determine the structure of odd-odd nuclei.

In  $^{205}\text{Tl}$ , the experimental energy spectrum,  $B(E2)$  values, and electromagnetic moments are reproduced well except for the electromagnetic moments of the  $(5/2)_2^-$  state, which were experimentally measured once [108]. The authors assigned a spin-parity of  $5/2^+$  on the measured level at 2.63 MeV. In the present calculations several  $5/2^+$  states are predicted around 2.6 MeV. The electromagnetic moments of a calculated state at 2.823 MeV are  $\mu = 0.217 \mu_N$  and  $Q = -0.072 eb$ . We then conclude that  $5/2^+$  is preferable to the spin-parity assignment of the state where the electromagnetic moments were measured.

In  $^{204}\text{Tl}$ , a lot of states have been discovered in experiment. As shown in Fig. 3.1, the energy spectrum is systematically reproduced in this study. On the other hand, the magnetic moment of the theoretical  $7_1^+$  state is more than 4 times smaller than the experimentally measured value. The  $7_3^+$  state predicted at 1.541 MeV has a large magnetic moment of  $5.871 \mu_N$  in theory. The theoretical  $7_3^+$  state is never mixed with the  $7_1^+$  for the same argument on the  $7_1^+$  state in  $^{206}\text{Tl}$  does not decay to the  $5_1^+$  state in the  $E2$  channel. These inconsistencies may indicate that the mixing of the  $(\nu^+ \otimes \pi^+)$  and  $(\nu^- \otimes \pi^-)$  type configurations is crucial.

In  $^{203}\text{Tl}$ , the experimental energy spectrum,  $B(E2)$  values, and electromagnetic moments are well reproduced. Comparing the energy spectrum with experiment, some low-lying  $11/2^-$  states which are uncertain in spin-parity should be positive parity states.

In  $^{202}\text{Tl}$ , it has been repeatedly confirmed that the  $7_1^+$  state is an isomeric state and the weighted average of the half-life is  $591 \mu s$  [16, 105]. The long half-life can be theoretically understood in the situation that the  $6_1^+$  state is the lowest positive-parity state followed by the  $7_1^+$  state with a little energy difference of 11 keV.

### 3.3.2 Hg isotopes

Figure 3.2 shows the energy spectra of  $_{80}\text{Hg}$  isotopes. The experimental data of  $^{206}\text{Hg}$  nucleus, which has two neutrons outside the doubly closed core of  $^{208}\text{Pb}$ , is helpful to determine the two-body interactions between neutrons. All the experimentally observed states are identified as theoretical states in one-to-one correspondence if the spins and parities are uniquely assigned. The  $(10_1^+)$  state observed at 3.723 MeV is an isomeric state with a half-life of 92 ns. This isomer is caused by the small energy gap between the  $(10_1^+)$  and the  $(8_1^+)$  states and the small  $B(E2; 10_1^+ \rightarrow 8_1^+)$  value, which are reproduced well as shown in Fig. 3.2 and Table 3.5, respectively. Table 4.2 shows the electromagnetic moments of the  $_{80}\text{Hg}$  isotopes. The magnetic moment and the electric quadrupole

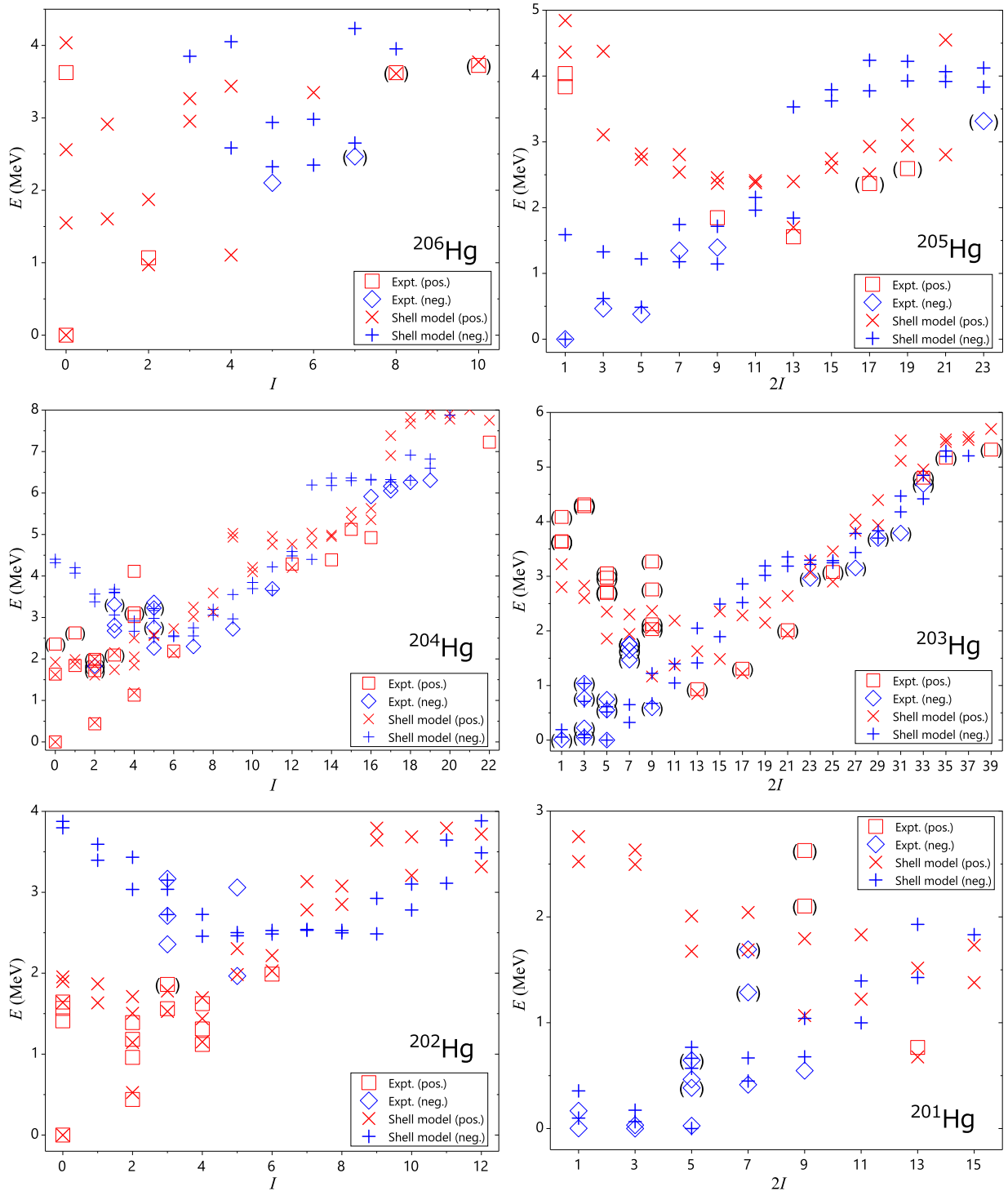


Figure 3.2: Same as Fig. 3.1, but for Hg isotopes. The experimental data are taken from ENSDF [16] and Nuclear Data Sheets [71, 102–105, 109]. High-spin states in  $^{205,204,203}\text{Hg}$  are reported in Ref. [81, 85, 110].

Table 3.5: The calculated  $B(E2)$  values in units of W.u. for Hg isotopes (Calc.) in comparison with the experimental data (Expt.) [16, 71, 86, 102–105, 109].

$^{206}\text{Hg}$	$B(E2)$	
	Expt.	Calc.
$2_1^+ \rightarrow 0_1^+$	$> 2.7 \times 10^{-4}$	5.732
$4_1^+ \rightarrow 2_1^+$		4.457
$6_1^+ \rightarrow 4_1^+$		0.088
$8_1^+ \rightarrow 6_1^+$		2.027
$10_1^+ \rightarrow 8_1^+$	0.99(18)	0.853
$^{204}\text{Hg}$	Expt.	Calc.
$2_1^+ \rightarrow 0_1^+$	11.96(9)	13.836
$4_1^+ \rightarrow 2_1^+$	17.0(13)	17.375
$6_1^+ \rightarrow 4_1^+$	20(3)	14.910
$8_1^+ \rightarrow 6_1^+$		3.425
$10_1^+ \rightarrow 8_1^+$		0.002
$^{202}\text{Hg}$	Expt.	Calc.
$2_1^+ \rightarrow 0_1^+$	17.34(14)	17.378
$2_2^+ \rightarrow 2_1^+$	5.6(15)	5.887
$2_2^+ \rightarrow 0_1^+$	0.087(21)	0.061
$4_1^+ \rightarrow 2_1^+$	26.5(8)	20.815
$6_1^+ \rightarrow 4_1^+$	$\sim 25$	17.302
$8_1^+ \rightarrow 6_1^+$		12.876
$10_1^+ \rightarrow 8_1^+$		0.025
$^{201}\text{Hg}$	Expt.	Calc.
$1/2_1^- \rightarrow 3/2_1^-$	25(9)	0.000
$1/2_2^- \rightarrow 3/2_1^-$	4(4)	23.454
$1/2_2^- \rightarrow 3/2_2^-$	3(+4 -3)	0.030
$1/2_2^- \rightarrow 5/2_1^-$	46(22)	5.674
$3/2_2^- \rightarrow 1/2_1^-$	10(6)	0.359
$3/2_2^- \rightarrow 3/2_1^-$	20(9)	0.253
$5/2_1^- \rightarrow 3/2_1^-$	2.4(8)	0.414
$7/2_2^- \rightarrow 3/2_1^-$	10.9(5)	5.471
$7/2_2^- \rightarrow 3/2_2^-$	13.5(6)	3.502
$7/2_2^- \rightarrow 5/2_2^-$	9.4(21)	13.265
$9/2_2^- \rightarrow 5/2_2^-$	$> 0.010$	15.511

Table 3.6: The results of magnetic dipole moments  $\mu$  in units of  $\mu_N$  and electric quadrupole moments  $Q$  in units of eb for Hg isotopes (Calc.) in comparison with the experimental data (Expt.) [16, 71, 102–105, 109].

$^{206}\text{Hg}$	$\mu$		$Q$	
	Expt.	Calc.	Expt.	Calc.
$2_1^+$		+2.098		+0.419
$4_1^+$		+4.165		+0.224
$6_1^+$		+6.884		+0.003
$8_1^+$		+9.302		+0.240
$10_1^+$		+11.627		+0.650
$5_1^-$	5.45(5)	+5.186	0.74(15)	+0.557
$^{205}\text{Hg}$	Expt.	Calc.	Expt.	Calc.
$1/2_1^-$	+0.601	+0.306		0
$^{204}\text{Hg}$	Expt.	Calc.	Expt.	Calc.
$2_1^+$	0.67(9)	+0.984	0.40(20)	+0.636
$4_1^+$		+2.731		+0.723
$6_1^+$		+3.635		+0.716
$8_1^+$		+4.082		+0.440
$10_1^+$		-1.359		+0.512
$^{203}\text{Hg}$	Expt.	Calc.	Expt.	Calc.
$5/2_1^-$	+0.849	+0.818	+0.343(36)	+0.356
$^{202}\text{Hg}$	Expt.	Calc.	Expt.	Calc.
$2_1^+$	+0.82(6)	+0.997	1.01(13)	+0.624
$4_1^+$	1.36(27)	+1.809		+0.841
$6_1^+$		+2.268		+0.992
$8_1^+$		+3.802		+0.845
$10_1^+$		-1.335		+0.756
$^{201}\text{Hg}$	Expt.	Calc.	Expt.	Calc.
$3/2_1^-$	-0.560	-0.396	+0.387(6)	+0.366

moment of the  $5_1^-$  state in  $^{206}\text{Hg}$  are reproduced well in theory.

In  $^{205}\text{Hg}$ , the  $13/2_1^+$  state is an isomeric state with a very long half-life of 1.09 ms. The  $13/2_1^+$  state is described in this study as

$$\begin{aligned} & |^{205}\text{Hg}; 13/2_1^+\rangle \\ &= \sqrt{0.43}|\nu i_{13/2} \otimes \pi s_{1/2}^2\rangle + \sqrt{0.33}|\nu i_{13/2} \otimes \pi d_{3/2}^2\rangle + \sqrt{0.09}|\nu i_{13/2} \otimes \pi h_{11/2}^2\rangle + \text{others}. \end{aligned} \quad (3.1)$$

Comparing this state with the configuration of the  $0_1^+$  state in  $^{206}\text{Hg}$ ,

$$\begin{aligned} & |^{206}\text{Hg}; 0_1^+\rangle \\ &= \sqrt{0.47}|\pi s_{1/2}^2\rangle + \sqrt{0.35}|\pi d_{3/2}^2\rangle + \sqrt{0.10}|\pi h_{11/2}^2\rangle + \sqrt{0.07}|\pi d_{5/2}^2\rangle + \sqrt{0.02}|\pi g_{7/2}^2\rangle, \end{aligned} \quad (3.2)$$

it is found that the  $13/2_1^+$  state can be simply depicted as  $|\nu i_{13/2}\rangle \otimes |^{206}\text{Hg}; 0_1^+\rangle$ . The  $13/2_1^+$  state is located at the significantly low energy since the  $0i_{13/2}$  is the only positive-parity orbital for neutron.

The  $13/2_1^+$  state can decay to the  $7/2_1^-$  and  $9/2_1^-$  states with  $B(E3; 13/2_1^+ \rightarrow 7/2_1^-) = 1.14(7)$  W.u. and  $B(M2; 13/2_1^+ \rightarrow 9/2_1^-) = 0.00047(3)$  W.u, respectively. In theory, the  $7/2_1^-$  and  $9/2_1^-$  states mainly consist of the  $|\nu p_{1/2} \otimes \pi(d_{3/2}d_{5/2})_{4+}\rangle$  and  $|\nu p_{1/2} \otimes \pi(d_{3/2}d_{5/2})_{4+}\rangle$  configurations with probabilities of 40.9% and 36.5%, respectively. The neutron  $2p_{1/2}$  orbital is not connected to the  $0i_{13/2}$  orbital in the  $E3$  and  $M2$  operators, so that the transitions are very rare.

The dominant configuration in the  $13/2_1^+$  state,  $|\nu i_{13/2} \otimes \pi s_{1/2}^2\rangle$ , with a probability of 43.2% can be connected with a configuration of  $|\nu f_{7/2} \otimes \pi s_{1/2}^2\rangle$  in the  $E3$  channel, and with a configuration of  $|\nu h_{9/2} \otimes \pi s_{1/2}^2\rangle$  in the  $M2$  channel. However, those probabilities are 0.7% in the  $7/2_1^-$  state and 0.2% in the  $9/2_1^-$  state, respectively.

In  $^{204}\text{Hg}$ , all the large  $B(E2)$  values from the  $2_1^+$ ,  $4_1^+$ , and  $6_1^+$  states and the electromagnetic moments of the  $2_1^+$  state are reproduced well. The  $(2_1^-)$  state has been experimentally observed at 1.829 MeV, but the theoretical  $2_1^-$  state is calculated at 3.073 MeV. It is difficult in the present framework to explain such a low-lying negative-parity state, and positive-parity states are densely populated around the experimental  $(2_1^-)$  state.

In  $^{203}\text{Hg}$ , all the low-lying states and the electromagnetic moments of the ground  $5/2^-$  state are reproduced well. Another low-lying negative-parity state has been confirmed in experiment with an excitation energy of 0.369 MeV.  $M1$  transitions from this state to the  $3/2_1^-$  state was measured in  $^{202}\text{Hg}(d, p\gamma)$  reaction [111]. The spin is suggested as  $(1/2, 3/2, 5/2)$ . It is inferred in the present calculations that the  $1/2_2^-$  state predicted at 0.257 MeV corresponds to the experimental low-lying state.

In  $^{202}\text{Hg}$ , the excitation energies of the yrast band and all the electromagnetic properties are reproduced well. The excitation energies of the yrare band are too high in comparison with the experiment. Since the  $^{202}\text{Hg}$  has four neutron holes, lower single-particle levels are important in determining the nuclear structure. In particular, the dependence of the coupling strengths on single-particle levels, which is neglected in this study, can be crucial.

Table 3.7: The calculated  $B(E2)$  values in units of W.u. for Pt isotopes (Calc.) in comparison with the experimental data (Expt.) [86].

$^{204}\text{Pt}$	$B(E2)$	
	Expt.	Calc.
$2_1^+ \rightarrow 0_1^+$		6.014
$4_1^+ \rightarrow 2_1^+$		0.005
$6_1^+ \rightarrow 4_1^+$		0.039
$8_1^+ \rightarrow 6_1^+$		0.125
$10_1^+ \rightarrow 8_1^+$	0.80(8)	0.102
$7_1^- \rightarrow 5_1^-$	0.017 $\rightarrow$ 0.0034 <sup>*1</sup>	0.529
$7_2^- \rightarrow 5_2^-$		0.098

In  $^{201}\text{Hg}$ , the  $B(E2)$  values have been measured in muonic X-ray spectroscopy [112], Coulomb excitations [113, 114], and  $^{201}\text{Tl}$  electron capture decay [87]. As shown in Table 4.2, some collective values are not reproduced in the present calculations.

### 3.3.3 Au isotopes

Figure 3.3 shows the energy spectra of  $_{79}\text{Au}$  isotopes. All the correct spins and parities of the ground states are reproduced except for  $^{205}\text{Au}$ . In  $^{205}\text{Au}$ , the  $1/2_1^+$  state is calculated with a slightly lower energy than the  $3/2_1^+$  state, which is the ground state in experiment. In  $^{203, 201, 200}\text{Au}$ , some low-lying states have been observed. Comparing the energy spectra between experiment and theory, it is seen that all the excited states are reproduced well. In  $^{200-205}\text{Au}$ , any  $B(E2)$  values and electromagnetic moments have not been measured in experiment.

### 3.3.4 Pt isotopes

Figure 3.4 shows the energy spectra of  $_{78}\text{Pt}$  isotopes. In  $^{204}\text{Pt}$ , three isomeric states,  $(5_1^-)$ ,  $(7_1^-)$ , and  $(10_1^+)$ , have been discovered with half-lives of  $5.5 \mu\text{s}$ ,  $55 \mu\text{s}$ , and  $146 \text{ ns}$ , respectively [86]. In this study the  $5_1^-$  state is the second lowest negative-parity state and the energy gap between the lowest one (the  $4_1^-$  state) is as narrow as  $57 \text{ keV}$ . The long half-life of the  $(7_1^-)$  state, where the excitation energy is unknown in experiment, is expected to be caused by a narrow energy gap between the  $7_1^-$  and the  $5_1^-$  states of  $17 \text{ keV}$  and the small  $B(E2; 7_1^- \rightarrow 5_1^-)$  value as shown in Table 3.7.

In  $^{203}\text{Pt}$ , the spin and parity of the ground state are assigned as  $(1/2^-)$  with uncertainty. In the present study, the spin-parity of the ground state is calculated as  $1/2^-$  and all the excited states are predicted higher than  $0.5 \text{ MeV}$ . Thus, the spin-parity assignment on the ground state is strongly supported.

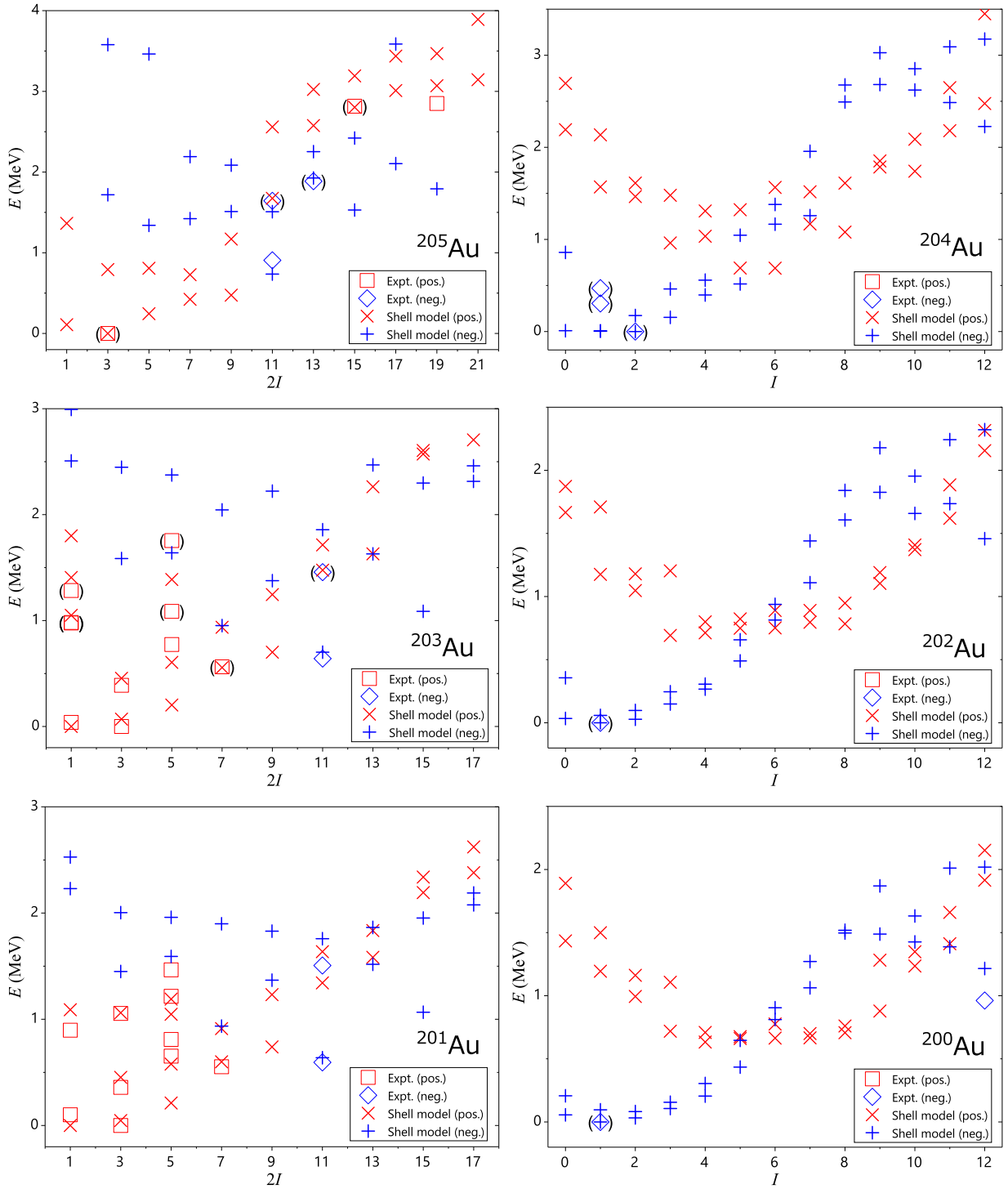


Figure 3.3: Same as Fig. 3.1, but for Au isotopes. The experimental data are taken from ENSDF [16] and Nuclear Data Sheets [102–105, 109, 115]. In the recent experiment [110, 116–118], the  $11/2_1^-$ ,  $(11/2_2^-)$ ,  $(13_1^-)$ ,  $(15/2^+)_1$ , and  $19/2_1^+$  states in  $^{205}\text{Au}$ , the  $(1/2_1^-)$  and  $(1/2_1^-)$  states in  $^{204}\text{Au}$ , the  $(1/2_2^+)$ ,  $(1/2_3^+)$ , and  $(7/2_1^+)$  states and the  $7/2_1^+$  state in  $^{201}\text{Au}$  are discovered.

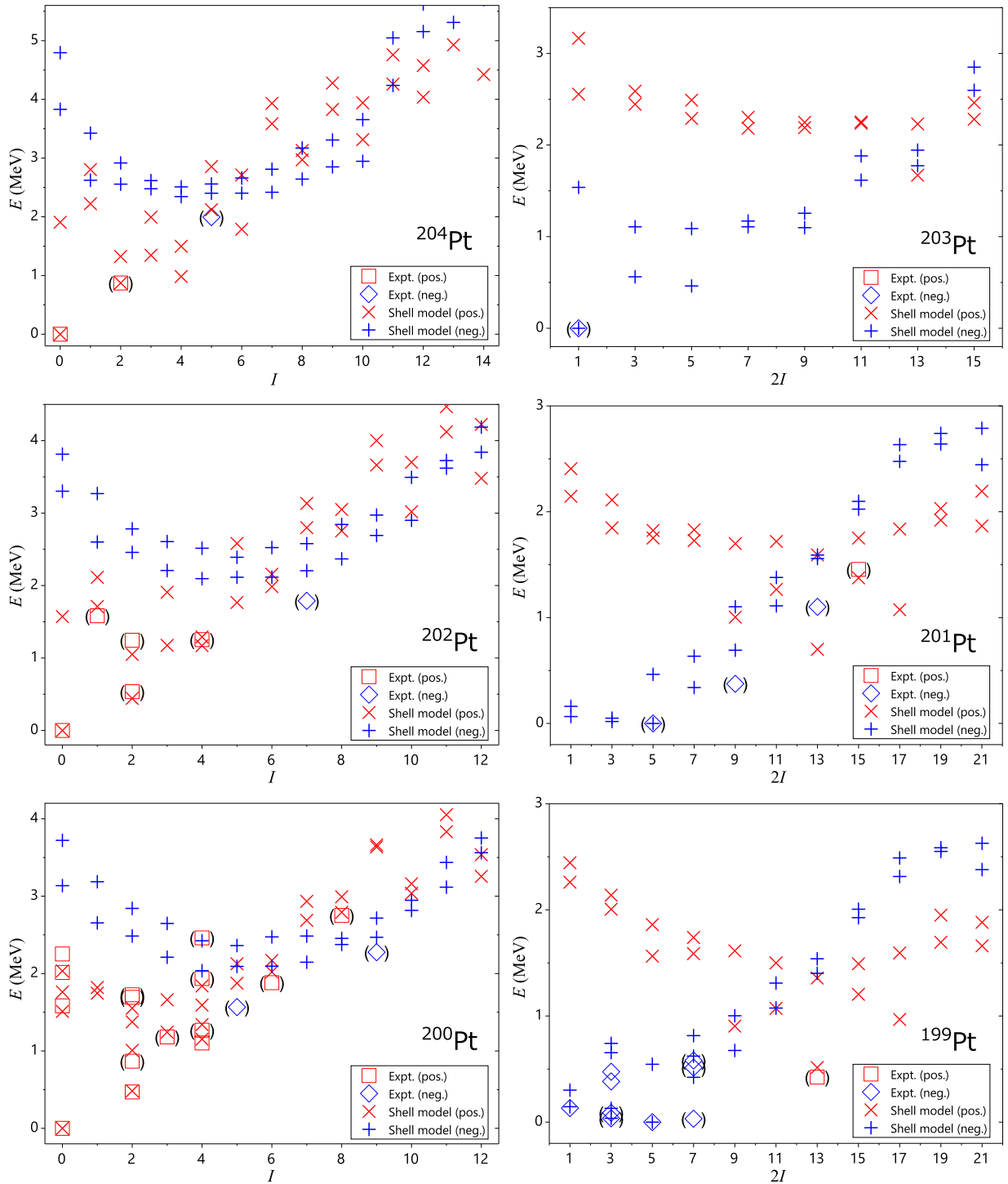


Figure 3.4: Same as Fig. 3.1, but for Pt isotopes. The experimental data are taken from ENSDF [16] and Nuclear Data Sheets [103–105, 109, 115, 119]. The  $(1_1^+)$  and  $(2_2^+)$  states in  $^{202}\text{Pt}$  are reported in Ref. [118]. The  $(6_1^+)$  and  $(8_1^+)$  states in  $^{200}\text{Pt}$  are reported in Ref. [120].

In  $^{202}\text{Pt}$ , the  $(1_1^+)$ ,  $(2_1^+)$ ,  $(2_2^+)$ ,  $(4_1^+)$ , and  $(7_1^-)$  states have been observed with the uncertain assignments on the spins and parities. These excited states are well reproduced in the present calculations.

In  $^{201}\text{Pt}$ , the  $\gamma$ -ray transitions have been observed once [88]. They assigned the  $(5/2^-)$ ,  $(9/2^-)$ ,  $(13/2^-)$ ,  $(15/2^+)$ , and  $(19/2^+)$  to observed levels. The ground  $(5/2^-)$  state and the  $(15/2^+)_1$  states are reproduced well in the present study, whereas the  $(9/2^-)$  and  $(13/2^-)$  states are not. In  $^{199}\text{Pt}$ , the  $(7/2)_1^-$  state was observed at 0.032 MeV [121]. This state is not described in the present framework and low-lying states with other spins are already assigned.

### 3.4 Summary

In the present study, the large-scale shell-model calculations have been carried out for even-even, odd-mass, and doubly odd nuclei of  $_{82}\text{Pb}$ ,  $_{81}\text{Tl}$ ,  $_{80}\text{Hg}$ ,  $_{79}\text{Au}$ , and  $_{78}\text{Pt}$  isotopes in the proton-deficient and neutron-deficient region around the double magic core of the  $^{208}\text{Pb}$  nucleus.

For neutron single-particle levels, seven orbitals above the magic number 126,  $1g_{9/2}$ ,  $0i_{11/2}$ ,  $0j_{15/2}$ ,  $2d_{5/2}$ ,  $3s_{1/2}$ ,  $1g_{7/2}$ , and  $2d_{3/2}$  orbitals, have been taken into account. For proton single-particle levels, all the six orbitals in the major shell between the magic numbers 82 and 126,  $0h_{9/2}$ ,  $1f_{7/2}$ ,  $0i_{13/2}$ ,  $2p_{3/2}$ ,  $1f_{5/2}$ , and  $2p_{1/2}$  orbitals, have been taken into account. The particle number dependence of the single-particle energies of the neutron  $0j_{15/2}$  and  $0i_{11/2}$  orbitals and the proton  $0i_{13/2}$  and  $1f_{7/2}$  orbitals have been assumed. They are changed linearly so as to reproduce the energy levels of low-lying states of the odd-mass nuclei. As for the effective two-body interaction, higher multipole-pairing interactions among like nucleons and the quadrupole-quadrupole interaction between neutrons and protons are employed in addition to the conventional pairing interactions. Only one set of the strengths of the two-body interactions has been adopted in all the nuclei considered.

Energy spectra,  $E2$  transition rates, magnetic moments, and electric quadrupole moments have been calculated and compared with the experimental data. Good agreements with experimental data have been obtained not only for even-even and odd-mass nuclei, but also for doubly-odd nuclei. Comparing our results and the experimental data, spins and parities of experimentally ambiguous states have been suggested.

Nine isomeric states are analyzed in terms of the shell-model configurations. Four isomeric states appearing in this region are classified as the spin-gap isomers, which do not take gamma transitions with low-spin changes, such as  $E2$  or  $M1$  transitions, because of the large spin difference between initial and final states. The other five states become isomers even if they decay by the  $E2$  transition. They become isomers since the energy gaps between the initial and final states are small.



## Chapter 4

# Nuclear Schiff moment of $^{199}\text{Hg}$

### 4.1 Introduction

The *Planck* 2015 results on the Cosmic microwave background provide the baryon-to-photon ratio in the universe of  $\eta = n_b/n_\gamma = (6.09 \pm 0.06) \times 10^{-10}$  [122, 123], which is consistent with the result from the light-element abundances  $\eta = (5.8 - 6.6) \times 10^{-10}$  [124, 125]. In order to realize the baryon-abundant universe, the  $CP$ -violation is required as well as the baryon number violating process. In the Standard Model of particle physics, the  $CP$ -violation arises from the Cabibbo-Kobayashi-Maskawa (CKM) matrix. However, it is well known that the  $CP$ -violating phase is too small to produce the baryon-antibaryon asymmetry [126–129]. This is one of the noticeable problems that should be explained in physics beyond the Standard Model.

The permanent electric dipole moments (EDMs) of elementary particles and composite particles are  $CP$ -odd observables. The neutron EDM has been directly explored [130–134], and the recent upper limit is  $|d_n| < 3.6 \times 10^{-26} e \text{ cm}$ . The electron EDM has been measured in  $^{133}\text{Cs}$  [135, 136],  $^{205}\text{Tl}$  [137, 138] atoms, and some molecules [139–141]. The present situation is  $|d_e| < 1.1 \times 10^{-29} e \text{ cm}$ . The atomic EDM of  $^{199}\text{Hg}$  has been experimentally searched many times [89–94, 142]. The constraint of  $|d(^{199}\text{Hg})| < 7.4 \times 10^{-30} e \text{ cm}$  has been given so far.

The diamagnetic atoms such as  $^{199}\text{Hg}$  are mainly contributed from the nuclear Schiff moments. The Schiff moment of  $^{199}\text{Hg}$  has been calculated within some kinds of mean-field approximation [95–100, 143, 144]. In the first calculation [95], non-collective one-particle one-hole excitations due to the  $P$ ,  $T$ -odd nuclear interactions are considered. The authors take a Woods-Saxon potential as the mean field. The spin-orbit and isovector interactions are considered in addition to the Woods-Saxon potential as an isoscalar part in Ref. [96–98, 143, 144]. They take into account collective excitations in the manner of the random phase approximation (RPA). Fully self-consistent mean fields including pairing correlations are treated in Ref [99, 100]. They take Skyrme interactions as  $P$ ,  $T$ -even interactions.

In this paper, we perform the shell-model calculations of  $^{199}\text{Hg}$  and  $^{200}\text{Hg}$  with the use of a newly developed effective interactions. The energy spectra,  $E2$  transition strengths, and electromagnetic

moments are systematically reproduced for excited states as well.

## 4.2 Nuclear Schiff moment

The  $P$ ,  $T$ -odd  $\pi$ - $N$  interactions are generally given as

$$\mathcal{L}_{\pi NN} = \sum_{N=p,n} \left[ \sum_{a=1}^3 \bar{g}_{\pi NN}^{(0)} \bar{N} \tau^a N \pi^a + \bar{g}_{\pi NN}^{(1)} \bar{N} N \pi^0 + \sum_{a=1}^3 \bar{g}_{\pi NN}^{(2)} (\bar{N} \tau^a N \pi^a - 3 \bar{N} \tau^3 N \pi^0) \right], \quad (2.1)$$

where  $G_F$  is the Fermi coupling constant,  $F^{\mu\nu}$  the electromagnetic field tensor, and  $a$  denotes the isospin components. The non-relativistic potentials of the  $P$ ,  $T$ -odd  $\pi$ - $N$  interactions are given as [145–147]

$$V_{T=0}^{(PT)} = F_0 (\boldsymbol{\tau}_1 \cdot \boldsymbol{\tau}_2) (\boldsymbol{\sigma}_1 - \boldsymbol{\sigma}_2) \cdot \mathbf{r} f(r) \quad (2.2)$$

$$V_{T=1}^{(PT)} = F_1 [(\tau_1^z - \tau_2^z) (\boldsymbol{\sigma}_1 + \boldsymbol{\sigma}_2) + (\tau_1^z + \tau_2^z) (\boldsymbol{\sigma}_1 - \boldsymbol{\sigma}_2)] \cdot \mathbf{r} f(r) \quad (2.3)$$

$$V_{T=2}^{(PT)} = F_2 (3\tau_1^z \tau_2^z - \boldsymbol{\tau}_1 \cdot \boldsymbol{\tau}_2) (\boldsymbol{\sigma}_1 - \boldsymbol{\sigma}_2) \cdot \mathbf{r} f(r), \quad (2.4)$$

where

$$f(r) = \frac{e^{-m_\pi r}}{m_\pi r} \left( 1 + \frac{1}{m_\pi r} \right), \quad (2.5)$$

and

$$F_0 = -\frac{m_\pi^2}{8\pi m_N} \bar{g}_{\pi NN}^{(0)} g_{\pi NN}, \quad (2.6)$$

$$F_1 = -\frac{m_\pi^2}{16\pi m_N} \bar{g}_{\pi NN}^{(1)} g_{\pi NN}, \quad (2.7)$$

$$F_2 = -\frac{m_\pi^2}{8\pi m_N} \bar{g}_{\pi NN}^{(2)} g_{\pi NN}, \quad (2.8)$$

with the pion mass  $m_\pi$  and the nucleon mass  $m_N$ . The  $CP$ -odd  $\pi$ - $N$  interaction couplings are given within the standard model as [63]

$$\begin{aligned} \bar{g}_{\pi NN}^{(0)} &= -1.1 \times 10^{-17}, \\ \bar{g}_{\pi NN}^{(1)} &= -1.3 \times 10^{-17}, \\ \bar{g}_{\pi NN}^{(2)} &= 3.3 \times 10^{-21}. \end{aligned} \quad (2.9)$$

Adopting the standard value of the  $CP$ -even  $\pi$ - $N$  coupling [63] of

$$g_{\pi NN} = 14.11 \pm 0.20, \quad (2.10)$$

we have

$$\begin{aligned} \bar{G}_\pi^{(0)} &\equiv -\bar{g}_{\pi NN}^{(0)} g_{\pi NN} = 1.6 \times 10^{-16}, \\ \bar{G}_\pi^{(1)} &\equiv -\bar{g}_{\pi NN}^{(1)} g_{\pi NN} = 1.8 \times 10^{-16}, \\ \bar{G}_\pi^{(2)} &\equiv \bar{g}_{\pi NN}^{(2)} g_{\pi NN} = 4.7 \times 10^{-20}. \end{aligned} \quad (2.11)$$

The nuclear Schiff moment (NSM) caused by the asymmetry of the charge distribution in a nucleus is expressed as

$$S_{\text{ch}}^{(1)} = \frac{1}{10} \sum_{i=1}^A e_i \left( r_i^2 r_i^{(1)} - \frac{5}{3} \langle r^2 \rangle_{\text{ch}} r_i^{(1)} - \frac{2}{3} \langle Q_{ij} \rangle r_j^{(1)} \right). \quad (2.12)$$

The NSM is classified as

$$S = \sum_{T=0,1,2} S_T, \quad (2.13)$$

where the isospin components of NSM due to the  $PT$ -odd interactions are defined as

$$S_T = \frac{\langle I_{\text{g.s.}}^- | S_0^{(1)} | I_k^+ \rangle \langle I_k^+ | V_T^{(PT)} | I_{\text{g.s.}}^- \rangle}{E_{\text{g.s.}} - E_k} + c.c. \quad (2.14)$$

Since the ground state of  $^{199}\text{Hg}$  has a spin-parity of  $1/2^-$ , all the excited states with a spin-parity of  $1/2^+$  should be taken into account as intermediate states.  $E_{\text{g.s.}}$  and  $E_k$  indicate the energies of the ground state and the  $k$ th excited state with a spin-parity of  $1/2^+$ , respectively.

In this paper, the intermediate states are expressed only by one-particle-one-hole configurations defined as

$$|I_k^+\rangle = |\psi_{(ij)_{L;I}}^{\text{(ph)}}\rangle = N \left[ [c_{\pi i}^\dagger \tilde{c}_{\pi j}]^{(L)} \otimes |I_{\text{g.s.}}^-\rangle \right]^{(I)}, \quad (2.15)$$

where  $c_{\pi im}^\dagger$  and  $c_{\pi jm}$  are proton ( $\pi$ ) creation and annihilation operators, respectively. The spherical tensor accompanied with  $c_{\pi jm}$  is defined as  $\tilde{c}_{\pi jm} = (-1)^{j-m} c_{\pi jm}$ . The single-particle orbital  $i$  should have the opposite parity to that of the single-hole orbital  $j$ . Moreover, the creation and annihilation operators are coupled only with  $L = 0, 1$  in order to let the excited states have the same spin  $I$  as the ground state. The proton orbitals between the magic numbers 50 and 82 are  $2s_{1/2}$ ,  $1d_{3/2}$ ,  $1d_{5/2}$ ,  $0g_{7/2}$ , and  $0h_{11/2}$ . Thus, there are no combinations of two orbitals satisfy the above conditions within the valence space.

All the single-particle orbitals of the harmonic oscillator potential are taken into account as the contributions to the one-particle-one-hole excited states. As the excited energies  $E_k$ , the energy differences of the Nilsson single-particle energies outside the valence space and the adopted single-particle energies within the valence space are employed.

### 4.3 Numerical results

In the previous chapter,  $^{201-206}\text{Hg}$  nuclei are studied in the nuclear shell model with a newly developed effective interaction. In order to perform the shell-model calculation of the  $^{199}\text{Hg}$  nucleus, the lower four single-neutron orbitals,  $2p_{1/2}$ ,  $2p_{3/2}$ ,  $1f_{5/2}$ , and  $0i_{13/2}$ , are taken into account. The single-particle energies and the two-body interaction strengths are given in the previous chapter. Figure 4.1 shows the energy spectra of  $^{200}\text{Hg}$  and  $^{199}\text{Hg}$ .

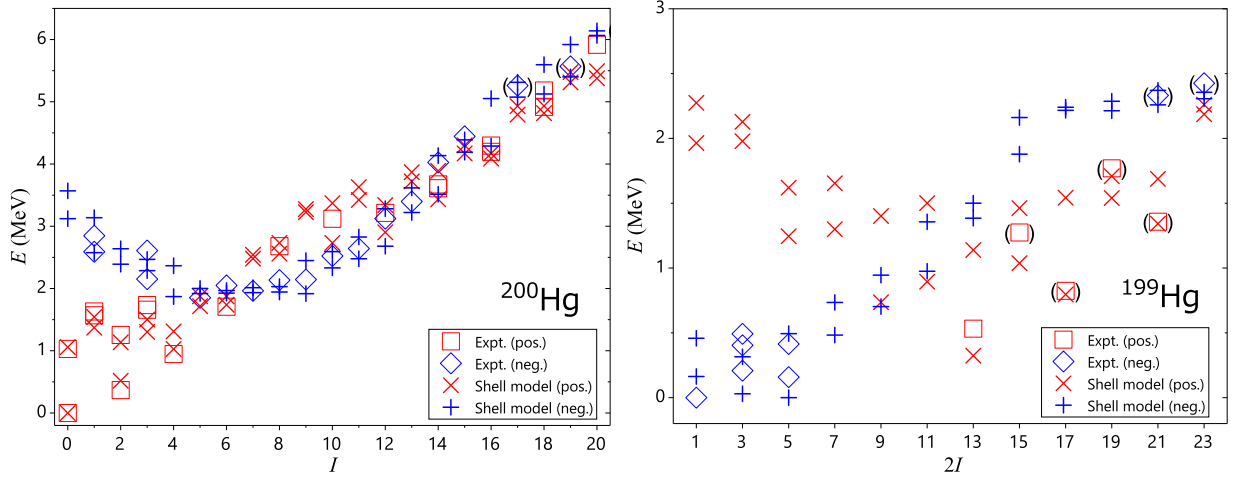


Figure 4.1: The energy spectra of  $^{200}\text{Hg}$  and  $^{199}\text{Hg}$  calculated in the nuclear shell model, which are compared with the experimental data [16, 115, 119].

Table 4.1: The calculated  $B(E2)$  values in units of W.u. for  $^{200}\text{Hg}$  (Calc.) in comparison with the experimental data (Expt.) [16, 115].

$^{200}\text{Hg}$	$B(E2)$	
	Expt.	Calc.
$2_1^+ \rightarrow 0_1^+$	24.57(22)	15.017
$4_1^+ \rightarrow 2_1^+$	37.8(6)	15.880
$6_1^+ \rightarrow 4_1^+$	46(4)	14.691
$8_1^+ \rightarrow 6_1^+$	41(14)	12.530
$2_2^+ \rightarrow 0_1^+$	0.23(6)	0.009
$2_2^+ \rightarrow 2_1^+$	2.4(6)	4.160
$9_1^- \rightarrow 7_1^-$	25.1(10)	15.477

As shown in Fig. 4.2, the experimentally measured values of the electromagnetic moments are well reproduced with the present parameters. The same quenching factors as the previous chapter are taken for the effective operators. It is also found that the results are little depend on the monopole pairing strengths for the neutron  $p_{3/2}$  and  $f_{5/2}$  orbitals.

We adopt another truncation process to get wavefunctions of  $^{200}\text{Hg}$  and  $^{199}\text{Hg}$ . The lowest 100 eigenstates in each neutron or proton system are labeled as  $|\psi_i^{(\nu)}\rangle$  or  $|\psi_j^{(\pi)}\rangle$ . The  $CP$ -even effective Hamiltonian is diagonalized in the  $10^4$  bases, which are given as  $|\psi_i^{(\nu)}\rangle \otimes |\psi_j^{(\pi)}\rangle$ . The energy convergence is discussed for mass  $A = 130$  region [14].

Table 4.2: The results of magnetic dipole moments  $\mu$  in units of  $\mu_N$  and electric quadrupole moments  $Q$  in units of  $eb$  for Hg isotopes (Calc.) in comparison with the experimental data (Expt.) [16, 115, 119].

$^{200}\text{Hg}$	$\mu$		$Q$	
	Expt.	Calc.	Expt.	Calc.
$2_1^+$	0.65(5)	+0.996	+1.09	+0.583
$4_1^+$	1.02(16)	+1.266		
$^{199}\text{Hg}$	Expt.	Calc.	Expt.	Calc.
$1/2_1^-$	+0.506	+0.298		0
$5/2_1^-$	+0.88(3)	+0.719	+0.95(7)	-0.025
$3/2_1^-$	-0.56(9)	-0.625	+0.50(12)	+0.252
$5/2_2^-$	+0.80(9)	+0.677		
$13/2_1^+$	-1.015	-0.912	+1.2(5)	+0.624

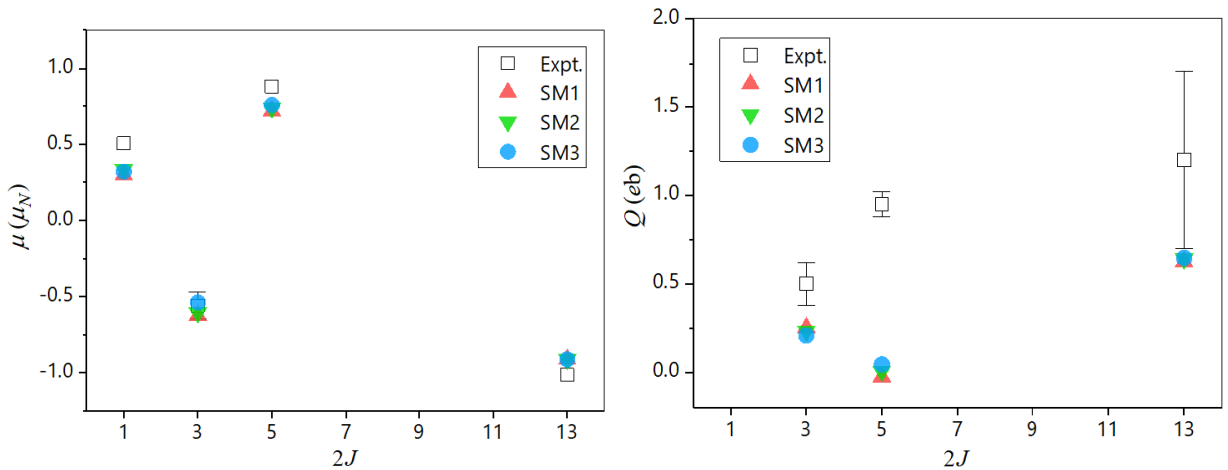


Figure 4.2: Electromagnetic moments.

Table 4.3: The numerical results of the nuclear Schiff moment in units of  $10^{-3}efm^3$ . The one-particle-one-hole excitations from the valence space are shown in the first line. The second and third lines correspond to those from the core to the valence space and to beyond the valence space, respectively.

	$a_0$	$a_1$	$a_2$
valence	25.9	25.1	49.3
core	-0.9	-0.8	-1.36
over-shell	1.0	1.1	2.3
sum	26.0	25.4	50.2

The results shown in Table 4.3 are given in the form as

$$S = \sum_{T=0,1,2} a_T \bar{g}^{(T)} g. \quad (3.1)$$

For all the components  $T = 0, 1, 2$ , the contributions of one-particle-one-hole excitations from the valence space are dominant, whereas those from the core region are comparable in  $^{129}\text{Xe}$ . In the  $^{199}\text{Hg}$  nucleus the valence space of proton is almost fully occupied, whereas the  $^{129}\text{Xe}$  nucleus has only four valence protons, so that there are large energy gaps from the core in  $^{199}\text{Hg}$ .

Each component of  $a_T$  is 30% smaller than the result in the simple shell model [95]. In the simple shell model, they employed contact  $CP$ -odd interactions and the Woods-Saxon potential as the mean field. In addition to those points of difference, it is crucial to decrease the Schiff moment that a lot of configurations within the valence space are admixed. The population of the  $|\nu p_{1/2} f_{5/2}^6 \otimes \pi s_{1/2}^2\rangle$  configuration is only 2.4% in the  $1/2^-$  state.

The sensitivity of the results on the energy denominator is checked by using the Nilsson values also for the valence orbitals. In this case the isoscalar component is  $a_0 = 29.0 \times 10^{-3} \text{efm}^3$ . The spin of the ground state in  $^{199}\text{Hg}$  is not reproduced with the adopted effective interactions. As shown in Fig. 4.3, the actual spin of  $1/2$  is realized by introducing the monopole pairing for the  $\nu p_{3/2}$  and  $\nu f_{5/2}$  orbitals (SM2 and SM3). The NSMs are  $a_0 = 33.2 \times 10^{-3} \text{efm}^3$  and  $a_0 = 34.1 \times 10^{-3} \text{efm}^3$ , respectively. Thus, the accuracy of the results would be estimated as 30%.

The nuclear Schiff moment produces the  $P$ ,  $T$ -odd electrostatic potential such as

$$\phi(\mathbf{r}) = -4\pi \mathbf{S} \cdot \nabla \delta(\mathbf{r}). \quad (3.2)$$

The interaction violates the parity conservation in atoms and induces the atomic EDM. The EDM of  $^{199}\text{Hg}$  atom has been calculated as [148]

$$d(^{199}\text{Hg}) = -2.8 \times 10^{-17} \left( \frac{S}{e \text{fm}^3} \right) e \text{cm}. \quad (3.3)$$

If the SM2 result for the NSM of  $^{199}\text{Hg}$  is adopted, the atomic EDM is given as

$$d(^{199}\text{Hg}) = 3.15 \times 10^{-34} e \text{cm}. \quad (3.4)$$

The QCD  $\theta$ -term contributes to the  $CP$ -odd couplings. The coupling constants are evaluated in the chiral effective field theory as

$$\bar{g}_\pi^{(0)} = (0.015 \pm 0.003) \bar{\theta}, \quad \bar{g}_\pi^{(1)} = 0.003 \bar{\theta}, \quad (3.5)$$

whereas the isotensor coupling is suppressed [149, 150]. The SM2 results and the experimental upper limit on the  $^{199}\text{Hg}$  atomic EDM provide the constraint on the  $\theta$ -term as  $|\bar{\theta}| < 6.63 \times 10^{-10}$ .

The upper limit on the magnitude of the neutron EDM of  $3.6 \times 10^{-26} e \text{cm}$  [134] provides  $|\bar{\theta}| < 1.3 \times 10^{-10}$ , which is the most limited value.

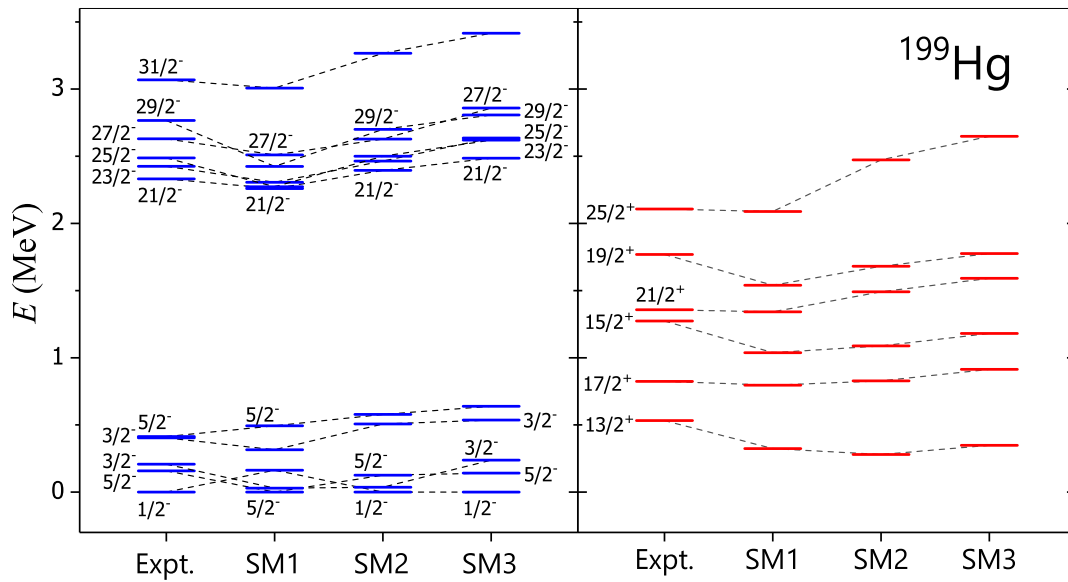


Figure 4.3: Low-lying states of  $^{199}\text{Hg}$  in which the monopole pairing interactions peculiar to the  $\nu p_{3/2}$  and  $\nu f_{5/2}$  orbitals are adopted (SM2, SM3). SM1 shows the results with the original interactions. The experimental states are compared in the far left column.



## Appendix A

# Racah algebra

### A.1 Orthogonal functions

#### A.1.1 Legendre polynomials

The Legendre polynomials are defined through a generating function of

$$g_P(t, x) = \frac{1}{\sqrt{1 - 2tx + t^2}} = \sum_{n=0}^{\infty} P_n(x)t^n. \quad (\text{A.1.1})$$

The generating function is expanded as

$$\begin{aligned} g_P(t, x) &= \sum_{m=0}^{\infty} \frac{(2m-1)!!}{2^m m!} (2tx - t^2)^m \\ &= \sum_{m=0}^{\infty} \frac{(2m-1)!!}{2^m m!} t^m \sum_{k=0}^m \binom{m}{k} (2x)^{m-k} (-t)^k \\ &= \sum_{n=0}^{\infty} \sum_{k=0}^{[n/2]} \frac{(2n-2k-1)!!}{2^k (n-k)!} (-1)^k \binom{n-k}{k} x^{n-2k} t^n \\ &= \sum_{n=0}^{\infty} \sum_{k=0}^{[n/2]} (-1)^k \frac{(2n-2k)!}{2^n k! (n-k)! (n-2k)!} x^{n-2k} t^n, \end{aligned} \quad (\text{A.1.2})$$

where  $n = m + k$  and  $[n/2]$  indicates the maximum integer which does not exceed  $n/2$ . Thus the Legendre polynomials can be expanded as

$$P_n(x) = \sum_{k=0}^{[n/2]} (-1)^k \frac{(2n-2k)!}{2^n k! (n-k)! (n-2k)!} x^{n-2k}. \quad (\text{A.1.3})$$

This expression is given also by the Rodrigues formula

$$P_n(x) = \frac{1}{2^n n!} \frac{d^n}{dx^n} (x^2 - 1)^n. \quad (\text{A.1.4})$$

The Legendre polynomials are orthogonal as

$$\int_{-1}^1 P_m(x) P_n(x) dx = \frac{2}{2n+1} \delta_{mn}, \quad (\text{A.1.5})$$

which is given by

$$\begin{aligned}
\int_{-1}^1 g_P(t, x) g_P(s, x) dx &= \frac{1}{2\sqrt{ts}} \int_{-1}^1 \frac{1}{\sqrt{\frac{1+t^2}{2t} - x} \sqrt{\frac{1+s^2}{2s} - x}} dx \\
&= -\frac{1}{\sqrt{ts}} \left[ \ln \left( \sqrt{\frac{1+t^2}{2t} - x} + \sqrt{\frac{1+s^2}{2s} - x} \right) \right]_{x=-1}^1 \\
&= \frac{1}{\sqrt{ts}} \ln \frac{1 + \sqrt{ts}}{1 - \sqrt{ts}} \\
&= \sum_{n=0}^{\infty} \frac{2}{2n+1} (ts)^n. \tag{A.1.6}
\end{aligned}$$

The associated Legendre polynomials are defined by the Legendre polynomials  $P_n(x)$  as

$$\begin{aligned}
P_{lm}(x) &\equiv (1-x^2)^{m/2} \frac{d^m}{dx^m} P_l(x) \\
&= \frac{1}{2^l l!} (1-x^2)^{m/2} \frac{d^{l+m}}{dx^{l+m}} (x^2-1)^l. \tag{A.1.7}
\end{aligned}$$

This can be expanded as

$$\begin{aligned}
P_{lm}(x) &= \frac{1}{2^l l!} (1-x^2)^{m/2} \sum_n \binom{l+m}{n} \frac{d^{l+m-n}}{dx^{l+m-n}} (x+1)^l \frac{d^n}{dx^n} (x-1)^l \\
&= \frac{1}{2^l l!} (1-x^2)^{m/2} \sum_n \binom{l+m}{n} \frac{l!}{(n-m)!} (x+1)^{n-m} \frac{l!}{(l-n)!} (x-1)^{l-n} \\
&= \frac{1}{2^l l!} (1-x^2)^{m/2} (l+m)! \sum_n \binom{l}{n-m} \binom{l}{n} (x+1)^{n-m} (x-1)^{l-n} \\
P_{l,-m}(x) &= \frac{1}{2^l l!} (1-x^2)^{-m/2} (l-m)! \sum_n \binom{l}{n+m} \binom{l}{n} (x+1)^{n+m} (x-1)^{l-n} \\
&= (-1)^m \frac{1}{2^l l!} (1-x^2)^{m/2} (l-m)! \sum_n \binom{l}{n+m} \binom{l}{n} (x+1)^n (x-1)^{l-n-m} \\
&= (-1)^m \frac{1}{2^l l!} (1-x^2)^{m/2} (l-m)! \sum_{n'} \binom{l}{n'} \binom{l}{n'-m} (x+1)^{n'-m} (x-1)^{l-n'}, \tag{A.1.8}
\end{aligned}$$

where  $n' = n - m$ , and then

$$P_{l,-m}(x) = (-1)^m \frac{(l-m)!}{(l+m)!} P_{lm}(x). \tag{A.1.9}$$

The orthogonality is given as

$$\int_{-1}^1 P_{lm}(x) P_{l'm}(x) dx = \frac{2}{2l+1} \frac{(l+m)!}{(l-m)!} \delta_{ll'}. \tag{A.1.10}$$

### A.1.2 Spherical harmonics

Spherical harmonics are defined as

$$Y_{lm}(\theta, \phi) = (-1)^m \sqrt{\frac{2l+1}{4\pi} \frac{(l-m)!}{(l+m)!}} P_{lm}(\cos \theta) e^{im\phi}, \quad (\text{A.1.11})$$

where  $0 \leq \theta \leq \pi$  and  $0 \leq \phi \leq 2\pi$ . The complex conjugate is given as

$$Y_{l,m}^*(\theta, \phi) = (-1)^m Y_{l,-m}(\theta, \phi). \quad (\text{A.1.12})$$

### A.1.3 Jacobi polynomials

Jacobi polynomials are given through the Rodrigues formula as

$$P_n^{(\alpha, \beta)}(x) = \frac{(-1)^n}{2^n n!} (1-x)^{-\alpha} (1+x)^{-\beta} \frac{d^n}{dx^n} (1-x)^{n+\alpha} (1+x)^{n+\beta}, \quad (\text{A.1.13})$$

and then by the series expansion of

$$\begin{aligned} P_n^{(\alpha, \beta)}(x) &= \frac{(-1)^n}{2^n n!} (1-x)^{-\alpha} (1+x)^{-\beta} \\ &\quad \times \sum_{\nu=0}^n \binom{n}{\nu} (-1)^\nu \frac{(n+\alpha)!}{(n+\alpha-\nu)!} (1-x)^{n+\alpha-\nu} \frac{(n+\beta)!}{(\beta+\nu)!} (1+x)^{\beta+\nu} \\ &= \frac{(-1)^n}{2^n} \sum_{\nu=0}^n (-1)^\nu \binom{n+\alpha}{\nu} \binom{n+\beta}{n-\nu} (1-x)^{n-\nu} (1+x)^\nu \\ &= \frac{1}{2^n} \sum_{\nu=0}^n \binom{n+\alpha}{\nu} \binom{n+\beta}{n-\nu} (x-1)^{n-\nu} (x+1)^\nu. \end{aligned} \quad (\text{A.1.14})$$

The orthogonality is given as

$$\begin{aligned} &\int_{-1}^1 dx (1-x)^\alpha (1+x)^\beta P_n^{(\alpha, \beta)}(x) P_m^{(\alpha, \beta)}(x) \\ &= \frac{2^{\alpha+\beta+1}}{2n+\alpha+\beta+1} \frac{\Gamma(n+\alpha+1)\Gamma(n+\beta+1)}{n!\Gamma(n+\alpha+\beta+1)} \delta_{nm}. \end{aligned} \quad (\text{A.1.15})$$

### A.1.4 Associated Laguerre polynomials

The associated Laguerre polynomials are defined by the Laguerre polynomials  $L_n(x)$  as

$$L_{nl}(x) = \frac{d^l}{dx^l} L_n(x), \quad (\text{A.1.16})$$

or through a generating function of

$$g_L(t, x) = \frac{(-1)^l}{(1-t)^{l+1}} \exp\left(-\frac{xt}{1-t}\right) = \sum_{n=l}^{\infty} L_{nl}(x) \frac{t^{n-l}}{n!}. \quad (\text{A.1.17})$$

This can be expanded as

$$\begin{aligned}
g_L(t, x) &= \frac{(-1)^l}{(1-t)^{l+1}} \sum_{m=0}^{\infty} \frac{1}{m!} \left( -\frac{xt}{1-t} \right)^m \\
&= \sum_{m=0}^{\infty} \frac{(-1)^{l+m}}{m!} x^m \frac{t^m}{(1-t)^{l+m+1}} \\
&= \sum_{m=0}^{\infty} \frac{(-1)^{l+m}}{m!} x^m \sum_{k=0}^{\infty} \frac{(l+m+k)!}{k!(l+m)!} t^{k+m} \\
&= \sum_{m=0}^{\infty} \frac{(-1)^{l+m}}{m!} x^m \sum_{n=m+l}^{\infty} \frac{n!}{(n-l-m)!(l+m)!} t^{n-l} \\
&= \sum_{n=l}^{\infty} \sum_{m=0}^{n-l} \frac{(-1)^{l+m}}{m!} x^m \frac{n!}{(n-l-m)!(l+m)!} t^{n-l},
\end{aligned} \tag{A.1.18}$$

and thus the series expansions of associated Laguerre polynomials are given as

$$L_{nl}(x) = \sum_{m=0}^{n-l} (-1)^{l+m} \frac{(n!)^2}{m!(n-l-m)!(l+m)!} x^m, \tag{A.1.19}$$

where  $L_{nl}(x) = 0$  for  $n < l$ .

In order to derive recursion formulas,

$$\begin{aligned}
\ln g_L(t, x) &= \ln(-1)^l - (l+1) \ln(1-t) - \frac{xt}{1-t} \\
\therefore \frac{\partial g_L(t, x)}{\partial t} &= [(l-x+1) - (l+1)t] g_L(t, x),
\end{aligned} \tag{A.1.20}$$

and

$$\begin{aligned}
t g_L(t, x) &= \sum_{n=l}^{\infty} L_{nl}(x) \frac{t^{n-l+1}}{n!} = \sum_{n=l}^{\infty} n L_{n-1,l}(x) \frac{t^{n-l}}{n!}, \\
\frac{\partial g_L(t, x)}{\partial t} &= \sum_{n=l}^{\infty} (n-l) L_{nl}(x) \frac{t^{n-l-1}}{n!} = \sum_{n=l}^{\infty} \frac{n-l+1}{n+1} L_{n+1,l}(x) \frac{t^{n-l}}{n!}, \\
t \frac{\partial g_L(t, x)}{\partial t} &= \sum_{n=l}^{\infty} (n-l) L_{nl}(x) \frac{t^{n-l}}{n!}, \\
t^2 \frac{\partial g_L(t, x)}{\partial t} &= \sum_{n=l}^{\infty} n(n-l-1) L_{n-1,l}(x) \frac{t^{n-l}}{n!}
\end{aligned} \tag{A.1.21}$$

are utilized. Substituting these series expansions to Eq. (A.1.20), we obtain

$$\left(1 - \frac{l}{n+1}\right) L_{n+1,l}(x) + (x+k-2n-1) L_{nl}(x) + n^2 L_{n-1,l}(x) = 0. \tag{A.1.22}$$

The associated Laguerre polynomials are orthogonal with a weight function  $x^l e^{-x}$  as

$$\int_0^{\infty} L_{nl}(x) L_{ml}(x) x^l e^{-x} dx = \frac{(n!)^3}{(n-l)!} \delta_{nm}. \tag{A.1.23}$$

This orthogonality is derived from the relations of

$$\begin{aligned}
\int_0^\infty g_L(t, x)g_L(s, x)x^l e^{-x} dx &= \frac{1}{(1-t)^{l+1}(1-s)^{l+1}} \int_0^\infty \exp\left[-\frac{1-ts}{(1-t)(1-s)}x\right] x^l dx \\
&= \frac{1}{(1-t)^{l+1}(1-s)^{l+1}} \times l! \left(\frac{(1-t)(1-s)}{1-ts}\right)^{l+1} \\
&= \frac{l!}{(1-ts)^{l+1}} \\
&= \sum_{n=0}^\infty \frac{(l+n)!}{n!} t^n s^n \\
&= \sum_{n=l}^\infty \frac{n!}{(n-l)!} t^{n-l} s^{n-l}, \tag{A.1.24}
\end{aligned}$$

and

$$\sum_{n,m=l}^\infty \frac{t^{n-l} s^{m-l}}{n!m!} \int_0^\infty L_{nl}(x)L_{ml}(x)x^l e^{-x} dx. \tag{A.1.25}$$

### A.1.5 Sonine polynomials

Sonine polynomials are generalized Laguerre polynomials with  $\alpha$  which is not limited to integers. Those are defined through generating functions of

$$g_S(t, x) = \frac{1}{(1-t)^{\alpha+1}} \exp\left(-\frac{xt}{1-t}\right) = \sum_{n=0}^\infty S_{n\alpha}(x)t^n, \tag{A.1.26}$$

where  $\text{Re } \alpha > -1$ . The generating functions are expanded as

$$\begin{aligned}
g_S(t, x) &= \sum_{m=0}^\infty \frac{(-1)^m}{m!} x^m \frac{t^m}{(1-t)^{\alpha+m+1}} \\
&= \sum_{m=0}^\infty \frac{(-1)^m}{m!} x^m \sum_{k=0}^\infty \frac{\Gamma(\alpha+m+1+k)}{k!\Gamma(\alpha+m+1)} t^{m+k} \\
&= \sum_{m=0}^\infty \frac{(-1)^m}{m!} x^m \sum_{n=m}^\infty \frac{\Gamma(\alpha+n+1)}{(n-m)!\Gamma(\alpha+m+1)} t^n \\
&= \sum_{n=0}^\infty \sum_{m=0}^n \frac{(-1)^m}{m!} x^m \frac{\Gamma(\alpha+n+1)}{(n-m)!\Gamma(\alpha+m+1)} t^n. \tag{A.1.27}
\end{aligned}$$

Thus the Sonine polynomials are expanded as

$$S_{n\alpha}(x) = \sum_{m=0}^n (-1)^m \frac{\Gamma(\alpha+n+1)}{m!(n-m)!\Gamma(\alpha+m+1)} x^m, \tag{A.1.28}$$

which are related to associated Laguerre polynomials  $L_{nl}(x)$  as

$$L_{nl}(x) = (-1)^l n! S_{n-l, l}(x). \tag{A.1.29}$$

Here, the Gamma function defined as

$$\Gamma(x) = \int_0^{\infty} e^{-t} t^{x-1} dt, \quad (\text{A.1.30})$$

satisfies the recursion relation of  $\Gamma(x+1) = x\Gamma(x)$ . The orthogonality of

$$\int_0^{\infty} S_{n\alpha}(x) S_{m\alpha}(x) x^\alpha e^{-x} dx = \frac{1}{n!} \Gamma(\alpha+n+1) \delta_{nm} \quad (\text{A.1.31})$$

is derived from the relations of

$$\begin{aligned} \int_0^{\infty} g_S(t, x) g_S(s, x) x^\alpha e^{-x} dx &= \frac{1}{(1-t)^{\alpha+1} (1-s)^{\alpha+1}} \int_0^{\infty} \exp\left[-\frac{1-ts}{(1-t)(1-s)} x\right] x^\alpha dx \\ &= \frac{1}{(1-ts)^{\alpha+1}} \Gamma(\alpha+1) \\ &= \sum_{n=0}^{\infty} \frac{1}{n!} \Gamma(\alpha+n+1) t^n s^n, \end{aligned} \quad (\text{A.1.32})$$

and

$$\sum_{n,m=0}^{\infty} t^n s^m \int_0^{\infty} S_{n\alpha}(x) S_{m\alpha}(x) x^\alpha e^{-x} dx. \quad (\text{A.1.33})$$

## A.2 Recoupling Coefficients

### A.2.1 Clebsch-Gordan Coefficients

Let us consider the angular momentum operators  $\mathbf{J}_1$  and  $\mathbf{J}_2$ , which follow the SU(2) algebra as

$$[J_{1i}, J_{1j}] = i\varepsilon_{ijk} J_{1k}, \quad [J_{2i}, J_{2j}] = i\varepsilon_{ijk} J_{2k}. \quad (\text{A.2.1})$$

If those operators refer to independent systems, they are commute with each other as

$$[J_{1i}, J_{2j}] = 0. \quad (\text{A.2.2})$$

The angular momentum operators of the combined system, which is defined as

$$\mathbf{J} = \mathbf{J}_1 \oplus \mathbf{J}_2, \quad (\text{A.2.3})$$

follow that

$$[J_i, J_j] = i\varepsilon_{ijk} J_k. \quad (\text{A.2.4})$$

There are two different sets of simultaneous eigenstates in the combined system with respect to  $(\Gamma, \mathbf{J}_1^2, J_{1z}, \mathbf{J}_2^2, J_{2z})$  and  $(\Gamma, \mathbf{J}_1^2, \mathbf{J}_2^2, \mathbf{J}^2, J_z)$ , where  $\Gamma$  indicates other conservative quantities. The

eigenstates are represented as  $|\gamma j_1 m_1 j_2 m_2\rangle$  and  $|\gamma j_1 j_2 j m\rangle$ , which can be expanded with the other through the unitary transformations as

$$\begin{aligned} |\gamma j_1 j_2 j m\rangle &= \sum_{m_1 m_2} |\gamma j_1 m_1 j_2 m_2\rangle \langle j_1 m_1 j_2 m_2 | j m\rangle, \\ |\gamma j_1 m_1 j_2 m_2\rangle &= \sum_{j m} |\gamma j_1 j_2 j m\rangle \langle j m | j_1 m_1 j_2 m_2\rangle, \end{aligned} \quad (\text{A.2.5})$$

where the Clebsch-Gordan (CG) coefficients are expressed by  $\langle j_1 m_1 j_2 m_2 | j m\rangle$  and the complex conjugates by  $\langle j m | j_1 m_1 j_2 m_2\rangle$ . The CG coefficients have the unitary properties as

$$\begin{aligned} \sum_{j m} \langle j_1 m'_1 j_2 m'_2 | j m\rangle \langle j m | j_1 m_1 j_2 m_2\rangle &= \delta_{m'_1 m_1} \delta_{m'_2 m_2}, \\ \sum_{m_1 m_2} \langle j' m' | j_1 m_1 j_2 m_2\rangle \langle j_1 m_1 j_2 m_2 | j m\rangle &= \delta_{j' j} \delta_{m' m} \delta(j_1 j_2; j), \end{aligned} \quad (\text{A.2.6})$$

where

$$\delta(j_1 j_2; j) = \begin{cases} 1 & |j_1 - j_2| \leq j \leq j_1 + j_2 \\ 0 & \text{others} \end{cases}. \quad (\text{A.2.7})$$

The well-known phase convention of the CG coefficients, Condon-Shortley phase convention, is defined as

$$\langle j_1 j_1 j_2 j_2 | j_1 + j_2 j_1 + j_2\rangle = 1. \quad (\text{A.2.8})$$

This choice is very useful because all the CG coefficients are real. In the Condon-Shortley convention, the CG coefficients have symmetric properties as

$$\langle j_1 m_1 j_2 m_2 | j m\rangle = (-1)^{j_1 + j_2 - j} \langle j_2 m_2 j_1 m_1 | j m\rangle, \quad (\text{A.2.9})$$

$$\langle j_1 m_1 j_2 m_2 | j m\rangle = (-1)^{j_1 + j_2 - j} \langle j_1 - m_1 j_2 - m_2 | j - m\rangle, \quad (\text{A.2.10})$$

$$\langle j_1 m_1 j_2 m_2 | j m\rangle = \langle j_2 - m_2 j_1 - m_1 | j - m\rangle, \quad (\text{A.2.11})$$

and some explicit values are given as

$$\langle j m 0 0 | j m\rangle = 1, \quad \langle j m j - m | 0 0\rangle = \frac{(-1)^{j-m}}{\sqrt{2j+1}}. \quad (\text{A.2.12})$$

### A.2.2 Wigner 3- $j$ Symbols

Wigner 3- $j$  symbol is defined through the CG coefficients as

$$\begin{pmatrix} j_1 & j_2 & j_3 \\ m_1 & m_2 & m_3 \end{pmatrix} = (-1)^{j_1 - j_2 - m_3} \frac{\langle j_1 m_1 j_2 m_2 | j_3 - m_3\rangle}{\sqrt{2j_3 + 1}}, \quad (\text{A.2.13})$$

which has symmetry properties for even permutations of columns as

$$\begin{pmatrix} j_1 & j_2 & j_3 \\ m_1 & m_2 & m_3 \end{pmatrix} = \begin{pmatrix} j_2 & j_3 & j_1 \\ m_2 & m_3 & m_1 \end{pmatrix} = \begin{pmatrix} j_3 & j_1 & j_2 \\ m_3 & m_1 & m_2 \end{pmatrix}, \quad (\text{A.2.14})$$

for odd permutations become equivalent by the multiplication of  $(-1)^{j_1+j_2+j_3}$  as

$$\begin{aligned} & (-1)^{j_1+j_2+j_3} \begin{pmatrix} j_1 & j_2 & j_3 \\ m_1 & m_2 & m_3 \end{pmatrix} \\ &= \begin{pmatrix} j_2 & j_1 & j_3 \\ m_2 & m_1 & m_3 \end{pmatrix} = \begin{pmatrix} j_1 & j_3 & j_2 \\ m_1 & m_3 & m_2 \end{pmatrix} = \begin{pmatrix} j_3 & j_2 & j_1 \\ m_3 & m_2 & m_1 \end{pmatrix}, \end{aligned} \quad (\text{A.2.15})$$

and for negative directions of all the angular momenta  $\mathbf{J}_1$ ,  $\mathbf{J}_2$ , and  $\mathbf{J}_3$  as

$$\begin{pmatrix} j_1 & j_2 & j_3 \\ m_1 & m_2 & m_3 \end{pmatrix} = (-1)^{j_1+j_2+j_3} \begin{pmatrix} j_1 & j_2 & j_3 \\ -m_1 & -m_2 & -m_3 \end{pmatrix}. \quad (\text{A.2.16})$$

The CG-coefficients follow the similar symmetric properties, which are derived as

$$\begin{aligned} \langle j_1 m_1 j_2 m_2 | j m \rangle &= (-1)^{-j_1+j_2-m} \sqrt{2j+1} \begin{pmatrix} j_1 & j_2 & j \\ m_1 & m_2 & -m \end{pmatrix} \\ &= (-1)^{-j_1+j_2-m} \sqrt{2j+1} \begin{pmatrix} j_2 & j & j_1 \\ m_2 & -m & m_1 \end{pmatrix} \\ &= (-1)^{-j_1+2j_2-j-m_1-m} \sqrt{\frac{2j+1}{2j_1+1}} \langle j_2 m_2 j - m | j_1 - m_1 \rangle, \end{aligned} \quad (\text{A.2.17})$$

$$\begin{aligned} \langle j_1 m_1 j_2 m_2 | j m \rangle &= (-1)^{-j_1+j_2-m} \sqrt{2j+1} \begin{pmatrix} j_1 & j_2 & j \\ m_1 & m_2 & -m \end{pmatrix} \\ &= (-1)^{-j_1+j_2-m} \sqrt{2j+1} \begin{pmatrix} j & j_1 & j_2 \\ -m & m_1 & m_2 \end{pmatrix} \\ &= (-1)^{-2j_1+j_2+j-m_2-m} \sqrt{\frac{2j+1}{2j_2+1}} \langle j - m j_1 m_1 | j_2 - m_2 \rangle. \end{aligned} \quad (\text{A.2.18})$$

### A.2.3 Wigner 6- $j$ symbol

Wigner 6- $j$  symbols are defined as

$$\left\{ \begin{matrix} j_1 & j_2 & j_{12} \\ j_3 & j & j_{23} \end{matrix} \right\} = \frac{(-1)^{j_1+j_2+j_3+j}}{\sqrt{(2j_{12}+1)(2j_{23}+1)}} \langle (j_1 j_2) j_{12} j_3 j | j_1 (j_2 j_3) j_{23} j \rangle. \quad (\text{A.2.19})$$

Since the phase of  $(-1)^{j_1+j_2+j_3+j}$  should be an integer, the inverse transformation is given as

$$\begin{aligned} & \langle (j_1 j_2) j_{12} j_3 j | j_1 (j_2 j_3) j_{23} j \rangle \\ &= (-1)^{j_1+j_2+j_3+j} \sqrt{(2j_{12}+1)(2j_{23}+1)} \left\{ \begin{matrix} j_1 & j_2 & j_{12} \\ j_3 & j & j_{23} \end{matrix} \right\}. \end{aligned} \quad (\text{A.2.20})$$

The unitary nature of

$$\begin{aligned} & \sum_{j_{23}} \langle (j_1 j_2) j_{12} j_3 J | j_1 (j_2 j_3) j_{23} J \rangle \langle j_1 (j_2 j_3) j_{23} J | j_2 (j_3 j_1) j_{31} J \rangle \\ &= \langle (j_1 j_2) j_{12} j_3 J | j_2 (j_3 j_1) j_{31} J \rangle \end{aligned} \quad (\text{A.2.21})$$

gives the unitary properties for the 6- $j$  symbols as

$$\begin{aligned} \sum_{j_{23}} (-1)^{j_{12}+j_{23}+j_{31}} (2j_{23} + 1) \begin{Bmatrix} j_1 & j_2 & j_{12} \\ j_3 & j & j_{23} \end{Bmatrix} \begin{Bmatrix} j_2 & j_3 & j_{23} \\ j_1 & j & j_{31} \end{Bmatrix} \\ = \begin{Bmatrix} j_3 & j_1 & j_{31} \\ j_2 & j & j_{12} \end{Bmatrix}. \end{aligned} \quad (\text{A.2.22})$$

Similar arguments give sum rules as

$$\sum_J (-1)^{j_1+j_2+J} (2J + 1) \begin{Bmatrix} j_1 & j_1 & J' \\ j_2 & j_2 & J \end{Bmatrix} = \sqrt{(2j_1 + 1)(2j_2 + 1)} \delta_{J'0}, \quad (\text{A.2.23})$$

$$\sum_J (2J + 1) \begin{Bmatrix} j_1 & j_2 & J' \\ j_1 & j_2 & J \end{Bmatrix} = (-1)^{2(j_1+j_2)}, \quad (\text{A.2.24})$$

$$\sum_J (-1)^{2J} (2J + 1) \begin{Bmatrix} j_1 & j_2 & J \\ j_1 & j_2 & J' \end{Bmatrix} = 1. \quad (\text{A.2.25})$$

The 6- $j$  symbols are invariant by any permutation of columns

$$\begin{aligned} \begin{Bmatrix} j_1 & j_2 & j_3 \\ j_4 & j_5 & j_6 \end{Bmatrix} &= \begin{Bmatrix} j_3 & j_1 & j_2 \\ j_6 & j_4 & j_5 \end{Bmatrix} = \begin{Bmatrix} j_2 & j_3 & j_1 \\ j_5 & j_6 & j_4 \end{Bmatrix} \\ &= \begin{Bmatrix} j_2 & j_1 & j_3 \\ j_5 & j_4 & j_6 \end{Bmatrix} = \begin{Bmatrix} j_1 & j_3 & j_2 \\ j_4 & j_6 & j_5 \end{Bmatrix} = \begin{Bmatrix} j_3 & j_2 & j_1 \\ j_6 & j_5 & j_4 \end{Bmatrix}, \end{aligned} \quad (\text{A.2.26})$$

and against interchanges of the upper and lower arguments in each of any two columns, e.g.

$$\begin{Bmatrix} j_1 & j_2 & j_3 \\ j_4 & j_5 & j_6 \end{Bmatrix} = \begin{Bmatrix} j_1 & j_5 & j_6 \\ j_4 & j_2 & j_3 \end{Bmatrix}. \quad (\text{A.2.27})$$

If  $j_{23} = 0$  in the definition, the 6- $j$  symbols can be reduced as

$$\begin{Bmatrix} j_1 & j_2 & j_{12} \\ j_3 & j & 0 \end{Bmatrix} = \delta_{j_1,j} \delta_{j_2,j_3} \begin{Bmatrix} j_1 & j_2 & j_{12} \\ j_2 & j_1 & 0 \end{Bmatrix} = \delta_{j_1,j} \delta_{j_2,j_3} \frac{(-1)^{j_1+j_2+j_{12}}}{\sqrt{(2j_1+1)(2j_2+1)}}. \quad (\text{A.2.28})$$

#### A.2.4 Wigner 9- $j$ symbol

The 9- $j$  symbol is defined by the relation of

$$\begin{aligned} \langle (j_1 j_2) j_{12}, (j_3 j_4) j_{34}, J | (j_1 j_3) j_{13}, (j_2 j_4) j_{24}, J \rangle \\ = \sqrt{(2j_{12} + 1)(2j_{34} + 1)(2j_{13} + 1)(2j_{24} + 1)} \begin{Bmatrix} j_1 & j_2 & j_{12} \\ j_3 & j_4 & j_{34} \\ j_{13} & j_{24} & J \end{Bmatrix}. \end{aligned} \quad (\text{A.2.29})$$

The 9- $j$  symbols are invariant under the transposition as

$$\begin{Bmatrix} j_1 & j_2 & j_3 \\ k_1 & k_2 & k_3 \\ l_1 & l_2 & l_3 \end{Bmatrix} = \begin{Bmatrix} j_1 & k_1 & l_1 \\ j_2 & k_2 & l_2 \\ j_3 & k_3 & l_3 \end{Bmatrix}, \quad (\text{A.2.30})$$

and have cyclic symmetry properties both for column and row as

$$\begin{Bmatrix} j_1 & j_2 & j_3 \\ k_1 & k_2 & k_3 \\ l_1 & l_2 & l_3 \end{Bmatrix} = \begin{Bmatrix} k_1 & k_2 & k_3 \\ l_1 & l_2 & l_3 \\ j_1 & j_2 & j_3 \end{Bmatrix} = \begin{Bmatrix} j_2 & j_3 & j_1 \\ k_2 & k_3 & k_1 \\ l_2 & l_3 & l_1 \end{Bmatrix}, \quad (\text{A.2.31})$$

which are deduced from the property under an exchange of any two columns or rows as

$$\begin{Bmatrix} j_1 & j_2 & j_3 \\ k_1 & k_2 & k_3 \\ l_1 & l_2 & l_3 \end{Bmatrix} = (-1)^{j_1+j_2+j_3+k_1+k_2+k_3+l_1+l_2+l_3} \begin{Bmatrix} k_1 & k_2 & k_3 \\ j_1 & j_2 & j_3 \\ l_1 & l_2 & l_3 \end{Bmatrix}. \quad (\text{A.2.32})$$

If  $J = 0$ , the 9- $j$  symbols can be reduced to the 6- $j$  symbols as

$$\begin{aligned} \begin{Bmatrix} j_1 & j_2 & j_{12} \\ j_3 & j_4 & j_{34} \\ j_{13} & j_{24} & 0 \end{Bmatrix} &= \delta_{j_{12},j_{34}} \delta_{j_{13},j_{24}} \frac{(-1)^{j_{12}+j_{13}+j_2+j_3}}{\sqrt{(2j_{12}+1)(2j_{13}+1)}} \begin{Bmatrix} j_1 & j_2 & j_{12} \\ j_4 & j_3 & j_{13} \end{Bmatrix}, \\ \begin{Bmatrix} j_1 & j_2 & j_{12} \\ j_3 & j_4 & j_{34} \\ 0 & 0 & 0 \end{Bmatrix} &= \delta_{j_{12},j_{34}} \delta_{j_1,j_3} \delta_{j_2,j_4} \frac{(-1)^{j_{12}+j_1+j_2}}{\sqrt{2j_{12}+1}} \begin{Bmatrix} j_1 & j_2 & j_{12} \\ j_2 & j_1 & 0 \end{Bmatrix} \\ &= \delta_{j_{12},j_{34}} \delta_{j_1,j_3} \delta_{j_2,j_4} \frac{(-1)^{2(j_1+j_2+j_{12})}}{\sqrt{(2j_1+1)(2j_2+1)(2j_{12}+1)}}. \end{aligned} \quad (\text{A.2.33})$$

## A.3 Representations of Rotations

### A.3.1 Wigner $D$ -matrix

The rotation operators with finite angles are generated through the  $SU(2)$  operator  $\mathbf{J}$  as

$$D(\alpha, \beta, \gamma) = e^{i\gamma J_z} e^{i\beta J_y} e^{i\alpha J_z}, \quad (\text{A.3.1})$$

where  $(\alpha, \beta, \gamma)$  indicate a set of the Euler angles. The matrix elements of a rotation operator  $D(\alpha, \beta, \gamma)$  are symbolized as

$$\mathcal{D}_{m',m}^{(j)}(\alpha, \beta, \gamma) \equiv \langle jm' | D(\alpha, \beta, \gamma) | jm \rangle, \quad (\text{A.3.2})$$

and the corresponding matrix is called Wigner  $D$ -matrix. Wigner  $d$ -matrix defined through the  $D$ -matrix as

$$d_{m',m}^{(j)}(\beta) \equiv \mathcal{D}_{m',m}^{(j)}(0, \beta, 0). \quad (\text{A.3.3})$$

is also useful. In the representation where  $J_z$  is diagonal, the  $D$ -matrix is written as

$$\mathcal{D}_{m',m}^{(j)}(\alpha, \beta, \gamma) \equiv e^{im'\gamma} d_{m',m}^{(j)}(\beta) e^{im\alpha}. \quad (\text{A.3.4})$$

Since the simplest representation of  $j = 1/2$  is given by

$$J_x = \frac{1}{2} \begin{pmatrix} 0 & 1 \\ 1 & 0 \end{pmatrix}, \quad J_y = \frac{1}{2} \begin{pmatrix} 0 & -i \\ i & 0 \end{pmatrix}, \quad J_z = \frac{1}{2} \begin{pmatrix} 1 & 0 \\ 0 & -1 \end{pmatrix}, \quad (\text{A.3.5})$$

the  $d$ -matrix is given as

$$d^{(j=1/2)}(\beta) = \begin{pmatrix} \cos \frac{\beta}{2} & \sin \frac{\beta}{2} \\ -\sin \frac{\beta}{2} & \cos \frac{\beta}{2} \end{pmatrix}. \quad (\text{A.3.6})$$

Here, we express the eigenfunctions by independent variables

$$\chi_{\uparrow} \equiv |j = \frac{1}{2}, m = \frac{1}{2}\rangle, \quad \chi_{\downarrow} \equiv |j = \frac{1}{2}, m = -\frac{1}{2}\rangle, \quad (\text{A.3.7})$$

and the differential operators are defined as

$$\partial_{\uparrow} \equiv \frac{\partial}{\partial \chi_{\uparrow}}, \quad \partial_{\downarrow} \equiv \frac{\partial}{\partial \chi_{\downarrow}}. \quad (\text{A.3.8})$$

In this expression, the angular momentum operators are given as

$$\begin{aligned} J_x &= \frac{1}{2} (\chi_{\downarrow} \partial_{\uparrow} + \chi_{\uparrow} \partial_{\downarrow}), & J_y &= \frac{i}{2} (\chi_{\downarrow} \partial_{\uparrow} - \chi_{\uparrow} \partial_{\downarrow}), & J_z &= \frac{1}{2} (\chi_{\uparrow} \partial_{\uparrow} - \chi_{\downarrow} \partial_{\downarrow}), \\ J_+ &= \frac{1}{2} \chi_{\uparrow} \partial_{\downarrow}, & J_- &= \frac{1}{2} \chi_{\downarrow} \partial_{\uparrow}, \\ \mathbf{J}^2 &= j(j+1), & j &= \frac{1}{2} (\chi_{\uparrow} \partial_{\uparrow} + \chi_{\downarrow} \partial_{\downarrow}). \end{aligned} \quad (\text{A.3.9})$$

This expression leads to a useful way of representing the normalized eigenvectors of the angular momentum as

$$u(j, m) = \frac{\chi_{\uparrow}^{j+m} \chi_{\downarrow}^{j-m}}{\sqrt{(j+m)!(j-m)!}}, \quad (\text{A.3.10})$$

where the eigenvalues of  $\mathbf{J}^2$  and  $J_z$  are  $j(j+1)$  and  $m$ , respectively. The products mean the direct products of spinors and this representation is called spinor representations. Finite rotations are represented as

$$e^{i\beta J_y} = \begin{pmatrix} \cos \frac{\beta}{2} & \sin \frac{\beta}{2} \\ -\sin \frac{\beta}{2} & \cos \frac{\beta}{2} \end{pmatrix}, \quad (\text{A.3.11})$$

so that the generating function of the  $d$ -matrix is derived as

$$\begin{aligned} D(0, \beta, 0)u(j, m) &= \frac{\left(\chi_{\uparrow} \cos \frac{\beta}{2} - \chi_{\downarrow} \sin \frac{\beta}{2}\right)^{j+m} \left(\chi_{\uparrow} \sin \frac{\beta}{2} + \chi_{\downarrow} \cos \frac{\beta}{2}\right)^{j-m}}{\sqrt{(j+m)!(j-m)!}} \equiv g_d(\chi_{\uparrow}, \chi_{\downarrow}) \\ &= \sum_{m'} \frac{\chi_{\uparrow}^{j+m'} \chi_{\downarrow}^{j-m'}}{\sqrt{(j+m')!(j-m')!}} d_{m'm}^{(j)}(\beta). \end{aligned} \quad (\text{A.3.12})$$

Expanding the generating function with  $\chi_\uparrow$  and  $\chi_\downarrow$ ,

$$\begin{aligned}
gd(\chi_\uparrow, \chi_\downarrow) &= \frac{1}{\sqrt{(j+m)!(j-m)!}} \sum_{kn} \binom{j+m}{j+m-k} \binom{j-m}{n} \\
&\quad \times (-1)^{j+m-k} \left(\cos \frac{\beta}{2}\right)^{k+n} \left(\sin \frac{\beta}{2}\right)^{2j-k-n} \chi_\uparrow^{j-m+k-n} \chi_\downarrow^{j+m-k+n} \\
&= \frac{1}{\sqrt{(j+m)!(j-m)!}} \sum_{m'n} \binom{j+m}{j-m'-n} \binom{j-m}{n} \\
&\quad \times (-1)^{j-m'-n} \left(\cos \frac{\beta}{2}\right)^{2n+m'+m} \left(\sin \frac{\beta}{2}\right)^{2j-2n-m'-m} \chi_\uparrow^{j+m'} \chi_\downarrow^{j-m'}, \quad (\text{A.3.13})
\end{aligned}$$

where  $m' = k - m - n$ , the Wigner  $d$ -matrix is explicitly given as

$$\begin{aligned}
d_{m'm}^{(j)}(\beta) &= \sqrt{\frac{(j+m')!(j-m')!}{(j+m)!(j-m)!}} \sum_n \binom{j+m}{j-m'-n} \binom{j-m}{n} \\
&\quad \times (-1)^{j-m'-n} \left(\cos \frac{\beta}{2}\right)^{2n+m'+m} \left(\sin \frac{\beta}{2}\right)^{2j-2n-m'-m}. \quad (\text{A.3.14})
\end{aligned}$$

Thus, it can be concluded that the  $d$ -matrix is real.

### A.3.2 The symmetries of the $d$ -matrix and the $D$ -matrix

It is easily shown from Eq. (A.3.12) that

$$d_{m'm}^{(j)}(\pi) = (-1)^{j+m} \delta_{m,-m'}, \quad d_{m'm}^{(j)}(-\pi) = (-1)^{j-m} \delta_{m,-m'}, \quad (\text{A.3.15})$$

and thus, for example,

$$d_{m'm}^{(j)}(\beta - \pi) = \sum_{m''} d_{m'm''}^{(j)}(-\pi) d_{m''m}^{(j)}(\beta) = (-1)^{j+m'} d_{-m',m}(\beta). \quad (\text{A.3.16})$$

Therefore,

$$\begin{aligned}
d_{m'm}^{(j)}(\beta) &= \sum_{m''} d_{m'm''}^{(j)}(\beta + \pi) d_{m''m}^{(j)}(-\pi) = (-1)^{j-m} d_{m',-m}^{(j)}(\beta + \pi) \\
&= (-1)^{m'-m} d_{-m',-m}^{(j)}(\beta). \quad (\text{A.3.17})
\end{aligned}$$

It follows from Eq. (A.3.14) that

$$d_{m'm}^{(j)}(-\beta) = d_{mm'}^{(j)}(\beta). \quad (\text{A.3.18})$$

Thus the complex conjugate of a  $D$ -matrix is given by

$$\begin{aligned}
\mathcal{D}_{m'm}^{(j)*}(\alpha, \beta, \gamma) &= e^{-im'\gamma} d_{mm'}^{(j)}(-\beta) e^{-im\alpha} = e^{-im'\gamma} d_{m'm}^{(j)}(\beta) e^{-im\alpha} = \mathcal{D}_{m'm}^{(j)}(-\alpha, \beta, -\gamma) \\
&= (-1)^{m'-m} \mathcal{D}_{-m',-m}^{(j)}(\alpha, \beta, \gamma), \quad (\text{A.3.19})
\end{aligned}$$

where Eq. (A.3.17) is utilized in the equality on the second line.

A.3.3  $D$ -matrix and orthogonal polynomials

Using Eqs. (A.1.8, A.3.14), we obtain

$$\begin{aligned} P_{l,-m}(\cos \beta) &= \frac{1}{2^l l!} (\sin \beta)^{-m} (l-m)! \sum_n \binom{l}{n+m} \binom{l}{n} (-1)^{l-n} \left(2 \cos^2 \frac{\beta}{2}\right)^{n+m} \left(2 \sin^2 \frac{\beta}{2}\right)^{l-n} \\ &= \frac{1}{l!} (l-m)! \sum_n \binom{l}{n+m} \binom{l}{n} (-1)^{l-n} \left(\cos \frac{\beta}{2}\right)^{2n+m} \left(\sin \frac{\beta}{2}\right)^{2l-2n-m}, \end{aligned} \quad (\text{A.3.20})$$

$$\begin{aligned} d_{m0}^{(l)}(\beta) &= \frac{1}{l!} \sqrt{(l+m)!(l-m)!} \sum_n \binom{l}{l-m-n} \binom{l}{n} \\ &\quad \times (-1)^{l-m-n} \left(\cos \frac{\beta}{2}\right)^{2n+m} \left(\sin \frac{\beta}{2}\right)^{2l-2n-m}, \end{aligned} \quad (\text{A.3.21})$$

and then

$$d_{m0}^{(l)}(\beta) = \sqrt{\frac{(l+m)!}{(l-m)!}} (-1)^m P_{l,-m}(\cos \beta) = \sqrt{\frac{(l-m)!}{(l+m)!}} P_{l,m}(\cos \beta), \quad (\text{A.3.22})$$

where Eq. (A.1.9) is utilized in the second equality.

It follows from Eqs. (A.3.4), (A.3.22), and (A.1.11) that

$$\mathcal{D}_{m0}^{(l)}(\alpha, \beta, \gamma) = (-1)^m \sqrt{\frac{4\pi}{2l+1}} Y_{lm}(\beta, \gamma) \quad (\text{A.3.23})$$

$$\mathcal{D}_{0m}^{(l)}(\alpha, \beta, \gamma) = \sqrt{\frac{4\pi}{2l+1}} Y_{lm}(\beta, \alpha) \quad (\text{A.3.24})$$

$$\mathcal{D}_{00}^{(l)}(\alpha, \beta, \gamma) = P_l(\cos \beta). \quad (\text{A.3.25})$$

Using the definition of the 3- $j$  symbols (A.2.13) and Eq. (A.3.19), the products of  $D$ -matrices are given by

$$\begin{aligned} &\mathcal{D}_{m'_1 m_1}^{(j_1)}(\omega) \mathcal{D}_{m'_2 m_2}^{(j_2)}(\omega) \\ &= \langle j_1 m'_1 | D(\omega) | j_1 m_1 \rangle \langle j_2 m'_2 | D(\omega) | j_2 m_2 \rangle \\ &= \sum_{jm'm} \langle j_1 m'_1 j_2 m'_2 | jm'm \rangle \langle j_1 m_1 j_2 m_2 | jm'm \rangle \mathcal{D}_{m',m}^{(j)}(\omega) \\ &= \sum_{jm'm} (-1)^{-2j_1+2j_2-m-m'} (2j+1) \begin{pmatrix} j_1 & j_2 & j \\ m'_1 & m'_2 & -m' \end{pmatrix} \begin{pmatrix} j_1 & j_2 & j \\ m_1 & m_2 & -m \end{pmatrix} \mathcal{D}_{m',m}^{(j)}(\omega) \\ &= \sum_{jm'm} (-1)^{-2j_1+2j_2-2m} (2j+1) \begin{pmatrix} j_1 & j_2 & j \\ m'_1 & m'_2 & -m' \end{pmatrix} \begin{pmatrix} j_1 & j_2 & j \\ m_1 & m_2 & -m \end{pmatrix} \mathcal{D}_{-m',-m}^{(j)*}(\omega) \\ &= \sum_{jm'm} (2j+1) \begin{pmatrix} j_1 & j_2 & j \\ m'_1 & m'_2 & m' \end{pmatrix} \begin{pmatrix} j_1 & j_2 & j \\ m_1 & m_2 & m \end{pmatrix} \mathcal{D}_{m',m}^{(j)*}(\omega). \end{aligned} \quad (\text{A.3.26})$$

It follows from Eq. (A.1.14) that

$$\begin{aligned} P_{j-m'}^{(m'-m, m'+m)}(\cos \beta) &= \sum_{\nu=0}^{j-m'} \binom{j-m}{\nu} \binom{j+m}{j-m'-\nu} (-1)^{j-m'-\nu} \left(\sin \frac{\beta}{2}\right)^{2j-2m'-2\nu} \left(\cos \frac{\beta}{2}\right)^{2\nu} \end{aligned} \quad (\text{A.3.27})$$

Comparing with Eq. (A.3.14), we obtain

$$d_{m'm}^{(j)}(\beta) = \sqrt{\frac{(j+m')!(j-m')!}{(j+m)!(j-m)!}} \left(\cos \frac{\beta}{2}\right)^{m'+m} \left(\sin \frac{\beta}{2}\right)^{m'-m} P_{j-m'}^{(m'-m, m'+m)}(\cos \beta). \quad (\text{A.3.28})$$

### A.3.4 Integrals involving $D$ -matrix

The  $D$ -matrix follows the orthogonality as

$$\begin{aligned} \frac{1}{8\pi^2} \int_0^{2\pi} \int_0^\pi \int_0^{2\pi} d\alpha \sin \beta d\beta d\gamma \mathcal{D}_{m'_1, m_1}^{(j_1)*}(\alpha, \beta, \gamma) \mathcal{D}_{m'_2, m_2}^{(j_2)}(\alpha, \beta, \gamma) \\ = \delta_{j_1 j_2} \delta_{m'_1 m'_2} \delta_{m_1 m_2} \frac{1}{2j_1 + 1}. \end{aligned} \quad (\text{A.3.29})$$

Combining this result and the products of  $D$ -matrices given in Eq. (A.3.26),

$$\begin{aligned} \frac{1}{8\pi^2} \int_0^{2\pi} \int_0^\pi \int_0^{2\pi} d\alpha \sin \beta d\beta d\gamma \mathcal{D}_{m'_1, m_1}^{(j_1)}(\alpha, \beta, \gamma) \mathcal{D}_{m'_2, m_2}^{(j_2)}(\alpha, \beta, \gamma) \mathcal{D}_{m'_3, m_3}^{(j_3)}(\alpha, \beta, \gamma) \\ = \begin{pmatrix} j_1 & j_2 & j_3 \\ m'_1 & m'_2 & m'_3 \end{pmatrix} \begin{pmatrix} j_1 & j_2 & j_3 \\ m_1 & m_2 & m_3 \end{pmatrix} \end{aligned} \quad (\text{A.3.30})$$

is obtained. Thus, Eq. (A.3.25) is applied, in which  $m'_1 = m'_2 = m'_3 = 0$ , to give

$$\begin{aligned} \frac{1}{8\pi^2} \int_0^{2\pi} \int_0^\pi \sin \theta d\theta d\phi Y_{l_1 m_1}(\theta, \phi) Y_{l_2 m_2}(\theta, \phi) Y_{l_3 m_3}(\theta, \phi) \\ = \sqrt{\frac{(2l_1 + 1)(2l_2 + 1)(2l_3 + 1)}{4\pi}} \begin{pmatrix} l_1 & l_2 & l_3 \\ 0 & 0 & 0 \end{pmatrix} \begin{pmatrix} l_1 & l_2 & l_3 \\ m_1 & m_2 & m_3 \end{pmatrix}. \end{aligned} \quad (\text{A.3.31})$$

## A.4 Tensor Operators

### A.4.1 Definition of Irreducible Tensor Operator

The rotation operator with respect to a set of Euler angles  $\omega = \{\alpha, \beta, \gamma\}$  is given as

$$D(\omega) \equiv D(\alpha, \beta, \gamma) = e^{i\gamma J_z} e^{i\beta J_y} e^{i\alpha J_z}. \quad (\text{A.4.1})$$

The representations of rotation operators in terms of  $|jm\rangle$ , which are eigenvectors of the angular momentum operators  $\mathbf{J}^2$  and  $J_z$  with eigenvalues of  $j$  and  $m$ , respectively, are given as

$$\mathcal{D}_{m'm}^{(j)}(\omega) = \langle jm' | D(\omega) | jm \rangle. \quad (\text{A.4.2})$$

Thus,

$$D(\omega)|jm\rangle = \sum_{m'} |jm'\rangle \langle jm'|D(\omega)|jm\rangle = \sum_{m'} \mathcal{D}_{m'm}^{(j)}(\omega)|jm'\rangle. \quad (\text{A.4.3})$$

The irreducible tensor operator (ITO)  $T^{(k)}$ , which is a set of  $2k + 1$  operators  $T_q^{(k)}$  ( $q = -k, -k + 1, \dots, k - 1, k$ ), is defined by the property of the transformation under rotations of the frame of coordinates as

$$D(\omega)T_q^{(k)}D^{-1}(\omega) = \sum_{q'=-k}^k T_{q'}^{(k)}\mathcal{D}_{q'q}^{(k)}(\omega). \quad (\text{A.4.4})$$

The Hermite conjugate of the definition (A.4.4) is

$$D(\omega)T_q^{(k)\dagger}D^{-1}(\omega) = \sum_{q'} T_{q'}^{(k)\dagger}\mathcal{D}_{q'q}^{(k)*}(\omega) = \sum_{q'} T_{q'}^{(k)\dagger}(-1)^{q'-q}\mathcal{D}_{-q'-q}^{(k)}(\omega). \quad (\text{A.4.5})$$

Here, the complex conjugate of the  $D$ -matrix is given in Eq. (A.3.19). It can be shown from this equation that  $\tilde{T}_q^{(k)} \equiv (-1)^{k-q}T_{-q}^{(k)\dagger}$  satisfies the definition of the ITO as

$$D(\omega)(-1)^{k-q}T_{-q}^{(k)\dagger}D^{-1}(\omega) = (-1)^k \sum_{q'} T_{-q'}^{(k)\dagger}(-1)^{-q'}\mathcal{D}_{q'q}^{(k)}(\omega). \quad (\text{A.4.6})$$

The particle creation operator  $c_{jm}^\dagger$  is one of the ITOs. That acts on the vacuum to create an eigenstate of  $\mathbf{J}^2$  and  $J_z$  as

$$c_{jm}^\dagger|0\rangle = |jm\rangle, \quad (\text{A.4.7})$$

so that

$$D(\omega)c_{jm}^\dagger|0\rangle = \sum_{m'} |jm'\rangle \langle jm'|D(\omega)|jm\rangle = \sum_{m'} \mathcal{D}_{m'm}^{(j)}c_{jm'}^\dagger|0\rangle. \quad (\text{A.4.8})$$

If ITOs are operated on the eigenvectors of  $\mathbf{J}^2$  and  $J_z$ , we have

$$D(\omega)T_q^{(k)}|jm\rangle = \sum_{q'm'} \mathcal{D}_{q'q}^{(k)}(\omega)\mathcal{D}_{m'm}^{(j)}(\omega)T_{q'}^{(k)}|jm'\rangle. \quad (\text{A.4.9})$$

This means that the vector  $T_q^{(k)}|jm\rangle$  is transformed as the product representation  $\mathcal{D}^{(k)} \otimes \mathcal{D}^{(j)}$  of the rotation group.

The annihilation operator  $\tilde{c}_{jm} = (-1)^{j-m}c_{j-m}$  is another ITO, which is shown by taking the conjugate of this relation as

$$\begin{aligned} \langle 0|c_{jm}D^\dagger(\omega) &= \sum_{m'} \langle jm|D^\dagger(\omega)|jm'\rangle \langle jm'| = \langle 0|\sum_{m'} c_{jm'}\mathcal{D}_{m'm}^{(j)*}(\omega) \\ &= \langle 0|\sum_{m'} c_{jm'}(-1)^{m'-m}\mathcal{D}_{-m'-m}^{(j)}(\omega). \end{aligned} \quad (\text{A.4.10})$$

In fact, it follows that

$$\langle 0 | \tilde{c}_{jm} D^\dagger(\omega) = \sum_{m'} \langle 0 | \tilde{c}_{jm'} \mathcal{D}_{m'm}^{(j)}(\omega). \quad (\text{A.4.11})$$

The inverted expression is given as

$$c_{jm} = (-1)^{j+m} \tilde{c}_{j-m}. \quad (\text{A.4.12})$$

A non-relativistic wavefunction is represented as

$$\phi_{nljm}(\mathbf{r}) = \langle \mathbf{r} | nljm \rangle = i^l R_{nl}(r) \sum_{m_l m_s} \langle l m_l \frac{1}{2} m_s | j m \rangle Y_{lm_l}(\theta, \phi) \chi_{m_s}. \quad (\text{A.4.13})$$

The time-reversal of the single-particle wavefunction is given by multiplying the operator  $K$  taking the complex conjugate and the unitary operator

$$i\sigma_2 = e^{-i\pi\sigma_2} \quad (\text{A.4.14})$$

in this order as shown in § XX. That can be explicitly given as

$$\begin{aligned} \phi'_{nljm}(\mathbf{r}) &= T \phi_{nljm}(\mathbf{r}) \\ &= (-i)^l R_{nl}(r) \sum_{m_l m_s} (-1)^{-m_l} (-1)^{-\frac{1}{2}-m_s} \langle l m_l \frac{1}{2} m_s | j m \rangle Y_{l, -m_l}(\theta, \phi) \chi_{-m_s} \\ &= (-1)^{l-m-\frac{1}{2}} (-1)^{l+\frac{1}{2}-j} \phi_{nlj, -m}(\mathbf{r}) \\ &= (-1)^{j+m} \phi_{nlj, -m}(\mathbf{r}) \end{aligned} \quad (\text{A.4.15})$$

where  $Y_{lm_l}^*(\theta, \phi) = (-1)^{-m_l} Y_{l, -m_l}(\theta, \phi)$  and  $i\sigma_2 \chi_{m_s} = (-1)^{-\frac{1}{2}-m_s} \chi_{-m_s}$  are used. For the many-particle system,

#### A.4.2 Products of Irreducible Tensor Operators

Tensor products of two ITOs are given by

$$T_q^{(k)} = \left[ T^{(k_1)} \otimes T^{(k_2)} \right]_q^{(k)} \equiv \sum_{q_1 q_2} T_{q_1}^{(k_1)} T_{q_2}^{(k_2)} \langle k_1 q_1 k_2 q_2 | k q \rangle. \quad (\text{A.4.16})$$

The scalar product is defined by

$$T^{(k)} \cdot T^{(k)} \equiv \sum_q (-1)^q T_q^{(k)} T_{-q}^{(k)}, \quad (\text{A.4.17})$$

which is related to a tensor product as

$$T^{(k)} \cdot T^{(k)} = (-1)^{-k} \sqrt{2k+1} \left[ T^{(k)} \otimes T^{(k)} \right]_0^{(0)}. \quad (\text{A.4.18})$$

The inverse transformation to Eq. (A.4.16) is derived from the unitary properties of the CG coefficients in Eq. (A.2.6) as

$$\begin{aligned} \sum_{kq} T_q^{(k)} \langle kq | k_1 q_1 k_2 q_2 \rangle &= \sum_{kq} \sum_{q'_1 q'_2} T_{q'_1}^{(k_1)} T_{q'_2}^{(k_2)} \langle k_1 q'_1 k_2 q'_2 | kq \rangle \langle kq | k_1 q_1 k_2 q_2 \rangle \\ &= T_{q_1}^{(k_1)} T_{q_2}^{(k_2)} \end{aligned} \quad (\text{A.4.19})$$

The propagators of the ITO products are given as

$$\begin{aligned} \langle 0 | T_{q_1}^{(k_1)} T_{q_2}^{(k_2)} | 0 \rangle &= \delta_{k_1, k_2} \delta_{q_1, -q_2} \sum_{q'} \langle 0 | T_{q'}^{(k)} T_{-q'}^{(k)} | 0 \rangle \langle k_1 q' k_1 - q' | 00 \rangle \langle 00 | k_1 q_1 k_1 - q_1 \rangle \\ &= \delta_{k_1, k_2} \delta_{q_1, -q_2} \frac{(-1)^{k_1 - q_1}}{\sqrt{2k_1 + 1}} \langle 0 | [T^{(k)} \otimes T^{(k)}]_0^{(0)} | 0 \rangle, \end{aligned} \quad (\text{A.4.20})$$

where the condition of  $k = q = 0$  reflects the rotational symmetry of the vacuum.

The recouplings of ITOs can be obtained by using a symmetric property in Eq. (A.2.11) as

$$\left[ T^{(k_1)} \otimes T^{(k_2)} \right]_Q^{(K)} = (-1)^{k_1 + k_2 - K} \left[ T^{(k_2)} \otimes T^{(k_1)} \right]_Q^{(K)}, \quad (\text{A.4.21})$$

and then two single ITOs of rank  $k$  can be recoupled as

$$\left[ T^{(k)} \otimes T^{(k)} \right]_Q^{(K)} = (-1)^K \left[ T^{(k)} \otimes T^{(k)} \right]_Q^{(K)}, \quad (\text{A.4.22})$$

and then odd  $K$  terms should be vanished.

For the recouplings of three ITOs, using the 6- $j$  symbols, we get

$$\begin{aligned} &\left[ \left[ T^{(k_1)} \otimes T^{(k_2)} \right]^{(k_{12})} \otimes T^{(k_3)} \right]_Q^{(K)} \\ &= \sum_{k_{23}} (-1)^{k_1 + k_2 + k_3 + K} \sqrt{(2k_{12} + 1)(2k_{23} + 1)} \left\{ \begin{array}{ccc} k_1 & k_2 & k_{12} \\ k_3 & K & k_{23} \end{array} \right\} \\ &\quad \times \left[ T^{(k_1)} \otimes \left[ T^{(k_2)} \otimes T^{(k_3)} \right]^{(k_{23})} \right]_Q^{(K)}. \end{aligned} \quad (\text{A.4.23})$$

This transformation and the inverse transformation are discovered by using the 9- $j$  symbols as

$$\begin{aligned} &\left[ \left[ T^{(k_1)} \otimes T^{(k_2)} \right]^{(k_{12})} \otimes T^{(k_3)} \right]_Q^{(K)} \\ &= \left[ \left[ T^{(k_1)} \otimes T^{(k_2)} \right]^{(k_{12})} \otimes \left[ 1 \otimes T^{(k_3)} \right]^{(k_3)} \right]_Q^{(K)} \\ &= \sum_{k_{23}} \sqrt{(2k_{12} + 1)(2k_3 + 1)(2k_1 + 1)(2k_{23} + 1)} \left\{ \begin{array}{ccc} k_1 & k_2 & k_{12} \\ 0 & k_3 & k_3 \\ k_1 & k_{23} & K \end{array} \right\} \\ &\quad \times \left[ \left[ T^{(k_1)} \otimes 1 \right]^{(k_1)} \otimes \left[ T^{(k_2)} \otimes T^{(k_3)} \right]^{(k_{23})} \right]_Q^{(K)} \end{aligned}$$

$$\begin{aligned}
&= \sum_{k_{23}} (-1)^{k_1+k_2+k_3+K} \sqrt{(2k_{12}+1)(2k_{23}+1)} \left\{ \begin{matrix} k_{23} & K & k_1 \\ k_{12} & k_2 & k_3 \end{matrix} \right\} \\
&\quad \times \left[ \left[ T^{(k_1)} \otimes 1 \right]^{(k_1)} \otimes \left[ T^{(k_2)} \otimes T^{(k_3)} \right]^{(k_{23})} \right]_Q^{(K)} \\
&= \sum_{k_{23}} (-1)^{k_1+k_2+k_3+K} \sqrt{(2k_{12}+1)(2k_{23}+1)} \left\{ \begin{matrix} k_1 & k_2 & k_{12} \\ k_3 & K & k_{23} \end{matrix} \right\} \\
&\quad \times \left[ T^{(k_1)} \otimes \left[ T^{(k_2)} \otimes T^{(k_3)} \right]^{(k_{23})} \right]_Q^{(K)}, \tag{A.4.24}
\end{aligned}$$

$$\begin{aligned}
&\left[ T^{(k_1)} \otimes \left[ T^{(k_2)} \otimes T^{(k_3)} \right]^{(k_{23})} \right]_Q^{(K)} \\
&= \left[ \left[ T^{(k_1)} \otimes 1 \right]^{(k_1)} \otimes \left[ T^{(k_2)} \otimes T^{(k_3)} \right]^{(k_{23})} \right]_Q^{(K)} \\
&= \sum_{k_{12}} \sqrt{(2k_1+1)(2k_{23}+1)(2k_{12}+1)(2k_3+1)} \left\{ \begin{matrix} k_1 & 0 & k_1 \\ k_2 & k_3 & k_{23} \\ k_{12} & k_3 & K \end{matrix} \right\} \\
&\quad \times \left[ \left[ T^{(k_1)} \otimes T^{(k_2)} \right]^{(k_{12})} \otimes \left[ 1 \otimes T^{(k_3)} \right]^{(k_3)} \right]_Q^{(K)} \\
&= \sum_{k_{12}} (-1)^{k_1+k_2+k_3+K} \sqrt{(2k_{23}+1)(2k_{12}+1)} \left\{ \begin{matrix} k_{23} & k_2 & k_3 \\ k_{12} & K & k_1 \end{matrix} \right\} \\
&\quad \times \left[ \left[ T^{(k_1)} \otimes T^{(k_2)} \right]^{(k_{12})} \otimes \left[ 1 \otimes T^{(k_3)} \right]^{(k_3)} \right]_Q^{(K)} \\
&= \sum_{k_{12}} (-1)^{k_1+k_2+k_3+K} \sqrt{(2k_{23}+1)(2k_{12}+1)} \left\{ \begin{matrix} k_3 & k_2 & k_{23} \\ k_1 & K & k_{12} \end{matrix} \right\} \\
&\quad \times \left[ \left[ T^{(k_1)} \otimes T^{(k_2)} \right]^{(k_{12})} \otimes T^{(k_3)} \right]_Q^{(K)}. \tag{A.4.25}
\end{aligned}$$

For  $k_{12} = 0$ ,

$$\begin{aligned}
&\left[ \left[ T^{(k_1)} \otimes T^{(k_2)} \right]^{(0)} \otimes T^{(k_3)} \right]_Q^{(K)} \\
&= \delta_{k_1, k_2} \delta_{k_3, K} \sum_{k_{23}} (-1)^{2k_1+2k_3} \sqrt{2k_{23}+1} \left\{ \begin{matrix} k_1 & k_1 & 0 \\ k_3 & k_3 & k_{23} \end{matrix} \right\} \\
&\quad \times \left[ T^{(k_1)} \otimes \left[ T^{(k_1)} \otimes T^{(k_3)} \right]^{(k_{23})} \right]_Q^{(k_3)} \\
&= \delta_{k_1, k_2} \delta_{k_3, K} \sum_{k_{23}} (-1)^{3k_1+3k_3+k_{23}} \sqrt{\frac{2k_{23}+1}{(2k_1+1)(2k_3+1)}} \\
&\quad \times \left[ T^{(k_1)} \otimes \left[ T^{(k_2)} \otimes T^{(k_3)} \right]^{(k_{23})} \right]_Q^{(K)}. \tag{A.4.26}
\end{aligned}$$

For  $k_{23} = 0$ ,

$$\begin{aligned}
& \left[ T^{(k_1)} \otimes \left[ T^{(k_2)} \otimes T^{(k_3)} \right]^{(0)} \right]^{(K)} \Big|_Q \\
&= \delta_{k_2, k_3} \delta_{k_1, K} \sum_{k_{12}} (-1)^{2k_1 + 2k_2} \sqrt{2k_{12} + 1} \begin{Bmatrix} k_2 & k_2 & 0 \\ k_1 & k_1 & k_{12} \end{Bmatrix} \\
&\quad \times \left[ \left[ T^{(k_1)} \otimes T^{(k_2)} \right]^{(k_{12})} \otimes T^{(k_3)} \right]^{(k_1)} \Big|_Q \\
&= \delta_{k_2, k_3} \delta_{k_1, K} \sum_{k_{12}} (-1)^{3k_1 + 3k_2 + k_{12}} \sqrt{\frac{2k_{12} + 1}{(2k_1 + 1)(2k_2 + 1)}} \\
&\quad \times \left[ \left[ T^{(k_1)} \otimes T^{(k_2)} \right]^{(k_{12})} \otimes T^{(k_3)} \right]^{(k_1)} \Big|_Q. \tag{A.4.27}
\end{aligned}$$

For  $K = 0$ ,

$$\begin{aligned}
& \left[ \left[ T^{(k_1)} \otimes T^{(k_2)} \right]^{(k_{12})} \otimes T^{(k_3)} \right]^{(0)} \Big|_0 \\
&= \delta_{k_{12}, k_3} (-1)^{k_1 + k_2 + k_3} \sqrt{(2k_3 + 1)(2k_1 + 1)} \begin{Bmatrix} k_1 & k_2 & k_3 \\ k_3 & 0 & k_1 \end{Bmatrix} \\
&\quad \times \left[ T^{(k_1)} \otimes \left[ T^{(k_2)} \otimes T^{(k_3)} \right]^{(k_1)} \right]^{(0)} \Big|_0 \\
&= \delta_{k_{12}, k_3} (-1)^{2k_1 + 2k_2 + 2k_3} \left[ T^{(k_1)} \otimes \left[ T^{(k_2)} \otimes T^{(k_3)} \right]^{(k_1)} \right]^{(0)} \Big|_0, \tag{A.4.28}
\end{aligned}$$

and

$$\begin{aligned}
& \left[ T^{(k_1)} \otimes \left[ T^{(k_2)} \otimes T^{(k_3)} \right]^{(k_{23})} \right]^{(0)} \Big|_0 \\
&= \delta_{k_1, k_{23}} (-1)^{k_1 + k_2 + k_3} \sqrt{(2k_1 + 1)(2k_3 + 1)} \begin{Bmatrix} k_3 & k_2 & k_1 \\ k_1 & 0 & k_3 \end{Bmatrix} \\
&\quad \times \left[ \left[ T^{(k_1)} \otimes T^{(k_2)} \right]^{(k_3)} \otimes T^{(k_3)} \right]^{(0)} \Big|_0 \\
&= \delta_{k_1, k_{23}} (-1)^{2k_1 + 2k_2 + 2k_3} \left[ \left[ T^{(k_1)} \otimes T^{(k_2)} \right]^{(k_3)} \otimes T^{(k_3)} \right]^{(0)} \Big|_0. \tag{A.4.29}
\end{aligned}$$

By using the 9- $j$  symbols,

$$\begin{aligned}
& \left[ \left[ T^{(k_1)} \otimes T^{(k_2)} \right]^{(k_{12})} \otimes \left[ T^{(k_3)} \otimes T^{(k_4)} \right]^{(k_{34})} \right]^{(K)} \Big|_Q \\
&= \sum_{k_{13} k_{24}} \sqrt{(2k_{12} + 1)(2k_{34} + 1)(2k_{13} + 1)(2k_{24} + 1)} \begin{Bmatrix} k_1 & k_2 & k_{12} \\ k_3 & k_4 & k_{34} \\ k_{13} & k_{24} & K \end{Bmatrix}
\end{aligned}$$

$$\times \left[ \left[ T^{(k_1)} \otimes T^{(k_3)} \right]^{(k_{13})} \otimes \left[ T^{(k_2)} \otimes T^{(k_4)} \right]^{(k_{24})} \right]_Q^{(K)}. \quad (\text{A.4.30})$$

For three single ITOs of rank 1,

$$\begin{aligned} & \left[ \left[ T^{(1)} \otimes T^{(1)} \right]^{(k_{12})} \otimes T^{(1)} \right]_Q^{(2)} \\ &= \left[ \left[ T^{(1)} \otimes T^{(1)} \right]^{(2)} \otimes T^{(1)} \right]_Q^{(2)} \delta_{k_{12},2} \\ &= -5 \begin{Bmatrix} 1 & 1 & 2 \\ 1 & 2 & 2 \end{Bmatrix} \left[ T^{(1)} \otimes \left[ T^{(1)} \otimes T^{(1)} \right]^{(2)} \right]_Q^{(2)} \\ &= 5 \begin{Bmatrix} 1 & 1 & 2 \\ 1 & 2 & 2 \end{Bmatrix} \left[ \left[ T^{(1)} \otimes T^{(1)} \right]^{(2)} \otimes T^{(1)} \right]_Q^{(2)} \\ &= -\frac{1}{2} \left[ \left[ T^{(1)} \otimes T^{(1)} \right]^{(2)} \otimes T^{(1)} \right]_Q^{(2)} \\ \therefore & \left[ \left[ T^{(1)} \otimes T^{(1)} \right]^{(2)} \otimes T^{(1)} \right]_Q^{(2)} = \left[ T^{(1)} \otimes \left[ T^{(1)} \otimes T^{(1)} \right]^{(2)} \right]_Q^{(2)} = 0. \end{aligned} \quad (\text{A.4.31})$$

### A.4.3 Spherical Tensors

The coordinate vector is expressed in the spherical coordinates  $(r, \theta, \phi)$  as

$$\mathbf{r} = \begin{pmatrix} x \\ y \\ z \end{pmatrix} = \begin{pmatrix} r \sin \theta \cos \phi \\ r \sin \theta \sin \phi \\ r \cos \theta \end{pmatrix}, \quad (\text{A.4.32})$$

and then

$$r = \sqrt{x^2 + y^2 + z^2}, \quad \tan \theta = \frac{\sqrt{x^2 + y^2}}{z}, \quad \tan \phi = \frac{y}{x}. \quad (\text{A.4.33})$$

The spherical components of  $\mathbf{r}$  are defined as

$$r_0 = z = r \cos \theta, \quad r_{\pm 1} = \mp \frac{1}{\sqrt{2}} (x \pm iy) = \mp \frac{1}{\sqrt{2}} r \sin \theta e^{\pm i\phi}, \quad (\text{A.4.34})$$

and then

$$x = -\frac{1}{\sqrt{2}} (r_{+1} - r_{-1}), \quad y = \frac{i}{\sqrt{2}} (r_{+1} + r_{-1}). \quad (\text{A.4.35})$$

The differential operator is defined in the Cartesian coordinate as

$$\begin{aligned} \frac{\partial}{\partial x} &= \sin \theta \cos \phi \frac{\partial}{\partial r} + \frac{\cos \theta \cos \phi}{r} \frac{\partial}{\partial \theta} - \frac{\sin \phi}{r \sin \theta} \frac{\partial}{\partial \phi}, \\ \frac{\partial}{\partial y} &= \sin \theta \sin \phi \frac{\partial}{\partial r} + \frac{\cos \theta \sin \phi}{r} \frac{\partial}{\partial \theta} + \frac{\cos \phi}{r \sin \theta} \frac{\partial}{\partial \phi}, \\ \frac{\partial}{\partial z} &= \cos \theta \frac{\partial}{\partial r} - \frac{\sin \theta}{r} \frac{\partial}{\partial \theta}, \end{aligned} \quad (\text{A.4.36})$$

and the spherical components are defined through

$$\mathbf{r} \cdot \nabla = r_\mu^{(1)} \nabla_\mu^{(1)} = r_0^{(1)} \nabla_0^{(1)} - r_{+1}^{(1)} \nabla_{-1}^{(1)} - r_{-1}^{(1)} \nabla_{+1}^{(1)}. \quad (\text{A.4.37})$$

The explicit forms are given as

$$\begin{aligned} \nabla_0^{(1)} &= \frac{\partial}{\partial z} = \cos \theta \frac{\partial}{\partial r} - \frac{\sin \theta}{r} \frac{\partial}{\partial \theta}, \\ \nabla_{\pm 1}^{(1)} &= -\frac{\partial}{\partial r_{\mp 1}^{(1)}} = \mp \frac{1}{\sqrt{2}} \left( \frac{\partial}{\partial x} \pm i \frac{\partial}{\partial y} \right) \\ &= \mp \frac{1}{\sqrt{2}} e^{\pm i \phi} \left( \sin \theta \frac{\partial}{\partial r} + \frac{\cos \theta}{r} \frac{\partial}{\partial \theta} \pm i \frac{1}{r \sin \theta} \frac{\partial}{\partial \phi} \right). \end{aligned} \quad (\text{A.4.38})$$

Note that the differential operator, counterpart of each spherical components of  $\mathbf{r}$ , is reversely defined in the scalar product (e.g.  $\nabla_{+1}$  corresponds to  $r_{+1}$ ). It follows the commutation relation of

$$[\nabla_\mu^{(1)}, r_\nu^{(1)}] = (-1)^\mu \delta_{\mu, -\nu}; \quad \mu, \nu = 0, \pm 1. \quad (\text{A.4.39})$$

#### A.4.4 Creation-Annihilation Operators

Let us consider multi-particle system. A two-particle system is given as

$$|\psi_{JM}^{(2)}\rangle = [c_{j_1}^\dagger \otimes c_{j_2}^\dagger]_M^{(J)} |0\rangle = \sum_{m_1 m_2} \langle j_1 m_1 j_2 m_2 | J M \rangle c_{j_1 m_1}^\dagger c_{j_2 m_2}^\dagger |0\rangle. \quad (\text{A.4.40})$$

The conjugate is

$$\begin{aligned} \langle \psi_{JM}^{(2)} | &= \langle 0 | \sum_{m_1 m_2} \langle j_1 m_1 j_2 m_2 | J M \rangle c_{j_2 m_2} c_{j_1 m_1} \\ &= (-1)^{j_1 + j_2 + M} \langle 0 | \sum_{m_1 m_2} \langle j_2 -m_2 j_1 -m_1 | J -M \rangle \tilde{c}_{j_2 -m_2} \tilde{c}_{j_1 -m_1} \\ &= (-1)^{j_1 + j_2 + M} \langle 0 | [\tilde{c}_{j_2} \otimes \tilde{c}_{j_1}]_{-M}^{(J)}. \end{aligned} \quad (\text{A.4.41})$$

A three-particle system is made of the two-particle system as

$$|\psi_{JM}^{(3)}\rangle = \left[ [c_{j_1}^\dagger \otimes c_{j_2}^\dagger]_{M_{12}}^{(J_{12})} \otimes c_{j_3}^\dagger \right]_M^{(J)} |0\rangle, \quad (\text{A.4.42})$$

and the conjugate is given as

$$\langle \psi_{JM}^{(3)} | = (-1)^{j_1 + j_2 + j_3 + M} \langle 0 | \left[ \tilde{c}_{j_3} \otimes [\tilde{c}_{j_2} \otimes \tilde{c}_{j_1}]_{-M_{12}}^{(J_{12})} \right]_{-M}^{(J)}. \quad (\text{A.4.43})$$

Similarly, the conjugate of a many-particle system, which is defined as

$$|\psi_{JM}^{(n)}\rangle = \left[ \cdots \left[ [c_{j_1}^\dagger \otimes c_{j_2}^\dagger]_{M_{12}}^{(J_{12})} \otimes c_{j_3}^\dagger \right]_{M_{123}}^{(J_{123})} \cdots \otimes c_{j_n}^\dagger \right]_M^{(J)} |0\rangle, \quad (\text{A.4.44})$$

is given as

$$\langle \psi_{JM}^{(n)} | = (-1)^{j_1+j_2+j_3+\dots+j_n+M} \langle 0 | \left[ c_{j_n}^\dagger \otimes \dots \left[ \tilde{c}_{j_3} \otimes \left[ \tilde{c}_{j_2} \otimes \tilde{c}_{j_1} \right]_{-M_{12}}^{(J_{12})} \right]_{-M_{123}}^{(J_{123})} \dots \right]_{-M}^{(J)}. \quad (\text{A.4.45})$$

The number operator in a  $j$ -shell defined by

$$N_{\tau j} = \sum_m a_{\tau j m}^\dagger a_{\tau j m}, \quad (\text{A.4.46})$$

are related as

$$\begin{aligned} \left[ \tilde{a}_{\tau j} \otimes a_{\tau j}^\dagger \right]_0^{(0)} &= \sum_m \langle j m j - m | 0 0 \rangle \tilde{a}_{\tau j m} a_{\tau j - m}^\dagger \\ &= \sum_m \langle j m j - m | 0 0 \rangle \left( (-1)^{j-m} \delta_{m, -m} - a_{\tau j - m}^\dagger \tilde{a}_{\tau j m} \right) \\ &= \sum_m \langle j - m j m | 0 0 \rangle a_{\tau j - m}^\dagger \tilde{a}_{\tau j m} \\ &= \left[ a_{\tau j}^\dagger \otimes \tilde{a}_{\tau j} \right]_0^{(0)}, \end{aligned} \quad (\text{A.4.47})$$

$$\begin{aligned} \left[ a_{\tau j}^\dagger \otimes \tilde{a}_{\tau j} \right]_0^{(0)} &= \sum_m \langle j m j - m | 0 0 \rangle a_{\tau j m}^\dagger \tilde{a}_{\tau j - m} \\ &= \sum_m \frac{(-1)^{j-m}}{\sqrt{2j+1}} a_{\tau j m}^\dagger (-1)^{j+m} a_{\tau j m} \\ &= -\frac{1}{\sqrt{2j+1}} N_{\tau j}. \end{aligned} \quad (\text{A.4.48})$$

## A.5 Matrix elements of tensor operators

### A.5.1 Wigner-Eckart Theorem

The reduced matrix elements of an irreducible tensor operator  $T^{(k)}$  are defined through the Wigner-Eckart theorem as

$$\begin{aligned} \langle j' m' | T_q^{(k)} | j m \rangle &= (-1)^{j-m} \frac{\langle j' m' j - m | k q \rangle}{\sqrt{2k+1}} \langle j' \| T^{(k)} \| j \rangle \\ &= (-1)^{k-j+j'} \frac{\langle k q j m | j' m' \rangle}{\sqrt{2j'+1}} \langle j' \| T^{(k)} \| j \rangle \\ &= (-1)^{j'-m'} \begin{pmatrix} j' & k & j \\ -m' & q & m \end{pmatrix} \langle j' \| T^{(k)} \| j \rangle. \end{aligned} \quad (\text{A.5.1})$$

Let us consider that  $k$  is an integer. If  $j'$  and  $j$  are integers, we have

$$\langle j' m' | T_q^{(k)} | j m \rangle = (-1)^m \frac{\langle j' m' j - m | k q \rangle}{\langle j' 0 j 0 | k 0 \rangle} \langle j' 0 | T_0^{(k)} | j 0 \rangle. \quad (\text{A.5.2})$$

If  $j'$  and  $j$  are half-integers, we have

$$\langle j' m' | T_q^{(k)} | j m \rangle = (-1)^m \frac{\langle j' m' j - m | k q \rangle}{\langle j' \frac{1}{2} j - \frac{1}{2} | k 0 \rangle} \langle j' \frac{1}{2} | T_0^{(k)} | j \frac{1}{2} \rangle. \quad (\text{A.5.3})$$

The unitary properties of the CG coefficients (A.2.6) enable us to get the alternative expressions as

$$\langle j' \| T^{(k)} \| j \rangle = \sqrt{2k+1} \sum_{mm'} (-1)^{j-m} \langle j' m' j - m | k q \rangle \langle j' m' | T_q^{(k)} | j m \rangle. \quad (\text{A.5.4})$$

The reduced matrix elements is computed in practice by choosing the easiest values of  $q, m, m'$  to evaluate the CG coefficients  $\langle k' q' | j' m' j - m \rangle$ . For example, the reduced matrix elements of rank-1 ITOs are computed with the use of the Wigner-Eckart theorem (A.5.1) with  $q = m = m' = 0$  as

$$\begin{aligned} \langle l' \| L^{(1)} \| l \rangle &= \sqrt{2l'+1} (-1)^{1-l+l'} \frac{\langle l' 0 | L_0^{(1)} | l 0 \rangle}{\langle 1 0 l 0 | l' 0 \rangle} = \sqrt{2l'+1} \frac{\langle l' m' | L_q^{(1)} | l m \rangle}{\langle l m 1 q | l' m' \rangle} \\ &= \delta_{ll'} \sqrt{l(l+1)(2l+1)}, \end{aligned} \quad (\text{A.5.5})$$

and

$$\begin{aligned} \langle l' \| Y^{(k)} \| l \rangle &= (-1)^{l'} \sqrt{\frac{(2l'+1)(2k+1)(2l+1)}{4\pi}} \begin{pmatrix} l' & k & l \\ 0 & 0 & 0 \end{pmatrix} \\ &= (-1)^k \sqrt{\frac{(2l'+1)(2k+1)}{4\pi}} \langle l' 0 k 0 | l 0 \rangle. \end{aligned} \quad (\text{A.5.6})$$

For the case of half-integer  $j$ , choosing  $q = 0, m = m' = \frac{1}{2}$ ,

$$\langle \frac{1}{2} \| S^{(1)} \| \frac{1}{2} \rangle = \sqrt{\frac{3}{2}}. \quad (\text{A.5.7})$$

Note that the reduced matrix elements of the identity are not one, but

$$\langle j' \| 1 \| j \rangle = \delta_{j'j} \sqrt{2j+1}. \quad (\text{A.5.8})$$

## A.5.2 Reduced matrix elements of tensor products

Let us consider tensor products of two ITOs  $T^{(k_1)}$  and  $T^{(k_2)}$ . The matrix elements are given as

$$\begin{aligned} &\langle J' M' | [T^{(k_1)} \otimes T^{(k_2)}]_Q^{(K)} | J M \rangle \\ &= \sum_{q_1 q_2} \langle k_1 q_1 k_2 q_2 | K Q \rangle \langle J' M' | T_{q_1}^{(k_1)} T_{q_2}^{(k_2)} | J M \rangle \\ &= \sum_{q_1 q_2} \langle k_1 q_1 k_2 q_2 | K Q \rangle \sum_{J'' M''} \langle J' M' | T_{q_1}^{(k_1)} | J'' M'' \rangle \langle J'' M'' | T_{q_2}^{(k_2)} | J M \rangle, \end{aligned} \quad (\text{A.5.9})$$

and the reduced matrix elements are then given by using Eq. (A.5.4) as

$$\begin{aligned}
& \left\langle J' \left\| \left[ T^{(k_1)} \otimes T^{(k_2)} \right]^{(K)} \right\| J \right\rangle \\
&= \sqrt{2K+1} \sum_{q_1 q_2} \langle k_1 q_1 k_2 q_2 | K Q \rangle \sum_{J'' M''} \sum_{M' M} (-1)^{J-M} \langle J' M' J - M | K Q \rangle \\
&\quad \times \left\langle J' M' \left| T_{q_1}^{(k_1)} \right| J'' M'' \right\rangle \left\langle J'' M'' \left| T_{q_2}^{(k_2)} \right| J M \right\rangle. \tag{A.5.10}
\end{aligned}$$

### A.5.3 Two different systems

Consider two tensor operators  $T^{(k_1)}$  and  $U^{(k_2)}$  which operate on different systems such as the orbital part associated with  $(j_1, m_1)$  and the spin part  $(j_2, m_2)$ . The reduced matrix element of a tensor product is given by using

$$\begin{aligned}
& \left\langle (j'_1 j'_2) J' M' \left| \left[ T^{(k_1)} \otimes T^{(k_2)} \right]^{(K)} \right| (j_1 j_2) J M \right\rangle \\
&= \sum_{m'_1 m'_2 m_1 m_2} \langle j'_1 m'_1 j'_2 m'_2 | J' M' \rangle \langle j_1 m_1 j_2 m_2 | J M \rangle \\
&\quad \times \left\langle j'_1 m'_1 j'_2 m'_2 \left| \left[ T^{(k_1)} \otimes T^{(k_2)} \right]^{(K)} \right| j_1 m_1 j_2 m_2 \right\rangle, \tag{A.5.11}
\end{aligned}$$

as

$$\begin{aligned}
& \left\langle (j'_1 j'_2) J' \left\| \left[ T^{(k_1)} \otimes T^{(k_2)} \right]^{(K)} \right\| (j_1 j_2) J \right\rangle \\
&= \sqrt{(2J+1)(2J'+1)(2K+1)} \begin{Bmatrix} j'_1 & j_1 & k_1 \\ j'_2 & j_2 & k_2 \\ J' & J & K \end{Bmatrix} \left\langle j'_1 \left\| T^{(k_1)} \right\| j_1 \right\rangle \left\langle j'_2 \left\| T^{(k_2)} \right\| j_2 \right\rangle. \tag{A.5.12}
\end{aligned}$$

In the case of  $U^{(k_2)} = 1$ , where  $k_1 = K$  and  $k_2 = 0$ ,

$$\begin{aligned}
& \left\langle (j'_1 j'_2) J' \left\| T^{(K)} \right\| (j_1 j_2) J \right\rangle \\
&= \delta_{j'_2 j_2} \delta_{J' J} \sqrt{(2J+1)(2J'+1)(2K+1)(2j_2+1)} \begin{Bmatrix} j'_1 & j_1 & K \\ j_2 & j_2 & 0 \\ J' & J & K \end{Bmatrix} \left\langle j'_1 \left\| T^{(K)} \right\| j_1 \right\rangle \\
&= \delta_{j'_2 j_2} \delta_{J' J} \sqrt{(2J+1)(2J'+1)(2K+1)(2j_2+1)} \\
&\quad \times \frac{(-1)^{j'_1+j_2+J+K}}{\sqrt{(2j_2+1)(2K+1)}} \begin{Bmatrix} J' & j'_1 & j_2 \\ j_1 & J & K \end{Bmatrix} \left\langle j'_1 \left\| T^{(K)} \right\| j_1 \right\rangle \\
&= \delta_{j'_2 j_2} \delta_{J' J} (-1)^{j'_1+j_2+J+K} \sqrt{(2J+1)(2J'+1)} \begin{Bmatrix} J' & j'_1 & j_2 \\ j_1 & J & K \end{Bmatrix} \left\langle j'_1 \left\| T^{(K)} \right\| j_1 \right\rangle. \tag{A.5.13}
\end{aligned}$$

Here,  $\langle j_2 \| 1 \| j_2 \rangle = \sqrt{2j_2 + 1}$  is used. In the case of  $T^{(k_1)} = 1$ ,

$$\begin{aligned}
& \langle (j'_1 j'_2) J' \| U^{(K)} \| (j_1 j_2) J \rangle \\
&= \delta_{j'_1 j_1} \delta_{J' J} \sqrt{(2J+1)(2J'+1)(2K+1)(2j_1+1)} \begin{Bmatrix} j_1 & j_1 & 0 \\ j'_2 & j_2 & K \\ J' & J & K \end{Bmatrix} \langle j'_2 \| U^{(K)} \| j_2 \rangle \\
&= \delta_{j'_1 j_1} \delta_{J' J} \sqrt{(2J+1)(2J'+1)(2K+1)(2j_1+1)} \\
&\quad \times \frac{(-1)^{j_1+j_2+J'+K}}{\sqrt{(2j_1+1)(2K+1)}} \begin{Bmatrix} j'_2 & j_2 & K \\ J & J' & j_1 \end{Bmatrix} \langle j'_2 \| U^{(K)} \| j_2 \rangle \\
&= \delta_{j'_1 j_1} \delta_{J' J} (-1)^{j_1+j_2+J'+K} \sqrt{(2J+1)(2J'+1)} \begin{Bmatrix} j'_2 & j_2 & K \\ J & J' & j_1 \end{Bmatrix} \langle j'_2 \| U^{(K)} \| j_2 \rangle. \quad (\text{A.5.14})
\end{aligned}$$

Let us consider one of the most typical functions as  $f(r)Y_{\lambda\mu}(\theta, \phi)$ . Using the reduced matrix elements of  $Y^{(\lambda)}$  (A.5.6) and the relation of

$$\langle l' 0 \lambda 0 | l 0 \rangle \begin{Bmatrix} j' & \lambda & j \\ l & \frac{1}{2} & l' \end{Bmatrix} = \frac{(-1)^{j+l+\frac{1}{2}}}{\sqrt{(2l'+1)(2j+1)}} \langle j' \frac{1}{2} \lambda 0 | j \frac{1}{2} \rangle, \quad (\text{A.5.15})$$

we obtain

$$\begin{aligned}
& \langle n', (l' \frac{1}{2}) j' \| f(r) Y^{(\lambda)} \| n, (l \frac{1}{2}) j \rangle \\
&= \delta_{j' j} (-1)^{l'+\frac{1}{2}+j+\lambda} \sqrt{(2j+1)(2j'+1)} \begin{Bmatrix} j' & l' & \frac{1}{2} \\ l & j & \lambda \end{Bmatrix} \langle n', l' \| f(r) Y^{(\lambda)} \| n, l \rangle \\
&= \delta_{j' j} (-1)^{l'+\frac{1}{2}+j+\lambda} \sqrt{(2j+1)(2j'+1)} \begin{Bmatrix} j' & l' & \frac{1}{2} \\ l & j & \lambda \end{Bmatrix} \\
&\quad \times \langle n', l' | f(r) | n, l \rangle \times (-1)^\lambda \sqrt{\frac{(2l'+1)(2\lambda+1)}{4\pi}} \langle l' 0 \lambda 0 | l 0 \rangle \\
&= \delta_{j' j} (-1)^{l'+\frac{1}{2}+j} \sqrt{\frac{(2j+1)(2j'+1)(2l'+1)(2\lambda+1)}{4\pi}} \langle n', l' | f(r) | n, l \rangle \\
&\quad \times \frac{(-1)^{j+l+\frac{1}{2}}}{\sqrt{(2l'+1)(2j+1)}} \langle j' \frac{1}{2} \lambda 0 | j \frac{1}{2} \rangle \\
&= \delta_{j' j} (-1)^{l+l'} \sqrt{\frac{(2j'+1)(2\lambda+1)}{4\pi}} \langle n', l' | f(r) | n, l \rangle \langle j' \frac{1}{2} \lambda 0 | j \frac{1}{2} \rangle. \quad (\text{A.5.16})
\end{aligned}$$



## Appendix B

# Nuclear effective interactions

### B.1 Pairing interactions

Two-body interactions are generally given as

$$V = \frac{1}{2} \sum_{ijkl} V_{ijkl} c_i^\dagger c_j^\dagger c_l c_k, \quad (\text{B.1.1})$$

where two particles lying in single-particle levels  $k$  and  $l$  are scattered into levels  $i$  and  $j$ . The two-body matrix elements  $V_{ijkl}$  of the interactions  $V$  are anti-symmetrized as

$$V_{ijkl} = \frac{1}{4} \left[ \langle ij | V | kl \rangle - \langle ji | V | kl \rangle - \langle ij | V | lk \rangle + \langle ji | V | lk \rangle \right], \quad (\text{B.1.2})$$

which follow the relation of

$$V_{ijkl} = -V_{jikl} = -V_{ijlk} = V_{jilk}. \quad (\text{B.1.3})$$

Since an atomic nucleus is a spherically symmetric system, the angular momentum is one of the good quantum numbers. The pairing operators of like-particles are defined as [14]

$$A_{\kappa\mu JM}^\dagger(j_1 j_2) = \left[ c_{j_1}^\dagger \otimes c_{j_2}^\dagger \right]_M^{(J)} = \sum_{m_1 m_2} \langle j_1 m_1 j_2 m_2 | J M \rangle c_{j_1 m_1}^\dagger c_{j_2 m_2}^\dagger, \quad (\text{B.1.4})$$

$$B_{JM}^\dagger(j_1 j_2) = \left[ c_{j_1}^\dagger \otimes \tilde{c}_{j_2} \right]_M^{(J)} = \sum_{m_1 m_2} \langle j_1 m_1 j_2 m_2 | J M \rangle c_{j_1 m_1}^\dagger \tilde{c}_{j_2 m_2}. \quad (\text{B.1.5})$$

The conjugate operators are given as

$$\begin{aligned} A_{JM}(j_1 j_2) &= \sum_{m_1 m_2} \langle j_1 m_1 j_2 m_2 | J M \rangle c_{j_2 m_2} c_{j_1 m_1} \\ &= \sum_{m_1 m_2} \langle j_1 m_1 j_2 m_2 | J M \rangle (-1)^{j_1 + j_2 + m_1 + m_2} \tilde{c}_{j_2 - m_2} \tilde{c}_{j_1 - m_1} \\ &= (-1)^{j_1 + j_2 + M} \sum_{m_1 m_2} \langle j_2 - m_2 j_1 - m_1 | J - M \rangle \tilde{c}_{j_2 - m_2} \tilde{c}_{j_1 - m_1} \\ &= (-1)^{j_1 + j_2 + M} \left[ \tilde{c}_{j_2} \otimes \tilde{c}_{j_1} \right]_{-M}^{(J)}. \end{aligned} \quad (\text{B.1.6})$$

The nuclear interactions are assumed to conserve the rotational symmetry. The two-body interactions are then expanded in terms of the scalar products of the irreducible tensor operators as

$$\begin{aligned} V &= \sum_{j_1 j_2 j_3 j_4} \sum_{JM} G_J(j_1 j_2 j_3 j_4) A_{JM}^\dagger(j_1 j_2) A_{JM}(j_3 j_4) \\ &= \sum_{j_1 j_2 j_3 j_4} \sum_J G_J(j_1 j_2 j_3 j_4) \sqrt{2J+1} (-1)^{j_3+j_4-J} \left[ \left[ c_{j_1}^\dagger \otimes c_{j_2}^\dagger \right]^{(J)} \otimes \left[ \tilde{c}_{j_4} \otimes \tilde{c}_{j_3} \right]^{(J)} \right]_0^{(0)}, \end{aligned} \quad (\text{B.1.7})$$

where the interaction strengths  $G_J(j_1 j_2 j_3 j_4)$  satisfy the relations that

$$\begin{aligned} G_J(j_1 j_2 j_3 j_4) &= G_J(j_3 j_4 j_1 j_2) \\ &= -(-1)^{j_1+j_2-J} G_J(j_2 j_1 j_3 j_4) \\ &= -(-1)^{j_3+j_4-J} G_J(j_1 j_2 j_4 j_3) \\ &= (-1)^{j_1+j_2+j_3+j_4} G_J(j_2 j_1 j_4 j_3). \end{aligned} \quad (\text{B.1.8})$$

In order to calculate the matrix elements with respect to many-body wavefunctions, the Wick's theorem saying that any time-ordered products of creation and annihilation operators are given as

$$T \left[ c_1 c_2 c_3^\dagger \cdots \right] = N \left[ c_1 c_2 c_3^\dagger \cdots + (\text{all possible contractions}) \right]. \quad (\text{B.1.9})$$

The contractions of two operators are defined as the difference of the time-ordered product and the normal-ordered product. They are explicitly given as

$$\overline{c_i^\dagger c_j^\dagger} = c_i c_j^\dagger - N [c_i c_j^\dagger] = c_i c_j^\dagger + c_j^\dagger c_i = \{c_i, c_j^\dagger\} = \delta_{ij}, \quad (\text{B.1.10})$$

$$\overline{c_i c_j} = 0, \quad \overline{c_i^\dagger c_j^\dagger} = 0. \quad (\text{B.1.11})$$

If two irreducible tensor operators are coupled with a rank  $J$ , the contraction is given as

$$\begin{aligned} \left[ \overline{\tilde{c}_{j'} \otimes c_j^\dagger} \right]_M^{(J)} &= \sum_{m', m} \langle j' m' j m | J M \rangle \overline{\tilde{c}_{j' m'} c_{j m}^\dagger} \\ &= \sum_{m', m} \langle j' m' j m | J M \rangle (-1)^{j'-m'} \overline{c_{j', -m'}^\dagger c_{j m}^\dagger} \\ &= \sum_m \langle j - m j m | 0 0 \rangle (-1)^{j+m} \delta_{j' j} \delta_{J 0} \delta_{M 0} \\ &= \delta_{j' j} \delta_{J 0} \delta_{M 0} \sqrt{2j+1}. \end{aligned} \quad (\text{B.1.12})$$

The reduced matrix elements of the contraction are given as

$$\begin{aligned} \langle I' \| \left[ \overline{\tilde{c}_{j'} \otimes c_j^\dagger} \right]_M^{(J)} \| I \rangle &= \frac{(-1)^{I-M_I}}{\langle I' M_I' I - M_I | 0 0 \rangle} \langle I' M_I' | \left[ \overline{\tilde{c}_{j'} \otimes c_j^\dagger} \right]_M^{(J)} | I M_I \rangle \\ &= \delta_{I' I} \delta_{j' j} \delta_{J 0} \delta_{M 0} \sqrt{(2I+1)(2j+1)}. \end{aligned} \quad (\text{B.1.13})$$

The contractions of two operators in a product of more than two operators are defined as

$$\begin{aligned} \overline{c_i c_{i_1} \cdots c_{i_n} c_j^\dagger c_{j_1} \cdots c_{j_m}} &= (-1)^n \overline{c_i c_j^\dagger} c_{i_1} \cdots c_{i_n} c_{j_1} \cdots c_{j_m} \\ &= (-1)^n \delta_{ij} c_{i_1} \cdots c_{i_n} c_{j_1} \cdots c_{j_m}. \end{aligned} \quad (\text{B.1.14})$$

Since the two possible contractions of the two-body interactions are evaluated as

$$\begin{aligned}
& \left[ \overbrace{\left[ \tilde{c}_{j_2}' \otimes \tilde{c}_{j_1}' \right]^{(J)} \otimes \left[ c_{j_1}^\dagger \otimes c_{j_2}^\dagger \right]^{(J)}}^{(J)} \right]_0^{(0)} \\
&= - \sum_K (2J+1)(2K+1) \begin{Bmatrix} j_2' & j_1' & J \\ j_1 & j_2 & J \\ K & K & 0 \end{Bmatrix} \left[ \overbrace{\left[ \tilde{c}_{j_2}' \otimes c_{j_1}^\dagger \right]^{(K)}}^{(K)} \otimes \overbrace{\left[ \tilde{c}_{j_1}' \otimes c_{j_2}^\dagger \right]^{(K)}}^{(K)} \right]_0^{(0)} \\
&= -(2J+1) \begin{Bmatrix} j_1 & j_2 & J \\ j_1 & j_2 & J \\ 0 & 0 & 0 \end{Bmatrix} \times \delta_{j_2', j_1} \delta_{j_1', j_2} \sqrt{(2j_1+1)(2j_2+1)} \\
&= -\delta_{j_2', j_1} \delta_{j_1', j_2} \sqrt{2J+1}, \tag{B.1.15}
\end{aligned}$$

$$\left[ \overbrace{\left[ \tilde{c}_{j_2}' \otimes \tilde{c}_{j_1}' \right]^{(J)} \otimes \left[ c_{j_1}^\dagger \otimes c_{j_2}^\dagger \right]^{(J)}}^{(J)} \right]_0^{(0)} = (-1)^{j_1+j_2-J} \times \delta_{j_1', j_1} \delta_{j_2', j_2} \sqrt{2J+1}, \tag{B.1.16}$$

the propagators of the two-body interactions are given as

$$\begin{aligned}
& \langle 0 | \left[ \overbrace{\left[ \tilde{c}_{j_2}' \otimes \tilde{c}_{j_1}' \right]^{(J)} \otimes \left[ c_{j_1}^\dagger \otimes c_{j_2}^\dagger \right]^{(J)}}^{(J)} \right]_0^{(0)} | 0 \rangle \\
&= \left[ \overbrace{\left[ \tilde{c}_{j_2}' \otimes \tilde{c}_{j_1}' \right]^{(J)} \otimes \left[ c_{j_1}^\dagger \otimes c_{j_2}^\dagger \right]^{(J)}}^{(J)} \right]_0^{(0)} + \left[ \overbrace{\left[ \tilde{c}_{j_2}' \otimes \tilde{c}_{j_1}' \right]^{(J)} \otimes \left[ c_{j_1}^\dagger \otimes c_{j_2}^\dagger \right]^{(J)}}^{(J)} \right]_0^{(0)} \\
&= [(-1)^{j_1+j_2-J} \delta_{j_1', j_1} \delta_{j_2', j_2} - \delta_{j_2', j_1} \delta_{j_1', j_2}] \sqrt{2J+1}. \tag{B.1.17}
\end{aligned}$$

Let us construct two-particles states, which obey the orthonormalized condition of

$$\langle j_1 j_2; J' M' | j_1 j_2; J M \rangle = \delta_{J' J} \delta_{M' M}, \tag{B.1.18}$$

where

$$|j_1 j_2; J M \rangle = \mathcal{N} A_{JM}^\dagger(j_1 j_2) |0 \rangle \tag{B.1.19}$$

is a two-particle state and  $\mathcal{N}$  is the normalization constant. The overlap is calculated as

$$\begin{aligned}
& \langle j_1 j_2; J' M' | j_1 j_2; J M \rangle \\
&= \mathcal{N}^2 \langle 0 | A_{J'M'}(j_1 j_2) A_{JM}^\dagger(j_1 j_2) | 0 \rangle \\
&= \mathcal{N}^2 (-1)^{j_1+j_2+M'} \langle 0 | \left[ \tilde{c}_{j_2}' \otimes \tilde{c}_{j_1}' \right]_{-M'}^{(J')} \left[ c_{j_1}^\dagger \otimes c_{j_2}^\dagger \right]_M^{(J)} | 0 \rangle \\
&= \mathcal{N}^2 \delta_{J' J} \delta_{M' M} \frac{(-1)^{j_1+j_2+J}}{\sqrt{2J+1}} \langle 0 | \left[ \left[ \tilde{c}_{j_2}' \otimes \tilde{c}_{j_1}' \right]^{(J)} \otimes \left[ c_{j_1}^\dagger \otimes c_{j_2}^\dagger \right]^{(J)} \right]_0^{(0)} | 0 \rangle \\
&= \mathcal{N}^2 \delta_{J' J} \delta_{M' M} [1 - \delta_{j_1, j_2} (-1)^{j_1+j_2+J}]. \tag{B.1.20}
\end{aligned}$$

The whole tensor operator should be coupled with rank-0 due to the rotational symmetry of the vacuum. The terms in the square bracket become two if  $j_1 = j_2$ , and the two-particle state is then

orthonormalized as

$$|j_1 j_2; JM\rangle = \sqrt{\frac{1}{1 + \delta_{j_1, j_2}}} A_{JM}^\dagger(j_1 j_2) |0\rangle. \quad (\text{B.1.21})$$

The two-body matrix elements of the tensor operator in the two-body interactions are given as

$$\begin{aligned} \langle 0 | A_{J'0}(j_1 j_2) \left[ \left[ c_{j'_1}^\dagger \otimes c_{j'_2}^\dagger \right]^{(K)} \otimes \left[ \tilde{c}_{j'_4} \otimes \tilde{c}_{j'_3} \right]^{(K)} \right]_0^{(0)} A_{J0}^\dagger(j_3 j_4) |0\rangle \\ = (-1)^{J+K} \sum_{K'} \sqrt{\frac{2K'+1}{(2J+1)(2K+1)}} \langle 0 | A_{J'0}(j_1 j_2) \\ \times \left[ \left[ c_{j'_1}^\dagger \otimes c_{j'_2}^\dagger \right]^{(K)} \otimes \left[ \left[ \tilde{c}_{j'_4} \otimes \tilde{c}_{j'_3} \right]^{(K)} \otimes \left[ c_{j_3}^\dagger \otimes c_{j_4}^\dagger \right]^{(J)} \right]^{(K')} \right]_0^{(J)} |0\rangle \\ = (-1)^{j_1+j_2+K} \sum_{K'} \frac{1}{2J+1} \sqrt{\frac{2K'+1}{2K+1}} \delta_{J',J} \\ \times \langle 0 | \left[ \left[ \tilde{c}_{j_2} \otimes \tilde{c}_{j_1} \right]^{(J)} \otimes \left[ \left[ c_{j'_1}^\dagger \otimes c_{j'_2}^\dagger \right]^{(K)} \otimes \left[ \left[ \tilde{c}_{j'_4} \otimes \tilde{c}_{j'_3} \right]^{(K)} \otimes \left[ c_{j_3}^\dagger \otimes c_{j_4}^\dagger \right]^{(J)} \right]^{(K')} \right]_0^{(J)} |0\rangle \\ = (-1)^{j_1+j_2+K} \sum_{K'} \frac{1}{2J+1} \sqrt{\frac{2K'+1}{2K+1}} \delta_{J',J} \\ \times \langle 0 | \left[ \left[ \left[ \tilde{c}_{j_2} \otimes \tilde{c}_{j_1} \right]^{(J)} \otimes \left[ c_{j'_1}^\dagger \otimes c_{j'_2}^\dagger \right]^{(K)} \right]^{(K')} \otimes \left[ \left[ \tilde{c}_{j'_4} \otimes \tilde{c}_{j'_3} \right]^{(K)} \otimes \left[ c_{j_3}^\dagger \otimes c_{j_4}^\dagger \right]^{(J)} \right]^{(K')} \right]_0^{(0)} |0\rangle \\ = \delta_{J',J} \delta_{K,J} (-1)^{j_1+j_2+J} \frac{1}{\sqrt{2J+1}} \\ \times \left[ (-1)^{j'_1+j'_2-J} \delta_{j_1, j'_1} \delta_{j_2, j'_2} - \delta_{j_2, j'_1} \delta_{j_1, j'_2} \right] \\ \times \left[ (-1)^{j_3+j_4-J} \delta_{j'_3, j_3} \delta_{j'_4, j_4} - \delta_{j'_4, j_3} \delta_{j'_3, j_4} \right], \quad (\text{B.1.22}) \end{aligned}$$

where the left four and the right four operators should be reduced separately among them in each half. Thus, we have

$$\begin{aligned} \langle j_1 j_2; J' M' | V | j_3 j_4; JM \rangle &= \delta_{J',J} \delta_{M',M} \langle j_1 j_2; J0 | V | j_3 j_4; J0 \rangle \\ &= \delta_{J',J} \delta_{M',M} \frac{1}{\sqrt{(1 + \delta_{j_1 j_2})(1 + \delta_{j_3 j_4})}} \sum_{j'_1 j'_2 j'_3 j'_4} \sum_K G_K(j'_1 j'_2 j'_3 j'_4) \sqrt{2K+1} (-1)^{j'_3+j'_4-K} \\ &\quad \times \langle 0 | A_{J'0}(j_1 j_2) \left[ \left[ c_{j'_1}^\dagger \otimes c_{j'_2}^\dagger \right]^{(K)} \otimes \left[ \tilde{c}_{j'_4} \otimes \tilde{c}_{j'_3} \right]^{(K)} \right]_0^{(0)} A_{J0}^\dagger(j_3 j_4) |0\rangle \\ &= \delta_{J',J} \delta_{M',M} \frac{1}{\sqrt{(1 + \delta_{j_1 j_2})(1 + \delta_{j_3 j_4})}} \sum_{j'_1 j'_2 j'_3 j'_4} (-1)^{j_1+j_2+j'_3+j'_4} G_J(j'_1 j'_2 j'_3 j'_4) \\ &\quad \times \left[ (-1)^{j'_1+j'_2-J} \delta_{j_1, j'_1} \delta_{j_2, j'_2} - \delta_{j_2, j'_1} \delta_{j_1, j'_2} \right] \\ &\quad \times \left[ (-1)^{j_3+j_4-J} \delta_{j'_3, j_3} \delta_{j'_4, j_4} - \delta_{j'_4, j_3} \delta_{j'_3, j_4} \right] \\ &= \delta_{J',J} \delta_{M',M} \frac{4}{\sqrt{(1 + \delta_{j_1 j_2})(1 + \delta_{j_3 j_4})}} G_J(j_1 j_2 j_3 j_4). \quad (\text{B.1.23}) \end{aligned}$$

## B.2 Monopole-pairing Interaction

The pair-creation operator  $P_{\mu,M}^{(1,J)\dagger}$  and the quadrupole operator  $Q_{\tau,M}^{(1,2)\dagger}$  are defined by

$$P_{\mu,M}^{(1,J)\dagger} = \sum_{j_1,j_2} p_J(j_1j_2) A_{1\mu JM}^\dagger(j_1j_2), \quad Q_{\mu,M}^{(1,2)\dagger} = \sum_{j_1,j_2} q(j_1j_2) B_{1\mu,2M}(j_1j_2), \quad (\text{B.2.1})$$

with

$$p_0(j_1j_2) = \frac{\sqrt{2j_1+1}}{2} \delta_{j_1j_2}, \quad (\text{B.2.2})$$

$$p_2(j_1j_2) = q(j_1j_2) = \frac{1}{\sqrt{5}} \langle j_1 \| r^2 Y^{(2)} \| j_2 \rangle = \frac{1}{\sqrt{5}} \langle n_1 l_1 \| r^2 \| n_2 l_2 \rangle \langle l_1 j_1 \| Y^{(2)} \| l_2 j_2 \rangle. \quad (\text{B.2.3})$$

In this paper, we adopt  $p_J = 1$  for higher order ( $J > 2$ ) pairing operators. The conjugate of pair-creation operator is given by

$$\begin{aligned} \tilde{P}_{\mu,M}^{(1,J)} &\equiv (-1)^M P_{\mu,-M}^{(1,J)} \\ &= \sum_{j_1,j_2} p_J(j_1j_2) (-1)^{j_1+j_2} \left[ \tilde{c}_{j_2} \otimes \tilde{c}_{j_1} \right]_{\mu,M}^{(1,J)} \\ &= \sum_{j_1,j_2} p_J(j_1j_2) (-1)^{1+\kappa-M} A_{1\mu JM}(j_1j_2) \\ &= (-1)^{J+1} \sum_{j_1,j_2} p_J(j_1j_2) \left[ \tilde{c}_{j_1} \otimes \tilde{c}_{j_2} \right]_{\mu,M}^{(1,J)}. \end{aligned} \quad (\text{B.2.4})$$

Assuming that the effective interactions are Hermite and rotational, parity, and time-reversal invariant, the isovector pairing ( $P$ ) interactions and the quadrupole-quadrupole ( $QQ$ ) interactions are given by

$$H_{\mu,J}^{(\text{pair})} = -g_{\mu J} P_{\mu}^{(1,J)\dagger} \cdot \tilde{P}_{\mu}^{(1,J)} = -g_{\mu J} (-1)^J \sqrt{2J+1} \left[ P_{\mu}^{(1,J)\dagger} \otimes \tilde{P}_{\mu}^{(1,J)} \right]_0^{(0)}, \quad (\text{B.2.5})$$

$$H_{\mu,\mu'}^{(QQ)} = -\chi_{\mu\mu'} N \left[ Q_{\mu}^{(2)\dagger} \cdot Q_{\mu'}^{(2)} \right] = -\sqrt{5} \chi_{\mu\mu'} N \left[ \left[ Q_{\mu}^{(2)\dagger} \otimes Q_{\mu'}^{(2)} \right]_0^{(0)} \right]. \quad (\text{B.2.6})$$

It should be noted that the scalar product is taken only for  $J$ -space except for isospin space.

$\mu = \pm 1$  for the pairing interactions between like particles, and  $\mu = 0$  for isovector  $np$  pairing interactions.  $\mu = \mu' = \pm 1$  for the  $QQ$  interactions between like particles, and  $(\mu, \mu') = (+1, -1)$  or  $(-1, +1)$  for those between neutron and proton. The phenomenological coupling strengths  $g_{J\mu}$  and  $\chi_{\mu\mu'}$  are determined to represent spectra and electromagnetic transition rates.

In the later sections we will utilize abbreviated forms of the pairing interactions as

$$\begin{aligned} H_{\mu,J}^{(\text{pair})} &= -g_{\mu J} P_{\mu}^{(1,J)\dagger} \cdot \tilde{P}_{\mu}^{(1,J)} \\ &= -g_{\mu J} \sum_M (-1)^M \sum_{j_1,j_2} p_J(j_1j_2) A_{1\mu JM}^\dagger(j_1j_2) \sum_{j_3,j_4} p_J(j_3j_4) (-1)^{1+\kappa-M} A_{1\mu J-M}(j_3j_4) \\ &= -g_{\mu J} (-1)^{1+\kappa} \sum_{j_1,j_2,j_3,j_4} p_J(j_1j_2) p_J(j_3j_4) \sum_M A_{1\mu JM}^\dagger(j_1j_2) A_{1\mu J-M}(j_3j_4), \end{aligned} \quad (\text{B.2.7})$$

or

$$\begin{aligned}
H_{\mu,J}^{(\text{pair})} &= -g_{\mu J} P_{\mu}^{(1,J)\dagger} \cdot \tilde{P}_{\mu}^{(1,J)} \\
&= g_{\mu J} (-1)^J \sum_{j_1 j_2 j_3 j_4} p_J(j_1 j_2) p_J(j_3 j_4) \left[ c_{j_1}^{\dagger} \otimes c_{j_2}^{\dagger} \right]_{\mu}^{(1,J)} \cdot \left[ \tilde{c}_{j_3} \otimes \tilde{c}_{j_4} \right]_{\mu}^{(1,J)} \\
&\equiv \sum_{j_1 j_2 j_3 j_4} G_{\mu}(j_1 j_2, j_3 j_4; J) \left[ c_{j_1}^{\dagger} \otimes c_{j_2}^{\dagger} \right]_{\mu}^{(1,J)} \cdot \left[ \tilde{c}_{j_3} \otimes \tilde{c}_{j_4} \right]_{\mu}^{(1,J)}, \tag{B.2.8}
\end{aligned}$$

where

$$G_{\mu}(j_1 j_2, j_3 j_4; J) = g_{\mu J} (-1)^J p_J(j_1 j_2) p_J(j_3 j_4). \tag{B.2.9}$$

Since the Hermitian nature of the Hamiltonian and the reality of the CG coefficients,

$$G_{\mu}(j_1 j_2, j_3 j_4; J) = G_{\mu}(j_3 j_4, j_1 j_2; J). \tag{B.2.10}$$

For the monopole-pairing interactions between like particles,

$$\begin{aligned}
&\left\langle j_1 j_2; J \left| H_{\mu=\pm 1, J}^{(\text{pair})} \right| j_3 j_4; J \right\rangle \\
&= g_{\mu J} (-1)^{J+M} \sum_{j'_1 j'_2} p_0(j'_1 j'_2) \sum_{j'_3 j'_4} p_0(j'_3 j'_4) \left\langle j_1 j_2; J \left| A_{1\mu JM}^{\dagger}(j'_1 j'_2) \cdot A_{1\mu JM}(j'_3 j'_4) \right| j_3 j_4; J \right\rangle \\
&= \frac{g_{\mu J}}{\sqrt{2J+1}} p_0(j_1 j_2) p_0(j_3 j_4) \sqrt{1 + (-1)^J \delta_{j_1 j_2}} \sqrt{1 + (-1)^J \delta_{j_3 j_4}}. \tag{B.2.11}
\end{aligned}$$

### B.3 Quadrupole-Quadrupole interactions

The quadrupole-quadrupole ( $QQ$ ) interaction between like nucleons is given by a normal-ordered form of

$$H_{\tau=\nu,\pi}^{(QQ)} = N \left[ Q^{(2)} \cdot Q^{(2)} \right] = N \left[ \sqrt{5} \left[ Q^{(2)} \otimes Q^{(2)} \right]_0^{(0)} \right], \tag{B.3.1}$$

where the quadrupole operator is defined as

$$Q^{(2)} = \sum_{j_1 j_2} Q_{j_1, j_2} \left[ c_{j_1}^{\dagger} \otimes \tilde{c}_{j_2} \right]^{(2)}. \tag{B.3.2}$$

The  $QQ$  interaction can be decomposed as

$$\begin{aligned}
H^{(QQ)} &= \sqrt{5} \sum_{j_1 j_2 j_3 j_4} Q_{j_1, j_2} Q_{j_3, j_4} N \left[ \left[ \left[ c_{j_1}^\dagger \otimes \tilde{c}_{j_2} \right]^{(2)} \otimes \left[ c_{j_3}^\dagger \otimes \tilde{c}_{j_4} \right]^{(2)} \right]_0^{(0)} \right] \\
&= -\sqrt{5} \sum_{j_1 j_2 j_3 j_4} Q_{j_1, j_2} Q_{j_3, j_4} \sum_K 5(2K+1) \begin{Bmatrix} j_1 & j_2 & 2 \\ j_3 & j_4 & 2 \\ K & K & 0 \end{Bmatrix} \\
&\quad \times \left[ \left[ c_{j_1}^\dagger \otimes c_{j_3}^\dagger \right]^{(K)} \otimes \left[ \tilde{c}_{j_2} \otimes \tilde{c}_{j_4} \right]^{(K)} \right]_0^{(0)} \\
&= -5 \sum_{j_1 j_2 j_3 j_4} Q_{j_1, j_2} Q_{j_3, j_4} \sum_K (-1)^{K+j_2+j_3} \sqrt{2K+1} \begin{Bmatrix} j_1 & j_2 & 2 \\ j_4 & j_3 & K \end{Bmatrix} \\
&\quad \times \left[ \left[ c_{j_1}^\dagger \otimes c_{j_3}^\dagger \right]^{(K)} \otimes \left[ \tilde{c}_{j_2} \otimes \tilde{c}_{j_4} \right]^{(K)} \right]_0^{(0)} \\
&= -5 \sum_{j_1 j_2 j_3 j_4} Q_{j_1, j_2} Q_{j_3, j_4} \sum_K (-1)^{j_3+j_4} \sqrt{2K+1} \begin{Bmatrix} j_1 & j_2 & 2 \\ j_4 & j_3 & K \end{Bmatrix} \\
&\quad \times \left[ \left[ c_{j_1}^\dagger \otimes c_{j_3}^\dagger \right]^{(K)} \otimes \left[ \tilde{c}_{j_4} \otimes \tilde{c}_{j_2} \right]^{(K)} \right]_0^{(0)}. \tag{B.3.3}
\end{aligned}$$

Here the reduced matrix elements of the spherical harmonics is given by

$$\langle l' \parallel Y^{(k)} \parallel l \rangle = (-1)^{l'} \sqrt{\frac{(2l'+1)(2k+1)(2l+1)}{4\pi}} \begin{Bmatrix} l' & k & l \\ 0 & 0 & 0 \end{Bmatrix}, \tag{B.3.4}$$

$$\langle l' \parallel C^{(k)} \parallel l \rangle = (-1)^{l'} \sqrt{(2l'+1)(2l+1)} \begin{Bmatrix} l' & k & l \\ 0 & 0 & 0 \end{Bmatrix}. \tag{B.3.5}$$

Then

$$Q_{j_1, j_2} = -\frac{1}{\sqrt{5}} \langle j_1 \parallel Q^{(2)} \parallel j_2 \rangle = (-1)^{j_1-j_2} Q_{j_2, j_1}. \tag{B.3.6}$$

There is only one contracted term given by

$$\begin{aligned}
&\langle 0 \parallel H_{\tau\tau'}^{(QQ)} \parallel 0 \rangle \\
&= \sqrt{5} \sum_{j_1 j_2 j_3 j_4} Q_{j_1, j_2} Q_{j_3, j_4} \langle 0 \parallel \left[ \left[ a_{\tau j_1}^\dagger \otimes \tilde{a}_{\tau j_2} \right]^{(2)} \otimes \left[ a_{\tau' j_3}^\dagger \otimes \tilde{a}_{\tau' j_4} \right]^{(2)} \right]_0^{(0)} \parallel 0 \rangle \\
&= -\sqrt{5} \sum_{j_1 j_2 j_3 j_4} (-1)^{j_3+j_4} Q_{j_1, j_2} Q_{j_3, j_4} \langle 0 \parallel \left[ \left[ a_{\tau j_1}^\dagger \otimes \tilde{a}_{\tau j_2} \right]^{(2)} \otimes \left[ \tilde{a}_{\tau' j_4} \otimes a_{\tau' j_3}^\dagger \right]^{(2)} \right]_0^{(0)} \parallel 0 \rangle \\
&= \sqrt{5} \sum_{j_1 j_2 j_3 j_4} (-1)^{j_3+j_4} Q_{j_1, j_2} Q_{j_3, j_4} 5 \begin{Bmatrix} j_1 & j_2 & 2 \\ j_4 & j_3 & 2 \\ 0 & 0 & 0 \end{Bmatrix} \delta_{j_1 j_4} \delta_{j_2 j_3} \\
&\quad \times \langle 0 \parallel \left[ \left[ a_{\tau j_1}^\dagger \otimes \tilde{a}_{\tau' j_4} \right]^{(0)} \otimes \left[ \tilde{a}_{\tau j_2} \otimes a_{\tau' j_3}^\dagger \right]^{(0)} \right]_0^{(0)} \parallel 0 \rangle
\end{aligned}$$

$$\begin{aligned}
&= 5 \sum_{j_1 j_2} Q_{j_1, j_2} Q_{j_2, j_1} \begin{Bmatrix} j_1 & j_2 & 2 \\ j_2 & j_1 & 0 \end{Bmatrix} \langle 0 | [a_{\tau j_1}^\dagger \otimes \tilde{a}_{\tau' j_1}]^{(0)} | 0 \rangle \sqrt{2j_2 + 1} \delta_{\tau \tau'} \\
&= -5 \sum_{j_1 j_2} Q_{j_1, j_2} Q_{j_2, j_1} \begin{Bmatrix} j_1 & j_2 & 2 \\ j_2 & j_1 & 0 \end{Bmatrix} \frac{1}{\sqrt{2j_1 + 1}} N_{\tau j_1} \sqrt{2j_2 + 1} \delta_{\tau \tau'} \\
&= -5 \sum_{j_1 j_2} (-1)^{j_1 + j_2} Q_{j_1, j_2} Q_{j_2, j_1} \frac{1}{2j_1 + 1} N_{\tau j_1} \delta_{\tau \tau'} \\
&= 5 \sum_{j_1 j_2} (Q_{j_1, j_2})^2 \frac{1}{2j_1 + 1} N_{\tau j_1} \delta_{\tau \tau'}. \tag{B.3.7}
\end{aligned}$$

The octupole-octupole interaction is similarly given as

$$H^{(\text{Octupole})} = N [\hat{Q}^{(3)} \cdot \hat{Q}^{(3)}], \tag{B.3.8}$$

where

$$\hat{Q}^{(3)} = \sum_{j_1 j_2} Q_{j_1, j_2}^{(3)} [c_{j_1}^\dagger \otimes \tilde{c}_{j_2}]^{(3)} \tag{B.3.9}$$

are octupole operators. Then,

$$\begin{aligned}
H^{(\text{Octupole})} &= \sqrt{7} \sum_{j_1 j_2 j_3 j_4} Q_{j_1, j_2}^{(3)} Q_{j_3, j_4}^{(3)} N \left[ \left[ [c_{j_1}^\dagger \otimes \tilde{c}_{j_2}]^{(3)} \otimes [c_{j_3}^\dagger \otimes \tilde{c}_{j_4}]^{(3)} \right]_0^{(0)} \right] \\
&= -\sqrt{7} \sum_{j_1 j_2 j_3 j_4} Q_{j_1, j_2}^{(3)} Q_{j_3, j_4}^{(3)} \sum_K 7(2K + 1) \begin{Bmatrix} j_1 & j_2 & 3 \\ j_3 & j_4 & 3 \\ K & K & 0 \end{Bmatrix} \\
&\quad \times \left[ [c_{j_1}^\dagger \otimes c_{j_3}^\dagger]^{(K)} \otimes [\tilde{c}_{j_2} \otimes \tilde{c}_{j_4}]^{(K)} \right]_0^{(0)} \\
&= 7 \sum_{j_1 j_2 j_3 j_4} Q_{j_1, j_2}^{(3)} Q_{j_3, j_4}^{(3)} \sum_K (-1)^{j_2 + j_3 + K} \sqrt{2K + 1} \begin{Bmatrix} j_1 & j_2 & 3 \\ j_4 & j_3 & K \end{Bmatrix} \\
&\quad \times \left[ [c_{j_1}^\dagger \otimes c_{j_3}^\dagger]^{(K)} \otimes [\tilde{c}_{j_2} \otimes \tilde{c}_{j_4}]^{(K)} \right]_0^{(0)} \\
&= 7 \sum_{j_1 j_2 j_3 j_4} Q_{j_1, j_2}^{(3)} Q_{j_3, j_4}^{(3)} \sum_K (-1)^{j_3 + j_4} \sqrt{2K + 1} \begin{Bmatrix} j_1 & j_2 & 3 \\ j_4 & j_3 & K \end{Bmatrix} \\
&\quad \times \left[ [c_{j_1}^\dagger \otimes c_{j_3}^\dagger]^{(K)} \otimes [\tilde{c}_{j_4} \otimes \tilde{c}_{j_2}]^{(K)} \right]_0^{(0)}. \tag{B.3.10}
\end{aligned}$$

## B.4 Neutron-proton monopole-pairing interactions

### B.4.1 Isovector-pairing

Let us consider the monopole-pairing interaction between neutron and proton. Since

$$\begin{aligned}
A_{0010}^\dagger(jj) &= \frac{1}{\sqrt{2}} \sum_{m\tau} \langle j m j - m | 00 \rangle \langle \frac{1}{2} \tau \frac{1}{2} - \tau | 10 \rangle c_{\tau jm}^\dagger c_{-\tau j - m}^\dagger \\
&= \frac{1}{2} \sum_{m\tau} \langle j m j - m | 00 \rangle c_{\tau jm}^\dagger c_{-\tau j - m}^\dagger \\
&= \frac{1}{2} \sum_m \langle j m j - m | 00 \rangle \left( c_{\nu jm}^\dagger c_{\pi j - m}^\dagger + c_{\pi jm}^\dagger c_{\nu j - m}^\dagger \right) \\
&= \left[ c_{\nu j}^\dagger \otimes c_{\pi j}^\dagger \right]_0^{(0)}, \tag{B.4.1}
\end{aligned}$$

$$\begin{aligned}
A_{0010}(jj) &= \frac{1}{2} \sum_m \langle j m j - m | 00 \rangle (c_{\pi j - m} c_{\nu jm} + c_{\nu j - m} c_{\pi jm}) \\
&= -\frac{1}{2} \sum_m \langle j m j - m | 00 \rangle (\tilde{c}_{\pi jm} \tilde{c}_{\nu j - m} + \tilde{c}_{\nu jm} \tilde{c}_{\pi j - m}) \\
&= -\left[ \tilde{c}_{\nu j} \otimes \tilde{c}_{\pi j} \right]_0^{(0)}, \tag{B.4.2}
\end{aligned}$$

the neutron-proton pairing interaction is given as

$$\begin{aligned}
H_{J=0, \mu=0}^{(\text{pair})} &= -\frac{1}{2} g_{00} \sum_{j_1 \leq j_2} P_{0010}^\dagger(j_1 j_2) \sum_{j_3 \leq j_4} P_{0010}(j_3 j_4) \\
&= \frac{1}{2} g_{00} \sum_{jj'} \sqrt{(2j+1)(2j'+1)} \left[ c_{\nu j}^\dagger \otimes c_{\pi j}^\dagger \right]_0^{(0)} \left[ \tilde{c}_{\nu j'} \otimes \tilde{c}_{\pi j'} \right]_0^{(0)} \\
&= \frac{1}{2} g_{00} \sum_{jj'} \sqrt{(2j+1)(2j'+1)} \left[ \left[ c_{\nu j}^\dagger \otimes c_{\pi j}^\dagger \right]_0^{(0)} \otimes \left[ \tilde{c}_{\nu j'} \otimes \tilde{c}_{\pi j'} \right]_0^{(0)} \right]_0^{(0)} \\
&= -\frac{1}{2} g_{00} \sum_{jj'} \sqrt{(2j+1)(2j'+1)} \\
&\quad \times \sum_K (2K+1) \begin{Bmatrix} j & j & 0 \\ j' & j' & 0 \\ K & K & 0 \end{Bmatrix} \left[ \left[ c_{\nu j}^\dagger \otimes \tilde{c}_{\nu j'} \right]^{(K)} \otimes \left[ c_{\pi j}^\dagger \otimes \tilde{c}_{\pi j'} \right]^{(K)} \right]_0^{(0)} \\
&= -\frac{1}{2} g_{00} \sum_{jj'} \sqrt{(2j+1)(2j'+1)} \\
&\quad \times \sum_K (2K+1) \frac{(-1)^{2K}}{\sqrt{2K+1}} \begin{Bmatrix} j & j & 0 \\ j' & j' & K \end{Bmatrix} \left[ \left[ c_{\nu j}^\dagger \otimes \tilde{c}_{\nu j'} \right]^{(K)} \otimes \left[ c_{\pi j}^\dagger \otimes \tilde{c}_{\pi j'} \right]^{(K)} \right]_0^{(0)} \\
&= -\frac{1}{2} g_{00} \sum_{jj'} \sqrt{(2j+1)(2j'+1)}
\end{aligned}$$

$$\begin{aligned}
& \times \sum_K \sqrt{2K+1} \frac{(-1)^{K+j+j'}}{\sqrt{(2j+1)(2j'+1)}} \left[ \left[ c_{\nu j}^\dagger \otimes \tilde{c}_{\nu j'} \right]^{(K)} \otimes \left[ c_{\pi j}^\dagger \otimes \tilde{c}_{\pi j'} \right]^{(K)} \right]_0^{(0)} \\
& = -\frac{1}{2} g_{00} \sum_K \sqrt{2K+1} \sum_{jj'} (-1)^{K+j+j'} \left[ \left[ c_{\nu j}^\dagger \otimes \tilde{c}_{\nu j'} \right]^{(K)} \otimes \left[ c_{\pi j}^\dagger \otimes \tilde{c}_{\pi j'} \right]^{(K)} \right]_0^{(0)}. \quad (\text{B.4.3})
\end{aligned}$$

### B.4.2 Isoscalar-pairing

The isoscalar pairing interaction is defined by

$$H_{\tau=0} = - \sum_{j_1 \leq j_2} \sum_{j_3 \leq j_4} \sum_J k_J (j_1 j_2, j_3 j_4) \sum_M A_{JM00}^\dagger(j_1 j_2) A_{JM00}(j_3 j_4). \quad (\text{B.4.4})$$

Here we adopt  $k_J(j_1 j_2, j_3 j_4) = k_0$  as a phenomenological constant common to any  $J$ . The isoscalar pairing operator is expressed as

$$\begin{aligned}
A_{JM00}^\dagger(j_1 j_2) &= \sum_{m_1 m_2} \sum_\tau \langle j_1 m_1 j_2 m_2 | JM \rangle \left\langle \frac{1}{2} \tau \frac{1}{2} - \tau \middle| 00 \right\rangle \frac{1}{\sqrt{1 + \delta_{j_1 j_2}}} c_{\tau j_1 m_1}^\dagger c_{-\tau j_2 m_2}^\dagger \\
&= \sum_{m_1 m_2} \langle j_1 m_1 j_2 m_2 | JM \rangle \frac{1}{\sqrt{1 + \delta_{j_1 j_2}}} \frac{1}{\sqrt{2}} \left[ c_{\nu j_1 m_1}^\dagger c_{\pi j_2 m_2}^\dagger - c_{\pi j_1 m_1}^\dagger c_{\nu j_2 m_2}^\dagger \right] \\
&= \frac{1}{\sqrt{2(1 + \delta_{j_1 j_2})}} \left[ \left[ c_{\nu j_1}^\dagger \otimes c_{\pi j_2}^\dagger \right]_M^{(J)} + (-1)^{j_1+j_2-J} \left[ c_{\nu j_2}^\dagger \otimes c_{\pi j_1}^\dagger \right]_M^{(J)} \right]. \quad (\text{B.4.5})
\end{aligned}$$

If  $\tau \neq \tau'$ , using  $c_{\tau j m} = (-1)^{j+m} \tilde{c}_{\tau j -m}$ ,

$$\begin{aligned}
\left( \left[ c_{\tau j_1}^\dagger \otimes c_{\tau' j_2}^\dagger \right]_M^{(J)} \right)^\dagger &= \sum_{m_1 m_2} \langle j_1 m_1 j_2 m_2 | JM \rangle \left( c_{\tau j_1 m_1}^\dagger c_{\tau' j_2 m_2}^\dagger \right)^\dagger \\
&= \sum_{m_1 m_2} \langle j_1 m_1 j_2 m_2 | JM \rangle c_{\tau' j_2 m_2} c_{\tau j_1 m_1} \\
&= - \sum_{m_1 m_2} (-1)^{j_1+j_2-J} \langle j_1 - m_1 j_2 - m_2 | J - M \rangle \\
&\quad \times (-1)^{j_1+m_1} \tilde{c}_{\tau j_1 -m_1} (-1)^{j_2+m_2} \tilde{c}_{\tau' j_2 -m_2} \\
&= -(-1)^{J+M} \left[ \tilde{c}_{\tau j_1} \otimes \tilde{c}_{\tau' j_2} \right]_{-M}^{(J)}. \quad (\text{B.4.6})
\end{aligned}$$

Thus,

$$A_{JM00}(j_1 j_2) = -\frac{(-1)^{J+M}}{\sqrt{2(1 + \delta_{j_1 j_2})}} \left[ \left[ \tilde{c}_{\nu j_1} \otimes \tilde{c}_{\pi j_2} \right]_{-M}^{(J)} + (-1)^{j_1+j_2-J} \left[ \tilde{c}_{\nu j_2} \otimes \tilde{c}_{\pi j_1} \right]_{-M}^{(J)} \right], \quad (\text{B.4.7})$$

and

$$\begin{aligned}
H_{\tau=0} &= -k_0 \sum_{j_1 \leq j_2} \sum_{JM} A_{JM00}^\dagger(j_1 j_2) A_{JM00}(j_1 j_2) \\
&= k_0 \sum_{j_1 \leq j_2} \sum_{JM} \frac{1}{\sqrt{2(1+\delta_{j_1 j_2})}} \left[ \left[ c_{\nu j_1}^\dagger \otimes c_{\pi j_2}^\dagger \right]_M^{(J)} + (-1)^{j_1+j_2-J} \left[ c_{\nu j_2}^\dagger \otimes c_{\pi j_1}^\dagger \right]_M^{(J)} \right] \\
&\quad \times \frac{(-1)^{J+M}}{\sqrt{2(1+\delta_{j_1 j_2})}} \left[ \left[ \tilde{c}_{\nu j_1} \otimes \tilde{c}_{\pi j_2} \right]_{-M}^{(J)} + (-1)^{j_1+j_2-J} \left[ \tilde{c}_{\nu j_2} \otimes \tilde{c}_{\pi j_1} \right]_{-M}^{(J)} \right] \\
&= \frac{k_0}{2} \sum_{j_1 \leq j_2} \sum_{JM} \frac{(-1)^{J+M}}{1+\delta_{j_1 j_2}} \left[ \left[ c_{\nu j_1}^\dagger \otimes c_{\pi j_2}^\dagger \right]_M^{(J)} + (-1)^{j_1+j_2-J} \left[ c_{\nu j_2}^\dagger \otimes c_{\pi j_1}^\dagger \right]_M^{(J)} \right] \\
&\quad \times \left[ \left[ \tilde{c}_{\nu j_1} \otimes \tilde{c}_{\pi j_2} \right]_{-M}^{(J)} + (-1)^{j_1+j_2-J} \left[ \tilde{c}_{\nu j_2} \otimes \tilde{c}_{\pi j_1} \right]_{-M}^{(J)} \right] \\
&= \frac{k_0}{2} \sum_{j_1 \leq j_2} \sum_{JM} \frac{(-1)^{J+M}}{1+\delta_{j_1 j_2}} \left[ \left[ c_{\nu j_1}^\dagger \otimes c_{\pi j_2}^\dagger \right]_M^{(J)} \left[ \tilde{c}_{\nu j_1} \otimes \tilde{c}_{\pi j_2} \right]_{-M}^{(J)} \right. \\
&\quad + (-1)^{j_1+j_2-J} \left[ c_{\nu j_1}^\dagger \otimes c_{\pi j_2}^\dagger \right]_M^{(J)} \left[ \tilde{c}_{\nu j_2} \otimes \tilde{c}_{\pi j_1} \right]_{-M}^{(J)} \\
&\quad + (-1)^{j_1+j_2-J} \left[ c_{\nu j_2}^\dagger \otimes c_{\pi j_1}^\dagger \right]_M^{(J)} \left[ \tilde{c}_{\nu j_1} \otimes \tilde{c}_{\pi j_2} \right]_{-M}^{(J)} \\
&\quad \left. + \left[ c_{\nu j_2}^\dagger \otimes c_{\pi j_1}^\dagger \right]_M^{(J)} \left[ \tilde{c}_{\nu j_2} \otimes \tilde{c}_{\pi j_1} \right]_{-M}^{(J)} \right], \tag{B.4.8}
\end{aligned}$$

where the anti-symmetric property is applied to get the last line. Using the explicit value of a CG coefficient  $(-1)^{J+M} = \sqrt{2J+1} \langle JM J - M | 00 \rangle$  for integer  $J$ , the first term is

$$\begin{aligned}
&\sum_{JM} (-1)^{J+M} \left[ c_{\nu j_1}^\dagger \otimes c_{\pi j_2}^\dagger \right]_M^{(J)} \left[ \tilde{c}_{\nu j_1} \otimes \tilde{c}_{\pi j_2} \right]_{-M}^{(J)} \\
&= \sum_J \sqrt{2J+1} \left[ \left[ c_{\nu j_1}^\dagger \otimes c_{\pi j_2}^\dagger \right]^{(J)} \otimes \left[ \tilde{c}_{\nu j_1} \otimes \tilde{c}_{\pi j_2} \right]^{(J)} \right]_0^{(0)} \\
&= - \sum_J \sqrt{2J+1} \sum_K (2J+1)(2K+1) \left\{ \begin{matrix} j_1 & j_2 & J \\ j_1 & j_2 & J \\ K & K & 0 \end{matrix} \right\} \\
&\quad \times \left[ \left[ c_{\nu j_1}^\dagger \otimes \tilde{c}_{\nu j_1} \right]^{(K)} \otimes \left[ c_{\pi j_2}^\dagger \otimes \tilde{c}_{\pi j_2} \right]^{(K)} \right]_0^{(0)} \\
&= - \sum_J (2J+1) \sum_K \sqrt{2K+1} (-1)^{j_1+j_2+J+K} \left\{ \begin{matrix} j_1 & j_2 & J \\ j_2 & j_1 & K \end{matrix} \right\} \\
&\quad \times \left[ \left[ c_{\nu j_1}^\dagger \otimes \tilde{c}_{\nu j_1} \right]^{(K)} \otimes \left[ c_{\pi j_2}^\dagger \otimes \tilde{c}_{\pi j_2} \right]^{(K)} \right]_0^{(0)} \\
&= - \sum_K (-1)^K \sqrt{2K+1} \sum_J (-1)^{j_1+j_2+J} (2J+1) \left\{ \begin{matrix} j_1 & j_1 & K \\ j_2 & j_2 & J \end{matrix} \right\} \\
&\quad \times \left[ \left[ c_{\nu j_1}^\dagger \otimes \tilde{c}_{\nu j_1} \right]^{(K)} \otimes \left[ c_{\pi j_2}^\dagger \otimes \tilde{c}_{\pi j_2} \right]^{(K)} \right]_0^{(0)}
\end{aligned}$$

$$\begin{aligned}
&= - \sum_K (-1)^K \sqrt{(2K+1)(2j_1+1)(2j_2+1)} \delta_{K0} \left[ \left[ c_{\nu j_1}^\dagger \otimes \tilde{c}_{\nu j_1} \right]^{(K)} \otimes \left[ c_{\pi j_2}^\dagger \otimes \tilde{c}_{\pi j_2} \right]^{(K)} \right]_0^{(0)} \\
&= - \sqrt{(2j_1+1)(2j_2+1)} \left[ c_{\nu j_1}^\dagger \otimes \tilde{c}_{\nu j_1} \right]^{(0)} \left[ c_{\pi j_2}^\dagger \otimes \tilde{c}_{\pi j_2} \right]^{(0)}, \tag{B.4.9}
\end{aligned}$$

and the second term is

$$\begin{aligned}
&\sum_{JM} (-1)^{j_1+j_2+M} \left[ c_{\nu j_1}^\dagger \otimes c_{\pi j_2}^\dagger \right]_M^{(J)} \left[ \tilde{c}_{\nu j_2} \otimes \tilde{c}_{\pi j_1} \right]_{-M}^{(J)} \\
&= \sum_J (-1)^{j_1+j_2+J} \sqrt{2J+1} \left[ \left[ c_{\nu j_1}^\dagger \otimes c_{\pi j_2}^\dagger \right]^{(J)} \otimes \left[ \tilde{c}_{\nu j_2} \otimes \tilde{c}_{\pi j_1} \right]^{(J)} \right]_0^{(0)} \\
&= - \sum_J (-1)^{j_1+j_2+J} \sqrt{2J+1} \sum_K (2J+1)(2K+1) \begin{Bmatrix} j_1 & j_2 & J \\ j_2 & j_1 & J \\ K & K & 0 \end{Bmatrix} \\
&\quad \times \left[ \left[ c_{\nu j_1}^\dagger \otimes \tilde{c}_{\nu j_2} \right]^{(K)} \otimes \left[ c_{\pi j_2}^\dagger \otimes \tilde{c}_{\pi j_1} \right]^{(K)} \right]_0^{(0)} \\
&= \sum_J (-1)^{j_1+j_2+J} (2J+1) \sum_K \sqrt{2K+1} (-1)^{J+K} \begin{Bmatrix} j_1 & j_2 & J \\ j_1 & j_2 & K \end{Bmatrix} \\
&\quad \times \left[ \left[ c_{\nu j_1}^\dagger \otimes \tilde{c}_{\nu j_2} \right]^{(K)} \otimes \left[ c_{\pi j_2}^\dagger \otimes \tilde{c}_{\pi j_1} \right]^{(K)} \right]_0^{(0)} \\
&= (-1)^{j_1+j_2} \sum_K (-1)^K \sqrt{2K+1} \sum_J (2J+1) \begin{Bmatrix} j_1 & j_2 & J \\ j_1 & j_2 & K \end{Bmatrix} \\
&\quad \times \left[ \left[ c_{\nu j_1}^\dagger \otimes \tilde{c}_{\nu j_2} \right]^{(K)} \otimes \left[ c_{\pi j_2}^\dagger \otimes \tilde{c}_{\pi j_1} \right]^{(K)} \right]_0^{(0)} \\
&= (-1)^{j_1+j_2} \sum_K (-1)^K \sqrt{2K+1} \left[ \left[ c_{\nu j_1}^\dagger \otimes \tilde{c}_{\nu j_2} \right]^{(K)} \otimes \left[ c_{\pi j_2}^\dagger \otimes \tilde{c}_{\pi j_1} \right]^{(K)} \right]_0^{(0)}. \tag{B.4.10}
\end{aligned}$$

Similarly the third and the last terms are given as

$$\begin{aligned}
&\sum_{JM} (-1)^{j_1+j_2+M} \left[ c_{\nu j_2}^\dagger \otimes c_{\pi j_1}^\dagger \right]_M^{(J)} \left[ \tilde{c}_{\nu j_1} \otimes \tilde{c}_{\pi j_2} \right]_{-M}^{(J)} \\
&= (-1)^{j_1+j_2} \sum_K (-1)^K \sqrt{2K+1} \left[ \left[ c_{\nu j_2}^\dagger \otimes \tilde{c}_{\nu j_1} \right]^{(K)} \otimes \left[ c_{\pi j_1}^\dagger \otimes \tilde{c}_{\pi j_2} \right]^{(K)} \right]_0^{(0)} \tag{B.4.11}
\end{aligned}$$

$$\begin{aligned}
&\sum_{JM} (-1)^{J+M} \left[ c_{\nu j_2}^\dagger \otimes c_{\pi j_1}^\dagger \right]_M^{(J)} \left[ \tilde{c}_{\nu j_2} \otimes \tilde{c}_{\pi j_1} \right]_{-M}^{(J)} \\
&= - \sqrt{(2j_1+1)(2j_2+1)} \left[ c_{\nu j_2}^\dagger \otimes \tilde{c}_{\nu j_2} \right]^{(0)} \left[ c_{\pi j_1}^\dagger \otimes \tilde{c}_{\pi j_1} \right]^{(0)}. \tag{B.4.12}
\end{aligned}$$

The first and the last term are combined as

$$\begin{aligned}
H_{\tau=0}(14) &= - \frac{k_0}{2} \sum_{j_1 \leq j_2} \frac{1}{1 + \delta_{j_1 j_2}} \sqrt{(2j_1+1)(2j_2+1)} \\
&\quad \times \left[ \left[ c_{\nu j_1}^\dagger \otimes \tilde{c}_{\nu j_1} \right]^{(0)} \left[ c_{\pi j_2}^\dagger \otimes \tilde{c}_{\pi j_2} \right]^{(0)} + \left[ c_{\nu j_2}^\dagger \otimes \tilde{c}_{\nu j_2} \right]^{(0)} \left[ c_{\pi j_1}^\dagger \otimes \tilde{c}_{\pi j_1} \right]^{(0)} \right]
\end{aligned}$$

$$\begin{aligned}
&= -\frac{k_0}{2} \sum_{j_1 \leq j_2} \frac{1}{1 + \delta_{j_1 j_2}} \sqrt{(2j_1 + 1)(2j_2 + 1)} \left[ c_{\nu j_1}^\dagger \otimes \tilde{c}_{\nu j_1} \right]^{(0)} \left[ c_{\pi j_2}^\dagger \otimes \tilde{c}_{\pi j_2} \right]^{(0)} \\
&\quad - \frac{k_0}{2} \sum_{j_1 \geq j_2} \frac{1}{1 + \delta_{j_1 j_2}} \sqrt{(2j_1 + 1)(2j_2 + 1)} \left[ c_{\nu j_1}^\dagger \otimes \tilde{c}_{\nu j_1} \right]^{(0)} \left[ c_{\pi j_2}^\dagger \otimes \tilde{c}_{\pi j_2} \right]^{(0)} \\
&= -k_0 \sum_{j_1} (2j_1 + 1) \left[ c_{\nu j_1}^\dagger \otimes \tilde{c}_{\nu j_1} \right]^{(0)} \left[ c_{\pi j_1}^\dagger \otimes \tilde{c}_{\pi j_1} \right]^{(0)} \\
&\quad - \frac{k_0}{2} \sum_{j_1 \neq j_2} \sqrt{(2j_1 + 1)(2j_2 + 1)} \left[ c_{\nu j_1}^\dagger \otimes \tilde{c}_{\nu j_1} \right]^{(0)} \left[ c_{\pi j_2}^\dagger \otimes \tilde{c}_{\pi j_2} \right]^{(0)} \\
&= -\frac{k_0}{2} \sum_{j_1, j_2} \sqrt{(2j_1 + 1)(2j_2 + 1)} \left[ c_{\nu j_1}^\dagger \otimes \tilde{c}_{\nu j_1} \right]^{(0)} \left[ c_{\pi j_2}^\dagger \otimes \tilde{c}_{\pi j_2} \right]^{(0)} \\
&= -\frac{k_0}{2} N_\nu N_\pi, \tag{B.4.13}
\end{aligned}$$

where

$$N_\tau \equiv \sum_{\tau j m} c_{\tau j m}^\dagger c_{\tau j m} = - \sum_j \sqrt{2j + 1} \left[ c_{\tau j}^\dagger \otimes \tilde{c}_{\tau j} \right]_0^{(0)} \tag{B.4.14}$$

is the number operator.

The second and the third terms are combined as

$$\begin{aligned}
&H_{\tau=0}(23) \\
&= \frac{k_0}{2} \sum_{j_1 \leq j_2} \frac{1}{1 + \delta_{j_1 j_2}} (-1)^{j_1 + j_2} \sum_K (-1)^K \sqrt{2K + 1} \\
&\quad \times \left[ \left[ \left[ c_{\nu j_1}^\dagger \otimes \tilde{c}_{\nu j_2} \right]^{(K)} \otimes \left[ c_{\pi j_2}^\dagger \otimes \tilde{c}_{\pi j_1} \right]^{(K)} \right]_0^{(0)} + \left[ \left[ c_{\nu j_2}^\dagger \otimes \tilde{c}_{\nu j_1} \right]^{(K)} \otimes \left[ c_{\pi j_1}^\dagger \otimes \tilde{c}_{\pi j_2} \right]^{(K)} \right]_0^{(0)} \right] \\
&= \frac{k_0}{2} \sum_{j_1, j_2} (-1)^{j_1 + j_2} \sum_K (-1)^K \sqrt{2K + 1} \left[ \left[ c_{\nu j_1}^\dagger \otimes \tilde{c}_{\nu j_2} \right]^{(K)} \otimes \left[ c_{\pi j_2}^\dagger \otimes \tilde{c}_{\pi j_1} \right]^{(K)} \right]_0^{(0)}. \tag{B.4.15}
\end{aligned}$$

The reduced matrix elements according to many-body bases

$$|(J_\nu J_\pi) JM\rangle = \sum_{M_\nu M_\pi} \langle J_\nu M_\nu J_\pi M_\pi | JM\rangle |J_\nu M_\nu\rangle |J_\pi M_\pi\rangle, \tag{B.4.16}$$

are given by

$$\begin{aligned}
&\langle J || H_{\tau=0}(23) || J \rangle \\
&= \frac{k_0}{2} \sum_{j_1, j_2} (-1)^{j_1 + j_2} \sum_K (-1)^K \sqrt{2K + 1} \left\langle J \left\| \left[ \left[ c_{\nu j_1}^\dagger \otimes \tilde{c}_{\nu j_2} \right]^{(K)} \otimes \left[ c_{\pi j_2}^\dagger \otimes \tilde{c}_{\pi j_1} \right]^{(K)} \right]_0^{(0)} \right\| J \right\rangle \\
&= \frac{k_0}{2} \sum_{j_1, j_2} (-1)^{j_1 + j_2} \sum_K (-1)^K \sqrt{2K + 1} (2J + 1) \begin{Bmatrix} J_\nu f & J_\pi f & J \\ J_\nu i & J_\pi i & J \\ K & K & 0 \end{Bmatrix} \\
&\quad \times \left\langle J_\nu f M_\nu f \left\| \left[ c_{\nu j_1}^\dagger \otimes \tilde{c}_{\nu j_2} \right]^{(K)} \right\| J_\nu i M_\nu i \right\rangle \left\langle J_\pi f M_\pi f \left\| \left[ c_{\pi j_2}^\dagger \otimes \tilde{c}_{\pi j_1} \right]^{(K)} \right\| J_\pi i M_\pi i \right\rangle
\end{aligned}$$

$$\begin{aligned}
&= \frac{k_0}{2} \sum_{j_1, j_2} (-1)^{j_1+j_2} \sum_K (-1)^K \sqrt{(2K+1)} (2J+1) \frac{(-1)^{J_{\nu i}+J_{\pi f}+J+K}}{\sqrt{(2J+1)(2K+1)}} \begin{Bmatrix} J_{\nu f} & J_{\pi f} & J \\ J_{\pi i} & J_{\nu i} & K \end{Bmatrix} \\
&\quad \times \left\langle J_{\nu f} M_{\nu f} \left\| \left[ c_{\nu j_1}^\dagger \otimes \tilde{c}_{\nu j_2} \right]^{(K)} \right\| J_{\nu i} M_{\nu i} \right\rangle \left\langle J_{\pi f} M_{\pi f} \left\| \left[ c_{\pi j_2}^\dagger \otimes \tilde{c}_{\pi j_1} \right]^{(K)} \right\| J_{\pi i} M_{\pi i} \right\rangle \\
&= \frac{k_0}{2} \sum_{j_1, j_2} (-1)^{j_1+j_2} \sum_K \sqrt{2J+1} (-1)^{J_{\nu i}+J_{\pi f}+J} \begin{Bmatrix} J_{\nu f} & J_{\pi f} & J \\ J_{\pi i} & J_{\nu i} & K \end{Bmatrix} \\
&\quad \times \left\langle J_{\nu f} M_{\nu f} \left\| \left[ c_{\nu j_1}^\dagger \otimes \tilde{c}_{\nu j_2} \right]^{(K)} \right\| J_{\nu i} M_{\nu i} \right\rangle \\
&\quad \times \left\langle J_{\pi f} M_{\pi f} \left\| \left[ c_{\pi j_2}^\dagger \otimes \tilde{c}_{\pi j_1} \right]^{(K)} \right\| J_{\pi i} M_{\pi i} \right\rangle. \tag{B.4.17}
\end{aligned}$$

### B.4.3 Isospin

We evaluate the expectation value of isospin

$$\mathbf{T}^2 = T_+ T_- + T_z^2 - T_z, \tag{B.4.18}$$

where  $T_\pm$  are ladder operators expressed in second quantized form as

$$\begin{aligned}
T_+ &\equiv \sum_{jm} c_{\nu jm}^\dagger c_{\pi jm} = \sum_{jm} (-1)^{j+m} c_{\nu jm}^\dagger \tilde{c}_{\pi j-m} \\
&= \sum_{jm} (-1)^{j+m} (-1)^{-j+m} \sqrt{2j+1} \langle j m j - m | 0 0 \rangle c_{\nu jm}^\dagger \tilde{c}_{\pi j-m} \\
&= - \sum_j \sqrt{2j+1} \left[ c_{\nu j}^\dagger \otimes \tilde{c}_{\pi j} \right]_0^{(0)}, \tag{B.4.19}
\end{aligned}$$

$$T_- \equiv \sum_{jm} c_{\pi jm}^\dagger c_{\nu jm} = - \sum_j \sqrt{2j+1} \left[ c_{\pi j}^\dagger \otimes \tilde{c}_{\nu j} \right]_0^{(0)}. \tag{B.4.20}$$

First the uncontracted term is given as

$$\begin{aligned}
T_+ T_- &= \left( - \sum_j \sqrt{2j+1} \left[ c_{\nu j}^\dagger \otimes \tilde{c}_{\pi j} \right]_0^{(0)} \right) \left( - \sum_{j'} \sqrt{2j'+1} \left[ c_{\pi j'}^\dagger \otimes \tilde{c}_{\nu j'} \right]_0^{(0)} \right) \\
&= \sum_{jj'} \sqrt{2j+1} \sqrt{2j'+1} \left[ \left[ c_{\nu j}^\dagger \otimes \tilde{c}_{\pi j} \right]^{(0)} \otimes \left[ c_{\pi j'}^\dagger \otimes \tilde{c}_{\nu j'} \right]^{(0)} \right]_0^{(0)} \\
&= \sum_{jj'} \sqrt{2j+1} \sqrt{2j'+1} \left[ \left[ c_{\nu j}^\dagger \otimes \tilde{c}_{\pi j} \right]^{(0)} \otimes \left[ \tilde{c}_{\nu j'} \otimes c_{\pi j'}^\dagger \right]^{(0)} \right]_0^{(0)} \\
&= - \sum_{jj'} \sqrt{2j+1} \sqrt{2j'+1} \sum_K (2K+1) \begin{Bmatrix} j & j & 0 \\ j' & j' & 0 \\ K & K & 0 \end{Bmatrix} \\
&\quad \times \left[ \left[ c_{\nu j}^\dagger \otimes \tilde{c}_{\nu j'} \right]^{(K)} \otimes \left[ \tilde{c}_{\pi j} \otimes c_{\pi j'}^\dagger \right]^{(K)} \right]_0^{(0)}
\end{aligned}$$

$$\begin{aligned}
&= - \sum_{jj'} \sqrt{2j+1} \sqrt{2j'+1} \sum_K (2K+1) \frac{(-1)^{j+j'+K}}{\sqrt{2K+1}} \begin{Bmatrix} j & j & 0 \\ j' & j' & K \end{Bmatrix} \\
&\quad \times \left[ \left[ c_{\nu j}^\dagger \otimes \tilde{c}_{\nu j'} \right]^{(K)} \otimes \left[ \tilde{c}_{\pi j} \otimes c_{\pi j'}^\dagger \right]^{(K)} \right]_0^{(0)} \\
&= - \sum_{jj'} \sqrt{2j+1} \sqrt{2j'+1} \sum_K (2K+1) \frac{(-1)^{j+j'+K}}{\sqrt{2K+1}} \frac{(-1)^{j+j'+K}}{\sqrt{(2j+1)(2j'+1)}} \\
&\quad \times \left[ \left[ c_{\nu j}^\dagger \otimes \tilde{c}_{\nu j'} \right]^{(K)} \otimes \left[ \tilde{c}_{\pi j} \otimes c_{\pi j'}^\dagger \right]^{(K)} \right]_0^{(0)} \\
&= - \sum_{jj'} \sum_K \sqrt{2K+1} \left[ \left[ c_{\nu j}^\dagger \otimes \tilde{c}_{\nu j'} \right]^{(K)} \otimes \left[ \tilde{c}_{\pi j} \otimes c_{\pi j'}^\dagger \right]^{(K)} \right]_0^{(0)} \\
&= \sum_{jj'} (-1)^{j+j'} \sum_K \sqrt{2K+1} (-1)^K \left[ \left[ c_{\nu j}^\dagger \otimes \tilde{c}_{\nu j'} \right]^{(K)} \otimes \left[ c_{\pi j'}^\dagger \otimes \tilde{c}_{\pi j} \right]^{(K)} \right]_0^{(0)} \\
&\quad + \sum_{jj'} (-1)^{j+j'} \sqrt{2j+1} \delta_{j,j'} \left[ c_{\nu j}^\dagger \otimes \tilde{c}_{\nu j'} \right]_0^{(0)} \\
&= \sum_{jj'} (-1)^{j+j'} \sum_K (-1)^K \sqrt{2K+1} \left[ \left[ c_{\nu j}^\dagger \otimes \tilde{c}_{\nu j'} \right]^{(K)} \otimes \left[ c_{\pi j'}^\dagger \otimes \tilde{c}_{\pi j} \right]^{(K)} \right]_0^{(0)} + N_\nu. \quad (\text{B.4.21})
\end{aligned}$$

The first term is same as a part of the isoscalar pairing interaction  $H_{\tau=0}(23)$  except for the factor.

#### B.4.4 Tensor interaction

Under the rotational invariance and the parity invariance, possible two-body interactions except of central forces are the spin-spin interactions proportional to  $\mathbf{s}_1 \cdot \mathbf{s}_2$ , and the tensor interactions defined as

$$\left[ s_1^{(1)} \otimes s_2^{(1)} \right]^{(2)} \cdot \left[ r^{(1)} \otimes r^{(1)} \right]^{(2)} = (\mathbf{s}_1 \cdot \mathbf{r})(\mathbf{s}_2 \cdot \mathbf{r}) - \frac{1}{3} (\mathbf{s}_1 \cdot \mathbf{s}_2) r^2, \quad (\text{B.4.22})$$

where  $\mathbf{s}_1$  and  $\mathbf{s}_2$  indicate the spin matrices, and  $\mathbf{r} = \mathbf{r}_1 - \mathbf{r}_2$  is the relative coordinate of two nucleons. The right expression can be deduced as follows. Starting from the the first term of the right-hand,

$$\begin{aligned}
&\left[ \left[ s_1^{(1)} \otimes r^{(1)} \right]^{(0)} \otimes \left[ s_2^{(1)} \otimes r^{(1)} \right]^{(0)} \right]_0^{(0)} \\
&= \sum_{k=0,2} (2k+1) \begin{Bmatrix} 1 & 1 & 0 \\ 1 & 1 & 0 \\ k & k & 0 \end{Bmatrix} \left[ \left[ s_1^{(1)} \otimes s_2^{(1)} \right]^{(k)} \otimes \left[ r^{(1)} \otimes r^{(1)} \right]^{(k)} \right]_0^{(0)} \\
&= \sum_{k=0,2} \sqrt{2k+1} \begin{Bmatrix} 1 & 1 & 0 \\ 1 & 1 & k \end{Bmatrix} \left[ \left[ s_1^{(1)} \otimes s_2^{(1)} \right]^{(k)} \otimes \left[ r^{(1)} \otimes r^{(1)} \right]^{(k)} \right]_0^{(0)} \\
&= \sum_{k=0,2} \frac{\sqrt{2k+1}}{3} \left[ \left[ s_1^{(1)} \otimes s_2^{(1)} \right]^{(k)} \otimes \left[ r^{(1)} \otimes r^{(1)} \right]^{(k)} \right]_0^{(0)}
\end{aligned}$$

$$\begin{aligned}
&= \frac{1}{3} \left[ \left[ s_1^{(1)} \otimes s_2^{(1)} \right]^{(0)} \otimes \left[ r^{(1)} \otimes r^{(1)} \right]^{(0)} \right]_0^{(0)} + \frac{\sqrt{5}}{3} \left[ \left[ s_1^{(1)} \otimes s_2^{(1)} \right]^{(2)} \otimes \left[ r^{(1)} \otimes r^{(1)} \right]^{(2)} \right]_0^{(0)} \\
&= \frac{1}{9} (\mathbf{s}_1 \cdot \mathbf{s}_2) r^2 + \frac{1}{3} \left[ s_1^{(1)} \otimes s_2^{(1)} \right]^{(2)} \cdot \left[ r^{(1)} \otimes r^{(1)} \right]^{(2)}. \tag{B.4.23}
\end{aligned}$$

Here,  $\left[ r^{(1)} \otimes r^{(1)} \right]^{(1)} = 0$  is used to abandon the  $k = 1$  term in the first equality. This relation for the rank-1 coupling of the same two tensor operators is deduced from the CG-coefficient properties of

$$\begin{aligned}
\langle 1 m_1 1 m_2 | 1 M \rangle &= -\langle 1 m_2 1 m_1 | 1 M \rangle, \\
\langle 1 m_1 1 m_2 | 1 M \rangle &= -\langle 1 -m_1 1 -m_2 | 1 -M \rangle. \tag{B.4.24}
\end{aligned}$$

The second term in the right-hand is given as

$$\begin{aligned}
\left[ s_1^{(1)} \otimes s_2^{(1)} \right]^{(2)} \cdot \left[ r^{(1)} \otimes r^{(1)} \right]^{(2)} &= 3 \left[ \left[ s_1^{(1)} \otimes r^{(1)} \right]^{(0)} \otimes \left[ s_2^{(1)} \otimes r^{(1)} \right]^{(0)} \right]_0^{(0)} - \frac{1}{3} (\mathbf{s}_1 \cdot \mathbf{s}_2) r^2 \\
&= (\mathbf{s}_1 \cdot \mathbf{r})(\mathbf{s}_2 \cdot \mathbf{r}) - \frac{1}{3} (\mathbf{s}_1 \cdot \mathbf{s}_2) r^2. \tag{B.4.25}
\end{aligned}$$

## B.5 Particle-Hole transformation for P+QQ interaction

### B.5.1 Particle-Hole transformation

Here we consider  $n$ -particle states  $|n\text{-particles}\rangle$  in a single  $j$ -shell. The particle-hole transformation operator  $\Gamma$  is defined by

$$\Gamma |n\text{-particles}\rangle = |n'\text{-holes}\rangle, \tag{B.5.1}$$

where  $n' = 2j + 1 - n$  is the number of holes in the same shell.  $\Gamma$  is an unitary operator, which satisfies

$$\Gamma^\dagger \Gamma = \Gamma \Gamma^\dagger = 1, \tag{B.5.2}$$

since  $\Gamma$  transforms one complete orthonormal set of  $|n\text{-particles}\rangle$  into another complete orthonormal set of  $|n\text{-particles}\rangle$ .

We define the hole operator as

$$b_{jm}^\dagger \equiv -\Gamma \tilde{a}_{jm} \Gamma^\dagger, \tag{B.5.3}$$

which is accompanied with one-hole states

$$|jm\rangle_h \equiv b_{jm}^\dagger |0\rangle_h. \tag{B.5.4}$$

The hole annihilation operator can be constructed by the same expression as the particle's as

$$\tilde{b}_{jm} \equiv (-1)^{j-m} b_{j-m} = -(-1)^{2j} \Gamma a_{jm}^\dagger \Gamma^\dagger = \Gamma a_{jm}^\dagger \Gamma^\dagger. \tag{B.5.5}$$

The hole vacuum state is defined by

$$|0\rangle_h \equiv \Gamma|\text{full shell}\rangle_p, \quad (\text{B.5.6})$$

where

$$|\text{full shell}\rangle_p = \frac{1}{\Omega!} (S_+)^{\Omega} |0\rangle \quad (\text{B.5.7})$$

is the normalized full occupied state with  $J = 0$ . Here

$$S_+ = \sum_{m>0} (-1)^{j-m} a_{jm}^{\dagger} a_{j-m}^{\dagger} \quad (\text{B.5.8})$$

is the  $S$ -pair creation operator and  $\Omega = j + 1/2$  is the degeneracy. It can be immediately shown that

$$\tilde{b}_{jm}|0\rangle_h = 0. \quad (\text{B.5.9})$$

Thus it is revealed that the hole operators  $b_{jm}^{\dagger}$  and  $\tilde{b}_{jm}$  are ITOs. These states are related as follows:

$$0 = \Gamma a_{jm}^{\dagger} |\text{full shell}\rangle_p = \Gamma a_{jm}^{\dagger} \Gamma^{\dagger} \Gamma |\text{full shell}\rangle_p = \tilde{b}_{jm} |0\rangle_h \quad (\text{B.5.10})$$

$$0 = \Gamma b_{jm}^{\dagger} |\text{full shell}\rangle_h = \Gamma b_{jm}^{\dagger} \quad (\text{B.5.11})$$

Let us consider the fermion characters. The hole operator is defined by  $\tilde{c}_{jm} = (-1)^{j-m} c_{j-m}$ . The anti-commutation relations are given by

$$\{\tilde{c}_{jm}, c_{j'm'}^{\dagger}\} = (-1)^{j-m} \delta_{j,j'} \delta_{m,-m'}. \quad (\text{B.5.12})$$

The contraction is then

$$\begin{aligned} \left[ \overline{\tilde{c}_{jm} \otimes c_{j'm'}^{\dagger}} \right]_M^{(J)} &= \sum_{mm'} \langle j m j' m' | J M \rangle \overline{\tilde{c}_{jm} c_{j'm'}^{\dagger}} \\ &= \sum_m \langle j m j - m | J M \rangle (-1)^{j-m} \delta_{j,j'}. \end{aligned} \quad (\text{B.5.13})$$

For any two-body interactions,  $J = 0$ , then

$$\left[ \overline{\tilde{c}_{jm} \otimes c_{j'm'}^{\dagger}} \right]_0^{(0)} = \sum_m \langle j m j - m | 0 0 \rangle (-1)^{j-m} \delta_{j,j'} = \sqrt{2j+1} \delta_{j,j'}. \quad (\text{B.5.14})$$

## B.5.2 Pairing Interactions

The pairing interactions are given by

$$\begin{aligned} H_{\mu,J}^{(\text{pair})} &= \sum_{j_1 j_2 j_3 j_4} G_{\mu}(j_1 j_2, j_3 j_4; J) \left[ c_{\tau j_1}^{\dagger} \otimes c_{\tau' j_2}^{\dagger} \right]^{(J)} \cdot \left[ \tilde{c}_{\tau j_3} \otimes \tilde{c}_{\tau' j_4} \right]^{(J)} \\ &= (-1)^{-J} \sqrt{2J+1} \sum_{j_1 j_2 j_3 j_4} G_{\mu}(j_1 j_2, j_3 j_4; J) \left[ c_{\tau j_1}^{\dagger} \otimes c_{\tau' j_2}^{\dagger} \right]^{(J)} \otimes \left[ \tilde{c}_{\tau j_3} \otimes \tilde{c}_{\tau' j_4} \right]^{(J)} \Big|_0^{(0)}. \end{aligned} \quad (\text{B.5.15})$$

Applying the particle-hole translation  $b_{jm}^\dagger = -\tilde{a}_{jm}$ ,  $\tilde{b}_{jm} = a_{jm}^\dagger$ ,

$$\begin{aligned} H_{\mu,J}^{(\text{pair})} &= \sum_{j_1 j_2 j_3 j_4} G_\mu(j_1 j_2, j_3 j_4; J) \left[ b_{\tau j_1}^\dagger \otimes b_{\tau' j_2}^\dagger \right]^{(J)} \cdot \left[ \tilde{b}_{\tau j_3} \otimes \tilde{b}_{\tau' j_4} \right]^{(J)} \\ &= \sum_{j_1 j_2 j_3 j_4} G_\mu(j_1 j_2, j_3 j_4; J) \left[ \tilde{a}_{\tau j_1} \otimes \tilde{a}_{\tau' j_2} \right]^{(J)} \cdot \left[ a_{\tau j_3}^\dagger \otimes a_{\tau' j_4}^\dagger \right]^{(J)}. \end{aligned} \quad (\text{B.5.16})$$

First we consider the two-body interactions in the normal ordered form, namely, uncontracted term in Eq. (B.5.16). That term is

$$\begin{aligned} H_{\mu,J}^{(\text{pair})} (\text{hole; uncontracted}) &= \sum_{j_1 j_2 j_3 j_4} G_\mu(j_1 j_2, j_3 j_4; J) \left[ a_{\tau j_3}^\dagger \otimes a_{\tau' j_4}^\dagger \right]^{(J)} \cdot \left[ \tilde{a}_{\tau j_1} \otimes \tilde{a}_{\tau' j_2} \right]^{(J)} \\ &= \sum_{j_1 j_2 j_3 j_4} G_\mu(j_1 j_2, j_3 j_4; J) \left[ a_{\tau j_1}^\dagger \otimes a_{\tau' j_2}^\dagger \right]^{(J)} \cdot \left[ \tilde{a}_{\tau j_3} \otimes \tilde{a}_{\tau' j_4} \right]^{(J)}, \end{aligned} \quad (\text{B.5.17})$$

Here  $G_\mu(j_3 j_4, j_1 j_2; J) = G_\mu(j_1 j_2, j_3 j_4; J)$  readily obtained from the definition is used. This is the same form as in the particle picture. Thus in the following we concentrate on one-body and constant parts which are arisen by the particle-hole transformation.

In order to form the one-body part, we first consider the contraction of  $a_{\tau j_1}^\dagger$  and  $\tilde{a}_{\tau j_3}$ . In this case  $a_{\tau' j_2}^\dagger$  and  $\tilde{a}_{\tau' j_4}$  can be anti-commuted with each other. Thus this term can be recoupled as follows

$$\begin{aligned} &\overline{\left[ \tilde{a}_{\tau j_1} \otimes \tilde{a}_{\tau' j_2} \right]^{(J)} \cdot \left[ a_{\tau j_3}^\dagger \otimes a_{\tau' j_4}^\dagger \right]^{(J)}} \\ &= -(2J+1) \begin{Bmatrix} j_1 & j_2 & J \\ j_3 & j_4 & J \\ 0 & 0 & 0 \end{Bmatrix} \left[ \left[ \tilde{a}_{\tau j_1} \otimes a_{\tau j_3}^\dagger \right]^{(0)} \otimes \left[ \tilde{a}_{\tau' j_2} \otimes a_{\tau' j_4}^\dagger \right]^{(0)} \right]^{(0)} \delta_{j_1 j_3} \delta_{j_2 j_4} \\ &= -(2J+1) \frac{(-1)^{j_2+j_1+J}}{\sqrt{2J+1}} \begin{Bmatrix} j_1 & j_2 & J \\ j_2 & j_1 & 0 \end{Bmatrix} \\ &\quad \times \left[ \left[ \tilde{a}_{\tau j_1} \otimes a_{\tau j_1}^\dagger \right]^{(0)} \otimes \left[ \tilde{a}_{\tau' j_2} \otimes a_{\tau' j_2}^\dagger \right]^{(0)} \right]^{(0)} \delta_{j_1 j_3} \delta_{j_2 j_4} \\ &= -\sqrt{2J+1} (-1)^{j_2+j_1+J} \frac{(-1)^{j_1+j_2+J}}{\sqrt{(2j_1+1)(2j_2+1)}} \\ &\quad \times \left[ \left[ \tilde{a}_{\tau j_1} \otimes a_{\tau j_1}^\dagger \right]^{(0)} \otimes \left[ \tilde{a}_{\tau' j_2} \otimes a_{\tau' j_2}^\dagger \right]^{(0)} \right]^{(0)} \delta_{j_1 j_3} \delta_{j_2 j_4} \\ &\stackrel{c}{=} -\sqrt{\frac{2J+1}{(2j_1+1)(2j_2+1)}} \sqrt{2j_1+1} \left[ \tilde{a}_{\tau' j_2} \otimes a_{\tau' j_2}^\dagger \right]^{(0)} \delta_{j_1 j_3} \delta_{j_2 j_4} \\ &= \frac{\sqrt{2J+1}}{2j_2+1} \delta_{j_1 j_3} \delta_{j_2 j_4} N_{\tau' j_2}, \end{aligned} \quad (\text{B.5.18})$$

where  $\stackrel{c}{=}$  means taking a contraction.

The other contractions are given by the same way as

$$\begin{aligned}
& \left[ \overline{\left[ \tilde{a}_{\tau j_1} \otimes \tilde{a}_{\tau' j_2} \right]^{(J)}} \cdot \left[ a_{\tau j_3}^\dagger \otimes a_{\tau' j_4}^\dagger \right]^{(J)} \right. \\
&= -(-1)^{j_3+j_4-J} \left[ \left[ \tilde{a}_{\tau j_1} \otimes \tilde{a}_{\tau' j_2} \right]^{(J)} \otimes \left[ a_{\tau' j_4}^\dagger \otimes a_{\tau j_3}^\dagger \right]^{(J)} \right]^{(0)} \\
&= (-1)^{j_3+j_4-J} (2J+1) \begin{Bmatrix} j_1 & j_2 & J \\ j_4 & j_3 & J \\ 0 & 0 & 0 \end{Bmatrix} \\
&\quad \times \left[ \left[ \tilde{a}_{\tau j_1} \otimes a_{\tau' j_4}^\dagger \right]^{(0)} \otimes \left[ \tilde{a}_{\tau' j_2} \otimes a_{\tau j_3}^\dagger \right]^{(0)} \right]^{(0)} \delta_{j_1 j_4} \delta_{j_2 j_3} \\
&= (-1)^{j_1+j_2-J} (2J+1) \frac{(-1)^{j_1+j_2+J}}{\sqrt{2J+1}} \begin{Bmatrix} j_1 & j_2 & J \\ j_2 & j_1 & 0 \end{Bmatrix} \\
&\quad \times \left[ \left[ \tilde{a}_{\tau j_1} \otimes a_{\tau' j_1}^\dagger \right]^{(0)} \otimes \left[ \tilde{a}_{\tau' j_2} \otimes a_{\tau j_2}^\dagger \right]^{(0)} \right]^{(0)} \delta_{j_1 j_4} \delta_{j_2 j_3} \\
&= \sqrt{2J+1} \frac{(-1)^{j_1+j_2+J}}{\sqrt{(2j_1+1)(2j_2+1)}} \left[ \left[ \tilde{a}_{\tau j_1} \otimes a_{\tau' j_1}^\dagger \right]^{(0)} \otimes \left[ \tilde{a}_{\tau' j_2} \otimes a_{\tau j_2}^\dagger \right]^{(0)} \right]^{(0)} \delta_{j_1 j_4} \delta_{j_2 j_3} \\
&= \frac{(-1)^{j_1+j_2+J}}{c} \sqrt{\frac{2J+1}{(2j_1+1)(2j_2+1)}} \sqrt{2j_1+1} \delta_{\tau\tau'} \left[ \tilde{a}_{\tau j_2} \otimes a_{\tau j_2}^\dagger \right]^{(0)} \delta_{j_1 j_4} \delta_{j_2 j_3} \\
&= -(-1)^{j_1+j_2+J} \frac{\sqrt{2J+1}}{2j_2+1} N_{\tau j_2} \delta_{\tau\tau'} \delta_{j_1 j_4} \delta_{j_2 j_3}, \tag{B.5.19}
\end{aligned}$$

$$\begin{aligned}
& \left[ \tilde{a}_{\tau j_1} \otimes \overline{\left[ \tilde{a}_{\tau' j_2} \right]^{(J)}} \cdot \left[ a_{\tau j_3}^\dagger \otimes a_{\tau' j_4}^\dagger \right]^{(J)} \right. \\
&= \frac{(-1)^{j_1+j_2+J}}{c} \sqrt{\frac{2J+1}{(2j_1+1)(2j_2+1)}} \sqrt{2j_2+1} \delta_{\tau\tau'} \left[ \tilde{a}_{\tau j_1} \otimes a_{\tau j_1}^\dagger \right]^{(0)} \delta_{j_1 j_4} \delta_{j_2 j_3} \\
&= -(-1)^{j_1+j_2+J} \frac{\sqrt{2J+1}}{2j_1+1} N_{\tau j_1} \delta_{\tau\tau'} \delta_{j_1 j_4} \delta_{j_2 j_3}, \tag{B.5.20}
\end{aligned}$$

$$\begin{aligned}
& \left[ \overline{\left[ \tilde{a}_{\tau j_1} \otimes \tilde{a}_{\tau' j_2} \right]^{(J)}} \cdot \left[ a_{\tau j_3}^\dagger \otimes a_{\tau' j_4}^\dagger \right]^{(J)} \right. \\
&= \frac{(-1)^{j_1+j_2+J}}{c} \sqrt{\frac{2J+1}{(2j_1+1)(2j_2+1)}} \sqrt{2j_2+1} \left[ \tilde{a}_{\tau j_1} \otimes a_{\tau j_1}^\dagger \right]^{(0)} \delta_{j_1 j_3} \delta_{j_2 j_4} \\
&= \frac{\sqrt{2J+1}}{2j_1+1} N_{\tau j_1} \delta_{j_1 j_3} \delta_{j_2 j_4}. \tag{B.5.21}
\end{aligned}$$

For the monopole pairing interaction,  $J = 0$  and  $j_1 = j_2$ , between like particles  $\tau = \tau'$ , there are no contributions to the one-body Hamiltonian.

For the quadrupole pairing interaction,  $J = 2$ , between like particles  $\tau = \tau'$ , we take couplings as

$$G(j_1 j_2, j_3 j_4; 2) = Q_{j_1, j_2} Q_{j_3, j_4}. \tag{B.5.22}$$

Thus we get

$$\begin{aligned}
& \sqrt{5} \sum_{j_1 j_2 j_3 j_4} Q_{j_1, j_2} Q_{j_3, j_4} \\
& \times \left[ \frac{\sqrt{5}}{2j_2 + 1} N_{\tau j_2} \delta_{j_1 j_3} \delta_{j_2 j_4} - (-1)^{j_1 + j_2} \frac{\sqrt{5}}{2j_2 + 1} N_{\tau j_2} \delta_{j_1 j_4} \delta_{j_2 j_3} \right. \\
& \quad \left. - (-1)^{j_1 + j_2} \frac{\sqrt{5}}{2j_1 + 1} N_{\tau j_1} \delta_{j_1 j_4} \delta_{j_2 j_3} + \frac{\sqrt{5}}{2j_1 + 1} N_{\tau j_1} \delta_{j_1 j_3} \delta_{j_2 j_4} \right] \\
& = 5 \sum_{j_1 j_2} \frac{N_{\tau j_2}}{2j_2 + 1} (Q_{j_1, j_2})^2 \{1 - (-1)^{j_1 + j_2} (-1)^{j_2 - j_1}\} \\
& \quad + 5 \sum_{j_1 j_2} \frac{N_{\tau j_1}}{2j_1 + 1} (Q_{j_1, j_2})^2 \{1 - (-1)^{j_1 + j_2} (-1)^{j_2 - j_1}\} \\
& = 10 \sum_{j_1 j_2} (Q_{j_1, j_2})^2 \left[ \frac{N_{\tau j_1}}{2j_1 + 1} + \frac{N_{\tau j_2}}{2j_2 + 1} \right] \\
& = 20 \sum_{j_1 j_2} (Q_{j_1, j_2})^2 \frac{N_{\tau j_1}}{2j_1 + 1}. \tag{B.5.23}
\end{aligned}$$

For higher order multipole pairing interactions,  $J > 2$ , between like particles  $\tau = \tau'$ , we retain the property of  $p_J(j_1 j_2) = p_J(j_2 j_1)$ . Thus we have a contribution

$$4(2J + 1) \sum_{j_1 j_2} p_J^2(j_1 j_2) \frac{N_{\tau j_1}}{2j_1 + 1}. \tag{B.5.24}$$

### B.5.3 Quadrupole Quadrupole Interaction

The QQ interactions for holes are rewritten by the particle-hole translation as

$$\begin{aligned}
H_{\tau\tau'}^{(QQ)}(\text{hole}) & = \sqrt{5} \sum_{j_1 j_2 j_3 j_4} Q_{j_1, j_2} Q_{j_3, j_4} N \left[ \left[ [b_{\tau j_1}^\dagger \otimes \tilde{b}_{\tau j_2}]^{(2)} \otimes [b_{\tau' j_3}^\dagger \otimes \tilde{b}_{\tau' j_4}]^{(2)} \right]^{(0)} \right] \\
& = -5 \sum_{j_1 j_2 j_3 j_4} Q_{j_1, j_2} Q_{j_3, j_4} \sum_K \sqrt{2K + 1} (-1)^{j_3 + j_4} \begin{Bmatrix} j_1 & j_2 & 2 \\ j_4 & j_3 & K \end{Bmatrix} \\
& \quad \times \left[ [b_{\tau j_1}^\dagger \otimes b_{\tau' j_3}^\dagger]^{(K)} \otimes [\tilde{b}_{\tau' j_4} \otimes \tilde{b}_{\tau j_2}]^{(K)} \right]^{(0)} \\
& = -5 \sum_{j_1 j_2 j_3 j_4} Q_{j_1, j_2} Q_{j_3, j_4} \sum_K \sqrt{2K + 1} (-1)^{j_3 + j_4} \begin{Bmatrix} j_1 & j_2 & 2 \\ j_4 & j_3 & K \end{Bmatrix} \\
& \quad \times \left[ [\tilde{a}_{\tau j_1} \otimes \tilde{a}_{\tau' j_3}]^{(K)} \otimes [a_{\tau' j_4}^\dagger \otimes a_{\tau j_2}^\dagger]^{(K)} \right]^{(0)} \\
& = -5 \sum_{j_1 j_4 j_2 j_3} Q_{j_1, j_4} Q_{j_2, j_3} \sum_K \sqrt{2K + 1} (-1)^{j_2 + j_3} \begin{Bmatrix} j_1 & j_4 & 2 \\ j_3 & j_2 & K \end{Bmatrix} \\
& \quad \times \left[ [\tilde{a}_{\tau j_1} \otimes \tilde{a}_{\tau' j_2}]^{(K)} \otimes [a_{\tau' j_3}^\dagger \otimes a_{\tau j_4}^\dagger]^{(K)} \right]^{(0)}. \tag{B.5.25}
\end{aligned}$$

We should consider two contracted terms which may be coupled with  $J = 0$ , given as

$$\begin{aligned}
& H_{\tau\tau'}^{(QQ)}(\text{hole; contraction of } j_1 \text{ and } j_3) \\
&= 5 \sum_{j_1 j_2 j_3 j_4} Q_{j_1, j_4} Q_{j_2, j_3} \sum_K \sqrt{2K+1} (-1)^{j_2+j_3} \begin{Bmatrix} j_1 & j_4 & 2 \\ j_3 & j_2 & K \end{Bmatrix} \\
&\quad \times (2K+1) \begin{Bmatrix} j_1 & j_2 & K \\ j_3 & j_4 & K \\ 0 & 0 & 0 \end{Bmatrix} \\
&\quad \times \left[ \left[ \tilde{a}_{\tau j_1} \otimes a_{\tau' j_3}^\dagger \right]^{(0)} \otimes \left[ \tilde{a}_{\tau' j_2} \otimes a_{\tau j_4}^\dagger \right]^{(0)} \right]^{(0)} \delta_{j_1 j_3} \delta_{j_2 j_4} \\
&= 5 \sum_{j_1 j_2} Q_{j_1, j_2} Q_{j_2, j_1} \sum_K \sqrt{2K+1} (-1)^{j_2+j_1} \begin{Bmatrix} j_1 & j_2 & 2 \\ j_1 & j_2 & K \end{Bmatrix} \\
&\quad \times (2K+1) \frac{(-1)^{K+j_2+j_1}}{\sqrt{2K+1}} \begin{Bmatrix} j_1 & j_2 & K \\ j_2 & j_1 & 0 \end{Bmatrix} \\
&\quad \times \left[ \left[ \tilde{a}_{\tau j_1} \otimes a_{\tau' j_1}^\dagger \right]^{(0)} \otimes \left[ \tilde{a}_{\tau' j_2} \otimes a_{\tau j_2}^\dagger \right]^{(0)} \right]^{(0)} \\
&= 5 \sum_{j_1 j_2} Q_{j_1, j_2} Q_{j_2, j_1} \sum_K (-1)^K (2K+1) \begin{Bmatrix} j_1 & j_2 & 2 \\ j_1 & j_2 & K \end{Bmatrix} \begin{Bmatrix} j_1 & j_2 & K \\ j_2 & j_1 & 0 \end{Bmatrix} \\
&\quad \times \left[ \left[ \tilde{a}_{\tau j_1} \otimes a_{\tau' j_1}^\dagger \right]^{(0)} \otimes \left[ \tilde{a}_{\tau' j_2} \otimes a_{\tau j_2}^\dagger \right]^{(0)} \right]^{(0)} \\
&= 5 \sum_{j_1 j_2} Q_{j_1, j_2} Q_{j_2, j_1} \begin{Bmatrix} j_1 & j_1 & 0 \\ j_2 & j_2 & 2 \end{Bmatrix} \left[ \left[ \tilde{a}_{\tau j_1} \otimes a_{\tau' j_1}^\dagger \right]^{(0)} \otimes \left[ \tilde{a}_{\tau' j_2} \otimes a_{\tau j_2}^\dagger \right]^{(0)} \right]^{(0)} \\
&= \frac{5}{c} \sum_{j_1 j_2} Q_{j_1, j_2} Q_{j_2, j_1} \frac{(-1)^{j_1+j_2}}{\sqrt{(2j_1+1)(2j_2+1)}} \sqrt{2j_1+1} \delta_{\tau\tau'} \left[ \tilde{a}_{\tau j_2} \otimes a_{\tau j_2}^\dagger \right]^{(0)} \\
&= -5 \sum_{j_1 j_2} Q_{j_1, j_2} Q_{j_2, j_1} \frac{(-1)^{j_1+j_2}}{2j_2+1} \delta_{\tau\tau'} N_{\tau j_2} \\
&= 5 \sum_{j_1 j_2} (Q_{j_1, j_2})^2 \frac{1}{2j_2+1} \delta_{\tau\tau'} N_{\tau j_2}, \tag{B.5.26}
\end{aligned}$$

and

$$\begin{aligned}
& H_{\tau\tau'}^{(QQ)}(\text{hole; contraction of } j_2 \text{ and } j_4) \\
&= 5 \sum_{j_1 j_2} Q_{j_1, j_2} Q_{j_2, j_1} \begin{Bmatrix} j_1 & j_1 & 0 \\ j_2 & j_2 & 2 \end{Bmatrix} \left[ \left[ \tilde{a}_{\tau j_1} \otimes a_{\tau' j_1}^\dagger \right]^{(0)} \otimes \left[ \tilde{a}_{\tau' j_2} \otimes a_{\tau j_2}^\dagger \right]^{(0)} \right]^{(0)} \\
&= \frac{5}{c} \sum_{j_1 j_2} Q_{j_1, j_2} Q_{j_2, j_1} \frac{(-1)^{j_1+j_2}}{\sqrt{(2j_1+1)(2j_2+1)}} \sqrt{2j_2+1} \delta_{\tau\tau'} \left[ \tilde{a}_{\tau j_1} \otimes a_{\tau j_1}^\dagger \right]^{(0)} \\
&= -5 \sum_{j_1 j_2} Q_{j_1, j_2} Q_{j_2, j_1} \frac{(-1)^{j_1+j_2}}{2j_1+1} \delta_{\tau\tau'} N_{\tau j_1}
\end{aligned}$$

$$= 5 \sum_{j_1 j_2} (Q_{j_1, j_2})^2 \frac{1}{2j_1 + 1} \delta_{\tau\tau'} N_{\tau j_1}. \quad (\text{B.5.27})$$

Then the contracted terms are written by using this relation as

$$\begin{aligned} & 5 \sum_{j_1 j_2} (Q_{j_1, j_2})^2 \left( \frac{1}{2j_1 + 1} N_{\tau j_1} + \frac{1}{2j_2 + 1} N_{\tau j_2} \right) \delta_{\tau\tau'} \\ &= 10 \sum_{j_1 j_2} (Q_{j_1, j_2})^2 \frac{1}{2j_1 + 1} N_{\tau j_1} \delta_{\tau\tau'}. \end{aligned} \quad (\text{B.5.28})$$

## B.6 Two-body matrix elements

### B.6.1 Radial eigenfunctions in the spherically symmetric harmonic oscillator

The isotropic harmonic oscillator in the three-dimensional space is described with a potential of

$$V(r) = \frac{1}{2} m \omega^2 r^2. \quad (\text{B.6.1})$$

In general, the wavefunctions decomposed as  $\psi(\mathbf{r}) = R_l(r) Y_{lm}(\theta, \phi)$  in a spherically symmetric potential  $V(r)$  are given by

$$-\frac{1}{2m} \frac{d^2 \chi_l(r)}{dr^2} + \left[ V(r) + \frac{l(l+1)}{2mr^2} \right] \chi_l(r) = E \chi_l(r), \quad (\text{B.6.2})$$

where the radial part is defined as

$$R_l(r) = \frac{\chi_l(r)}{r}. \quad (\text{B.6.3})$$

The angular components  $Y_{lm}(\theta, \phi)$  are the spherical harmonics. For the harmonic oscillator potential, in the limit of  $r \rightarrow \infty$ , the centrifugal potential is negligible and the radial part is simply given as

$$\chi_l(r) \sim e^{-\frac{1}{2} m \omega r^2}, \quad r \rightarrow \infty. \quad (\text{B.6.4})$$

In the other limit of  $r \rightarrow 0$ , it is found that

$$\chi_l(r) \sim r^{l+1}, \quad r \rightarrow 0. \quad (\text{B.6.5})$$

Thus, an ansatz for the radial part defined as

$$\chi_l(r) = r^{l+1} e^{-\frac{1}{2} m \omega r^2} f(r) \quad (\text{B.6.6})$$

is considered.

The radial part can be regarded as a function of  $z = r^2$ , and the Schrödinger equation is then given as

$$-2z \frac{d^2 f(z)}{dz^2} + \{2m\omega z - (2l+3)\} \frac{df(z)}{dz} + \frac{2l+3}{2} m\omega f(z) = mE f(z). \quad (\text{B.6.7})$$

The series expansion of  $f(z)$ , which is explicitly given as

$$\begin{aligned} f(z) &= \sum_{k=0}^{\infty} a_k z^k, \\ \frac{df(z)}{dz} &= \sum_{k=0}^{\infty} k a_k z^{k-1} = \sum_{k=0}^{\infty} (k+1) a_{k+1} z^k, \\ \frac{d^2 f(z)}{dz^2} &= \sum_{k=0}^{\infty} k(k+1) a_{k+1} z^{k-1} = \sum_{k=0}^{\infty} (k+1)(k+2) a_{k+2} z^k, \end{aligned} \quad (\text{B.6.8})$$

leads to the equations for the coefficients  $a_k$  as

$$\sum_{k=0}^{\infty} z^k \left[ -2k(k+1)a_{k+1} + 2m\omega k a_k - (2l+3)(k+1)a_{k+1} + \frac{2l+3}{2} m\omega a_k \right] = mE \sum_{k=0}^{\infty} a_k z^k, \quad (\text{B.6.9})$$

and thus recursion relations as

$$\frac{a_{k+1}}{a_k} = \frac{E - \left(2k + \frac{2l+3}{2}\right) \omega}{(2k+2l+3)(k+1)} m \quad (\text{B.6.10})$$

are given. The series of  $f(z)$  should be zero at some  $k = n$ , so that the series will be converged in the far distance. This requirement is realized if the eigenvalues are given as

$$E = \left(2n + l + \frac{3}{2}\right) \omega. \quad (\text{B.6.11})$$

In order to get an explicit form of the eigenfunctions, the Schrödinger equation (Eq. (B.6.7)) is rewritten by  $x = m\omega z = m\omega r^2$  as

$$\left[ x \frac{d^2}{dx^2} + \left( \frac{2l+3}{2} - x \right) \frac{d}{dx} + n \right] f(x) = 0. \quad (\text{B.6.12})$$

Comparing this with the Sonine's differential equation, it is found that  $f(x)$  is given with the Sonine polynomial as  $f(x) \propto S_{n,l+1/2}(x)$ . Thus, the radial function is given as

$$R_{nl}(r) = \mathcal{N} x^{\frac{l}{2}} e^{-\frac{x}{2}} S_{n,l+1/2}(x), \quad (\text{B.6.13})$$

with normalization constant  $\mathcal{N}$ . Using the orthogonality of the Sonine polynomials,

$$\begin{aligned} \int_0^{\infty} R_{nl}(r) R_{n'l}(r) r^2 dr &= |\mathcal{N}|^2 \int x^l e^{-x} S_{n,l+1/2}(x) S_{n',l+1/2}(x) \times \frac{1}{2(m\omega)^{3/2}} x^{\frac{1}{2}} dx \\ &= \frac{|\mathcal{N}|^2}{2(m\omega)^{3/2}} \frac{\Gamma(n+l+\frac{3}{2})}{n!} \delta_{n'n}, \end{aligned} \quad (\text{B.6.14})$$

and thus

$$\begin{aligned} R_{nl}(r) &= (m\omega)^{\frac{l}{2} + \frac{3}{4}} \sqrt{\frac{2n!}{\Gamma(n+l+\frac{3}{2})}} r^l e^{-\frac{1}{2}m\omega r^2} S_{n,l+1/2}(x) \\ &= r^l e^{-\frac{1}{2}m\omega r^2} \sum_{k=0}^n a_{nlk} r^{2k}, \end{aligned} \quad (\text{B.6.15})$$

where

$$\begin{aligned}
a_{nlk} &= (m\omega)^{\frac{l}{2}+k+\frac{3}{4}} \sqrt{\frac{2n!}{\Gamma(n+l+\frac{3}{2})}} \frac{(-1)^k \Gamma(n+l+\frac{3}{2})}{k!(n-k)!\Gamma(l+k+\frac{3}{2})} \\
&= (m\omega)^{\frac{l}{2}+k+\frac{3}{4}} \frac{(-1)^k}{k!(n-k)!} \sqrt{\frac{2n!2^{n+l+1}}{(2n+2l+1)!!\sqrt{\pi}}} \frac{(2n+2l+1)!!}{(2l+2k+1)!!} 2^{k-n} \\
&= (m\omega)^{\frac{l}{2}+k+\frac{3}{4}} \frac{(-1)^k 2^{k+1}}{k!(n-k)!} \frac{1}{(2l+2k+1)!!} \sqrt{\frac{n!(2n+2l+1)!!}{2^{n-l}\sqrt{\pi}}}
\end{aligned} \tag{B.6.16}$$

is obtained. A system of units in which  $m = \omega = 1$  is used below.

This phase convention of  $a_{nlk}$  satisfies

$$\lim_{r \rightarrow 0} R_{nl}(r) = \lim_{r \rightarrow 0} r^l a_{nl,k=0} > 0. \tag{B.6.17}$$

$0 \leq k \leq n$ . Another convention is given by multiplying  $(-1)^n$  as

$$\begin{aligned}
R'_{nl}(r) &\equiv r^l e^{-\frac{1}{2}r^2} \sum_{k=0}^n a'_{nlk} r^{2k}, \\
a'_{nlk} &= \frac{(-1)^{n+k}}{k!(n-k)!} \frac{2^{k+1}}{(2k+2l+1)!!} \sqrt{\frac{n!(2n+2l+1)!!}{2^{n-l}\sqrt{\pi}}},
\end{aligned} \tag{B.6.18}$$

so that

$$\lim_{r \rightarrow \infty} R'_{nl}(r) = \lim_{r \rightarrow \infty} r^{l+2n} e^{-\frac{r^2}{2}} a_{nl,k=n} > 0. \tag{B.6.19}$$

## B.6.2 Matrix elements of $r$

In order to evaluate the matrix elements of  $r$ ,

$$\begin{aligned}
a_{n,l+1,k} &= \frac{(-1)^k}{k!(n-k)!} \frac{2^{k+1}}{(2k+2l+3)!!} \sqrt{\frac{n!(2n+2l+3)!!}{2^{n-l-1}\sqrt{\pi}}} \\
&= \frac{\sqrt{2(2n+2l+3)}}{2k+2l+3} a_{nlk},
\end{aligned} \tag{B.6.20}$$

$$\begin{aligned}
a_{n-1,l+1,k} &= \frac{(-1)^k}{k!(n-k-1)!} \frac{2^{k+1}}{(2k+2l+3)!!} \sqrt{\frac{(n-1)!(2n+2l+1)!!}{2^{n-l-2}\sqrt{\pi}}} \\
&= \frac{n-k}{2k+2l+3} \frac{2}{\sqrt{n}} a_{nlk} \quad (k < n)
\end{aligned} \tag{B.6.21}$$

are utilized. Here,

$$\begin{aligned}
R_{n,l+1}(r) &= r^{l+1} e^{-\frac{1}{2}r^2} \sum_{k=0}^n a_{n,l+1,k} r^{2k} \\
&= r^{l+1} e^{-\frac{1}{2}r^2} \sum_{k=0}^n \frac{\sqrt{2(2n+2l+3)}}{2k+2l+3} a_{nlk} r^{2k}, \\
R_{n-1,l+1}(r) &= r^{l+1} e^{-\frac{1}{2}r^2} \sum_{k=0}^{n-1} a_{n-1,l+1,k} r^{2k} \\
&= r^{l+1} e^{-\frac{1}{2}r^2} \sum_{k=0}^n \frac{n-k}{2k+2l+3} \frac{2}{\sqrt{n}} a_{nlk} r^{2k}.
\end{aligned} \tag{B.6.22}$$

Thus

$$rR_{nl}(r) = r^{l+1} e^{-\frac{1}{2}r^2} \sum_{k=0}^n a_{nlk} r^{2k} = \sqrt{n+l+\frac{3}{2}} R_{n,l+1}(r) - \sqrt{n} R_{n-1,l+1}(r) \tag{B.6.23}$$

is given for  $n \geq 1$ .

On the other hand,

$$\begin{aligned}
a_{n+1,l-1,k+1} &= \frac{(-1)^{k+1} 2^{k+2}}{(k+1)!(n-k)!} \frac{1}{(2l+2k+1)!!} \sqrt{\frac{(n+1)!(2n+2l+1)!!}{2^{n-l+2} \sqrt{\pi}}} \\
&= -\frac{\sqrt{n+1}}{k+1} a_{nlk},
\end{aligned} \tag{B.6.24}$$

$$\begin{aligned}
a_{n,l-1,k+1} &= \frac{(-1)^{k+1} 2^{k+2}}{(k+1)!(n-k-1)!} \frac{1}{(2l+2k+1)!!} \sqrt{\frac{n!(2n+2l-1)!!}{2^{n-l+1} \sqrt{\pi}}} \\
&= -\frac{2(n-k)}{k+1} \frac{1}{\sqrt{2(2n+2l+1)}} a_{nlk}
\end{aligned} \tag{B.6.25}$$

lead to

$$\begin{aligned}
R_{n+1,l-1}(r) &= r^{l-1} e^{-\frac{1}{2}m\omega r^2} \sum_{k=0}^{n+1} a_{n+1,l-1,k} r^{2k} \\
&= r^{l+1} e^{-\frac{1}{2}m\omega r^2} \sum_{k=0}^{n+1} a_{n+1,l-1,k} r^{2(k-1)} \\
&= r^{l+1} e^{-\frac{1}{2}m\omega r^2} \sum_{k=0}^n a_{n+1,l-1,k+1} r^{2k} \\
&= -r^{l+1} e^{-\frac{1}{2}m\omega r^2} \sum_{k=0}^n \frac{\sqrt{n+1}}{k+1} a_{nlk} r^{2k}, \\
R_{n,l-1}(r) &= r^{l-1} e^{-\frac{1}{2}m\omega r^2} \sum_{k=0}^n a_{n,l-1,k} r^{2k} \\
&= r^{l+1} e^{-\frac{1}{2}m\omega r^2} \sum_{k=0}^n a_{n,l-1,k} r^{2(k-1)}
\end{aligned} \tag{B.6.26}$$

$$\begin{aligned}
&= r^{l+1} e^{-\frac{1}{2}m\omega r^2} \sum_{k=-1}^{n-1} a_{n,l-1,k+1} r^{2k} \\
&= -r^{l+1} e^{-\frac{1}{2}m\omega r^2} \sum_{k=-1}^n \frac{2(n-k)}{k+1} \frac{1}{\sqrt{2(2n+2l+1)}} a_{nlk} r^{2k} \\
&= -r^{l+1} e^{-\frac{1}{2}m\omega r^2} \sum_{k=0}^n \frac{2(n-k)}{k+1} \frac{1}{\sqrt{2(2n+2l+1)}} a_{nlk} r^{2k}, \tag{B.6.27}
\end{aligned}$$

and thus, for  $l \geq 1$ ,

$$rR_{nl}(r) = r^{l+1} e^{-\frac{1}{2}r^2} \sum_{k=0}^n a_{nlk} r^{2k} = -\sqrt{n+1} R_{n+1,l-1}(r) + \sqrt{n+l+\frac{1}{2}} R_{n,l-1}(r). \tag{B.6.28}$$

In summary, using the recursion relations as

$$rR_{nl}(r) = \sqrt{n+l+\frac{3}{2}} R_{n,l+1}(r) - \sqrt{n} R_{n-1,l+1}(r), \quad n \geq 1, \tag{B.6.29}$$

$$rR_{nl}(r) = -\sqrt{n+1} R_{n+1,l-1}(r) + \sqrt{n+l+\frac{1}{2}} R_{n,l-1}(r), \quad l \geq 1, \tag{B.6.30}$$

the matrix elements of  $r$  are given as

$$\langle n, l+1 | r | n, l \rangle = \sqrt{n+l+\frac{3}{2}}, \quad \langle n-1, l+1 | r | n, l \rangle = -\sqrt{n}, \tag{B.6.31}$$

$$\langle n, l-1 | r | n, l \rangle = \sqrt{n+l+\frac{1}{2}}, \quad \langle n+1, l-1 | r | n, l \rangle = -\sqrt{n+1}. \tag{B.6.32}$$

### B.6.3 Matrix elements of $r^l$

The recursion relations in Eqs. (B.6.29) and (B.6.30) are utilized to calculate the matrix elements of higher order factorials of  $r$ .

For  $n \geq 2$ , using Eq. (B.6.29),

$$\begin{aligned}
r^2 R_{nl}(r) &= \sqrt{\left(n+l+\frac{3}{2}\right) \left(n+l+\frac{5}{2}\right)} R_{n,l+2}(r) \\
&\quad - 2\sqrt{n \left(n+l+\frac{3}{2}\right)} R_{n-1,l+2}(r) \\
&\quad + \sqrt{n(n-1)} R_{n-2,l+2}(r). \tag{B.6.33}
\end{aligned}$$

For  $n \geq 1$ , using Eqs. (B.6.29) and (B.6.30),

$$\begin{aligned}
r^2 R_{nl}(r) &= -\sqrt{(n+1) \left(n+l+\frac{3}{2}\right)} R_{n+1,l}(r) \\
&\quad + \left(2n+l+\frac{3}{2}\right) R_{nl}(r) \\
&\quad - \sqrt{n \left(n+l+\frac{1}{2}\right)} R_{n-1,l}(r). \tag{B.6.34}
\end{aligned}$$

For  $l \geq 2$ , using Eq. (B.6.30),

$$\begin{aligned}
r^2 R_{nl}(r) &= \sqrt{(n+1)(n+2)} R_{n+2, l-2}(r) \\
&\quad - 2\sqrt{(n+1)\left(n+l+\frac{1}{2}\right)} R_{n+1, l-2}(r) \\
&\quad + \sqrt{\left(n+l-\frac{1}{2}\right)\left(n+l+\frac{1}{2}\right)} R_{n, l-2}(r).
\end{aligned} \tag{B.6.35}$$

The matrix elements of  $\langle n'l'|r^2|nl\rangle$  are given in Table B.1.

Table B.1: Two-body matrix elements of  $\langle n'l'|r^2|nl\rangle$  are given.

	$l' = l + 2$	$l$	$l - 2$
$n' = n + 2$			$\sqrt{(n+1)(n+2)}$
$n + 1$		$-\sqrt{(n+1)\left(n+l+\frac{3}{2}\right)}$	$-2\sqrt{(n+1)\left(n+l+\frac{1}{2}\right)}$
$n$	$\sqrt{\left(n+l+\frac{3}{2}\right)\left(n+l+\frac{5}{2}\right)}$	$(2n+l+\frac{3}{2})$	$\sqrt{\left(n+l-\frac{1}{2}\right)\left(n+l+\frac{1}{2}\right)}$
$n - 1$	$-2\sqrt{n\left(n+l+\frac{3}{2}\right)}$	$-\sqrt{n\left(n+l+\frac{1}{2}\right)}$	
$n - 2$	$\sqrt{n(n-1)}$		

The same procedures are followed to get matrix elements of  $r^3$ . For  $n \geq 3$ , applying a recursion relation in Eq. (B.6.29) to Eq. (B.6.33),

$$\begin{aligned}
r^3 R_{nl}(r) &= \sqrt{\left(n+l+\frac{3}{2}\right)\left(n+l+\frac{5}{2}\right)} r R_{n, l+2}(r) \\
&\quad - 2\sqrt{n\left(n+l+\frac{3}{2}\right)} r R_{n-1, l+2}(r) \\
&\quad + \sqrt{n(n-1)} r R_{n-2, l+2}(r) \\
&= \sqrt{\left(n+l+\frac{3}{2}\right)\left(n+l+\frac{5}{2}\right)\left(n+l+\frac{7}{2}\right)} R_{n, l+3}(r) \\
&\quad - 3\sqrt{n\left(n+l+\frac{3}{2}\right)\left(n+l+\frac{5}{2}\right)} R_{n-1, l+3}(r) \\
&\quad + 3\sqrt{n(n-1)\left(n+l+\frac{3}{2}\right)} R_{n-2, l+3}(r) \\
&\quad - \sqrt{n(n-1)(n-2)} R_{n-3, l+3}(r).
\end{aligned} \tag{B.6.36}$$

For  $n \geq 2$ , applying a recursion relation in Eq. (B.6.30) to Eq. (B.6.33),

$$r^3 R_{nl}(r) = \sqrt{\left(n+l+\frac{3}{2}\right)\left(n+l+\frac{5}{2}\right)} r R_{n, l+2}(r)$$

$$\begin{aligned}
& -2\sqrt{n\left(n+l+\frac{3}{2}\right)}rR_{n-1,l+2}(r) \\
& +\sqrt{n(n-1)}rR_{n-2,l+2}(r) \\
= & -\sqrt{(n+1)\left(n+l+\frac{3}{2}\right)\left(n+l+\frac{5}{2}\right)}R_{n+1,l+1}(r) \\
& +\sqrt{n+l+\frac{3}{2}\left(3n+l+\frac{5}{2}\right)}R_{n,l+1}(r) \\
& -\sqrt{n(3n+2l+2)}R_{n-1,l+1}(r) \\
& +\sqrt{n(n-1)\left(n+l+\frac{1}{2}\right)}R_{n-2,l+1}(r). \tag{B.6.37}
\end{aligned}$$

For  $n \geq 3$ , applying a recursion relation in Eq. (B.6.29) to Eq. (B.6.34),

$$\begin{aligned}
r^3R_{nl}(r) = & -\sqrt{(n+1)\left(n+l+\frac{3}{2}\right)}rR_{n+1,l}(r) \\
& +\left(2n+l+\frac{3}{2}\right)rR_{nl}(r) \\
& -\sqrt{n\left(n+l+\frac{1}{2}\right)}rR_{n-1,l}(r) \\
= & -\sqrt{(n+1)\left(n+l+\frac{3}{2}\right)\left(n+l+\frac{5}{2}\right)}R_{n+1,l+1}(r) \\
& +\sqrt{n+l+\frac{3}{2}\left(3n+l+\frac{5}{2}\right)}R_{n,l+1}(r) \\
& -\sqrt{n(3n+2l+2)}R_{n-1,l+1}(r) \\
& +\sqrt{n(n-1)\left(n+l+\frac{1}{2}\right)}R_{n-2,l+1}(r). \tag{B.6.38}
\end{aligned}$$

This relation is identical to Eq. (B.6.37). For  $n \geq 2$ , applying a recursion relation in Eq. (B.6.30) to Eq. (B.6.34),

$$\begin{aligned}
r^3R_{nl}(r) = & -\sqrt{(n+1)\left(n+l+\frac{3}{2}\right)}rR_{n+1,l}(r) \\
& +\left(2n+l+\frac{3}{2}\right)rR_{nl}(r) \\
& -\sqrt{n\left(n+l+\frac{1}{2}\right)}rR_{n-1,l}(r) \\
= & \sqrt{(n+1)(n+2)\left(n+l+\frac{3}{2}\right)}R_{n+2,l-1}(r) \\
& -\sqrt{n+1(3n+2l+3)}R_{n+1,l-1}(r) \\
& +\sqrt{n+l+\frac{1}{2}\left(3n+l+\frac{3}{2}\right)}R_{n,l-1}(r)
\end{aligned}$$

$$- \sqrt{n \left( n + l - \frac{1}{2} \right) \left( n + l + \frac{1}{2} \right)} R_{n-1, l-1}(r). \quad (\text{B.6.39})$$

For  $n \geq 3$ , applying a recursion relation in Eq. (B.6.29) to Eq. (B.6.35),

$$\begin{aligned} r^3 R_{nl}(r) &= \sqrt{(n+1)(n+2)} r R_{n+2, l-2}(r) \\ &\quad - 2 \sqrt{(n+1) \left( n + l + \frac{1}{2} \right)} r R_{n+1, l-2}(r) \\ &\quad + \sqrt{\left( n + l - \frac{1}{2} \right) \left( n + l + \frac{1}{2} \right)} r R_{n, l-2}(r) \\ &= \sqrt{(n+1)(n+2) \left( n + l + \frac{3}{2} \right)} R_{n+2, l-1}(r) \\ &\quad - \sqrt{n+1} (3n+2l+3) R_{n+1, l-1}(r) \\ &\quad + \sqrt{n+l+\frac{1}{2}} \left( 3n+l+\frac{3}{2} \right) R_{n, l-1}(r) \\ &\quad - \sqrt{n \left( n + l - \frac{1}{2} \right) \left( n + l + \frac{1}{2} \right)} R_{n-1, l-1}(r). \end{aligned} \quad (\text{B.6.40})$$

This is identical to Eq. (B.6.39). For  $n \geq 2$ , applying a recursion relation in Eq. (B.6.30) to Eq. (B.6.35),

$$\begin{aligned} r^3 R_{nl}(r) &= \sqrt{(n+1)(n+2)} r R_{n+2, l-2}(r) \\ &\quad - 2 \sqrt{(n+1) \left( n + l + \frac{1}{2} \right)} r R_{n+1, l-2}(r) \\ &\quad + \sqrt{\left( n + l - \frac{1}{2} \right) \left( n + l + \frac{1}{2} \right)} r R_{n, l-2}(r) \\ &= -\sqrt{(n+1)(n+2)(n+3)} R_{n+3, l-3}(r) \\ &\quad + 3 \sqrt{(n+1)(n+2) \left( n + l + \frac{1}{2} \right)} R_{n+2, l-3}(r) \\ &\quad - 3 \sqrt{(n+1) \left( n + l - \frac{1}{2} \right) \left( n + l + \frac{1}{2} \right)} R_{n+1, l-3}(r) \\ &\quad + \sqrt{n+l-\frac{3}{2}} R_{n, l-3}(r). \end{aligned} \quad (\text{B.6.41})$$



## Appendix C

# $CP$ -odd nuclear moments

### C.1 Schiff's theorem

Let us consider a system consisting of non-relativistic point-like particles. It is well known that the electric dipole moments (EDMs) of the ingredients are invisible at least directly with the use of an external electric field  $\mathbf{E}_{\text{ext}}$ . The shielding effect was first indicated by L. I. Schiff [151], so that the assertion is called Schiff's theorem. The proof is given as follows.

The point-like particles interact with a homogeneous electric field  $\mathbf{E}_{\text{ext}}$  through the electric charges  $e_i$  and the EDMs  $\mathbf{d}_i$  as

$$\begin{aligned} V_{\text{ext}} &= V_{\text{ext}}^{(\text{charge})} + V_{\text{ext}}^{(\text{edm})}, \\ V_{\text{ext}}^{(\text{charge})} &= \sum_i e_i \phi_{\text{ext}}(\mathbf{r}_i), \\ V_{\text{ext}}^{(\text{edm})} &= - \sum_i \mathbf{d}_i \cdot \mathbf{E}_{\text{ext}}. \end{aligned} \quad (\text{C.1.1})$$

The constituent particles interact with each other as

$$\begin{aligned} V_{\text{int}} &= V_{\text{int}}^{(\text{charge})} + V_{\text{int}}^{(\text{edm})}, \\ V_{\text{int}}^{(\text{charge})} &= \frac{1}{2} \sum_{i \neq j} \frac{e_i e_j}{|\mathbf{r}_i - \mathbf{r}_j|}, \\ V_{\text{int}}^{(\text{edm})} &= - \sum_{i \neq j} \mathbf{d}_i \cdot \nabla_i \frac{e_j}{|\mathbf{r}_i - \mathbf{r}_j|}. \end{aligned} \quad (\text{C.1.2})$$

L. I. Schiff introduced a unitary operator of  $e^{iQ}$  accompanied with a Hermite operator of

$$Q = \frac{1}{e} \sum_{i=1}^Z \mathbf{d}_i \cdot \mathbf{p}_i. \quad (\text{C.1.3})$$

The interactions due to the electric charges of the particles are transformed as

$$\begin{aligned} e^{iQ} V_{\text{ext}}^{(\text{charge})} e^{-iQ} &\simeq V_{\text{ext}}^{(\text{charge})} + i \left[ Q, V_{\text{ext}}^{(\text{charge})} \right] = V_{\text{ext}}^{(\text{charge})} + V_{\text{ext}}^{(\text{edm})}, \\ e^{iQ} V_{\text{int}}^{(\text{charge})} e^{-iQ} &\simeq V_{\text{int}}^{(\text{charge})} + i \left[ Q, V_{\text{int}}^{(\text{charge})} \right] = V_{\text{int}}^{(\text{charge})} + V_{\text{int}}^{(\text{edm})}, \end{aligned} \quad (\text{C.1.4})$$

where the higher order terms of the EDMs are negligible. Thus, the Hamiltonian of this system can be written as

$$H = \sum_i \frac{\mathbf{p}_i^2}{2m_i} + e^{iQ} V^{(\text{charge})} e^{-iQ}, \quad (\text{C.1.5})$$

where the interaction terms due to charges are gathered as  $V^{(\text{charge})} = V_{\text{ext}}^{(\text{charge})} + V_{\text{int}}^{(\text{charge})}$ .

If the ingredients have no EDMs, the Hamiltonian can be written as

$$H_0 = \sum_i \frac{\mathbf{p}_i^2}{2m_i} + V^{(\text{charge})}. \quad (\text{C.1.6})$$

Let us denote the eigenstates of the unperturbative Hamiltonian  $H_0$  as  $|n\rangle$ . The eigenstates of the Hamiltonian  $H$  including EDMs are then written as  $e^{iQ}|n\rangle$ . Indeed,

$$H e^{iQ}|n\rangle = e^{iQ} H_0 |n\rangle = E_n e^{iQ}|n\rangle \quad (\text{C.1.7})$$

thanks to  $[\mathbf{p}_i, Q] = 0$ . Thus, it is concluded that the system is not affected by the EDMs. Here, it is assumed that stationary states  $|n\rangle$  exist, which requires that the total charge of the system is zero.

Another intuitive explanation is given as follows [152]. The non-relativistic Hamiltonian for a system consisting of point-like particles located at  $\mathbf{r}_k$  and with masses  $m_k$ , charges  $e_k$ , and intrinsic EDMs  $\mathbf{d}_k$  is given as

$$H = H_0 + H_d, \quad H_0 = \sum_k \frac{\mathbf{p}_k^2}{2m_k} + \sum_k e_k \phi(\mathbf{r}_k), \quad H_d = - \sum_k \mathbf{d}_k \cdot \mathbf{E}_{\text{int}}(\mathbf{r}_k), \quad (\text{C.1.8})$$

where the charged particles induce the internal electric field  $\mathbf{E}_{\text{int}}(\mathbf{r}_k) = -\nabla\phi(\mathbf{r}_k)$  with the electrostatic potential  $\phi(\mathbf{r}_k)$ . Considering the purely electrostatic interactions as above, the  $CP$ -odd interaction is written as

$$H_d = -\mathbf{d}_k \cdot \mathbf{E}_{\text{int}}(\mathbf{r}_k) = \mathbf{d}_k \cdot \frac{\partial \phi}{\partial \mathbf{r}_k} = i \frac{1}{e_k} [\mathbf{d}_k \cdot \mathbf{p}_k, H_0]. \quad (\text{C.1.9})$$

The  $CP$ -odd interactions would be perturbatively treated with respect to  $CP$ -even interactions. Let us denote the  $CP$ -conserving eigenstates of the system as  $|n\rangle$ . The  $CP$ -mixed state is then given as

$$|\overline{n}\rangle = |n\rangle + \sum_m \frac{|m\rangle \langle m| H_d |n\rangle}{E_n - E_m} = \left( 1 + i \sum_k \frac{1}{e_k} \mathbf{d}_k \cdot \mathbf{p}_k \right) |n\rangle. \quad (\text{C.1.10})$$

The interactions between the intrinsic EDMs and the internal electric field induce additional EDMs as

$$\begin{aligned} \langle \overline{n} | \sum_l e_l \mathbf{r}_l | \overline{n} \rangle &= \langle n | \left( 1 - i \sum_k \frac{1}{e_k} \mathbf{d}_k \cdot \mathbf{p}_k \right) \sum_l e_l \mathbf{r}_l \left( 1 + i \sum_k \frac{1}{e_k} \mathbf{d}_k \cdot \mathbf{p}_k \right) | n \rangle \\ &= \langle n | i \sum_{kl} \frac{e_l}{e_k} [\mathbf{r}_l, \mathbf{d}_k \cdot \mathbf{p}_k] | n \rangle \\ &= -\langle n | \sum_k \mathbf{d}_k | n \rangle. \end{aligned} \quad (\text{C.1.11})$$

The expectation values of the intrinsic EDMs are given as

$$\overline{\langle n | \mathbf{d}_k | n \rangle} = \langle n | \sum_k \mathbf{d}_k | n \rangle, \quad (\text{C.1.12})$$

where the second order contributions in perturbation are neglected. Thus, the intrinsic EDMs cause the rearrangement of the charge distribution to induce EDMs, which exactly cancel the intrinsic EDMs of the ingredients.

## C.2 Nuclear Schiff moment

Let us consider a finite-size nucleus with the charge distribution of  $\rho_q(\mathbf{r}')$ , which is normalized as

$$\int \rho_q(\mathbf{r}') d^3 \mathbf{r}' = 1. \quad (\text{C.2.1})$$

The charge distribution of the nucleus causes the electrostatic potential

$$\phi_{\text{charge}}(\mathbf{r}) = Ze \int d^3 \mathbf{r}' \frac{\rho_q(\mathbf{r}')}{|\mathbf{r} - \mathbf{r}'|} = Ze \int d^3 \mathbf{r}' \rho_q(\mathbf{r}') \left[ \frac{1}{r} + \mathbf{r}' \cdot \nabla \frac{1}{r} + O(r'^2) \right], \quad (\text{C.2.2})$$

where  $\mathbf{r}'$  indicating a position inside the nucleus is much smaller than  $\mathbf{r}$  indicating the positions of electrons in the atom. If the nucleus has a permanent EDM  $\mathbf{d}_N$  with the distribution of  $\rho_d(\mathbf{r}')$ , the EDM also contributes to the electrostatic potential in the form of

$$\phi_{\text{edm}}(\mathbf{r}) = \int d^3 \mathbf{r}' \rho_d(\mathbf{r}') \mathbf{d}_N \cdot \nabla \frac{1}{|\mathbf{r} - \mathbf{r}'|}. \quad (\text{C.2.3})$$

The first order contributions of  $r'/r$  in the electrostatic potential are given as

$$\begin{aligned} \phi^{(1)}(\mathbf{r}) &= \phi_{\text{charge}}^{(1)}(\mathbf{r}) + \phi_{\text{edm}}^{(1)}(\mathbf{r}) \\ &= Ze \int d^3 \mathbf{r}' \rho_q(\mathbf{r}') \mathbf{r}' \cdot \nabla \frac{1}{r} + \int d^3 \mathbf{r}' \rho_d(\mathbf{r}') \mathbf{d}_N \cdot \nabla \frac{1}{r}. \end{aligned} \quad (\text{C.2.4})$$

The Schiff's theorem says that the expectation value of the first term with the  $P$ -mixed state can be replaced by

$$Ze \int d^3 \mathbf{r}' \rho_q(\mathbf{r}') \langle \mathbf{r}' \rangle' \cdot \nabla \frac{1}{r} = - \int d^3 \mathbf{r}' \rho_d(\mathbf{r}') \langle \mathbf{d}_N \rangle' \cdot \nabla \frac{1}{r} = - \int d^3 \mathbf{r}' \rho_d(\mathbf{r}') \langle \mathbf{d}_N \rangle' \cdot \nabla \frac{1}{r}, \quad (\text{C.2.5})$$

where the bracket  $\langle \dots \rangle'$  means the expectation value with respect to the  $P$ -mixed state, and  $\langle \dots \rangle$  means that with respect to the  $P$ -even state. The EDM is  $T$ -odd and  $P$ -even, so that only the dominant parity state plays a role as  $\langle \mathbf{d}_N \rangle' = \langle \mathbf{d}_N \rangle$ . Here, one ignores the contribution from the subdominant parity state, which is the second order term of parity-mixing perturbation. Thus, the first order contributions are exactly canceled.

In the following, the charge distribution is simply denoted by  $\rho(\mathbf{r})$  and the nuclear EDM is expressed as

$$\mathbf{d} = Ze \int \mathbf{r}' \rho(\mathbf{r}') d^3 \mathbf{r}'. \quad (\text{C.2.6})$$

The nucleons are assumed as point-like particles located at  $\mathbf{r}'$ . The electrostatic potential of a nucleus is given as [153, 154]

$$\phi(\mathbf{r}) = \phi_{\text{charge}}(\mathbf{r}) + \phi_{\text{edm}}(\mathbf{r}), \quad (\text{C.2.7})$$

$$\phi_{\text{charge}}(\mathbf{r}) = e \int d^3\mathbf{r}' \frac{\rho(\mathbf{r}')}{|\mathbf{r} - \mathbf{r}'|}, \quad (\text{C.2.8})$$

$$\phi_{\text{edm}}(\mathbf{r}) = \mathbf{d} \cdot \nabla \phi_{\text{charge}}(\mathbf{r}) = (\mathbf{d} \cdot \nabla) \int d^3\mathbf{r}' \frac{\rho(\mathbf{r}')}{|\mathbf{r} - \mathbf{r}'|}, \quad (\text{C.2.9})$$

where  $\phi_{\text{edm}}(\mathbf{r})$  is introduced instead of the coupling of the nuclear EDM and a homogeneous external electric field. The electrons at  $\mathbf{r}$  in an atom interact with the electrostatic potential, so that the positions  $\mathbf{r}'$  in a nucleus are typically much smaller than  $\mathbf{r}$ . In order to explore the leading order contributions to the electrostatic potential, the elementary relations of

$$\begin{aligned} \partial'_i f(|\mathbf{r} - \mathbf{r}'|) &= -\partial_i f(|\mathbf{r} - \mathbf{r}'|), \\ \partial'_i \partial'_j f(|\mathbf{r} - \mathbf{r}'|) &= -\partial_i \partial'_j f(|\mathbf{r} - \mathbf{r}'|) = \partial_i \partial_j f(|\mathbf{r} - \mathbf{r}'|), \\ \partial'_i \partial'_j \partial'_k f(|\mathbf{r} - \mathbf{r}'|) &= -\partial_i \partial'_j \partial'_k f(|\mathbf{r} - \mathbf{r}'|) = -\partial_i \partial_j \partial_k f(|\mathbf{r} - \mathbf{r}'|) \end{aligned} \quad (\text{C.2.10})$$

are helpful. It can be shown from the first line that the zeroth order term of  $\phi_{\text{edm}}$ , which is given as

$$\phi_{\text{edm}}^{(0)}(\mathbf{r}) = \mathbf{d} \cdot \nabla \frac{1}{r}, \quad (\text{C.2.11})$$

must vanish with the first order term of  $\phi_{\text{charge}}$ , which is given as

$$\phi_{\text{charge}}^{(0)}(\mathbf{r}) = -e \int d^3\mathbf{r}' \rho(\mathbf{r}') \left( \nabla \frac{1}{r} \right) \cdot \mathbf{r}' = -\mathbf{d} \cdot \nabla \frac{1}{r}. \quad (\text{C.2.12})$$

This equality means the Schiff's theorem saying that the EDM of a nucleus as a point-like particle is screened by the charge-induced dipole moment. The second line shows that the second derivative of  $\phi_{\text{charge}}$  and the first derivative of  $\phi_{\text{edm}}$  are also canceled. Thus, the leading order contributions come from the third line and those are given as

$$\phi(\mathbf{r}) = -\frac{1}{6} e \left( \partial_i \partial_j \partial_k \frac{1}{r} \right) \int \rho(\mathbf{r}') r'_i r'_j r'_k d^3\mathbf{r}' + \frac{1}{2Z} d_i \left( \partial_i \partial_j \partial_k \frac{1}{r} \right) \int \rho(\mathbf{r}') r'_j r'_k d^3\mathbf{r}'. \quad (\text{C.2.13})$$

Here, the spherical components of the vector  $\mathbf{r}$  and the gradient operator  $\nabla^{(1)}$  are defined as

$$\begin{aligned} r_{\pm 1} &= \mp \frac{1}{\sqrt{2}} (x \pm iy), \quad r_0 = z \quad \Leftrightarrow \quad x = -\frac{1}{\sqrt{2}} (r_{+1} - r_{-1}), \quad y = \frac{i}{\sqrt{2}} (r_{+1} + r_{-1}) \\ \nabla_{\pm 1}^{(1)} &= -\frac{\partial}{\partial r_{\mp 1}}, \quad \nabla_0^{(1)} = \frac{\partial}{\partial r_0}. \end{aligned} \quad (\text{C.2.14})$$

The spherical components ( $\mu, \nu = 0, \pm 1$ ) follow the commutation relation of

$$\left[ \nabla_{\mu}^{(1)}, r_{\nu}^{(1)} \right] = (-1)^{\mu} \delta_{\mu, -\nu}. \quad (\text{C.2.15})$$

However, this relation is not related to the following argument since the spherical components of  $\mathbf{r}'$  are integrated out.

The tensor product of  $\partial_i \partial_j r'_i r'_j$  is given as

$$\begin{aligned}
& \frac{1}{3} \left( \nabla^{(1)} \cdot r'^{(1)} \right) \left( \nabla^{(1)} \cdot r'^{(1)} \right) \\
&= \left[ \left[ \nabla^{(1)} \otimes r'^{(1)} \right]^{(0)} \otimes \left[ \nabla^{(1)} \otimes r'^{(1)} \right]^{(0)} \right]_0^{(0)} \\
&= \sum_{k=0,2} (2k+1) \begin{Bmatrix} 1 & 1 & 0 \\ 1 & 1 & 0 \\ k & k & 0 \end{Bmatrix} \left[ \left[ \nabla^{(1)} \otimes \nabla^{(1)} \right]^{(k)} \otimes \left[ r'^{(1)} \otimes r'^{(1)} \right]^{(k)} \right]_0^{(0)} \\
&= \sum_{k=0,2} \sqrt{2k+1} \begin{Bmatrix} 1 & 1 & 0 \\ 1 & 1 & k \end{Bmatrix} \left[ \left[ \nabla^{(1)} \otimes \nabla^{(1)} \right]^{(k)} \otimes \left[ r'^{(1)} \otimes r'^{(1)} \right]^{(k)} \right]_0^{(0)} \\
&= \sum_{k=0,2} \frac{\sqrt{2k+1}}{3} \left[ \left[ \nabla^{(1)} \otimes \nabla^{(1)} \right]^{(k)} \otimes \left[ r'^{(1)} \otimes r'^{(1)} \right]^{(k)} \right]_0^{(0)} \\
&= \frac{1}{3} \left[ \left[ \nabla^{(1)} \otimes \nabla^{(1)} \right]^{(0)} \otimes \left[ r'^{(1)} \otimes r'^{(1)} \right]^{(0)} \right]_0^{(0)} \\
&\quad + \frac{\sqrt{5}}{3} \left[ \left[ \nabla^{(1)} \otimes \nabla^{(1)} \right]^{(2)} \otimes \left[ r'^{(1)} \otimes r'^{(1)} \right]^{(2)} \right]_0^{(0)} \\
&= \frac{1}{9} \left( \nabla^{(1)} \cdot \nabla^{(1)} \right) \left( r'^{(1)} \cdot r'^{(1)} \right) + \frac{\sqrt{5}}{3} \left[ \left[ \nabla^{(1)} \otimes \nabla^{(1)} \right]^{(2)} \otimes \left[ r'^{(1)} \otimes r'^{(1)} \right]^{(2)} \right]_0^{(0)}, \quad (\text{C.2.16})
\end{aligned}$$

and then

$$\begin{aligned}
\partial_i \partial_j r_i r_j &= \frac{1}{3} \partial_i \partial_j r'^2 \delta_{ij} + \sqrt{5} \left[ \left[ \nabla^{(1)} \otimes \nabla^{(1)} \right]^{(2)} \otimes \left[ r'^{(1)} \otimes r'^{(1)} \right]^{(2)} \right]_0^{(0)} \\
&= \partial_i \partial_j \left[ \frac{1}{3} r'^2 \delta_{ij} + \left( r'_i r'_j - \frac{1}{3} r'^2 \delta_{ij} \right) \right] = \frac{1}{3} \partial_i \partial_j \left[ r'^2 \delta_{ij} + Q_{ij} \right]. \quad (\text{C.2.17})
\end{aligned}$$

The first term is an irreducible rank-0 tensor operator, and the remaining term is an irreducible rank-2 tensor operator. The quadrupole moment is defined as

$$Q_{ij} = \left( 3r'_i r'_j - r'^2 \delta_{ij} \right), \quad (\text{C.2.18})$$

and the spherical components are given by

$$Q^{(2)} = \sqrt{6} \left[ r'^{(1)} \otimes r'^{(1)} \right]^{(2)}. \quad (\text{C.2.19})$$

Actually, using explicit values of CG-coefficients as

$$\langle 1010 | 20 \rangle = \sqrt{\frac{2}{3}}, \quad \langle 111-1 | 20 \rangle = \sqrt{\frac{1}{6}}, \quad (\text{C.2.20})$$

it is found that

$$\begin{aligned}
\frac{1}{\sqrt{6}}Q_0^{(2)} &= [r'^{(1)} \otimes r'^{(1)}]^{(2)} \\
&= \langle 1010|20\rangle r'_0 r'_0 + 2\langle 111-1|20\rangle r'_{+1} r'_{-1} \\
&= \sqrt{\frac{2}{3}}z'^2 - \sqrt{\frac{1}{6}}(x'^2 + y'^2) \\
&= \sqrt{\frac{1}{6}}[3z'^2 - (x'^2 + y'^2 + z'^2)] \\
&= \sqrt{\frac{1}{6}}Q_{zz}.
\end{aligned} \tag{C.2.21}$$

The rank-2 part can be reduced further as

$$\begin{aligned}
& -\frac{1}{\sqrt{3}}(d^{(1)} \cdot \nabla^{(1)}) \left[ [\nabla^{(1)} \otimes \nabla^{(1)}]^{(2)} \otimes [r'^{(1)} \otimes r'^{(1)}]^{(2)} \right]_0^{(0)} \\
&= \left[ [d^{(1)} \otimes \nabla^{(1)}]^{(0)} \otimes \left[ [\nabla^{(1)} \otimes \nabla^{(1)}]^{(2)} \otimes [r'^{(1)} \otimes r'^{(1)}]^{(2)} \right]_0^{(0)} \right]_0^{(0)} \\
&= \sum_{k=1,3} (2k+1) \begin{Bmatrix} 1 & 1 & 0 \\ 2 & 2 & 0 \\ k & k & 0 \end{Bmatrix} \\
&\quad \times \left[ [\nabla^{(1)} \otimes [\nabla^{(1)} \otimes \nabla^{(1)}]^{(2)}]^{(k)} \otimes [d^{(1)} \otimes [r'^{(1)} \otimes r'^{(1)}]^{(2)}]^{(k)} \right]_0^{(0)} \\
&= \sum_{k=1,3} \sqrt{2k+1} \begin{Bmatrix} 1 & 1 & 0 \\ 2 & 2 & k \end{Bmatrix} \\
&\quad \times \left[ [\nabla^{(1)} \otimes [\nabla^{(1)} \otimes \nabla^{(1)}]^{(2)}]^{(k)} \otimes [d^{(1)} \otimes [r'^{(1)} \otimes r'^{(1)}]^{(2)}]^{(k)} \right]_0^{(0)} \\
&= \sum_{k=1,3} \sqrt{\frac{2k+1}{15}} \left[ [\nabla^{(1)} \otimes [\nabla^{(1)} \otimes \nabla^{(1)}]^{(2)}]^{(k)} \otimes [d^{(1)} \otimes [r'^{(1)} \otimes r'^{(1)}]^{(2)}]^{(k)} \right]_0^{(0)} \\
&= \frac{2}{5} \left[ [\nabla^{(1)} \otimes [\nabla^{(1)} \otimes \nabla^{(1)}]^{(0)}]^{(1)} \otimes [d^{(1)} \otimes [r'^{(1)} \otimes r'^{(1)}]^{(2)}]^{(1)} \right]_0^{(0)} \\
&\quad + \sqrt{\frac{7}{15}} \left[ [\nabla^{(1)} \otimes [\nabla^{(1)} \otimes \nabla^{(1)}]^{(2)}]^{(3)} \otimes [d^{(1)} \otimes [r'^{(1)} \otimes r'^{(1)}]^{(2)}]^{(3)} \right]_0^{(0)} \\
&= \frac{2}{15} \left[ d^{(1)} \otimes [r'^{(1)} \otimes r'^{(1)}]^{(2)} \right]^{(1)} \cdot \nabla^{(1)} \nabla^2 \\
&\quad + \sqrt{\frac{7}{15}} \left[ [\nabla^{(1)} \otimes [\nabla^{(1)} \otimes \nabla^{(1)}]^{(2)}]^{(3)} \otimes [d^{(1)} \otimes [r'^{(1)} \otimes r'^{(1)}]^{(2)}]^{(3)} \right]_0^{(0)}. \tag{C.2.22}
\end{aligned}$$

Here,

$$\begin{aligned}
& \left[ \left[ \nabla^{(1)} \otimes \nabla^{(1)} \right]^{(0)} \otimes \nabla^{(1)} \right]^{(1)} \\
&= \left[ \left[ \nabla^{(1)} \otimes \nabla^{(1)} \right]^{(0)} \otimes \left[ \nabla^{(1)} \otimes 1 \right]^{(1)} \right]^{(1)} \\
&= \sum_{k=0,2} 3\sqrt{(2k+1)} \begin{Bmatrix} 1 & 1 & 0 \\ 1 & 0 & 1 \\ k & 1 & 1 \end{Bmatrix} \left[ \left[ \nabla^{(1)} \otimes \nabla^{(1)} \right]^{(k)} \otimes \left[ \nabla^{(1)} \otimes 1 \right]^{(1)} \right]^{(1)} \\
&= \sum_{k=0,2} \sqrt{(2k+1)} \begin{Bmatrix} 1 & 0 & 1 \\ 1 & k & 1 \end{Bmatrix} \left[ \left[ \nabla^{(1)} \otimes \nabla^{(1)} \right]^{(k)} \otimes \left[ \nabla^{(1)} \otimes 1 \right]^{(1)} \right]^{(1)} \\
&= \sum_{k=0,2} \frac{\sqrt{(2k+1)}}{3} \left[ \left[ \nabla^{(1)} \otimes \nabla^{(1)} \right]^{(k)} \otimes \left[ \nabla^{(1)} \otimes 1 \right]^{(1)} \right]^{(1)}, \tag{C.2.23}
\end{aligned}$$

namely,

$$\left[ \left[ \nabla^{(1)} \otimes \nabla^{(1)} \right]^{(2)} \otimes \nabla^{(1)} \right]^{(1)} = \frac{2}{\sqrt{5}} \left[ \left[ \nabla^{(1)} \otimes \nabla^{(1)} \right]^{(0)} \otimes \nabla^{(1)} \right]^{(1)} \tag{C.2.24}$$

is used. Using a CG-coefficient of

$$\langle 1020 | 10 \rangle = -\sqrt{\frac{2}{5}}, \tag{C.2.25}$$

we get

$$\begin{aligned}
& \left[ d^{(1)} \otimes \left[ r'^{(1)} \otimes r'^{(1)} \right]^{(2)} \right]_0^{(1)} \\
&= -\sqrt{\frac{2}{5}} d_0^{(1)} \left[ r'^{(1)} \otimes r'^{(1)} \right]_0^{(2)} + \dots \\
&= -\sqrt{\frac{2}{5}} \sqrt{\frac{1}{6}} d_0^{(1)} Q_0^{(2)} + \dots \\
&= -\sqrt{\frac{1}{15}} d_z Q_{zz} + \dots \tag{C.2.26}
\end{aligned}$$

Another tensor product  $\partial_i \partial_j \partial_k r'_i r'_j r'_k$  is decomposed as

$$\begin{aligned}
& \left( \nabla^{(1)} \cdot r'^{(1)} \right) \left( \nabla^{(1)} \cdot r'^{(1)} \right) \left( \nabla^{(1)} \cdot r'^{(1)} \right) \\
&= -3\sqrt{3} \left[ \left[ \left[ \nabla^{(1)} \otimes r'^{(1)} \right]^{(0)} \otimes \left[ \nabla^{(1)} \otimes r'^{(1)} \right]^{(0)} \right]^{(0)} \otimes \left[ \nabla^{(1)} \otimes r'^{(1)} \right]^{(0)} \right]_0^{(0)} \\
&= -\sqrt{3} \left[ \left[ \left[ \nabla^{(1)} \otimes \nabla^{(1)} \right]^{(0)} \otimes \left[ r'^{(1)} \otimes r'^{(1)} \right]^{(0)} \right]^{(0)} \otimes \left[ \nabla^{(1)} \otimes r'^{(1)} \right]^{(0)} \right]_0^{(0)} \\
&\quad - \sqrt{15} \left[ \left[ \left[ \nabla^{(1)} \otimes \nabla^{(1)} \right]^{(2)} \otimes \left[ r'^{(1)} \otimes r'^{(1)} \right]^{(2)} \right]^{(0)} \otimes \left[ \nabla^{(1)} \otimes r'^{(1)} \right]^{(0)} \right]_0^{(0)}. \tag{C.2.27}
\end{aligned}$$

The first term is given as

$$\begin{aligned}
& \left[ \left[ \left[ \nabla^{(1)} \otimes \nabla^{(1)} \right]^{(0)} \otimes \left[ r'^{(1)} \otimes r'^{(1)} \right]^{(0)} \right]^{(0)} \otimes \left[ \nabla^{(1)} \otimes r'^{(1)} \right]^{(0)} \right]_0^{(0)} \\
&= 3 \begin{Bmatrix} 0 & 0 & 0 \\ 1 & 1 & 0 \\ 1 & 1 & 0 \end{Bmatrix} \left[ \left[ \left[ \nabla^{(1)} \otimes \nabla^{(1)} \right]^{(0)} \otimes \nabla^{(1)} \right]^{(1)} \otimes \left[ \left[ r'^{(1)} \otimes r'^{(1)} \right]^{(0)} \otimes r'^{(1)} \right]^{(1)} \right]_0^{(0)} \\
&= \sqrt{3} \begin{Bmatrix} 0 & 0 & 0 \\ 1 & 1 & 1 \end{Bmatrix} \left[ \left[ \left[ \nabla^{(1)} \otimes \nabla^{(1)} \right]^{(0)} \otimes \nabla^{(1)} \right]^{(1)} \otimes \left[ \left[ r'^{(1)} \otimes r'^{(1)} \right]^{(0)} \otimes r'^{(1)} \right]^{(1)} \right]_0^{(0)} \\
&= \left[ \left[ \left[ \nabla^{(1)} \otimes \nabla^{(1)} \right]^{(0)} \otimes \nabla^{(1)} \right]^{(1)} \otimes \left[ \left[ r'^{(1)} \otimes r'^{(1)} \right]^{(0)} \otimes r'^{(1)} \right]^{(1)} \right]_0^{(0)} \\
&= -\frac{1}{3\sqrt{3}} \nabla^2 r'^2 (\nabla \cdot \mathbf{r}'), \tag{C.2.28}
\end{aligned}$$

and the second term is given as

$$\begin{aligned}
& \left[ \left[ \left[ \nabla^{(1)} \otimes \nabla^{(1)} \right]^{(2)} \otimes \left[ r'^{(1)} \otimes r'^{(1)} \right]^{(2)} \right]^{(0)} \otimes \left[ \nabla^{(1)} \otimes r'^{(1)} \right]^{(0)} \right]_0^{(0)} \\
&= \sum_{k=1,3} (2k+1) \begin{Bmatrix} 2 & 2 & 0 \\ 1 & 1 & 0 \\ k & k & 0 \end{Bmatrix} \\
&\quad \times \left[ \left[ \left[ \nabla^{(1)} \otimes \nabla^{(1)} \right]^{(2)} \otimes \nabla^{(1)} \right]^{(k)} \otimes \left[ \left[ r'^{(1)} \otimes r'^{(1)} \right]^{(2)} \otimes r'^{(1)} \right]^{(k)} \right]_0^{(0)} \\
&= \sum_{k=1,3} (-1)^{k+1} \sqrt{2k+1} \begin{Bmatrix} 2 & 2 & 0 \\ 1 & 1 & k \end{Bmatrix} \\
&\quad \times \left[ \left[ \left[ \nabla^{(1)} \otimes \nabla^{(1)} \right]^{(2)} \otimes \nabla^{(1)} \right]^{(k)} \otimes \left[ \left[ r'^{(1)} \otimes r'^{(1)} \right]^{(2)} \otimes r'^{(1)} \right]^{(k)} \right]_0^{(0)} \\
&= \sum_{k=1,3} \sqrt{\frac{2k+1}{15}} \left[ \left[ \left[ \nabla^{(1)} \otimes \nabla^{(1)} \right]^{(2)} \otimes \nabla^{(1)} \right]^{(k)} \otimes \left[ \left[ r'^{(1)} \otimes r'^{(1)} \right]^{(2)} \otimes r'^{(1)} \right]^{(k)} \right]_0^{(0)} \\
&= -\frac{4}{15\sqrt{15}} \nabla^2 r'^2 (\nabla \cdot \mathbf{r}') \\
&\quad + \sqrt{\frac{7}{15}} \left[ \left[ \left[ \nabla^{(1)} \otimes \nabla^{(1)} \right]^{(2)} \otimes \nabla^{(1)} \right]^{(3)} \otimes \left[ \left[ r'^{(1)} \otimes r'^{(1)} \right]^{(2)} \otimes r'^{(1)} \right]^{(3)} \right]_0^{(0)}. \tag{C.2.29}
\end{aligned}$$

In conclusion, we get

$$\begin{aligned}
& \partial_i \partial_j \partial_k r'_i r'_j r'_k \\
&= \frac{3}{5} \nabla^2 r'^2 (\nabla \cdot \mathbf{r}') - \sqrt{7} \left[ \left[ \left[ \nabla^{(1)} \otimes \nabla^{(1)} \right]^{(2)} \otimes \nabla^{(1)} \right]^{(3)} \otimes \left[ \left[ r'^{(1)} \otimes r'^{(1)} \right]^{(2)} \otimes r'^{(1)} \right]^{(3)} \right]_0^{(0)}
\end{aligned}$$

$$= \partial_i \partial_j \partial_k \left[ \frac{1}{5} r'^2 (r'_i \delta_{jk} + r'_j \delta_{ki} + r'_k \delta_{ij}) + \left\{ r'_i r'_j r'_k - \frac{1}{5} r'^2 (r'_i \delta_{jk} + r'_j \delta_{ki} + r'_k \delta_{ij}) \right\} \right]. \quad (\text{C.2.30})$$

The first term is an irreducible rank-1 tensor operator, and the remaining term is an irreducible rank-3 tensor operator.

It has shown that the leading order contributions to the electrostatic potential are given as

$$\phi_{\text{octupole}}(\mathbf{r}) = -\frac{1}{6} \left( \partial_i \partial_j \partial_k \frac{1}{r} \right) \int e\rho(\mathbf{r}') \left[ r'_i r'_j r'_k - \frac{1}{5} r'^2 (r'_i \delta_{jk} + r'_j \delta_{ki} + r'_k \delta_{ij}) \right] d^3 \mathbf{r}' \quad (\text{C.2.31})$$

$$\phi_{\text{Schiff}}(\mathbf{r}) = 4\pi \mathbf{S} \cdot \nabla \delta^{(3)}(\mathbf{r}), \quad (\text{C.2.32})$$

where  $\nabla^2(1/r) = -4\pi\delta^{(3)}(\mathbf{r})$  is used. The Schiff moment operator  $\mathbf{S}$  is expressed as

$$S_k = \frac{1}{10} \left[ \int e\rho(\mathbf{r}') r'^2 r'_k d^3 \mathbf{r}' - \frac{5}{3} d_k \langle r^2 \rangle_{\text{ch}} - \frac{2}{3} d_j \int \rho(\mathbf{r}') Q_{jk}(\mathbf{r}') d^3 \mathbf{r}' \right], \quad (\text{C.2.33})$$

where

$$\langle r^2 \rangle_{\text{ch}} = \int \rho(\mathbf{r}') r'^2 d^3 \mathbf{r}' \quad (\text{C.2.34})$$

is the charge mean square radius. The nuclear Schiff moment should be proportional to the nuclear spin. Thus, the  $T$ -odd nuclear moment produces a  $P$ ,  $T$ -odd electrostatic potential  $\phi_{\text{Schiff}}$ . The interactions of electrons with  $\phi_{\text{Schiff}}$  mix atomic states of opposite parity, and then induce a  $P$ ,  $T$ -odd atomic moment, atomic EDM.

If nucleons inside a nucleus are point-like particles, the charge distribution is given by

$$\rho(\mathbf{r}) = \sum_{i=1}^A \delta^{(3)}(\mathbf{r} - \mathbf{r}_i). \quad (\text{C.2.35})$$

In this case, the Schiff moment operator without the third term is rewritten as

$$\mathbf{S} = \frac{1}{10} \sum_{i=1}^A e_i \left[ r_i^2 \mathbf{r}_i - \frac{5}{3} \langle r^2 \rangle_{\text{ch}} \mathbf{r}_i \right]. \quad (\text{C.2.36})$$

In order to take into account the internal structure of nucleons, the positions of nucleons  $\mathbf{r}_i$  are replaced with the positions of charges inside nucleons  $\mathbf{r}_i + \boldsymbol{\xi}$ , and the terms are integrated with the charge distribution  $\rho(\mathbf{r}_i + \boldsymbol{\xi})$ . An integral over inside a nucleon can be carried out as

$$\int \rho(\mathbf{r}_i + \boldsymbol{\xi}) d^3 \boldsymbol{\xi} = 1, \quad (\text{C.2.37})$$

and the Schiff moment operator is then given as

$$\begin{aligned} \mathbf{S} &= \frac{1}{10} \sum_{i=1}^A e_i \int d^3 \boldsymbol{\xi} \rho(\mathbf{r}_i + \boldsymbol{\xi}) \left[ (\mathbf{r}_i + \boldsymbol{\xi})^2 (\mathbf{r}_i + \boldsymbol{\xi}) - \frac{5}{3} \langle r^2 \rangle_{\text{ch}} (\mathbf{r}_i + \boldsymbol{\xi}) \right] \\ &= \frac{1}{10} \sum_{i=1}^A e_i \int d^3 \boldsymbol{\xi} \rho(\mathbf{r}_i + \boldsymbol{\xi}) \left[ (r_i^2 + 2\mathbf{r}_i \cdot \boldsymbol{\xi}) \mathbf{r}_i + r_i^2 \boldsymbol{\xi} - \frac{5}{3} \langle r^2 \rangle_{\text{ch}} (\mathbf{r}_i + \boldsymbol{\xi}) \right] + O(\xi^2) \\ &= \mathbf{S}^{(\text{ch})} + \mathbf{S}^{(\text{int})}, \end{aligned} \quad (\text{C.2.38})$$

where

$$\begin{aligned}
\mathbf{S}^{(\text{ch})} &= \frac{1}{10} \sum_{i=1}^A e_i \left[ r_i^2 \mathbf{r}_i - \frac{5}{3} \langle r^2 \rangle_{\text{ch}} \mathbf{r}_i \right], \\
\mathbf{S}^{(\text{int})} &= \frac{1}{10} \sum_{i=1}^A \left[ 2 \left( \mathbf{r}_i \cdot \mathbf{d}_i^{(n)} \right) \mathbf{r}_i + r_i^2 \mathbf{d}_i^{(n)} - \frac{5}{3} \langle r^2 \rangle_{\text{ch}} \mathbf{d}_i^{(n)} \right] \\
&= \frac{1}{6} \sum_{i=1}^A \left[ r_i^2 - \langle r^2 \rangle_{\text{ch}} \right] \mathbf{d}_i^{(n)} + \frac{1}{5} \sum_{i=1}^A \left[ \left( \mathbf{r}_i \cdot \mathbf{d}_i^{(n)} \right) \mathbf{r}_i - \frac{1}{3} r_i^2 \mathbf{d}_i^{(n)} \right].
\end{aligned} \tag{C.2.39}$$

The first term is induced by the charge asymmetry in a nucleus, and the second term is caused by the nucleonic EDM. The nucleonic EDM is defined as

$$\mathbf{d}_i^{(n)} = e_i \int \rho(\mathbf{r}_i + \boldsymbol{\xi}) \boldsymbol{\xi} d^3 \boldsymbol{\xi}. \tag{C.2.40}$$

### C.3 Schiff moment calculations in the shell-model framework

In order to evaluate the expectation value of the nuclear Schiff moment, we express the Schiff moment operator and the  $PT$ -odd interaction in the form of tensor operator as

$$S^{(1)} = \sum_{i'j} s_{i'j} \left[ c_{\pi i'}^\dagger \otimes \tilde{c}_{\pi j} \right]^{(1)} + \sum_{ij'} s_{ij'} \left[ c_{\pi i}^\dagger \otimes \tilde{c}_{\pi j'} \right]^{(1)}, \tag{C.3.1}$$

$$\begin{aligned}
\hat{V}_{\tau_1 \tau_2}^{(PT)} &= \sum_J \sum_{i'jkl} v_{i'jkl}^{(J)} \left[ \left[ c_{\tau_1 i'}^\dagger \otimes c_{\tau_2 j}^\dagger \right]^{(J)} \otimes \left[ \tilde{c}_{\tau_1 k} \otimes \tilde{c}_{\tau_2 l} \right]^{(J)} \right]_0^{(0)} \\
&+ \sum_J \sum_{ij'kl} v_{ij'kl}^{(J)} \left[ \left[ c_{\tau_1 i}^\dagger \otimes c_{\tau_2 j'}^\dagger \right]^{(J)} \otimes \left[ \tilde{c}_{\tau_1 k} \otimes \tilde{c}_{\tau_2 l} \right]^{(J)} \right]_0^{(0)} \\
&+ \sum_J \sum_{ijk'l} v_{ijk'l}^{(J)} \left[ \left[ c_{\tau_1 i}^\dagger \otimes c_{\tau_2 j}^\dagger \right]^{(J)} \otimes \left[ \tilde{c}_{\tau_1 k'} \otimes \tilde{c}_{\tau_2 l} \right]^{(J)} \right]_0^{(0)} \\
&+ \sum_J \sum_{ijk'l'} v_{ijk'l'}^{(J)} \left[ \left[ c_{\tau_1 i}^\dagger \otimes c_{\tau_2 j}^\dagger \right]^{(J)} \otimes \left[ \tilde{c}_{\tau_1 k} \otimes \tilde{c}_{\tau_2 l'} \right]^{(J)} \right]_0^{(0)}
\end{aligned} \tag{C.3.2}$$

where a single-particle level indicated with  $i', j', k', l'$  has the opposite parity to those of the others in each term. Here, the Hermite conjugate of the first term in the Schiff moment operator is given as

$$\begin{aligned}
\left( \sum_{i'j} s_{i'j} \left[ c_{\pi i'}^\dagger \otimes \tilde{c}_{\pi j} \right]_M^{(1)} \right)^\dagger &= \sum_{i'j} s_{i'j} \langle i' m' j m | 1 M \rangle \left( c_{\pi i' m'}^\dagger \tilde{c}_{\pi j m} \right)^\dagger \\
&= \sum_{i'j} s_{i'j} \langle i' m' j m | 1 M \rangle (-1)^{j-m} (-1)^{i'+m'} c_{\pi j-m}^\dagger \tilde{c}_{\pi i'-m'} \\
&= \sum_{i'j} s_{i'j} (-1)^{i'-j+M} \langle j - m i' - m' | 1 - M \rangle c_{\pi j-m}^\dagger \tilde{c}_{\pi i'-m'}
\end{aligned}$$

$$= \sum_{i'j} s_{i'j} (-1)^{i'-j+M} \left[ c_{\pi j}^\dagger \otimes \tilde{c}_{\pi i'} \right]_{-M}^{(1)}. \quad (\text{C.3.3})$$

Thus, if the one-body matrix elements follow that

$$s_{ij'} = (-1)^{-i+j'+M} s_{j'i}, \quad (\text{C.3.4})$$

the Schiff moment operator  $S_M^{(1)}$  is simply given as

$$S^{(1)} = \sum_{i'j} s_{i'j} \left[ c_{\pi i'}^\dagger \otimes \tilde{c}_{\pi j} \right]^{(1)} + h.c. \quad (\text{C.3.5})$$

The  $PT$ -odd interaction can be summarized as

$$\hat{V}_{\tau_1 \tau_2}^{(PT)} = \hat{V}_{\tau_1 \tau_2}^{(PT1)} + \hat{V}_{\tau_1 \tau_2}^{(PT2)}, \quad (\text{C.3.6})$$

where

$$\begin{aligned} \hat{V}_{\tau_1 \tau_2}^{(PT1)} &= \sum_J \sum_{i'jkl} \tilde{v}_{i'jkl}^{(J)} \left[ \left[ c_{\tau_1 i'}^\dagger \otimes c_{\tau_2 j}^\dagger \right]^{(J)} \otimes \left[ \tilde{c}_{\tau_1 k} \otimes \tilde{c}_{\tau_2 l} \right]^{(J)} \right]_0^{(0)}, \\ \hat{V}_{\tau_1 \tau_2}^{(PT2)} &= \sum_J \sum_{ijk'l} \tilde{v}_{ijk'l}^{(J)} \left[ \left[ c_{\tau_1 i}^\dagger \otimes c_{\tau_2 j}^\dagger \right]^{(J)} \otimes \left[ \tilde{c}_{\tau_1 k'} \otimes \tilde{c}_{\tau_2 l} \right]^{(J)} \right]_0^{(0)}. \end{aligned} \quad (\text{C.3.7})$$

The two-body matrix elements defined as

$$\begin{aligned} \tilde{v}_{i'jkl}^{(J)} &= v_{i'jkl}^{(J)} - (-1)^{i'+j-J} v_{j'i'kl}^{(J)}, \\ \tilde{v}_{ijk'l}^{(J)} &= v_{ijk'l}^{(J)} - (-1)^{k'+l-J} v_{ijlk'}^{(J)} \end{aligned} \quad (\text{C.3.8})$$

follow that

$$\tilde{v}_{ijkl}^{(J)} = (-1)^{i+j-J+1} \tilde{v}_{jikl}^{(J)} = (-1)^{k+l-J+1} \tilde{v}_{jilk}^{(J)} = (-1)^{i+j+k+l} \tilde{v}_{jilk}^{(J)}. \quad (\text{C.3.9})$$

The Hermite conjugate of  $\hat{V}^{(PT)}$  is given as

$$\begin{aligned} \hat{V}_{\tau_1 \tau_2}^{(PT1)\dagger} &= \sum_J \sum_{i'jkl} \tilde{v}_{i'jkl}^{(J)} \left[ \left[ c_{\tau_1 k}^\dagger \otimes c_{\tau_2 l}^\dagger \right]^{(J)} \otimes \left[ \tilde{c}_{\tau_1 i'} \otimes \tilde{c}_{\tau_2 j} \right]^{(J)} \right]_0^{(0)}, \\ \hat{V}_{\tau_1 \tau_2}^{(PT2)\dagger} &= \sum_J \sum_{ijk'l} \tilde{v}_{ijk'l}^{(J)} \left[ \left[ c_{\tau_1 k'}^\dagger \otimes c_{\tau_2 l}^\dagger \right]^{(J)} \otimes \left[ \tilde{c}_{\tau_1 i} \otimes \tilde{c}_{\tau_2 j} \right]^{(J)} \right]_0^{(0)}. \end{aligned} \quad (\text{C.3.10})$$

Thus, if  $\tilde{v}_{ijkl}^{(J)} = \tilde{v}_{klij}^{(J)}$ , we have  $\hat{V}_{\tau_1 \tau_2}^{(PT1)\dagger} = \hat{V}_{\tau_1 \tau_2}^{(PT2)}$  and Hermite  $PT$ -odd interactions are given as

$$\hat{V}_{\tau_1 \tau_2}^{(PT)} = \sum_J \sum_{i'jkl} \tilde{v}_{i'jkl}^{(J)} \left[ \left[ c_{\tau_1 i'}^\dagger \otimes c_{\tau_2 j}^\dagger \right]^{(J)} \otimes \left[ \tilde{c}_{\tau_1 k} \otimes \tilde{c}_{\tau_2 l} \right]^{(J)} \right]_0^{(0)} + h.c. \quad (\text{C.3.11})$$

Even if  $CP$ -odd hadronic interactions exist, they should be greatly suppressed in comparison to the well-known  $CP$ -even hadronic interactions such as one-pion exchange. The ground state in the  $CP$ -even effective Hamiltonian is expressed as

$$|\psi_{\text{g.s.}; JM}\rangle = \sum_n \alpha_n^{(\text{g.s.})} |\psi_n^{(\nu)}; J_\nu^{\pi\nu}\rangle \otimes |\psi_n^{(\pi)}; J_\pi^{\pi\pi}\rangle, \quad (\text{C.3.12})$$

where  $|\psi_n^{(\tau)}\rangle$  is the neutron ( $\tau = \nu$ ) or proton ( $\tau = \pi$ ) part of the  $n$ th configuration with a spin-parity of  $J^{\pi_\tau}$ .

In the perturbative manner, the nuclear Schiff moment can be calculated as

$$\langle S_0^{(1)} \rangle = \sum_{\tau_1 \tau_2} \sum_k \frac{\langle \psi_{\text{g.s.}; JM} | S_0^{(1)} | \psi_k \rangle \langle \psi_k | \hat{V}_{\tau_1 \tau_2}^{(PT)} | \psi_{\text{g.s.}; JM} \rangle}{E_{\text{g.s.}} - E_k} + c.c., \quad (\text{C.3.13})$$

where  $|\psi_k\rangle$  is the  $k$ th excited state with the same spin and the opposite parity to the ground state, and  $E_k$  is the excited energy.

## C.4 Valence excitations

### C.4.1 One-particle-one-hole excited states

First, we consider the case that  $i, j, k, l$  are single-particle levels in the valence space. The intruder orbital is only the single-particle level which has the opposite parity to those of the other valence orbitals. However, that has a large angular momentum compared with the others, and that cannot be connected by the rank-1 Schiff moment operator. In fact, for  $^{129}\text{Xe}$  and  $^{199}\text{Hg}$ , the proton orbitals in the valence space are  $2s_{1/2}$ ,  $1d_{3/2}$ ,  $1d_{5/2}$ ,  $0g_{7/2}$ , and  $0h_{11/2}$ . Thus, the excited proton with  $i', j', k', l'$  should be in beyond the valence space. In order to emphasize this point, the proton creation and annihilation operators for the high-lying orbitals outside the valence space are indicated as  $a_{\pi i'}$  and  $a_{\pi i'}^\dagger$  instead of  $c_{\pi i'}$  and  $c_{\pi i'}^\dagger$ . This kind of excitation is called valence excitations.

As discussed above, all the excited states that can contribute to the nuclear Schiff moment are not given in the nuclear shell model with only one harmonic oscillator shell. We take just one-particle-hole excited states from the ground state, which is defined as

$$\begin{aligned}
 |\psi_{i'j,L}^{(\text{ph})}; IM\rangle &= \left[ [a_{\pi i'}^\dagger \otimes \tilde{c}_{\pi j}]^{(L)} \otimes |\psi_{\text{g.s.}}; J\rangle \right]_M^{(I)} \\
 &= \left[ [a_{\pi i'}^\dagger \otimes \tilde{c}_{\pi j}]^{(L)} \otimes T^{(J)\dagger} \right]_M^{(I)} |0\rangle \\
 &= \sum_{M_L M_J} \langle L M_L J M_J | I M \rangle [a_{\pi i'}^\dagger \otimes \tilde{c}_{\pi j}]_{M_L}^{(L)} T_{M_J}^{(J)\dagger} |0\rangle
 \end{aligned} \tag{C.4.1}$$

for the intermediate states in the perturbative formula (C.3.13). The ground state is created by a weighted sum  $T_{M_J}^{(J)\dagger}$  of tensor products of creation operators, where each terms are coupled with  $(J, M_J)$ . Here, the norm of the ground state is given as

$$\begin{aligned}
 \langle \psi_{\text{g.s.}}; JM_J | \psi_{\text{g.s.}}; JM_J \rangle &= \langle 0 | (-1)^{J+M} \tilde{T}_{-M_J}^{(J)} T_{M_J}^{(J)\dagger} |0\rangle \\
 &= (-1)^{J+M} \langle J - M_J J M_J | 00 \rangle \langle 0 | [\tilde{T}^{(J)} \otimes T^{(J)\dagger}]_0^{(0)} |0\rangle \\
 &= \frac{1}{\sqrt{2J+1}} \langle 0 | [\tilde{T}^{(J)} \otimes T^{(J)\dagger}]_0^{(0)} |0\rangle.
 \end{aligned} \tag{C.4.2}$$

Thus, in order to normalize the ground state,

$$\langle 0 | [\tilde{T}^{(J)} \otimes T^{(J)\dagger}]_0^{(0)} |0\rangle = \sqrt{2J+1}, \tag{C.4.3}$$

should be sustained. The excitation energies are approximately given as

$$E_{i'j}^{(\text{ph})} = \varepsilon_{i'} - \varepsilon_j, \tag{C.4.4}$$

where  $\varepsilon_i$  indicates a single-particle energy in the Nilsson potential.

In the valence excitations, we have the anti-commutation relations of

$$\left\{ a_{\pi i' m'}, c_{\pi j m}^\dagger \right\} = \left\{ a_{\pi i' m'}^\dagger, c_{\pi j m} \right\} = 0 \tag{C.4.5}$$

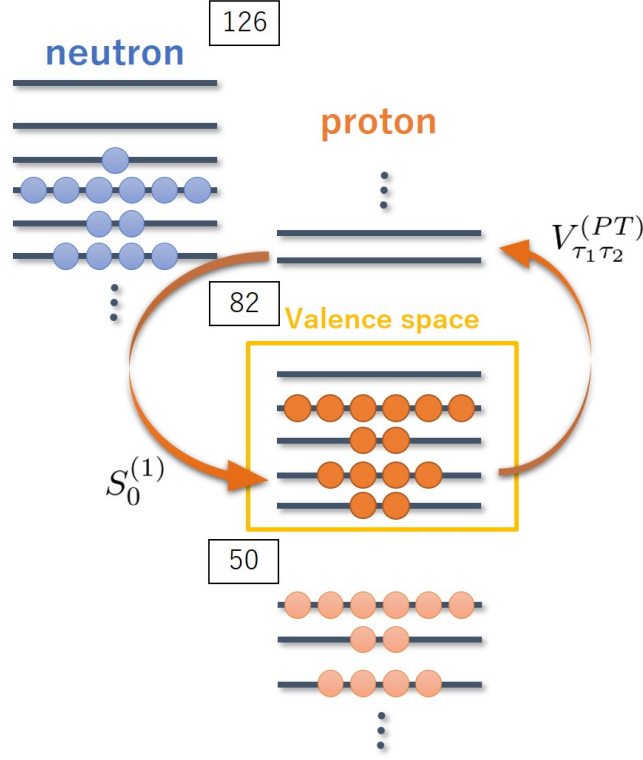


Figure C.1: The valence excitations indicate the contributions of excitations from the valence space, the single-proton orbitals between the magic numbers 50 and 82 for  $^{129}\text{Xe}$  and  $^{199}\text{Hg}$ , to the above by the  $PT$ -odd interactions.

for all the combinations of  $i'$  and  $j$ . The Hermite conjugate of the one-particle-hole operator is then given as

$$\begin{aligned}
 \left( [a_{\pi i'}^\dagger \otimes \tilde{c}_{\pi j}]_{M_L}^{(L)} \right)^\dagger &= \left( \sum_{m' m} \langle i' m' j m | L M_L \rangle a_{\pi i' m'}^\dagger \tilde{c}_{\pi j m} \right)^\dagger \\
 &= \sum_{m' m} \langle i' m' j m | L M_L \rangle (-1)^{i'+m'} (-1)^{j-m} c_{\pi j -m}^\dagger \tilde{a}_{\pi i' -m'} \\
 &= (-1)^{L+M_L} [\tilde{a}_{\pi i'} \otimes c_{\pi j}^\dagger]_{-M_L}^{(L)}.
 \end{aligned} \tag{C.4.6}$$

The conjugates of one-particle-hole excited states are given as

$$\begin{aligned}
 \langle \psi_{i' j, L}^{(\text{ph})}; IM | &= \langle 0 | \sum_{M_L M_J} \langle L M_L J M_J | I M \rangle (-1)^{J+M_J} \tilde{T}_{-M_J}^{(J)} \times (-1)^{L+M_L} [\tilde{a}_{\pi i'} \otimes c_{\pi j}^\dagger]_{-M_L}^{(L)} \\
 &= (-1)^{J+L+M} \langle 0 | \left[ \tilde{T}^{(J)} \otimes [\tilde{a}_{\pi i'} \otimes c_{\pi j}^\dagger]_{-M}^{(L)} \right]_{-M}^{(I)} \\
 &\equiv (-1)^{J+L+M} \left[ \langle \psi_{\text{g.s.}; J} | \otimes [\tilde{a}_{\pi i'} \otimes c_{\pi j}^\dagger]_{-M}^{(L)} \right]_{-M}^{(I)} \\
 &= \sum_{M_J M_L} (-1)^{L+M_L} \langle J - M_J L - M_L | I - M \rangle \langle \psi_{\text{g.s.}; J M_J | [\tilde{a}_{\pi i'} \otimes c_{\pi j}^\dagger]_{-M_L}^{(L)} \\
 & \tag{C.4.7}
 \end{aligned}$$

where  $\tilde{T}_{M_J}^{(J)} = (-1)^{J-M_J} T_{-M_J}^{(J)}$  are ITOs of rank- $J$ . The overlaps of one-particle-hole excited states are then given as

$$\begin{aligned}
& \langle \psi_{i'_f j_f, L'}^{(\text{ph})}; I' M' | \psi_{i'_j i, L}^{(\text{ph})}; I M \rangle \\
&= \delta_{I', I} \delta_{M', M} (-1)^{J+L'+M} \langle 0 | \left[ \tilde{T}^{(J)} \otimes [\tilde{a}_{\pi i'_f} \otimes c_{\pi j_f}^\dagger]^{(L')} \right]_{-M}^{(I)} \left[ [a_{\pi i'_i}^\dagger \otimes \tilde{c}_{\pi j_i}]^{(L)} \otimes T^{(J)\dagger} \right]_M^{(I)} | 0 \rangle \\
&= \delta_{I', I} \delta_{M', M} \frac{(-1)^{J+L'-I}}{\sqrt{2I+1}} \\
&\quad \times \langle 0 | \left[ \left[ \tilde{T}^{(J)} \otimes [\tilde{a}_{\pi i'_f} \otimes c_{\pi j_f}^\dagger]^{(L')} \right]^{(I)} \otimes \left[ [a_{\pi i'_i}^\dagger \otimes \tilde{c}_{\pi j_i}]^{(L)} \otimes T^{(J)\dagger} \right]^{(I)} \right]_0^{(0)} | 0 \rangle. \tag{C.4.8}
\end{aligned}$$

The matrix elements can be calculated as

$$\begin{aligned}
& \langle 0 | \left[ \left[ \tilde{T}^{(J)} \otimes [\tilde{a}_{\pi i'_f} \otimes c_{\pi j_f}^\dagger]^{(L')} \right]^{(I)} \otimes \left[ [a_{\pi i'_i}^\dagger \otimes \tilde{c}_{\pi j_i}]^{(L)} \otimes T^{(J)\dagger} \right]^{(I)} \right]_0^{(0)} | 0 \rangle \\
&= (2J+1)(2I+1) \begin{Bmatrix} J & L' & I \\ 0 & I & I \\ J & J & 0 \end{Bmatrix} \\
&\quad \times \langle 0 | \left[ \left[ \tilde{T}^{(J)} \otimes 1 \right]^{(J)} \otimes \left[ [\tilde{a}_{\pi i'_f} \otimes c_{\pi j_f}^\dagger]^{(L')} \otimes \left[ [a_{\pi i'_i}^\dagger \otimes \tilde{c}_{\pi j_i}]^{(L)} \otimes T^{(J)\dagger} \right]^{(I)} \right]^{(J)} \right]_0^{(0)} | 0 \rangle \\
&= \langle 0 | \left[ \tilde{T}^{(J)} \otimes \left[ [\tilde{a}_{\pi i'_f} \otimes c_{\pi j_f}^\dagger]^{(L')} \otimes \left[ [a_{\pi i'_i}^\dagger \otimes \tilde{c}_{\pi j_i}]^{(L)} \otimes T^{(J)\dagger} \right]^{(I)} \right]^{(J)} \right]_0^{(0)} | 0 \rangle \\
&= \sum_K \sqrt{(2L'+1)(2I+1)(2K+1)(2J+1)} \begin{Bmatrix} L' & 0 & L' \\ L & J & I \\ K & J & J \end{Bmatrix} \\
&\quad \times \langle 0 | \left[ \tilde{T}^{(J)} \otimes \left[ \left[ [\tilde{a}_{\pi i'_f} \otimes c_{\pi j_f}^\dagger]^{(L')} \otimes [a_{\pi i'_i}^\dagger \otimes \tilde{c}_{\pi j_i}]^{(L)} \right]^{(K)} \otimes [1 \otimes T^{(J)\dagger}]^{(J)} \right]^{(J)} \right]_0^{(0)} | 0 \rangle \\
&= \sum_K \sqrt{(2I+1)(2K+1)} (-1)^{2J+L+L'} \begin{Bmatrix} I & L & J \\ K & J & L' \end{Bmatrix} \\
&\quad \times \langle 0 | \left[ \tilde{T}^{(J)} \otimes \left[ \left[ [\tilde{a}_{\pi i'_f} \otimes c_{\pi j_f}^\dagger]^{(L')} \otimes [a_{\pi i'_i}^\dagger \otimes \tilde{c}_{\pi j_i}]^{(L)} \right]^{(K)} \otimes T^{(J)\dagger} \right]^{(J)} \right]_0^{(0)} | 0 \rangle \\
&= \sum_K \sqrt{(2I+1)(2K+1)} (-1)^{2J+L+L'} \begin{Bmatrix} I & L & J \\ K & J & L' \end{Bmatrix} \\
&\quad \times \sum_M \langle J - M \ J \ M | 0 \ 0 \rangle \sum_{Q, M'} \langle K \ Q \ J \ M' | J \ M \rangle \\
&\quad \times \langle 0 | \tilde{T}_{-M}^{(J)} \left[ [\tilde{a}_{\pi i'_f} \otimes c_{\pi j_f}^\dagger]^{(L')} \otimes [a_{\pi i'_i}^\dagger \otimes \tilde{c}_{\pi j_i}]^{(L)} \right]_Q^{(K)} T_{M'}^{(J)\dagger} | 0 \rangle \\
&= \sum_K \sqrt{\frac{(2I+1)(2K+1)}{2J+1}} (-1)^{2J+L+L'} \begin{Bmatrix} I & L & J \\ K & J & L' \end{Bmatrix} \sum_M (-1)^{J+M} \sum_{Q, M'} \langle K \ Q \ J \ M' | J \ M \rangle
\end{aligned}$$

$$\begin{aligned}
& \times \langle 0 | \tilde{T}_{-M}^{(J)} \left[ [\tilde{a}_{\pi i'_f} \otimes c_{\pi j_f}^\dagger]^{(L')} \otimes [a_{\pi i'_i}^\dagger \otimes \tilde{c}_{\pi j_i}]^{(L)} \right]_Q^{(K)} T_{M'}^{(J)\dagger} | 0 \rangle \\
& = \sum_K \sqrt{\frac{(2I+1)(2K+1)}{2J+1}} (-1)^{2J+L+L'} \left\{ \begin{array}{ccc} I & L & J \\ K & J & L' \end{array} \right\} \sum_M \sum_{Q, M'} \langle K Q J M' | J M \rangle \\
& \quad \times \langle \psi_{\text{g.s.}}; J M | \left[ [\tilde{a}_{\pi i'_f} \otimes c_{\pi j_f}^\dagger]^{(L')} \otimes [a_{\pi i'_i}^\dagger \otimes \tilde{c}_{\pi j_i}]^{(L)} \right]_Q^{(K)} | \psi_{\text{g.s.}}; J M' \rangle \\
& = \sum_K \sqrt{(2I+1)(2K+1)} (-1)^{2J+L+L'+K} \left\{ \begin{array}{ccc} I & L & J \\ K & J & L' \end{array} \right\} \\
& \quad \times \langle \psi_{\text{g.s.}}; J || \left[ [\tilde{a}_{\pi i'_f} \otimes c_{\pi j_f}^\dagger]^{(L')} \otimes [a_{\pi i'_i}^\dagger \otimes \tilde{c}_{\pi j_i}]^{(L)} \right]^{(K)} || \psi_{\text{g.s.}}; J \rangle \\
& = \sum_K \sqrt{(2I+1)(2K+1)} (-1)^{2J+L+L'+K} \left\{ \begin{array}{ccc} I & L & J \\ K & J & L' \end{array} \right\} \\
& \quad \times (-1) \sum_{L'' L'''} \sqrt{(2L+1)(2L'+1)(2L''+1)(2L''' + 1)} \left\{ \begin{array}{ccc} i'_f & j_f & L' \\ i'_i & j_i & L \\ L''' & L'' & K \end{array} \right\} \\
& \quad \times \langle \psi_{\text{g.s.}}; J || \left[ [\tilde{a}_{\pi i'_f} \otimes a_{\pi i'_i}^\dagger]^{(L''')} \otimes [c_{\pi j_f}^\dagger \otimes \tilde{c}_{\pi j_i}]^{(L'')} \right]^{(K)} || \psi_{\text{g.s.}}; J \rangle \\
& = \sum_K \sqrt{(2I+1)(2K+1)} (-1)^{2J+L+L'+K} \left\{ \begin{array}{ccc} I & L & J \\ K & J & L' \end{array} \right\} \\
& \quad \times (-1) \sqrt{(2L+1)(2L'+1)(2K+1)} \left\{ \begin{array}{ccc} i'_f & j_f & L' \\ i'_i & j_i & L \\ 0 & K & K \end{array} \right\} \\
& \quad \times \delta_{i'_f, i'_i} \sqrt{2i'_i + 1} \langle \psi_{\text{g.s.}}; J || [c_{\pi j_f}^\dagger \otimes \tilde{c}_{\pi j_i}]^{(K)} || \psi_{\text{g.s.}}; J \rangle \\
& = \delta_{i'_f, i'_i} \sum_K \sqrt{(2L+1)(2L'+1)(2I+1)(2K+1)} (-1)^{1+2J+i'_i+j_i+L} \\
& \quad \times \left\{ \begin{array}{ccc} I & L & J \\ K & J & L' \end{array} \right\} \left\{ \begin{array}{ccc} j_f & L' & i'_i \\ L & j_i & K \end{array} \right\} \langle \psi_{\text{g.s.}}; J || [c_{\pi j_f}^\dagger \otimes \tilde{c}_{\pi j_i}]^{(K)} || \psi_{\text{g.s.}}; J \rangle. \tag{C.4.9}
\end{aligned}$$

Thus, we have

$$\begin{aligned}
& \langle \psi_{i'_f j_f L'}^{(\text{ph})} | I' M' | \psi_{i'_i j_i L}^{(\text{ph})} | I M \rangle \\
& = \delta_{I', I} \delta_{M', M} \delta_{i'_f, i'_i} \sum_K \sqrt{(2L+1)(2L'+1)(2K+1)} (-1)^{1+3J+i'_i+j_i+L+L'-I} \\
& \quad \times \left\{ \begin{array}{ccc} I & L & J \\ K & J & L' \end{array} \right\} \left\{ \begin{array}{ccc} j_f & L' & i'_i \\ L & j_i & K \end{array} \right\} \langle \psi_{\text{g.s.}}; J || [c_{\pi j_f}^\dagger \otimes \tilde{c}_{\pi j_i}]^{(K)} || \psi_{\text{g.s.}}; J \rangle. \tag{C.4.10}
\end{aligned}$$

The spin of the one-particle-hole state is indicated with  $I$ , where  $I = J + L, J + L - 1, \dots, |J - L|$  can be realized. However, since the *PT*-odd scalar interactions are assumed, only one-particle-hole states with  $I = J$  and the same magnetic quantum number as the ground state can contribute to

the Schiff moment. The overlaps of one-particle-hole states are finally given as

$$\begin{aligned} & \langle \psi_{i'_f j_f, L'}^{(\text{ph})}; JM | \psi_{i'_i j_i, L}^{(\text{ph})}; JM \rangle \\ &= \delta_{i'_f, i'_i} \sum_K \sqrt{(2L+1)(2L'+1)(2K+1)} (-1)^{1+2J+i'_i+j_i+L+L'} \\ & \quad \times \left\{ \begin{matrix} J & L & J \\ K & J & L' \end{matrix} \right\} \left\{ \begin{matrix} j_f & L' & i'_i \\ L & j_i & K \end{matrix} \right\} \langle \psi_{\text{g.s.}; J} \| [c_{\pi j_f}^\dagger \otimes \tilde{c}_{\pi j_i}]^{(K)} \| \psi_{\text{g.s.}; J} \rangle, \end{aligned} \quad (\text{C.4.11})$$

and the norms used to normalize the one-particle-hole states are given as

$$\begin{aligned} & \langle \psi_{p'h, L}^{(\text{ph})}; JM | \psi_{p'h, L}^{(\text{ph})}; JM \rangle \\ &= (-1)^{1+2J+p'+h} (2L+1) \sum_K \sqrt{(2K+1)} \\ & \quad \times \left\{ \begin{matrix} J & L & J \\ K & J & L \end{matrix} \right\} \left\{ \begin{matrix} h & L & p' \\ L & h & K \end{matrix} \right\} \langle \psi_{\text{g.s.}; J} \| [c_{\pi h}^\dagger \otimes \tilde{c}_{\pi h}]^{(K)} \| \psi_{\text{g.s.}; J} \rangle. \end{aligned} \quad (\text{C.4.12})$$

#### C.4.2 $PT$ -odd interactions

Since the matrix elements of  $PT$ -odd interactions can be taken as real, we have

$$\begin{aligned} & \langle \psi_{p'h, L}^{(\text{ph})}; JM | \hat{V}_{\tau_1 \tau_2}^{(PT1)} | \psi_{\text{g.s.}; JM} \rangle = \langle \psi_{\text{g.s.}; JM | \hat{V}_{\tau_1 \tau_2}^{(PT1)\dagger} | \psi_{p'h, L}^{(\text{ph})}; JM \rangle \\ &= \sum_K \sum_{ijk'l} \tilde{v}_{ijk'l}^{(K)} \langle \psi_{\text{g.s.}; JM | \left[ [c_{\tau_1 i}^\dagger \otimes c_{\tau_2 j}^\dagger]^{(K)} \otimes [\tilde{a}_{\tau_1 k'} \otimes \tilde{c}_{\tau_2 l}]^{(K)} \right]_0^{(0)} | \psi_{p'h, L}^{(\text{ph})}; JM \rangle \\ &= \sum_K \sum_{ijk'l} \tilde{v}_{ijk'l}^{(K)} \langle \psi_{\text{g.s.}; JM | \\ & \quad \times \left[ [c_{\tau_1 i}^\dagger \otimes c_{\tau_2 j}^\dagger]^{(K)} \otimes [\tilde{a}_{\tau_1 k'} \otimes \tilde{c}_{\tau_2 l}]^{(K)} \right]_0^{(0)} \left[ [a_{\pi p'}^\dagger \otimes \tilde{c}_{\pi h}]^{(L)} \otimes |\psi_{\text{g.s.}; J} \rangle \right]_M^{(J)} \\ &= \sum_K \sum_{ijk'l} \tilde{v}_{ijk'l}^{(K)} \langle \psi_{\text{g.s.}; JM | \\ & \quad \times \left[ \left[ [c_{\tau_1 i}^\dagger \otimes c_{\tau_2 j}^\dagger]^{(K)} \otimes [\tilde{a}_{\tau_1 k'} \otimes \tilde{c}_{\tau_2 l}]^{(K)} \right]_0^{(0)} \otimes \left[ [a_{\pi p'}^\dagger \otimes \tilde{c}_{\pi h}]^{(L)} \otimes |\psi_{\text{g.s.}; J} \rangle \right]_M^{(J)} \right]_M^{(J)} \\ &= \sum_K \sum_{ijk'l} \tilde{v}_{ijk'l}^{(K)} \langle \psi_{\text{g.s.}; JM | \times (2J+1) \sqrt{2L+1} \left\{ \begin{matrix} 0 & 0 & 0 \\ L & J & J \\ L & J & J \end{matrix} \right\} \\ & \quad \times \left[ \left[ [c_{\tau_1 i}^\dagger \otimes c_{\tau_2 j}^\dagger]^{(K)} \otimes [\tilde{a}_{\tau_1 k'} \otimes \tilde{c}_{\tau_2 l}]^{(K)} \right]_0^{(0)} \otimes \left[ [a_{\pi p'}^\dagger \otimes \tilde{c}_{\pi h}]^{(L)} \right]^{(L)} \otimes |\psi_{\text{g.s.}; J} \rangle \right]_M^{(J)} \\ &= \sum_K \sum_{ijk'l} \tilde{v}_{ijk'l}^{(K)} \langle \psi_{\text{g.s.}; JM | \times \sum_{K'} \sqrt{(2K+1)(2L+1)(2K'+1)} \left\{ \begin{matrix} K & K & 0 \\ 0 & L & L \\ K & K' & L \end{matrix} \right\} \\ & \quad \times \left[ \left[ [c_{\tau_1 i}^\dagger \otimes c_{\tau_2 j}^\dagger]^{(K)} \otimes [\tilde{a}_{\tau_1 k'} \otimes \tilde{c}_{\tau_2 l}]^{(K)} \otimes [a_{\pi p'}^\dagger \otimes \tilde{c}_{\pi h}]^{(L)} \right]^{(K')} \right]^{(L)} \otimes |\psi_{\text{g.s.}; J} \rangle \right]_M^{(J)} \end{aligned}$$

$$\begin{aligned}
&= \sum_K \sum_{ijk'l} \tilde{v}_{ijk'l}^{(K)} \langle \psi_{\text{g.s.}}; JM | \times \sum_{K'} \sqrt{\frac{2K'+1}{(2K+1)(2L+1)}} (-1)^{K+L+K'} \\
&\quad \times \sqrt{(2K+1)(2L+1)(2K'+1)} \begin{Bmatrix} k' & l & K \\ p' & h & L \\ 0 & K' & K' \end{Bmatrix} \\
&\quad \times (-1) \left[ \left[ [c_{\tau_1 i}^\dagger \otimes c_{\tau_2 j}^\dagger]^{(K)} \otimes [\tilde{a}_{\tau_1 k'} \otimes a_{\tau p'}^\dagger]^{(0)} \otimes [\tilde{c}_{\tau_2 l} \otimes \tilde{c}_{\pi h}]^{(K')} \right]^{(K')} \right]^{(L)} \otimes |\psi_{\text{g.s.}}; J \rangle \Big]_M^{(J)} \\
&= \sum_K \sum_{ijk'l} \tilde{v}_{ijk'l}^{(K)} \langle \psi_{\text{g.s.}}; JM | \times \sum_{K'} \sqrt{\frac{2K'+1}{(2K+1)(2L+1)}} (-1)^{K+L+K'} \\
&\quad \times (-1)^{k'+h+K+K'} \sqrt{\frac{(2K+1)(2L+1)}{2k'+1}} \begin{Bmatrix} l & K & k' \\ L & h & K' \end{Bmatrix} \\
&\quad \times (-1) \delta_{\tau_1 \pi} \delta_{k' p'} \sqrt{2p'+1} \left[ \left[ [c_{\pi i}^\dagger \otimes c_{\tau_2 j}^\dagger]^{(K)} \otimes [\tilde{c}_{\tau_2 l} \otimes \tilde{c}_{\pi h}]^{(K')} \right]^{(L)} \otimes |\psi_{\text{g.s.}}; J \rangle \right]_M^{(J)} \\
&= \delta_{\tau_1 \pi} \sum_K \sum_{ijl} \tilde{v}_{ijp'l}^{(K)} \langle \psi_{\text{g.s.}}; JM | \times \sum_{K'} \sqrt{2K'+1} (-1)^{p'+h+L+1} \begin{Bmatrix} l & K & p' \\ L & h & K' \end{Bmatrix} \\
&\quad \times \left[ \left[ [c_{\pi i}^\dagger \otimes c_{\tau_2 j}^\dagger]^{(K)} \otimes [\tilde{c}_{\tau_2 l} \otimes \tilde{c}_{\pi h}]^{(K')} \right]^{(L)} \otimes |\psi_{\text{g.s.}}; J \rangle \right]_M^{(J)} \\
&= \delta_{\tau_1 \pi} \sum_K \sum_{ijl} \tilde{v}_{ijp'l}^{(K)} \langle \psi_{\text{g.s.}}; JM | \times \sum_{K'} \sqrt{2K'+1} (-1)^{p'+h+L+1} \begin{Bmatrix} l & K & p' \\ L & h & K' \end{Bmatrix} \\
&\quad \times \sum_{M_L M_J} \langle L M_L J M_J | J M \rangle \left[ [c_{\pi i}^\dagger \otimes c_{\tau_2 j}^\dagger]^{(K)} \otimes [\tilde{c}_{\tau_2 l} \otimes \tilde{c}_{\pi h}]^{(K')} \right]_{M_L}^{(L)} |\psi_{\text{g.s.}}; J M_J \rangle \\
&= \delta_{\tau_1 \pi} \sum_K \sum_{ijl} \tilde{v}_{ijp'l}^{(K)} \times \sum_{K'} \sqrt{2K'+1} (-1)^{p'+h+L+1} \begin{Bmatrix} l & K & p' \\ L & h & K' \end{Bmatrix} \\
&\quad \times \sum_{M_L M_J} \langle L M_L J M_J | J M \rangle \times (-1)^L \frac{\langle L M_L J M_J | J M \rangle}{\sqrt{2J+1}} \\
&\quad \times \langle \psi_{\text{g.s.}}; J \| \left[ [c_{\pi i}^\dagger \otimes c_{\tau_2 j}^\dagger]^{(K)} \otimes [\tilde{c}_{\tau_2 l} \otimes \tilde{c}_{\pi h}]^{(K')} \right]^{(L)} \| \psi_{\text{g.s.}}; J \rangle \\
&= \delta_{\tau_1 \pi} \sum_K \sum_{ijl} \tilde{v}_{ijp'l}^{(K)} \times \sum_{K'} \sqrt{\frac{2K'+1}{2J+1}} (-1)^{p'+h+1} \begin{Bmatrix} l & K & p' \\ L & h & K' \end{Bmatrix} \\
&\quad \times \langle \psi_{\text{g.s.}}; J \| \left[ [c_{\pi i}^\dagger \otimes c_{\tau_2 j}^\dagger]^{(K)} \otimes [\tilde{c}_{\tau_2 l} \otimes \tilde{c}_{\pi h}]^{(K')} \right]^{(L)} \| \psi_{\text{g.s.}}; J \rangle \\
&= \delta_{\tau_1 \pi} \sum_K \sum_{ijl} \tilde{v}_{jilp'}^{(K)} \times \sum_{K'} \sqrt{\frac{2K'+1}{2J+1}} (-1)^{l+h+K+1} \begin{Bmatrix} l & K & p' \\ L & h & K' \end{Bmatrix} \\
&\quad \times \langle \psi_{\text{g.s.}}; J \| \left[ [c_{\tau_2 j}^\dagger \otimes c_{\pi i}^\dagger]^{(K)} \otimes [\tilde{c}_{\tau_2 l} \otimes \tilde{c}_{\pi h}]^{(K')} \right]^{(L)} \| \psi_{\text{g.s.}}; J \rangle. \tag{C.4.13}
\end{aligned}$$

The expression for between two protons is given by taking  $\tau_2 = \pi$  in the general form as

$$\begin{aligned}
& \langle \psi_{p'h,L}^{(\text{ph})}; JM | \hat{V}_{\pi\pi}^{(PT1)} | \psi_{\text{g.s.}}; JM \rangle \\
&= \sum_K \sum_{ijl} \tilde{v}_{jilp'}^{(K)} \times \sum_{K'} \sqrt{\frac{2K'+1}{2J+1}} (-1)^{l+h+K+1} \left\{ \begin{array}{ccc} l & K & p' \\ L & h & K' \end{array} \right\} \\
& \quad \times \langle \psi_{\text{g.s.}}; J \| \left[ \left[ c_{\pi j}^\dagger \otimes c_{\pi i}^\dagger \right]^{(K)} \otimes \left[ \tilde{c}_{\pi l} \otimes \tilde{c}_{\pi h} \right]^{(K')} \right]^{(L)} \| \psi_{\text{g.s.}}; J \rangle,
\end{aligned} \tag{C.4.14}$$

and that for between neutron and proton is given as

$$\begin{aligned}
& \langle \psi_{p'h,L}^{(\text{ph})}; JM | \hat{V}_{\pi\pi}^{(PT1)} | \psi_{\text{g.s.}}; JM \rangle \\
&= \sum_K \sum_{ijl} \tilde{v}_{jilp'}^{(K)} \times \sum_{K'} \sqrt{\frac{2K'+1}{2J+1}} (-1)^{l+h+K+1} \left\{ \begin{array}{ccc} l & K & p' \\ L & h & K' \end{array} \right\} \\
& \quad \times \langle \psi_{\text{g.s.}}; J \| \left[ \left[ c_{\nu j}^\dagger \otimes c_{\pi i}^\dagger \right]^{(K)} \otimes \left[ \tilde{c}_{\nu l} \otimes \tilde{c}_{\pi h} \right]^{(K')} \right]^{(L)} \| \psi_{\text{g.s.}}; J \rangle \\
&= \sum_K \sum_{ijl} \tilde{v}_{jilp'}^{(K)} \times \sum_{K'} \sqrt{\frac{2K'+1}{2J+1}} (-1)^{l+h+K+1} \left\{ \begin{array}{ccc} l & K & p' \\ L & h & K' \end{array} \right\} \\
& \quad \times \sum_{NP} \sqrt{(2K+1)(2K'+1)(2N+1)(2P+1)} \left\{ \begin{array}{ccc} j & i & K \\ l & h & K' \\ N & P & L \end{array} \right\} \\
& \quad \times \langle \psi_{\text{g.s.}}; J \| \left[ \left[ c_{\nu j}^\dagger \otimes \tilde{c}_{\nu l} \right]^{(N)} \otimes \left[ c_{\pi i}^\dagger \otimes \tilde{c}_{\pi h} \right]^{(P)} \right]^{(L)} \| \psi_{\text{g.s.}}; J \rangle \\
&= \sum_K \sum_{ijl} \tilde{v}_{jilp'}^{(K)} (-1)^{l+h+K+1} \sum_{K'} (2K'+1) \left\{ \begin{array}{ccc} l & K & p' \\ L & h & K' \end{array} \right\} \\
& \quad \times \sum_{NP} \sqrt{\frac{(2K+1)(2N+1)(2P+1)}{2J+1}} \left\{ \begin{array}{ccc} j & i & K \\ l & h & K' \\ N & P & L \end{array} \right\} \\
& \quad \times (2J+1) \sqrt{2L+1} \left\{ \begin{array}{ccc} J'_\nu & J_\nu & N \\ J'_\pi & J_\pi & P \\ J & J & L \end{array} \right\} \sum_{n_i n_f m} \alpha_{n_f}^{(\text{g.s.})*} \alpha_{n_i}^{(\text{g.s.})} \\
& \quad \times \langle \psi_{n_f}^{(\nu)}; J'_\nu \pi'_\nu \| \left[ c_{\nu j}^\dagger \otimes \tilde{c}_{\nu l} \right]^{(N)} \| \psi_m^{(\nu)}; J_\nu \pi_\nu \rangle \langle \psi_m^{(\pi)}; J'_\pi \pi'_\pi \| \left[ c_{\pi i}^\dagger \otimes \tilde{c}_{\pi h} \right]^{(P)} \| \psi_{n_i}^{(\pi)}; J_\pi \pi_\pi \rangle.
\end{aligned} \tag{C.4.15}$$

### C.4.3 Schiff moment

It is assumed that the  $PT$ -odd interaction is scalar, so that we should take into account the one-particle-hole states with spin  $J$  and the third component  $M$ .

$$\langle \psi_{\text{g.s.}}; JM | S_0^{(1)} | \psi_{p'h,L}^{(\text{ph})}; JM \rangle$$

$$\begin{aligned}
&= \langle \psi_{\text{g.s.}}; JM | \sum_{ij'} s_{ij'} [c_{\pi i}^\dagger \otimes \tilde{a}_{\pi j'}]_0^{(1)} \left[ [a_{\pi p'}^\dagger \otimes \tilde{c}_{\pi h}]^{(L)} \otimes |\psi_{\text{g.s.}}; J \rangle \right]_M^{(J)} \\
&= \langle \psi_{\text{g.s.}}; JM | \sum_{ij'} s_{ij'} \sum_{J'M'} \langle 10 JM | J' M' \rangle \left[ [c_{\pi i}^\dagger \otimes \tilde{a}_{\pi j'}]^{(1)} \otimes [a_{\pi p'}^\dagger \otimes \tilde{c}_{\pi h}]^{(L)} \otimes |\psi_{\text{g.s.}}; J \rangle \right]_{M'}^{(J)} \\
&= \langle \psi_{\text{g.s.}}; JM | \sum_{ij'} s_{ij'} \sum_{J'M'} \langle 10 JM | J' M' \rangle \sum_K \sqrt{3(2K+1)}(2J+1) \begin{Bmatrix} 1 & 0 & 1 \\ L & J & J \\ K & J & J' \end{Bmatrix} \\
&\quad \times \left[ [c_{\pi i}^\dagger \otimes \tilde{a}_{\pi j'}]^{(1)} \otimes [a_{\pi p'}^\dagger \otimes \tilde{c}_{\pi h}]^{(L)} \right]^{(K)} \otimes |\psi_{\text{g.s.}}; J \rangle \Big]_{M'}^{(J')} \\
&= \sum_{ij'} s_{ij'} \sum_{J'M'} \langle 10 JM | J' M' \rangle \sum_K \sqrt{3(2K+1)}(2J+1) \times \frac{(-1)^{1+2J+L}}{\sqrt{3(2J+1)}} \begin{Bmatrix} J & L & J \\ K & J & 1 \end{Bmatrix} \\
&\quad \times \delta_{J'J} \delta_{M'M} \frac{(-1)^K}{\sqrt{2J+1}} \langle \psi_{\text{g.s.}}; J | \left[ [c_{\pi i}^\dagger \otimes \tilde{a}_{\pi j'}]^{(1)} \otimes [a_{\pi p'}^\dagger \otimes \tilde{c}_{\pi h}]^{(L)} \right]^{(K)} \| \psi_{\text{g.s.}}; J \rangle \\
&= \sum_{ij'} s_{ij'} \langle 10 JM | JM \rangle \sum_K (-1)^{1+2J+L+K} \sqrt{2K+1} \begin{Bmatrix} J & L & J \\ K & J & 1 \end{Bmatrix} \\
&\quad \times \langle \psi_{\text{g.s.}}; J | \left[ [c_{\pi i}^\dagger \otimes \tilde{a}_{\pi j'}]^{(1)} \otimes [a_{\pi p'}^\dagger \otimes \tilde{c}_{\pi h}]^{(L)} \right]^{(K)} \| \psi_{\text{g.s.}}; J \rangle \\
&= \sum_{ij'} s_{ij'} \langle 10 JM | JM \rangle \sum_K (-1)^{1+2J+L+K} \sqrt{2K+1} \begin{Bmatrix} J & L & J \\ K & J & 1 \end{Bmatrix} \\
&\quad \times (-1)^{i+j'} \langle \psi_{\text{g.s.}}; J | \left[ [\tilde{a}_{\pi j'} \otimes c_{\pi i}^\dagger]^{(1)} \otimes [a_{\pi p'}^\dagger \otimes \tilde{c}_{\pi h}]^{(L)} \right]^{(K)} \| \psi_{\text{g.s.}}; J \rangle \\
&= \sum_{ij'} s_{ij'} \langle 10 JM | JM \rangle \sum_K (-1)^{1+2J+L+K+i+j'} \sqrt{2K+1} \begin{Bmatrix} J & L & J \\ K & J & 1 \end{Bmatrix} \\
&\quad \times (-1) \sqrt{3(2L+1)(2K+1)} \begin{Bmatrix} j' & i & 1 \\ p' & h & L \\ 0 & K & K \end{Bmatrix} \\
&\quad \times \langle \psi_{\text{g.s.}}; J | \left[ [\tilde{a}_{\pi j'} \otimes a_{\pi p'}^\dagger]^{(0)} \otimes [c_{\pi i}^\dagger \otimes \tilde{c}_{\pi h}]^{(K)} \right]^{(K)} \| \psi_{\text{g.s.}}; J \rangle \\
&= \sum_{ij'} s_{ij'} \langle 10 JM | JM \rangle \sum_K (-1)^{2J+L+K+i+j'} \sqrt{3(2L+1)}(2K+1) \begin{Bmatrix} J & L & J \\ K & J & 1 \end{Bmatrix} \\
&\quad \times \frac{(-1)^{1+h+j'+K}}{\sqrt{(2j'+1)(2K+1)}} \begin{Bmatrix} i & 1 & j' \\ L & h & K \end{Bmatrix} \\
&\quad \times \delta_{j',p'} \sqrt{2p'+1} \langle \psi_{\text{g.s.}}; J | [c_{\pi i}^\dagger \otimes \tilde{c}_{\pi h}]^{(K)} \| \psi_{\text{g.s.}}; J \rangle \\
&= \sum_i s_{ip'} \langle 10 JM | JM \rangle \sum_K (-1)^{2J+L+i+h} \sqrt{3(2L+1)}(2K+1) \\
&\quad \times \begin{Bmatrix} J & L & J \\ K & J & 1 \end{Bmatrix} \begin{Bmatrix} i & 1 & p' \\ L & h & K \end{Bmatrix} \langle \psi_{\text{g.s.}}; J | [c_{\pi i}^\dagger \otimes \tilde{c}_{\pi h}]^{(K)} \| \psi_{\text{g.s.}}; J \rangle. \tag{C.4.16}
\end{aligned}$$

## C.5 Core excitations

### C.5.1 One-particle-one-hole excited states

In the nuclear shell model, it is assumed that all the single-proton levels below the magic number 50 are fully occupied for  $^{129}\text{Xe}$  and  $^{199}\text{Hg}$  and then those protons compose an inert core. In this section, we consider the one-particle-one-hole excitations from the core to the valence space. The excited configurations are given as

$$\begin{aligned}
|\psi_{ij',L}^{(\text{ph})}; IM\rangle &= - \left[ [c_{\pi i}^\dagger \otimes d_{\pi j'}^\dagger]^{(L)} \otimes |\psi_{\text{g.s.}; J}\rangle \right]_M^{(I)} \\
&= - \left[ [c_{\pi i}^\dagger \otimes d_{\pi j'}^\dagger]^{(L)} \otimes T^{(J)\dagger} \right]_M^{(I)} |0\rangle \\
&= - \sum_{M_L M_J} \langle L M_L J M_J | I M \rangle [c_{\pi i}^\dagger \otimes d_{\pi j'}^\dagger]_{M_L}^{(L)} T_{M_J}^{(J)\dagger} |0\rangle.
\end{aligned} \tag{C.5.1}$$

Here, the proton annihilation operator in the core region is transformed to the proton-hole creation operator as

$$\tilde{c}_{\pi j m} \rightarrow -d_{\pi j m}^\dagger, \quad c_{\pi j m}^\dagger \rightarrow \tilde{d}_{\pi j m}. \tag{C.5.2}$$

The proton creation and annihilation operators in the core region follow that

$$\{c_{\pi i m}, d_{\pi j' m'}^\dagger\} = \{c_{\pi i m}^\dagger, d_{\pi j' m'}\} = 0. \tag{C.5.3}$$

The Hermite conjugate of the one-particle-hole operator is then given as

$$\begin{aligned}
\left( [c_{\pi i}^\dagger \otimes d_{\pi j'}^\dagger]_{M_L}^{(L)} \right)^\dagger &= \left( \sum_{mm'} \langle i m j' m' | L M_L \rangle c_{\pi i m}^\dagger d_{\pi j' m'}^\dagger \right)^\dagger \\
&= \sum_{mm'} \langle i m j' m' | L M_L \rangle (-1)^{j'+m'} (-1)^{i+m} \tilde{d}_{\pi j' -m'} \tilde{c}_{\pi i -m} \\
&= (-1)^{i+j'+M_L+1} \sum_{mm'} \langle i m j' m' | L M_L \rangle \tilde{c}_{\pi i -m} \tilde{d}_{\pi j' -m'} \\
&= (-1)^{L+M_L+1} [\tilde{c}_{\pi i'} \otimes \tilde{d}_{\pi j'}]_{-M_L}^{(L)}.
\end{aligned} \tag{C.5.4}$$

The conjugates of one-particle-hole excited states are given as

$$\begin{aligned}
\langle \psi_{ij',L}^{(\text{ph})}; IM | &= \langle 0 | \sum_{M_L M_J} \langle L M_L J M_J | I M \rangle (-1)^{J+M_J} \tilde{T}_{-M_J}^{(J)} \times (-1)^{L+M_L+1} [\tilde{c}_{\pi i} \otimes \tilde{d}_{\pi j'}]_{-M_L}^{(L)} \\
&= (-1)^{J+L+M+1} \langle 0 | \left[ \tilde{T}^{(J)} \otimes [\tilde{c}_{\pi i} \otimes \tilde{d}_{\pi j'}]^{(L)} \right]_{-M}^{(I)},
\end{aligned} \tag{C.5.5}$$

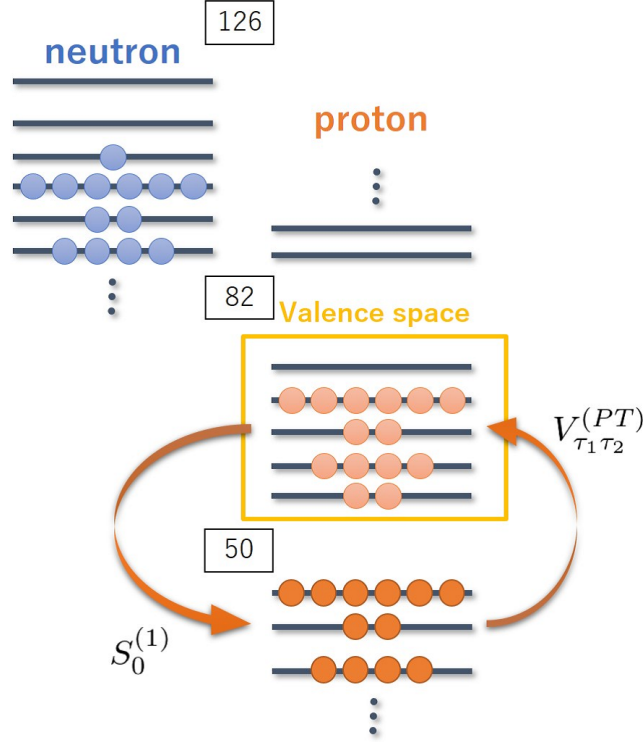


Figure C.2: The contributions of the excitations from the inert core to the valence space are called core excitations.

and the overlaps are then given as

$$\begin{aligned}
& \langle \psi_{i_f j'_f, L'}^{(\text{ph})}; I' M' | \psi_{i_i j'_i, L}^{(\text{ph})}; I M \rangle \\
&= \delta_{I', I} \delta_{M', M} (-1)^{J+L'+M+1} \langle 0 | \left[ \tilde{T}^{(J)} \otimes [\tilde{c}_{\pi i_f} \otimes \tilde{d}_{\pi j'_f}]^{(L')} \right]_{-M}^{(I)} \left[ [c_{\pi i_i}^\dagger \otimes d_{\pi j'_i}^\dagger]^{(L)} \otimes T^{(J)\dagger} \right]_M^{(I)} | 0 \rangle \\
&= \delta_{I', I} \delta_{M', M} \frac{(-1)^{J+L'-I+1}}{\sqrt{2I+1}} \\
&\quad \times \langle 0 | \left[ \left[ \tilde{T}^{(J)} \otimes [\tilde{c}_{\pi i_f} \otimes \tilde{d}_{\pi j'_f}]^{(L')} \right]^{(I)} \otimes \left[ [c_{\pi i_i}^\dagger \otimes d_{\pi j'_i}^\dagger]^{(L)} \otimes T^{(J)\dagger} \right]^{(I)} \right]_0^{(0)} | 0 \rangle. \tag{C.5.6}
\end{aligned}$$

The matrix elements can be calculated as

$$\begin{aligned}
& \langle 0 | \left[ \left[ \tilde{T}^{(J)} \otimes [\tilde{c}_{\pi i_f} \otimes \tilde{d}_{\pi j'_f}]^{(L')} \right]^{(I)} \otimes \left[ [c_{\pi i_i}^\dagger \otimes d_{\pi j'_i}^\dagger]^{(L)} \otimes T^{(J)\dagger} \right]^{(I)} \right]_0^{(0)} | 0 \rangle \\
&= \sum_K \sqrt{(2I+1)(2K+1)} (-1)^{2J+L+L'+K} \left\{ \begin{array}{ccc} I & L & J \\ K & J & L' \end{array} \right\} \\
&\quad \times \langle \psi_{\text{g.s.}; J} | \left[ [\tilde{c}_{\pi i_f} \otimes \tilde{d}_{\pi j'_f}]^{(L')} \otimes [c_{\pi i_i}^\dagger \otimes d_{\pi j'_i}^\dagger]^{(L)} \right]^{(K)} | \psi_{\text{g.s.}; J} \rangle \\
&= \sum_K \sqrt{(2I+1)(2K+1)} (-1)^{2J+L+L'+K} \left\{ \begin{array}{ccc} I & L & J \\ K & J & L' \end{array} \right\}
\end{aligned}$$

$$\begin{aligned}
& \times (-1) \sqrt{(2L+1)(2L'+1)(2K+1)} \begin{Bmatrix} i_f & j'_f & L' \\ i_i & j'_i & L \\ K & 0 & K \end{Bmatrix} \\
& \times \langle \psi_{\text{g.s.}}; J \parallel [\tilde{c}_{\pi i_f} \otimes c_{\pi i_i}^\dagger]^{(K)} \otimes [\tilde{d}_{\pi j'_f} \otimes d_{\pi j'_i}^\dagger]^{(0)} \parallel \psi_{\text{g.s.}}; J \rangle \\
& = \sum_K (2K+1) \sqrt{(2L+1)(2L'+1)(2I+1)} (-1)^{2J+L+L'+K+1} \begin{Bmatrix} I & L & J \\ K & J & L' \end{Bmatrix} \\
& \times \frac{(-1)^{i_f+j'_f+L+K}}{\sqrt{(2j'_f+1)(2K+1)}} \begin{Bmatrix} L' & i_f & j'_f \\ i_i & L & K \end{Bmatrix} \\
& \times \delta_{j'_f, j'_i} \sqrt{2j'_i+1} \langle \psi_{\text{g.s.}}; J \parallel [\tilde{c}_{\pi i_f} \otimes c_{\pi i_i}^\dagger]^{(K)} \parallel \psi_{\text{g.s.}}; J \rangle \\
& = \delta_{j'_f, j'_i} \sum_K \sqrt{(2L+1)(2L'+1)(2I+1)(2K+1)} (-1)^{1+2J+i_f+j'_f+L'} \\
& \times \begin{Bmatrix} I & L & J \\ K & J & L' \end{Bmatrix} \begin{Bmatrix} L' & i_f & j'_f \\ i_i & L & K \end{Bmatrix} \langle \psi_{\text{g.s.}}; J \parallel [\tilde{c}_{\pi i_f} \otimes c_{\pi i_i}^\dagger]^{(K)} \parallel \psi_{\text{g.s.}}; J \rangle \\
& = \delta_{j'_f, j'_i} \sum_K \sqrt{(2L+1)(2L'+1)(2I+1)(2K+1)} (-1)^{1+2J+i_f+j'_f+L'} \\
& \times \begin{Bmatrix} I & L & J \\ K & J & L' \end{Bmatrix} \begin{Bmatrix} L' & i_f & j'_f \\ i_i & L & K \end{Bmatrix} \times \delta_{i_f, i_i} \delta_{K, 0} \sqrt{(2i_i+1)(2J+1)} \\
& + \delta_{j'_f, j'_i} \sum_K \sqrt{(2L+1)(2L'+1)(2I+1)(2K+1)} (-1)^{1+2J+i_f+j'_f+L'} \\
& \times \begin{Bmatrix} I & L & J \\ K & J & L' \end{Bmatrix} \begin{Bmatrix} L' & i_f & j'_f \\ i_i & L & K \end{Bmatrix} \times (-1)^{i_i+i_f-K+1} \langle \psi_{\text{g.s.}}; J \parallel [c_{\pi i_i}^\dagger \otimes \tilde{c}_{\pi i_f}]^{(K)} \parallel \psi_{\text{g.s.}}; J \rangle \\
& = \delta_{j'_f, j'_i} \delta_{i_f, i_i} (-1)^{1+3J+I+L} \sqrt{2I+1} \\
& + \delta_{j'_f, j'_i} \sum_K \sqrt{(2L+1)(2L'+1)(2I+1)(2K+1)} (-1)^{2J+i_i+j'_f+L'+K} \\
& \times \begin{Bmatrix} I & L & J \\ K & J & L' \end{Bmatrix} \begin{Bmatrix} L' & i_f & j'_f \\ i_i & L & K \end{Bmatrix} \langle \psi_{\text{g.s.}}; J \parallel [c_{\pi i_i}^\dagger \otimes \tilde{c}_{\pi i_f}]^{(K)} \parallel \psi_{\text{g.s.}}; J \rangle, \tag{C.5.7}
\end{aligned}$$

where  $\langle \psi_{\text{g.s.}}; J \parallel 1 \parallel \psi_{\text{g.s.}}; J \rangle = \sqrt{2J+1}$  is used. Since the above calculations provides

$$\begin{aligned}
& \langle \psi_{i_f j'_f, L'; JM}^{(\text{ph})} \mid \psi_{i_i j'_i, L; JM}^{(\text{ph})} \rangle \\
& = \delta_{i_f, i_i} \delta_{j'_f, j'_i} (-1)^{L+L'} \\
& + \delta_{j'_f, j'_i} \sum_K (-1)^{2J+i_i+j'_f+K+1} \sqrt{(2L+1)(2L'+1)(2K+1)} \\
& \times \begin{Bmatrix} J & L & J \\ K & J & L' \end{Bmatrix} \begin{Bmatrix} L' & i_f & j'_f \\ i_i & L & K \end{Bmatrix} \langle \psi_{\text{g.s.}}; J \parallel [c_{\pi i_i}^\dagger \otimes \tilde{c}_{\pi i_f}]^{(K)} \parallel \psi_{\text{g.s.}}; J \rangle, \tag{C.5.8}
\end{aligned}$$

the norms are given as

$$\langle \psi_{ph', L; JM}^{(\text{ph})} \mid \psi_{ph', L; JM}^{(\text{ph})} \rangle$$

$$\begin{aligned}
&= 1 + \sum_K (-1)^{2J+p+h'+K} (2L+1) \sqrt{2K+1} \\
&\quad \times \left\{ \begin{array}{ccc} J & L & J \\ K & J & L' \end{array} \right\} \left\{ \begin{array}{ccc} L' & p & h' \\ p & L & K \end{array} \right\} \langle \psi_{\text{g.s.}}; J \| [c_{\pi p}^\dagger \otimes \tilde{c}_{\pi p}]^{(K)} \| \psi_{\text{g.s.}}; J \rangle. \tag{C.5.9}
\end{aligned}$$

### C.5.2 $PT$ -odd interactions

The matrix elements of the  $PT$ -odd interactions with the one-particle-one-hole excited states, which are contributed from the core excitations are calculated as

$$\begin{aligned}
&\langle \psi_{p'h,L}^{(\text{ph})}; JM | \hat{V}_{\tau_1 \tau_2}^{(PT2)} | \psi_{\text{g.s.}}; JM \rangle = \langle \psi_{\text{g.s.}}; JM | \hat{V}_{\tau_1 \tau_2}^{(PT2)\dagger} | \psi_{p'h,L}^{(\text{ph})}; JM \rangle \\
&= \sum_K \sum_{ijk'l} \tilde{v}_{ijk'l}^{(K)} \langle \psi_{\text{g.s.}}; JM | \\
&\quad \times \left[ [d_{\tau_1 k'}^\dagger \otimes c_{\tau_2 l}^\dagger]^{(K)} \otimes [\tilde{c}_{\tau_1 i} \otimes \tilde{c}_{\tau_2 j}]^{(K)} \right]_0^{(0)} \left[ [c_{\pi p'}^\dagger \otimes \tilde{d}_{\pi h}]^{(L)} \otimes |\psi_{\text{g.s.}}; J \rangle \right]_M^{(J)} \\
&= \sum_K \sum_{ijk'l} \tilde{v}_{ijk'l}^{(K)} \langle \psi_{\text{g.s.}}; JM | \\
&\quad \times \left[ \left[ [d_{\tau_1 k'}^\dagger \otimes c_{\tau_2 l}^\dagger]^{(K)} \otimes [\tilde{c}_{\tau_1 i} \otimes \tilde{c}_{\tau_2 j}]^{(K)} \right]_0^{(0)} \otimes \left[ [c_{\pi p'}^\dagger \otimes \tilde{d}_{\pi h}]^{(L)} \otimes |\psi_{\text{g.s.}}; J \rangle \right]_M^{(J)} \right]_M^{(J)} \\
&= \sum_K \sum_{ijk'l} \tilde{v}_{ijk'l}^{(K)} \langle \psi_{\text{g.s.}}; JM | \times (-1)^{k'+l-K+1} \times (-1)^{k'+j-K'+1} \\
&\quad \times \sum_{K'} (2K+1)(2K'+1) \left\{ \begin{array}{ccc} l & k' & K \\ i & j & K \\ K' & K' & 0 \end{array} \right\} \\
&\quad \times \left[ \left[ [c_{\tau_2 l}^\dagger \otimes \tilde{c}_{\tau_1 i}]^{(K')} \otimes [\tilde{c}_{\tau_2 j} \otimes d_{\tau_1 k'}^\dagger]^{(K')} \right]_0^{(0)} \otimes \left[ [c_{\pi p'}^\dagger \otimes \tilde{d}_{\pi h}]^{(L)} \otimes |\psi_{\text{g.s.}}; J \rangle \right]_M^{(J)} \right]_M^{(J)} \\
&= \sum_K \sum_{ijk'l} \tilde{v}_{ijk'l}^{(K)} \langle \psi_{\text{g.s.}}; JM | \times (-1)^{j+l-K-K'+1} \\
&\quad \times \sum_{K'} (-1)^{i+k'+K+K'} \sqrt{(2K+1)(2K'+1)} \left\{ \begin{array}{ccc} l & k' & K \\ j & i & K' \end{array} \right\} \\
&\quad \times (2J+1) \sqrt{2L+1} \left\{ \begin{array}{ccc} 0 & 0 & 0 \\ L & J & J \\ L & J & J \end{array} \right\} \\
&\quad \times \left[ \left[ [c_{\tau_2 l}^\dagger \otimes \tilde{c}_{\tau_1 i}]^{(K')} \otimes [\tilde{c}_{\tau_2 j} \otimes d_{\tau_1 k'}^\dagger]^{(K')} \right]_0^{(0)} \otimes [c_{\pi p'}^\dagger \otimes \tilde{d}_{\pi h}]^{(L)} \right]_M^{(L)} \otimes |\psi_{\text{g.s.}}; J \rangle \Big]_M^{(J)} \\
&= \sum_K \sum_{ijk'l} \tilde{v}_{ijk'l}^{(K)} \langle \psi_{\text{g.s.}}; JM | \times \sum_{K'} (-1)^{i+j+k'+l+1} \sqrt{(2K+1)(2K'+1)} \left\{ \begin{array}{ccc} l & k' & K \\ j & i & K' \end{array} \right\}
\end{aligned}$$

$$\begin{aligned}
& \times \sum_{K''} \sqrt{(2L+1)(2K'+1)(2K''+1)} \begin{Bmatrix} K' & K' & 0 \\ 0 & L & L \\ K' & K'' & L \end{Bmatrix} \\
& \times \left[ \left[ \left[ c_{\tau_2 l}^\dagger \otimes \tilde{c}_{\tau_1 i} \right]^{(K')} \otimes \left[ \left[ \tilde{c}_{\tau_2 j} \otimes d_{\tau_1 k'}^\dagger \right]^{(K')} \otimes \left[ c_{\pi p'}^\dagger \otimes \tilde{d}_{\pi h} \right]^{(L)} \right]^{(K'')} \right]^{(L)} \otimes |\psi_{\text{g.s.}; J}\rangle \right]_M^{(J)} \\
= & \sum_K \sum_{ijk'l} \tilde{v}_{ijk'l}^{(K)} \langle \psi_{\text{g.s.}; JM} | \times \sum_{K'} (-1)^{i+j+k'+l+1} \sqrt{(2K+1)(2K'+1)} \begin{Bmatrix} l & k' & K \\ j & i & K' \end{Bmatrix} \\
& \times \sum_{K''} \sqrt{(2L+1)(2K'+1)(2K''+1)} \times \frac{(-1)^{K'+K''+L}}{(2L+1)(2K'+1)} \\
& \times \begin{Bmatrix} j & k' & K' \\ p' & h & L \\ K'' & 0 & K'' \end{Bmatrix} \\
& \times (-1) \left[ \left[ \left[ c_{\tau_2 l}^\dagger \otimes \tilde{c}_{\tau_1 i} \right]^{(K')} \otimes \left[ \left[ \tilde{c}_{\tau_2 j} \otimes c_{\pi p'}^\dagger \right]^{(K'')} \otimes \left[ d_{\tau_1 k'}^\dagger \otimes \tilde{d}_{\pi h} \right]^{(0)} \right]^{(K'')} \right]^{(L)} \otimes |\psi_{\text{g.s.}; J}\rangle \right]_M^{(J)} \\
= & \sum_K \sum_{ijl} \tilde{v}_{ijhl}^{(K)} \langle \psi_{\text{g.s.}; JM} | \times \sum_{K'K''} (-1)^{i+j+h+l+K'+K''+L} \sqrt{\frac{(2K+1)(2K''+1)}{2L+1}} \begin{Bmatrix} l & h & K \\ j & i & K' \end{Bmatrix} \\
& \times \frac{(-1)^{j+h+L+K''}}{\sqrt{(2h+1)(2K''+1)}} \begin{Bmatrix} K' & j & h \\ p' & L & K'' \end{Bmatrix} \\
& \times (-1) \sqrt{2h+1} \left[ \left[ \left[ c_{\tau_2 l}^\dagger \otimes \tilde{c}_{\tau_1 i} \right]^{(K')} \otimes \left[ \tilde{c}_{\tau_2 j} \otimes c_{\pi p'}^\dagger \right]^{(K'')} \right]^{(L)} \otimes |\psi_{\text{g.s.}; J}\rangle \right]_M^{(J)} \\
= & \sum_K \sum_{ijl} \tilde{v}_{ijhl}^{(K)} \sum_{K'K''} (-1)^{i+l+K'+1} \sqrt{\frac{2K+1}{2L+1}} \begin{Bmatrix} l & h & K \\ j & i & K' \end{Bmatrix} \begin{Bmatrix} K' & j & h \\ p' & L & K'' \end{Bmatrix} \\
& \times \langle \psi_{\text{g.s.}; JM} | \left[ \left[ \left[ c_{\tau_2 l}^\dagger \otimes \tilde{c}_{\tau_1 i} \right]^{(K')} \otimes \left[ \tilde{c}_{\tau_2 j} \otimes c_{\pi p'}^\dagger \right]^{(K'')} \right]^{(L)} \otimes |\psi_{\text{g.s.}; J}\rangle \right]_M^{(J)} \\
= & \sum_K \sum_{ijl} \tilde{v}_{ijhl}^{(K)} \sum_{K'K''} (-1)^{i+l+K'+L+1} \sqrt{\frac{2K+1}{(2L+1)(2J+1)}} \begin{Bmatrix} l & h & K \\ j & i & K' \end{Bmatrix} \begin{Bmatrix} K' & j & h \\ p' & L & K'' \end{Bmatrix} \\
& \times \langle \psi_{\text{g.s.}; J} | \left[ \left[ c_{\tau_2 l}^\dagger \otimes \tilde{c}_{\tau_1 i} \right]^{(K')} \otimes \left[ \tilde{c}_{\tau_2 j} \otimes c_{\pi p'}^\dagger \right]^{(K'')} \right]^{(L)} \| \psi_{\text{g.s.}; J}\rangle \\
= & \sum_K \sum_{ijl} \tilde{v}_{ijhl}^{(K)} \sum_{K'K''} (-1)^{i+l+K'+L+1} \sqrt{\frac{2K+1}{(2L+1)(2J+1)}} \begin{Bmatrix} l & h & K \\ j & i & K' \end{Bmatrix} \begin{Bmatrix} K' & j & h \\ p' & L & K'' \end{Bmatrix} \\
& \times \delta_{\tau_2, \pi} \delta_{j, p'} \sqrt{2p'+1} \delta_{K', L} \delta_{K'', 0} \langle \psi_{\text{g.s.}; J} | \left[ c_{\tau_2 l}^\dagger \otimes \tilde{c}_{\tau_1 i} \right]^{(L)} \| \psi_{\text{g.s.}; J}\rangle \\
& + \sum_K \sum_{ijl} \tilde{v}_{ijhl}^{(K)} \sum_{K'K''} (-1)^{i+l+K'+L+1} \sqrt{\frac{2K+1}{(2L+1)(2J+1)}} \begin{Bmatrix} l & h & K \\ j & i & K' \end{Bmatrix} \begin{Bmatrix} K' & j & h \\ p' & L & K'' \end{Bmatrix} \\
& \times (-1)^{j+p'-K''+1} \langle \psi_{\text{g.s.}; J} | \left[ \left[ c_{\tau_2 l}^\dagger \otimes \tilde{c}_{\tau_1 i} \right]^{(K')} \otimes \left[ c_{\pi p'}^\dagger \otimes \tilde{c}_{\tau_2 j} \right]^{(K'')} \right]^{(L)} \| \psi_{\text{g.s.}; J}\rangle
\end{aligned}$$

$$\begin{aligned}
&= \delta_{\tau_2, \pi} \sum_K \sum_{il} \tilde{v}_{ip'hl}^{(K)} (-1)^{i+l+1} \sqrt{\frac{2K+1}{(2L+1)(2J+1)}} \left\{ \begin{matrix} l & h & K \\ p' & i & L \end{matrix} \right\} \times \frac{(-1)^{p'+h+L}}{\sqrt{(2p'+1)(2L+1)}} \\
&\quad \times \sqrt{2p'+1} \langle \psi_{\text{g.s.}}; J \| [c_{\tau_2 l}^\dagger \otimes \tilde{c}_{\tau_1 i}]^{(L)} \| \psi_{\text{g.s.}}; J \rangle \\
&+ \sum_K \sum_{ijl} \tilde{v}_{ijhl}^{(K)} \sum_{K'K''} (-1)^{i+j+l+p'+K'-K''+L} \sqrt{\frac{2K+1}{(2L+1)(2J+1)}} \\
&\quad \times \left\{ \begin{matrix} l & h & K \\ j & i & K' \end{matrix} \right\} \left\{ \begin{matrix} K' & j & h \\ p' & L & K'' \end{matrix} \right\} \\
&\quad \times \langle \psi_{\text{g.s.}}; J \| \left[ [c_{\tau_2 l}^\dagger \otimes \tilde{c}_{\tau_1 i}]^{(K')} \otimes [c_{\pi p'}^\dagger \otimes \tilde{c}_{\tau_2 j}]^{(K'')} \right]^{(L)} \| \psi_{\text{g.s.}}; J \rangle \tag{C.5.10}
\end{aligned}$$

### C.5.3 Schiff moment

The matrix elements of the Schiff moment operator with one-particle-one-hole excited states contributed from the core excitations are calculated as

$$\begin{aligned}
&\langle \psi_{\text{g.s.}}; JM | S_0^{(1)} | \psi_{ph',L}^{(\text{ph})}; JM \rangle \\
&= -\langle \psi_{\text{g.s.}}; JM | \sum_{i'j} s_{i'j} [\tilde{d}_{\pi i'} \otimes \tilde{c}_{\pi j}]_0^{(1)} [c_{\pi p}^\dagger \otimes d_{\pi h'}^\dagger]^{(L)} \otimes | \psi_{\text{g.s.}}; J \rangle_M^{(J)} \\
&= -\sum_{i'j} s_{i'j} \langle 10 JM | JM \rangle \sum_K (-1)^{1+2J+L+K} \sqrt{2K+1} \left\{ \begin{matrix} J & L & J \\ K & J & 1 \end{matrix} \right\} \\
&\quad \times \langle \psi_{\text{g.s.}}; J \| [\tilde{d}_{\pi i'} \otimes \tilde{c}_{\pi j}]^{(1)} \otimes [c_{\pi p}^\dagger \otimes d_{\pi h'}^\dagger]^{(L)} \| \psi_{\text{g.s.}}; J \rangle^{(K)} \\
&= \sum_{i'j} s_{i'j} \langle 10 JM | JM \rangle \sum_K (-1)^{2J+L+K} \sqrt{2K+1} \left\{ \begin{matrix} J & L & J \\ K & J & 1 \end{matrix} \right\} \\
&\quad \times (-1)^{i'+j} \langle \psi_{\text{g.s.}}; J \| [\tilde{c}_{\pi j} \otimes \tilde{d}_{\pi i'}]^{(1)} \otimes [c_{\pi p}^\dagger \otimes d_{\pi h'}^\dagger]^{(L)} \| \psi_{\text{g.s.}}; J \rangle^{(K)} \\
&= \sum_{i'j} s_{i'j} \langle 10 JM | JM \rangle \sum_K (-1)^{2J+L+K+i'+j} \sqrt{2K+1} \left\{ \begin{matrix} J & L & J \\ K & J & 1 \end{matrix} \right\} \\
&\quad \times (-1) \sqrt{3(2L+1)(2K+1)} \left\{ \begin{matrix} j & i' & 1 \\ p & h' & L \\ K & 0 & K \end{matrix} \right\} \\
&\quad \times \langle \psi_{\text{g.s.}}; J \| [\tilde{c}_{\pi j} \otimes c_{\pi p}^\dagger]^{(K)} \otimes [\tilde{d}_{\pi i'} \otimes d_{\pi h'}^\dagger]^{(0)} \| \psi_{\text{g.s.}}; J \rangle^{(K)} \\
&= \sum_{i'j} s_{i'j} \langle 10 JM | JM \rangle \sum_K (-1)^{2J+L+K+i'+j+1} \sqrt{3(2L+1)(2K+1)} \left\{ \begin{matrix} J & L & J \\ K & J & 1 \end{matrix} \right\} \\
&\quad \times \frac{(-1)^{i'+j+L+K}}{\sqrt{(2i'+1)(2K+1)}} \left\{ \begin{matrix} 1 & j & i' \\ p & L & K \end{matrix} \right\} \\
&\quad \times \delta_{i',h'} \sqrt{2h'+1} \langle \psi_{\text{g.s.}}; J \| [\tilde{c}_{\pi j} \otimes c_{\pi p}^\dagger]^{(K)} \| \psi_{\text{g.s.}}; J \rangle
\end{aligned}$$

$$\begin{aligned}
&= \sum_j s_{h'j} \langle 10 JM | JM \rangle \sum_K (-1)^{2J+1} \sqrt{3(2L+1)(2K+1)} \\
&\quad \times \left\{ \begin{matrix} J & L & J \\ K & J & 1 \end{matrix} \right\} \left\{ \begin{matrix} 1 & j & h' \\ p & L & K \end{matrix} \right\} \langle \psi_{\text{g.s.}}; J \| [\tilde{c}_{\pi j} \otimes c_{\pi p}^\dagger]^{(K)} \| \psi_{\text{g.s.}}; J \rangle \\
&= \sum_j s_{h'j} \langle 10 JM | JM \rangle \sum_K (-1)^{2J+1} \sqrt{3(2L+1)(2K+1)} \\
&\quad \times \left\{ \begin{matrix} J & L & J \\ K & J & 1 \end{matrix} \right\} \left\{ \begin{matrix} 1 & j & h' \\ p & L & K \end{matrix} \right\} \times \delta_{j,p} \delta_{K,0} \sqrt{(2p+1)(2J+1)} \\
&+ \sum_j s_{h'j} \langle 10 JM | JM \rangle \sum_K (-1)^{2J+1} \sqrt{3(2L+1)(2K+1)} \\
&\quad \times \left\{ \begin{matrix} J & L & J \\ K & J & 1 \end{matrix} \right\} \left\{ \begin{matrix} 1 & j & h' \\ p & L & K \end{matrix} \right\} \times (-1)^{j+p-K+1} \langle \psi_{\text{g.s.}}; J \| [c_{\pi p}^\dagger \otimes \tilde{c}_{\pi j}]^{(K)} \| \psi_{\text{g.s.}}; J \rangle \\
&= s_{h'p} \langle 10 JM | JM \rangle (-1)^{2J+1} \sqrt{3(2L+1)(2p+1)(2J+1)} \\
&\quad \times \delta_{j,p} \delta_{L,1} \frac{(-1)^{2J+1}}{\sqrt{3(2J+1)}} \frac{(-1)^{1+p+h'}}{\sqrt{(2p+1)(2L+1)}} \\
&+ \sum_j s_{h'j} \langle 10 JM | JM \rangle \sum_K (-1)^{2J+j+p-K} \sqrt{3(2L+1)(2K+1)} \\
&\quad \times \left\{ \begin{matrix} J & L & J \\ K & J & 1 \end{matrix} \right\} \left\{ \begin{matrix} 1 & j & h' \\ p & L & K \end{matrix} \right\} \langle \psi_{\text{g.s.}}; J \| [c_{\pi p}^\dagger \otimes \tilde{c}_{\pi j}]^{(K)} \| \psi_{\text{g.s.}}; J \rangle \\
&= s_{h'p} \langle 10 JM | JM \rangle (-1)^{p+h'+1} \\
&+ \sum_j s_{h'j} \langle 10 JM | JM \rangle \sum_K (-1)^{2J+j+p-K} \sqrt{3(2L+1)(2K+1)} \\
&\quad \times \left\{ \begin{matrix} J & L & J \\ K & J & 1 \end{matrix} \right\} \left\{ \begin{matrix} 1 & j & h' \\ p & L & K \end{matrix} \right\} \langle \psi_{\text{g.s.}}; J \| [c_{\pi p}^\dagger \otimes \tilde{c}_{\pi j}]^{(K)} \| \psi_{\text{g.s.}}; J \rangle. \tag{C.5.11}
\end{aligned}$$

By exchanging the subscripts of the one-body matrix elements, we have

$$\begin{aligned}
&\langle \psi_{\text{g.s.}}; JM | S_0^{(1)} | \psi_{ph',L}^{(\text{ph})}; JM \rangle \\
&= s_{ph'} \langle 10 JM | JM \rangle \\
&\quad + \sum_j s_{jh'} \langle 10 JM | JM \rangle \sum_K (-1)^{2J+p+h'-K} \sqrt{3(2L+1)(2K+1)} \\
&\quad \times \left\{ \begin{matrix} J & L & J \\ K & J & 1 \end{matrix} \right\} \left\{ \begin{matrix} 1 & j & h' \\ p & L & K \end{matrix} \right\} \langle \psi_{\text{g.s.}}; J \| [c_{\pi p}^\dagger \otimes \tilde{c}_{\pi j}]^{(K)} \| \psi_{\text{g.s.}}; J \rangle. \tag{C.5.12}
\end{aligned}$$

## C.6 Over-shell excitations

### C.6.1 One-particle-one-hole excited states

Finally, we consider the excitations from the core region to beyond the valence space. Those kinds of contributions are called over-shell excitations in this paper. The excited configurations are given

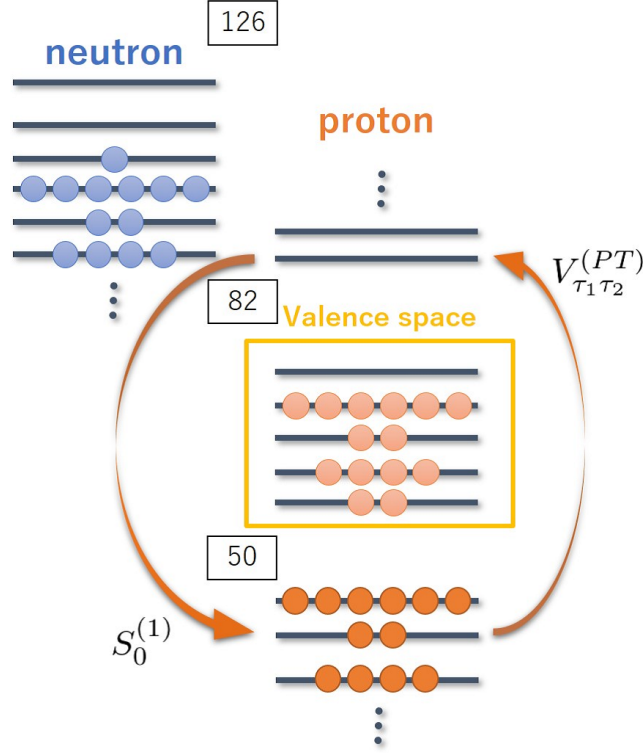


Figure C.3: The protons in the inert core can be excited beyond the valence space. Those contributions are indicated by over-shell excitations.

as

$$\begin{aligned}
 |\psi_{ij',L}^{(\text{ph})}; IM\rangle &= - \left[ [a_{\pi i}^\dagger \otimes d_{\pi j'}^\dagger]^{(L)} \otimes |\psi_{\text{g.s.}}; J\rangle \right]_M^{(I)} \\
 &= - \left[ [a_{\pi i}^\dagger \otimes d_{\pi j'}^\dagger]^{(L)} \otimes T^{(J)\dagger} \right]_M^{(I)} |0\rangle \\
 &= - \sum_{M_L M_J} \langle L M_L J M_J | I M \rangle [a_{\pi i}^\dagger \otimes d_{\pi j'}^\dagger]_{M_L}^{(L)} T_{M_J}^{(J)\dagger} |0\rangle.
 \end{aligned} \tag{C.6.1}$$

The notations of the creation and annihilation operators are the same as above subsections.

The overlaps of the one-particle-one hole excited states can be calculated as the same with the core excitations. The results are given as

$$\langle \psi_{i_f j'_f, L'}^{(\text{ph})}; JM | \psi_{i_i j'_i, L}^{(\text{ph})}; JM \rangle = \delta_{i_f, i_i} \delta_{j'_f, j'_i} (-1)^{L+L'}, \tag{C.6.2}$$

and it is found that those states are automatically normalized as

$$\langle \psi_{ph',L}^{(\text{ph})}; JM | \psi_{ph',L}^{(\text{ph})}; JM \rangle = 1. \tag{C.6.3}$$

## References

- [1] K. Yanase, E. Teruya, K. Higashiyama, and N. Yoshinaga. Shell-model study of pb, bi, po, at, rn, and fr isotopes with masses from 210 to 217. *Phys. Rev. C*, Vol. 98, p. 014308, Jul 2018.
- [2] L. Chen, P. M. Walker, H. Geissel, Yu. A. Litvinov, K. Beckert, P. Beller, F. Bosch, D. Boutin, L. Caceres, J. J. Carroll, D. M. Cullen, I. J. Cullen, B. Franzke, J. Gerl, M. Górska, G. A. Jones, A. Kishada, R. Knöbel, C. Kozhuharov, J. Kurcewicz, S. A. Litvinov, Z. Liu, S. Mandal, F. Montes, G. Münzenberg, F. Nolden, T. Ohtsubo, Z. Patyk, W. R. Plaß, Zs. Podolyák, S. Rigby, N. Saito, T. Saito, C. Scheidenberger, E. C. Simpson, M. Shindo, M. Steck, B. Sun, S. J. Williams, H. Weick, M. Winkler, H.-J. Wollersheim, and T. Yamaguchi. Direct observation of long-lived isomers in  $^{212}\text{Bi}$ . *Phys. Rev. Lett.*, Vol. 110, p. 122502, Mar 2013.
- [3] Alain Astier and Marie-Geneviève Porquet. High-spin states in the five-valence-particle nucleus  $^{213}\text{Po}$ . *Phys. Rev. C*, Vol. 83, p. 034302, Mar 2011.
- [4] G.J. Lane, K.H. Maier, A.P. Byrne, G.D. Dracoulis, R. Brodac, B. Fornal, M.P. Carpenter, R.M. Clark, M. Cromaz, R.V.F. Janssens, A.O. Macchiavelli, I. Wiedenhover, and K. Vetter. High-spin isomers and three-neutron valence configurations in  $^{211}\text{pb}$ . *Phys. Lett. B*, Vol. 606, pp. 34–42, Jan 2005.
- [5] G.J. Lane, R. Broda, B. Fornal, A.P. Byrne, G.D. Dracoulis, J. Blomqvist, R.M. Clark, M. Cromaz, M.A. Deleplanque, R.M. Diamond, P. Fallon, R.V.F. Janssens, I.Y. Lee, A.O. Macchiavelli, K.H. Maier, M. Rejmund, F.S. Stephens, C.E. Svensson, K. Vetter, D. Ward, I. Wiedenhover, and J. Wrzesinski. Structure of exotic nuclei near and above  $^{208}\text{pb}$  populated via deep-inelastic collisions. *Nucl. Phys. A*, Vol. 682, p. 71, Feb 2001.
- [6] P.A. Mello and J. Flores. Tensor forces and the energy levels of  $^{210}\text{bi}$ . *Nucl. Phys.*, Vol. 47, p. 177, 1963.
- [7] Yeong E. Kim and John O. Rasmussen. Energy levels of  $^{210}\text{bi}$  and  $^{210}\text{po}$  and the shell-model residual force. *Nucl. Phys.*, Vol. 47, p. 184, 1963.
- [8] G.H. Herling and T.T.S. Kuo. Two-particle states in  $^{210}\text{pb}$ ,  $^{210}\text{bi}$  and  $^{210}\text{po}$  with realistic forces. *Nucl. Phys. A*, Vol. 181, p. 113, 1972.
- [9] Petr Alexa, Jan Kvasil, Nguyen Viet Minh, and Raymond K. Sheline. Calculation of shell model energies for states in  $^{210}\text{bi}$ . *Phys. Rev. C*, Vol. 55, pp. 179–186, Jan 1997.
- [10] L. Coraggio, A. Covello, A. Gargano, and N. Itaco. Long standing problem of  $^{210}\text{Bi}$  and the

- realistic proton-neutron effective interaction. *Phys. Rev. C*, Vol. 76, p. 061303, Dec 2007.
- [11] L. W. Nordheim. Nuclear shell structure and beta-decay. ii. even  $a$  nuclei. *Rev. Mod. Phys.*, Vol. 23, pp. 322–327, Oct 1951.
- [12] Petr Alexa and Raymond K. Sheline. Shell model configurational trends in odd-odd nuclei beyond  $^{208}\text{Pb}$ . *Phys. Rev. C*, Vol. 56, pp. 3087–3091, Dec 1997.
- [13] Chin W. Ma and William W. True. Shell model in the lead region. *Phys. Rev. C*, Vol. 8, pp. 2313–2331, Dec 1973.
- [14] E. Teruya, N. Yoshinaga, K. Higashiyama, and A. Odahara. Shell-model calculations of nuclei around mass 130. *Phys. Rev. C*, Vol. 92, p. 034320, September 2015.
- [15] E. Teruya, K. Higashiyama, and N. Yoshinaga. Large-scale shell-model calculations of nuclei around mass 210. *Phys. Rev. C*, Vol. 93, p. 064327, Jun 2016.
- [16] Evaluated Nuclear Structure Data File (ENSDF). [www.nndc.bnl.gov/ensdf/](http://www.nndc.bnl.gov/ensdf/).
- [17] M. Shamsuzzoha Basunia. Nuclear data sheets for  $A = 210$ . *Nucl. Data Sheets*, Vol. 121, p. 561, September 2014.
- [18] Balraj Singh, Daniel Abriola, Coral Baglin, Vivian Demetriou, and Timothy Johnson. Nuclear data sheets for  $A = 211$ . *Nucl. Data Sheets*, Vol. 114, p. 661, June 2013.
- [19] E. Browne. Nuclear data sheets for  $A = 212$ . *Nucl. Data Sheets*, Vol. 104, p. 427, January 2005.
- [20] I. Hamamoto. Nuclear octupole vibrations in the isotopes of pb. *Nuclear Physics A*, Vol. 155, No. 2, pp. 362–384, 1970.
- [21] E.R. Flynn, G.J. Igo, R.A. Broglia, S. Landowne, V. Paar, and B. Nilsson. An experimental and theoretical investigation of the structure of  $^{210}\text{pb}$ . *Nucl. Phys. A*, Vol. 195, p. 97, November 1972.
- [22] M. S. Basunia. Nuclear data sheets for  $A = 213$ . *Nucl. Data Sheets*, Vol. 108, p. 633, March 2007.
- [23] A. Astier, P. Petkov, M.-G. Porquet, D. S. Delion, and P. Schuck. Novel manifestation of  $\alpha$ -clustering structures: New “ $\alpha + \text{pb } 208$ ” states in po 212 revealed by their enhanced e 1 decays. *Physical Review Letters*, Vol. 104, No. 4, p. 042701, 2010.
- [24] A. Astier, P. Petkov, M.-G. Porquet, D. S. Delion, and P. Schuck. Coexistence of  $\alpha + ^{208}\text{pb}$  cluster structures and single-particle excitations in 212 84 po 128. *The European Physical Journal A*, Vol. 46, No. 2, pp. 165–185, 2010.
- [25] Alain Astier and Marie-Geneviève Porquet. First observation of high-spin states in  $^{214}\text{Po}$ : Probing the valence space beyond  $^{208}\text{Pb}$ . *Phys. Rev. C*, Vol. 83, p. 014311, Jan 2011.
- [26] S.-C. Wu. Nuclear data sheets for  $A = 214$ . *Nucl. Data Sheets*, Vol. 110, p. 681, March 2009.
- [27] Y Suzuki and S Ohkubo. Enhanced e 1 transitions and  $\alpha + ^{208}\text{pb}$  (3-) clustering in po 212. *Physical Review C*, Vol. 82, No. 4, p. 041303, 2010.
- [28] D. S. Delion, R. J. Liotta, P. Schuck, A. Astier, and M. G. Porquet. Shell model plus cluster description of negative parity states in 212 po. *Physical Review C*, Vol. 85, No. 6, p. 064306,

- 2012.
- [29] H. W. Taylor, B. Singh, and D. A. Viggars. Mixing parameters of gamma transitions in  $^{214}\text{Po}$ . *Phys. Rev. C*, Vol. 34, pp. 2322–2325, Dec 1986.
- [30] D Kocheva, G Rainovski, J Jolie, N Pietralla, A Blazhev, R Altenkirch, S Ansari, A Astier, M Bast, M Beckers, et al. Low collectivity of the  $2\ 1+$  state of po 212. *Physical Review C*, Vol. 96, No. 4, p. 044305, 2017.
- [31] M. D. Seliverstov, T. E. Cocolios, W. Dexters, A. N. Andreyev, S. Antalic, A. E. Barzakh, B. Bastin, J. Büscher, I. G. Darby, D. V. Fedorov, V. N. Fedosseev, K. T. Flanagan, S. Franchoo, G. Huber, M. Huyse, M. Keupers, U. Köster, Yu. Kudryavtsev, B. A. Marsh, P. L. Molkanov, R. D. Page, A. M. Sjödin, I. Stefan, P. Van Duppen, M. Venhart, and S. G. Zemlyanov. Electromagnetic moments of odd- $a$   $^{193\sim 203,211}\text{Po}$  isotopes. *Phys. Rev. C*, Vol. 89, p. 034323, Mar 2014.
- [32] Balraj Singh. Nuclear data sheets for  $A = 215$ . *Nucl. Data Sheets*, Vol. 114, p. 2023, December 2013.
- [33] C. F. Liang, P. Paris, and R. K. Sheline. Shell model level structure in  $^{215}\text{At}$ . *Phys. Rev. C*, Vol. 47, pp. 1801–1803, Apr 1993.
- [34] S.-C. Wu. Nuclear data sheets for  $A = 216$ . *Nucl. Data Sheets*, Vol. 108, p. 1057, May 2007.
- [35] Y. A. Akovali. *Nucl. Data Sheets*, Vol. 100, p. 141, 2003.
- [36] N. Yoshinaga and K. Higashiyama. Systematic studies of nuclei around mass 130 in the pair-truncated shell model. *Physical Review C*, Vol. 69, No. 5, p. 054309, 2004.
- [37] Koji Higashiyama and Naotaka Yoshinaga. Pair-truncated shell-model analysis of nuclei around mass 130. *Physical Review C*, Vol. 83, No. 3, p. 034321, 2011.
- [38] Koji Higashiyama and Naotaka Yoshinaga. Pair-truncated shell-model analysis for doubly-odd nuclei around mass 130. *Physical Review C*, Vol. 88, No. 3, p. 034315, 2013.
- [39] N. Yoshinaga, K. Higashiyama, and P. H. Regan. High-spin structure of neutron-rich se, as, ge, and ga isotopes. *Physical Review C*, Vol. 78, No. 4, p. 044320, 2008.
- [40] Koji Higashiyama and Naotaka Yoshinaga. Shell model description of low-lying states in po and rn isotopes. In *EPJ Web of Conferences*, Vol. 66, p. 02050. EDP Sciences, 2014.
- [41] A. Bohr and B. R. Mottelson. *Nuclear Structure*. World Scientific Publishing Company, 1998.
- [42] P. Ring and P. Schuck. *The nuclear many-body problem*. Springer-Verlag Berlin Heidelberg, 1980.
- [43] D. Goutte, J. B. Bellicard, J. M. Cavedon, B. Frois, M. Huet, P. Leconte, Phan Xuan Ho, S. Platchkov, J. Heisenberg, J. Lichtenstadt, C. N. Papanicolas, and I. Sick. Determination of the transition charge density of the octupole vibration in pb 208. *Physical Review Letters*, Vol. 45, No. 20, p. 1618, 1980.
- [44] R. H. Spear, W. J. Vermeer, M. T. Esat, J. A. Kuehner, A. M. Baxter, and S. Hinds. An improved determination of the quadrupole moment of the first excited state of  $^{208}\text{pb}$ . *Physics Letters B*, Vol. 128, No. 1, pp. 29–32, 1983.

- [45] J. F. Ziegler and G. A. Peterson. Excitation of  $\text{pb}^{206}$ ,  $\text{pb}^{207}$ ,  $\text{pb}^{208}$ , and  $\text{bi}^{209}$  by inelastic electron scattering. *Phys. Rev.*, Vol. 165, pp. 1337–1351, Jan 1968.
- [46] D. J. Horen, R. L. Auble, J. R. Beene, F. E. Bertrand, M. L. Halbert, G. R. Satchler, M. Thoennessen, R. L. Varner, V. R. Brown, P. L. Anthony, and V. A. Madsen. Isospin character of transitions to bound states in  $^{204,206,208}\text{Pb}$  using inelastic scattering of  $^{17}\text{O}$  ions. *Phys. Rev. C*, Vol. 44, pp. 128–135, Jul 1991.
- [47] C. Ellegaard, P. D. Barnes, E. R. Flynn, and G. J. Igo. Inelastic scattering of tritons and protons from 210pb. *Nuclear Physics A*, Vol. 162, No. 1, pp. 1–11, 1971.
- [48] M. E. Debray, J. Davidson, M. Davidson, A. J. Kreiner, M. A. Cardona, D. Hojman, D. R. Napoli, S. Lenzi, G. de Angelis, D. Bazzacco, S. Lunardi, M. DePoli, C. Rossi-Alvarez, A. Gadea, N. Medina, and C. A. Ur. High-spin octupole yrast levels in  $^{216}\text{86}\text{rn}$ . *Physical Review C*, Vol. 73, No. 2, p. 024314, 2006.
- [49] Thomas Aumann, Pier F Bortignon, and Hans Emling. Multiphonon giant resonances in nuclei. *Annual Review of Nuclear and Particle Science*, Vol. 48, No. 1, pp. 351–399, 1998.
- [50] V. Yu. Ponomarev and P. von Neumann-Cosel. Fragmentation of the two-octupole phonon multiplet in  $^{208}\text{Pb}$ . *Phys. Rev. Lett.*, Vol. 82, pp. 501–504, Jan 1999.
- [51] B. Alex Brown. Double-octupole states in  $^{208}\text{pb}$ . *Phys. Rev. Lett.*, Vol. 85, pp. 5300–5303, Dec 2000.
- [52] B. D. Valnion, V. Yu. Ponomarev, Y. Eisermann, A. Gollwitzer, R. Hertenberger, A. Metz, P. Schiemenz, and G. Graw. Excitation of  $^{208}\text{Pb}$  in light ion induced reactions and the two octupole phonon multiplet. *Phys. Rev. C*, Vol. 63, p. 024318, Jan 2001.
- [53] E. Caurier, M. Rejmund, and H. Grawe. Large-scale shell model calculations for the  $n=126$  isotones  $\text{po-pu}$ . *Phys. Rev. C*, Vol. 67, p. 054310, May 2003.
- [54] A. Heusler, R. V. Jolos, and P. von Brentano. Excitation energies of particle-hole states in 208 pb and the surface delta interaction. *Physics of Atomic Nuclei*, Vol. 76, No. 7, pp. 807–827, 2013.
- [55] J. M. Yao and K. Hagino. Anharmonicity of multi-octupole-phonon excitations in  $^{208}\text{Pb}$ : Analysis with multireference covariant density functional theory and subbarrier fusion of  $^{16}\text{O} + ^{208}\text{Pb}$ . *Phys. Rev. C*, Vol. 94, p. 011303, Jul 2016.
- [56] A. Heusler, R. V. Jolos, T. Faestermann, R. Hertenberger, H.-F. Wirth, and P. von Brentano. Complete identification of states in  $^{208}\text{Pb}$  below  $E_x = 6.2$  mev. *Phys. Rev. C*, Vol. 93, p. 054321, May 2016.
- [57] E. Teruya, N. Yoshinaga, K. Higashiyama, H. Nishibata, A. Odahara, and T. Shimoda. Large-scale shell model study of the newly found isomer in  $^{136}\text{La}$ . *Phys. Rev. C*, Vol. 94, p. 014317, Jul 2016.
- [58] J. Engel, M. Bender, J. Dobaczewski, J. H. de Jesus, and P. Olbratowski. Time-reversal violating schiff moment of  $^{225}\text{Ra}$ . *Phys. Rev. C*, Vol. 68, p. 025501, Aug 2003.
- [59] O. P. Sushkov, V. V. Flambaum, and I. B. Khriplovich. Possibility of investigating p-and

- t-odd nuclear forces in atomic and molecular experiments. *Zh. Eksp. Teor. Fiz*, Vol. 87, p. 1521, 1984.
- [60] N. Auerbach, V. F. Dmitriev, V. V. Flambaum, A. Lisetskiy, R. A. Sen'kov, and V. G. Zelevinsky. Nuclear schiff moment in nuclei with soft octupole and quadrupole vibrations. *Phys. Rev. C*, Vol. 74, p. 025502, Aug 2006.
- [61] N Auerbach, VF Dmitriev, VV Flambaum, A Lisetskiy, RASen' kov, VG Zelevinsky. Is it possible to enhance the nuclear schiff moment by nuclear collective modes? *Physics of Atomic Nuclei*, Vol. 70, No. 9, pp. 1654–1660, 2007.
- [62] Nodoka Yamanaka and Emiko Hiyama. Enhancement of the  $cp$ -odd effect in the nuclear electric dipole moment of  ${}^6\text{Li}$ . *Phys. Rev. C*, Vol. 91, p. 054005, May 2015.
- [63] Nodoka Yamanaka and Emiko Hiyama. Standard model contribution to the electric dipole moment of the deuteron,  ${}^3\text{H}$ , and  ${}^3\text{He}$  nuclei. *Journal of High Energy Physics*, Vol. 2016, No. 2, p. 67, 2016.
- [64] Nodoka Yamanaka, Taiichi Yamada, Emiko Hiyama, and Yasuro Funaki. Electric dipole moment of  ${}^{13}\text{C}$ . *Phys. Rev. C*, Vol. 95, p. 065503, Jun 2017.
- [65] N. Yoshinaga, K. Higashiyama, R. Arai, and E. Teruya. Nuclear schiff moments for the lowest  $1/2^+$  states in Xe isotopes. *Phys. Rev. C*, Vol. 87, p. 044332, Apr 2013.
- [66] E. Teruya, N. Yoshinaga, K. Higashiyama, and K. Asahi. Effects of particle-hole excitations to nuclear schiff moments in Xe isotopes. *Phys. Rev. C*, Vol. 96, p. 015501, Jul 2017.
- [67] N. Yamanaka, B. K. Sahoo, N. Yoshinaga, T. Sato, K. Asahi, and B. P. Das. Probing exotic phenomena at the interface of nuclear and particle physics with the electric dipole moments of diamagnetic atoms: A unique window to hadronic and semi-leptonic  $cp$  violation. *The European Physical Journal A*, Vol. 53, No. 3, p. 54, 2017.
- [68] Naotaka Yoshinaga, Koji Higashiyama, and Ryoichi Arai. Shell model estimate of nuclear electric dipole moments. *Progress of Theoretical Physics*, Vol. 124, No. 6, pp. 1115–1123, 2010.
- [69] N. Yoshinaga, K. Higashiyama, R. Arai, and E. Teruya. Nuclear electric dipole moments for the lowest  $1/2^+$  states in Xe and Ba isotopes. *Phys. Rev. C*, Vol. 89, p. 045501, Apr 2014.
- [70] K. Yanase, N. Yoshinaga, K. Higashiyama, and N. Yamanaka. Electric dipole moment of  ${}^{199}\text{Hg}$  atom from  $p$ ,  $cp$ -odd electron-nucleon interaction. *arXiv preprint arXiv:1805.00419*, 2018.
- [71] F.G. Kondev. Nuclear data sheets for  $A = 206$ . *Nucl. Data Sheets*, Vol. 109, p. 1527, May 2008.
- [72] M. J. Martin. Nuclear data sheets for  $A = 208$ . *Nucl. Data Sheets*, Vol. 108, p. 1583, August 2007.
- [73] R. Broda, L. W. Iskra, R. V. F. Janssens, B. A. Brown, B. Fornal, J. Wrzesiński, N. Cieplicka-Oryńczak, M. P. Carpenter, C. J. Chiara, C. R. Hoffman, F. G. Kondev, G. J. Lane, T. Lauritsen, Zs. Podolyák, D. Seweryniak, W. B. Walters, and S. Zhu. Two-neutron and core-excited states in  ${}^{210}\text{Pb}$ : Tracing  $e3$  collectivity and evidence for a new  $\beta$ -decaying isomer in  ${}^{210}\text{Tl}$ . *Phys. Rev. C*, Vol. 98, p. 024324, Aug 2018.

- [74] G. D. Dracoulis, A. P. Byrne, A. E. Stuchbery, R. A. Bark, and A. R. Poletti. Valence configurations in  $^{214}\text{rn}$ . *Nuclear Physics A*, Vol. 467, No. 2, pp. 305 – 329, 1987.
- [75] S Bayer, AP Byrne, GD Dracoulis, AM Baxter, Tibor Kibedi, FG Kondev, SM Mullins, and TR McGoram. High-spin states, yrast isomers and residual interactions in the odd-odd nucleus  $^{212}\text{at}$ . *Nuclear Physics A*, Vol. 650, No. 1, pp. 3–36, 1999.
- [76] A. P. Byrne, S. Bayer, G. D. Dracoulis, and T. Kibédi. Blocking of octupole correlations deduced from the decay of a multiparticle isomer in  $^{212}\text{At}$ . *Phys. Rev. Lett.*, Vol. 80, pp. 2077–2080, Mar 1998.
- [77] AP Byrne, GJ Lane, GD Dracoulis, B Fabricius, T Kibédi, AE Stuchbery, AM Baxter, and KJ Schiffer. Octupole coupling and proton-neutron interactions in  $^{214}\text{fr}$ . *Nuclear Physics A*, Vol. 567, No. 2, pp. 445–476, 1994.
- [78] M. Piiparinen, P. Kleinheinz, S. Lunardi, M. Ogawa, G. de Angelis, F. Soramel, W. Meczynski, and J. Blomqvist. Shell model and octupole states in  $^{148}\text{gd}$  from in-beam experiments. *Zeitschrift für Physik A Atomic Nuclei*, Vol. 337, No. 4, pp. 387–406, 1990.
- [79] L. Rydström, J. Blomqvist, R. J. Liotta, and C. Pomar. Structure of proton-deficient nuclei near  $208\text{pb}$ . *Nuclear Physics A*, Vol. 512, No. 2, pp. 217–240, 1990.
- [80] E. K. Warburton and B. A. Brown. Appraisal of the kuo-herling shell-model interaction and application to  $A = 210 - 212$  nuclei. *Phys. Rev. C*, Vol. 43, pp. 602–617, Feb 1991.
- [81] B. Szpak, K. H. Maier, A. S. Smolkowska, B. Fornal, R. Broda, M. P. Carpenter, N. Cieplicka, R. V. F. Janssens, W. Królas, T. Pawlat, J. Wrzesiński, and S. Zhu. Yrast structure of the two-proton- and three-neutron-hole nucleus  $^{203}\text{Hg}$  from the decay of a  $53/2^+$  isomer. *Phys. Rev. C*, Vol. 83, p. 064315, Jun 2011.
- [82] F. I. Sharrad, A. A. Okhunov, H. Y. Abdullah, and H. A. Kassim. Shell model calculations on even nuclei near  $208\text{pb}$ . *International Journal of Physical Sciences*, Vol. 7, No. 38, pp. 5449–5454, 2012.
- [83] R. Broda, K. H. Maier, B. Fornal, J. Wrzesiński, B. Szpak, M. P. Carpenter, R. V. F. Janssens, W. Królas, T. Pawlat, and S. Zhu. High-spin states and isomers in the one-proton-hole and three-neutron-hole  $^{204}\text{tl}$  isotope. *Phys. Rev. C*, Vol. 84, p. 014330, Jul 2011.
- [84] N. Cieplicka-Orynczak, C. Michelagnoli, S. Leoni, B. Fornal, G. Benzoni, A. Blanc, S. Bottoni, F. C. L. Crespi, L. W. Iskra, M. Jentschel, et al. The low-spin structure of  $(206)\text{tl}$  studied by gamma-ray spectroscopy from thermal neutron capture reaction. *Acta Physica Polonica B*, Vol. 49, p. 561, 2018.
- [85] J. Wrzesiński, G. J. Lane, K. H. Maier, R. V. F. Janssens, G. D. Dracoulis, R. Broda, A. P. Byrne, M. P. Carpenter, R. M. Clark, M. Cromaz, B. Fornal, T. Lauritsen, A. O. Macchiavelli, M. Rejmund, B. Szpak, K. Vetter, and S. Zhu. High-spin yrast structure of  $^{204}\text{Hg}$  from the decay of a four-hole,  $22^+$  isomer. *Phys. Rev. C*, Vol. 92, p. 044327, Oct 2015.
- [86] S. J. Steer, Zs. Podolyák, S. Pietri, M. Górska, P. H. Regan, D. Rudolph, E. Werner-Malento, A. B. Garnsworthy, R. Hoischen, J. Gerl, H. J. Wollersheim, K. H. Maier, H. Grawe,

- F. Becker, P. Bednarczyk, L. Cáceres, P. Doornenbal, H. Geissel, J. Grebosz, A. Kelic, I. Kojouharov, N. Kurz, F. Montes, W. Prokopowicz, T. Saito, H. Schaffner, S. Tashenov, A. Heinz, M. Pfützner, T. Kurtukian-Nieto, G. Benzoni, A. Jungclaus, D. L. Balabanski, C. Brandau, B. A. Brown, A. M. Bruce, W. N. Catford, I. J. Cullen, Zs. Dombrádi, M. E. Estevez, W. Gelletly, G. Ilie, J. Jolie, G. A. Jones, M. Kmiecik, F. G. Kondev, R. Krücken, S. Lalkovski, Z. Liu, A. Maj, S. Myalski, S. Schwertel, T. Shizuma, P. M. Walker, and O. Wieland. Single-particle behavior at  $n = 126$ : Isomeric decays in neutron-rich  $^{204}\text{pt}$ . *Phys. Rev. C*, Vol. 78, p. 061302, Dec 2008.
- [87] V. Méot, J. Aupiais, P. Morel, G. Gosselin, F. Gobet, J. N. Scheurer, and M. Tarisien. Half-life of the first excited state of  $^{201}\text{Hg}$ . *Phys. Rev. C*, Vol. 75, p. 064306, Jun 2007.
- [88] M. Caamaño, P. M. Walker, P. H. Regan, M. Pfützner, Zs. Podolyák, J. Gerl, M. Hellström, P. Mayet, M. N. Mineva, A. Aprahamian, J. Benlliure, et al. Isomers in neutron-rich  $a \approx 190$  nuclides from 208 pb fragmentation. *The European Physical Journal A-Hadrons and Nuclei*, Vol. 23, No. 2, pp. 201–215, 2005.
- [89] S. K. Lamoreaux, J. P. Jacobs, B. R. Heckel, F. J. Raab, and N. Fortson. New constraints on time-reversal asymmetry from a search for a permanent electric dipole moment of  $^{199}\text{Hg}$ . *Phys. Rev. Lett.*, Vol. 59, pp. 2275–2278, Nov 1987.
- [90] J. P. Jacobs, W. M. Klipstein, S. K. Lamoreaux, B. R. Heckel, and E. N. Fortson. Testing time-reversal symmetry using  $^{199}\text{Hg}$ . *Phys. Rev. Lett.*, Vol. 71, pp. 3782–3785, Dec 1993.
- [91] J. P. Jacobs, W. M. Klipstein, S. K. Lamoreaux, B. R. Heckel, and E. N. Fortson. Limit on the electric-dipole moment of  $^{199}\text{Hg}$  using synchronous optical pumping. *Phys. Rev. A*, Vol. 52, pp. 3521–3540, Nov 1995.
- [92] M. V. Romalis, W. C. Griffith, J. P. Jacobs, and E. N. Fortson. New limit on the permanent electric dipole moment of  $^{199}\text{Hg}$ . *Phys. Rev. Lett.*, Vol. 86, pp. 2505–2508, Mar 2001.
- [93] W. C. Griffith, M. D. Swallows, T. H. Loftus, M. V. Romalis, B. R. Heckel, and E. N. Fortson. Improved limit on the permanent electric dipole moment of  $^{199}\text{Hg}$ . *Phys. Rev. Lett.*, Vol. 102, p. 101601, Mar 2009.
- [94] B. Graner, Y. Chen, E. G. Lindahl, and B. R. Heckel. Reduced limit on the permanent electric dipole moment of  $^{199}\text{Hg}$ . *Phys. Rev. Lett.*, Vol. 116, p. 161601, Apr 2016.
- [95] V. V. Flambaum, I. B. Khriplovich, and O. P. Sushkov. On the p- and t-nonconserving nuclear moments. *Nuclear Physics A*, Vol. 449, No. 4, pp. 750–760, 1986.
- [96] V. F. Dmitriev and R. A. Sen'kov. Schiff moment of the mercury nucleus and the proton dipole moment. *Phys. Rev. Lett.*, Vol. 91, p. 212303, Nov 2003.
- [97] V. F. Dmitriev and R. A. Sen'kov. P- and t-violating schiff moment of the mercury nucleus. *Physics of Atomic Nuclei*, Vol. 66, No. 10, pp. 1940–1945, 2003.
- [98] V. F. Dmitriev and V. V. Flambaum. Relativistic corrections to the nuclear schiff moment. *Phys. Rev. C*, Vol. 71, p. 068501, Jun 2005.
- [99] J. H. de Jesus and J. Engel. Time-reversal-violating schiff moment of  $^{199}\text{Hg}$ . *Phys. Rev. C*,

- Vol. 72, p. 045503, Oct 2005.
- [100] Shufang Ban, Jacek Dobaczewski, Jonathan Engel, and A. Shukla. Fully self-consistent calculations of nuclear schiff moments. *Phys. Rev. C*, Vol. 82, p. 015501, Jul 2010.
- [101] J. Engel and P. Vogel. Spin-dependent cross sections of weakly interacting massive particles on nuclei. *Phys. Rev. D*, Vol. 40, pp. 3132–3135, Nov 1989.
- [102] F.G. Kondev. Nuclear data sheets for  $A = 205$ . *Nucl. Data Sheets*, Vol. 101, p. 521, April 2004.
- [103] C. J. Chiara and F. G. Kondev. Nuclear data sheets for  $A = 204$ . *Nucl. Data Sheets*, Vol. 111, p. 141, January 2010.
- [104] F. G. Kondev. Nuclear data sheets for  $A = 203$ . *Nucl. Data Sheets*, Vol. 105, p. 1, June 2005.
- [105] S. Zhu and F. G. Kondev. Nuclear data sheets for  $A = 202$ . *Nuclear Data Sheets*, Vol. 109, No. 3, pp. 699–786, 2008.
- [106] N. Fotiades., R. O. Nelson, M. Devlin, and J. A. Becker. New levels and a lifetime measurement in  $^{202}\text{Tl}$ . *Phys. Rev. C*, Vol. 76, p. 014302, Jul 2007.
- [107] O. Häusser, B. Haas, and H. R. Andrews. The g-factors of excited states in  $^{205,203}\text{Tl}$  measured by transient field interaction at high recoil velocities. *Nuclear Physics A*, Vol. 314, No. 1, pp. 161–170, 1979.
- [108] M. Y. Chen, S. C. Cheng, W. Y. Lee, A. M. Rushton, and C. S. Wu. Resonance processes and nuclear excitation in muonic  $^{205}\text{Tl}$ . *Nuclear Physics A*, Vol. 181, No. 1, pp. 25–32, 1972.
- [109] F. G. Kondev. Nuclear data sheets for  $A = 201$ . *Nuclear Data Sheets*, Vol. 108, No. 2, pp. 365–454, 2007.
- [110] S. J. Steer, Zs. Podolyák, S. Pietri, M. Górska, H. Grawe, K. H. Maier, P. H. Regan, D. Rudolph, A. B. Garnsworthy, R. Hoischen, J. Gerl, H. J. Wollersheim, F. Becker, P. Bednarczyk, L. Cáceres, P. Doornenbal, H. Geissel, J. Grebosz, A. Kelic, I. Kojouharov, N. Kurz, F. Montes, W. Prokopwicz, T. Saito, H. Schaffner, S. Tashenov, A. Heinz, M. Pfützner, T. Kurtukian-Nieto, G. Benzoni, A. Jungclaus, D. L. Balabanski, M. Bowry, C. Brandau, A. Brown, A. M. Bruce, W. N. Catford, I. J. Cullen, Zs. Dombrádi, M. E. Estevez, W. Gelletly, G. Ilie, J. Jolie, G. A. Jones, M. Kmiecik, F. G. Kondev, R. Krücken, S. Lalkovski, Z. Liu, A. Maj, S. Myalski, S. Schwertel, T. Shizuma, P. M. Walker, E. Werner-Malento, and O. Wieland. Isomeric states observed in heavy neutron-rich nuclei populated in the fragmentation of a  $^{208}\text{Pb}$  beam. *Phys. Rev. C*, Vol. 84, p. 044313, Oct 2011.
- [111] P. Zeyen, K. Euler, V. Grafen, C. Günther, M. Marten-Tölle, P. Schüler, and R. Tolle. Investigation of  $^{203, 205}\text{Hg}$  with the  $(d, p\gamma)$  reaction—identification of the  $13/2$  neutron hole state in  $^{205}\text{Hg}$ . *Zeitschrift für Physik A Atomic Nuclei*, Vol. 325, No. 4, pp. 451–456, 1986.
- [112] A. A. Hahn, J. P. Miller, R. J. Powers, A. Zehnder, A. M. Rushton, R. E. Welsh, A. R. Kunselman, P. Roberson, and H. K. Walter. An experimental study of muonic x-ray transitions in mercury isotopes. *Nuclear Physics A*, Vol. 314, No. 2-3, pp. 361–386, 1979.
- [113] A. Bockisch, M. Miller, K. P. Lieb, and K. Heyde. Identification of the missing  $f_{5/2}$  state in

- 201hg by coulomb excitation. *Physics Letters B*, Vol. 90, No. 1-2, pp. 61–64, 1980.
- [114] P. Schüler, K. Hardt, C. Günther, K. Freitag, P. Herzog, H. Niederwestberg, H. Reif, E. B. Shera, and M. V. Hoehn. Experimental investigation of low lying excited states in 201 hg. *Zeitschrift für Physik A Atoms and Nuclei*, Vol. 313, No. 4, pp. 305–309, 1983.
- [115] F. G. Kondev and S. Lalkovski. Nuclear data sheets for  $A = 200$ . *Nuclear Data Sheets*, Vol. 108, No. 7, pp. 1471–1582, 2007.
- [116] Zs. Podolyák, G. F. Farrelly, P. H. Regan, A. B. Garnsworthy, S. J. Steer, M. Górska, J. Benlliure, E. Casarejos, S. Pietri, J. Gerl, et al. Proton-hole excitation in the closed shell nucleus 205au. *Physics Letters B*, Vol. 672, No. 2, pp. 116–119, 2009.
- [117] Zs. Podolyák, S. J. Steer, S. Pietri, M. Górska, P. H. Regan, D. Rudolph, A. B. Garnsworthy, R. Hoischen, J. Gerl, H. J. Wollersheim, et al. Structure of neutron-rich nuclei around the  $n=126$  closed shell; the yrast structure of 205au126 up to spin-parity  $i^\pi = (19/2+)$ . *The European Physical Journal A*, Vol. 42, No. 3, p. 489, 2009.
- [118] A. I. Morales, J. Benlliure, M. Górska, H. Grawe, S. Verma, P. H. Regan, Zs. Podolyák, S. Pietri, R. Kumar, E. Casarejos, A. Algora, N. Alkhomashi, H. Álvarez-Pol, G. Benzoni, A. Blazhev, P. Boutachkov, A. M. Bruce, L. S. Cáceres, I. J. Cullen, A. M. Denis Bacelar, P. Doornenbal, M. E. Estévez-Aguado, G. Farrelly, Y. Fujita, A. B. Garnsworthy, W. Gelletly, J. Gerl, J. Grebosz, R. Hoischen, I. Kojouharov, N. Kurz, S. Lalkovski, Z. Liu, C. Mihai, F. Molina, D. Mücher, W. Prokopowicz, B. Rubio, H. Schaffner, S. J. Steer, A. Tamii, S. Tashenov, J. J. Valiente-Dobón, P. M. Walker, H. J. Wollersheim, and P. J. Woods.  $\beta$ -delayed  $\gamma$ -ray spectroscopy of  $^{203,204}\text{au}$  and  $^{200-202}\text{pt}$ . *Phys. Rev. C*, Vol. 88, p. 014319, Jul 2013.
- [119] B. Singh. Nuclear data sheets for  $A = 199$ . *Nuclear Data Sheets*, Vol. 1, No. 108, pp. 79–196, 2007.
- [120] P. R. John, J. J. Valiente-Dobón, D. Mengoni, V. Modamio, S. Lunardi, D. Bazzacco, A. Gadea, C. Wheldon, T. R. Rodríguez, T. Alexander, G. de Angelis, N. Ashwood, M. Barr, G. Benzoni, B. Birkenbach, P. G. Bizzeti, A. M. Bizzeti-Sona, S. Bottoni, M. Bowry, A. Bracco, F. Browne, M. Bunce, F. Camera, L. Corradi, F. C. L. Crespi, B. Melon, E. Farnea, E. Fioretto, A. Gottardo, L. Grente, H. Hess, Tz. Kokalova, W. Korten, A. Kuşoğlu, S. Lenzi, S. Leoni, J. Ljungvall, R. Menegazzo, C. Michelagnoli, T. Mijatović, G. Montagnoli, D. Montanari, D. R. Napoli, Zs. Podolyák, G. Pollarolo, F. Recchia, P. Reiter, O. J. Roberts, E. Şahin, M.-D. Salsac, F. Scarlassara, M. Sferrazza, P.-A. Söderström, A. M. Stefanini, S. Szilner, C. A. Ur, A. Vogt, and J. Walshe. In-beam  $\gamma$ -ray spectroscopy of the neutron-rich platinum isotope  $^{200}\text{Pt}$  toward the  $n = 126$  shell gap. *Phys. Rev. C*, Vol. 95, p. 064321, Jun 2017.
- [121] M. A. Wahlgren and W. W. Meinke. Isomeric state of platinum-199. *Phys. Rev.*, Vol. 115, pp. 191–193, Jul 1959.
- [122] P. A. R. Ade, N. Aghanim, M. Arnaud, M. Ashdown, J. Aumont, C. Baccigalupi, A. J. Banday, R. B. Barreiro, J. G. Bartlett, N. Bartolo, et al. Planck 2015 results-xiii. cosmological

- parameters. *Astronomy & Astrophysics*, Vol. 594, p. A13, 2016.
- [123] M. Tanabashi, K. Hagiwara, K. Hikasa, K. Nakamura, Y. Sumino, F. Takahashi, J. Tanaka, K. Agashe, G. Aielli, C. Amsler, M. Antonelli, D. M. Asner, H. Baer, Sw. Banerjee, R. M. Barnett, T. Basaglia, C. W. Bauer, J. J. Beatty, V. I. Belousov, J. Beringer, S. Bethke, A. Bettini, H. Bichsel, O. Biebel, K. M. Black, E. Blucher, O. Buchmuller, V. Burkert, M. A. Bychkov, R. N. Cahn, M. Carena, A. Ceccucci, A. Cerri, D. Chakraborty, M.-C. Chen, R. S. Chivukula, G. Cowan, O. Dahl, G. D'Ambrosio, T. Damour, D. de Florian, A. de Gouvêa, T. DeGrand, P. de Jong, G. Dissertori, B. A. Dobrescu, M. D'Onofrio, M. Doser, M. Drees, H. K. Dreiner, D. A. Dwyer, P. Eerola, S. Eidelman, J. Ellis, J. Erler, V. V. Ezhela, W. Fetscher, B. D. Fields, R. Firestone, B. Foster, A. Freitas, H. Gallagher, L. Garren, H.-J. Gerber, G. Gerbier, T. Gershon, Y. Gershtein, T. Gherghetta, A. A. Godizov, M. Goodman, C. Grab, A. V. Gribsan, C. Grojean, D. E. Groom, M. Grünewald, A. Gurtu, T. Gutsche, H. E. Haber, C. Hanhart, S. Hashimoto, Y. Hayato, K. G. Hayes, A. Hebecker, S. Heinemeyer, B. Heltsley, J. J. Hernández-Rey, J. Hisano, A. Höcker, J. Holder, A. Holtkamp, T. Hyodo, K. D. Irwin, K. F. Johnson, M. Kado, M. Karliner, U. F. Katz, S. R. Klein, E. Klempt, R. V. Kowalewski, F. Krauss, M. Kreps, B. Krusche, Yu. V. Kuyanov, Y. Kwon, O. Lahav, J. Laiho, J. Lesgourgues, A. Liddle, Z. Ligeti, C.-J. Lin, C. Lippmann, T. M. Liss, L. Littenberg, K. S. Lugovsky, S. B. Lugovsky, A. Lusiani, Y. Makida, F. Maltoni, T. Mannel, A. V. Manohar, W. J. Marciano, A. D. Martin, A. Masoni, J. Matthews, U.-G. Meißner, D. Milstead, R. E. Mitchell, K. Mönig, P. Molaro, F. Moortgat, M. Moskovic, H. Murayama, M. Narain, P. Nason, S. Navas, M. Neubert, P. Nevski, Y. Nir, K. A. Olive, S. Pagan Griso, J. Parsons, C. Patrignani, J. A. Peacock, M. Pennington, S. T. Petcov, V. A. Petrov, E. Pianori, A. Piepke, A. Pomarol, A. Quadt, J. Rademacker, G. Raffelt, B. N. Ratcliff, P. Richardson, A. Ringwald, S. Roesler, S. Rolli, A. Romaniouk, L. J. Rosenberg, J. L. Rosner, G. Rybka, R. A. Ryutin, C. T. Sachrajda, Y. Sakai, G. P. Salam, S. Sarkar, F. Sauli, O. Schneider, K. Scholberg, A. J. Schwartz, D. Scott, V. Sharma, S. R. Sharpe, T. Shutt, M. Silari, T. Sjöstrand, P. Skands, T. Skwarnicki, J. G. Smith, G. F. Smoot, S. Spanier, H. Spieler, C. Spiering, A. Stahl, S. L. Stone, T. Sumiyoshi, M. J. Syphers, K. Terashi, J. Terning, U. Thoma, R. S. Thorne, L. Tiator, M. Titov, N. P. Tkachenko, N. A. Törnqvist, D. R. Tovey, G. Valencia, R. Van de Water, N. Varelas, G. Venanzoni, L. Verde, M. G. Vincter, P. Vogel, A. Vogt, S. P. Wakely, W. Walkowiak, C. W. Walter, D. Wands, D. R. Ward, M. O. Wascko, G. Weiglein, D. H. Weinberg, E. J. Weinberg, M. White, L. R. Wiencke, S. Willocq, C. G. Wohl, J. Womersley, C. L. Woody, R. L. Workman, W.-M. Yao, G. P. Zeller, O. V. Zenin, R.-Y. Zhu, S.-L. Zhu, F. Zimmermann, P. A. Zyla, J. Anderson, L. Fuller, V. S. Lugovsky, and P. Schaffner. Review of particle physics. *Phys. Rev. D*, Vol. 98, p. 030001, Aug 2018.
- [124] Craig J. Copi, David N. Schramm, and Michael S. Turner. Assessing big-bang nucleosynthesis. *Phys. Rev. Lett.*, Vol. 75, pp. 3981–3984, Nov 1995.
- [125] Craig J Copi, David N Schramm, and Michael S Turner. Big-bang nucleosynthesis and the

- baryon density of the universe. *Science*, Vol. 267, No. 5195, pp. 192–199, 1995.
- [126] M. B. Gavela, M. Lozano, J. Orloff, and O. Pène. Standard model cp-violation and baryon asymmetry (i). zero temperature. *Nuclear Physics B*, Vol. 430, No. 2, pp. 345–381, 1994.
- [127] M. B. Gavela, P. Hernández, J. Orloff, O. Pène, and C. Quimbay. Standard model cp-violation and baryon asymmetry (ii). finite temperature. *Nuclear Physics B*, Vol. 430, No. 2, pp. 382–426, 1994.
- [128] G. R. Farrar and M. E. Shaposhnikov. Baryon asymmetry of the universe in the standard model. *Phys. Rev. D*, Vol. 50, pp. 774–818, Jul 1994.
- [129] P. Huet and E. Sather. Electroweak baryogenesis and standard model cp violation. *Phys. Rev. D*, Vol. 51, pp. 379–394, Jan 1995.
- [130] J. H. Smith, E. M. Purcell, and N. F. Ramsey. Experimental limit to the electric dipole moment of the neutron. *Phys. Rev.*, Vol. 108, pp. 120–122, Oct 1957.
- [131] K. F. Smith, N. Crampin, J. M. Pendlebury, D. J. Richardson, D. Shiers, K. Green, A. I. Kilvington, J. Moir, H. B. Prosper, D. Thompson, et al. A search for the electric dipole moment of the neutron. *Physics Letters B*, Vol. 234, No. 1-2, pp. 191–196, 1990.
- [132] P. G. Harris, C. A. Baker, K. Green, P. Iaydjiev, S. Ivanov, D. J. R. May, J. M. Pendlebury, D. Shiers, K. F. Smith, M. van der Grinten, and P. Geltenbort. New experimental limit on the electric dipole moment of the neutron. *Phys. Rev. Lett.*, Vol. 82, pp. 904–907, Feb 1999.
- [133] C. A. Baker, D. D. Doyle, P. Geltenbort, K. Green, M. G. D. van der Grinten, P. G. Harris, P. Iaydjiev, S. N. Ivanov, D. J. R. May, J. M. Pendlebury, J. D. Richardson, D. Shiers, and K. F. Smith. Improved experimental limit on the electric dipole moment of the neutron. *Phys. Rev. Lett.*, Vol. 97, p. 131801, Sep 2006.
- [134] J. M. Pendlebury, S. Afach, N. J. Ayres, C. A. Baker, G. Ban, G. Bison, K. Bodek, M. Burghoff, P. Geltenbort, K. Green, W. C. Griffith, M. van der Grinten, Z. D. Grujić, P. G. Harris, V. Héléine, P. Iaydjiev, S. N. Ivanov, M. Kasprzak, Y. Kermaidic, K. Kirch, H.-C. Koch, S. Komposch, A. Kozela, J. Krempel, B. Lauss, T. Lefort, Y. Lemièrre, D. J. R. May, M. Musgrave, O. Naviliat-Cuncic, F. M. Piegsa, G. Pignol, P. N. Prashanth, G. Quémener, M. Rawlik, D. Rebreyend, J. D. Richardson, D. Ries, S. Rocchia, D. Rozpedzik, A. Schnabel, P. Schmidt-Wellenburg, N. Severijns, D. Shiers, J. A. Thorne, A. Weis, O. J. Winston, E. Wursten, J. Zejma, and G. Zsigmond. Revised experimental upper limit on the electric dipole moment of the neutron. *Phys. Rev. D*, Vol. 92, p. 092003, Nov 2015.
- [135] M. C. Weisskopf, J. P. Carrico, H. Gould, E. Lipworth, and T. S. Stein. Electric dipole moment of the cesium atom. a new upper limit to the electric dipole moment of the electron. *Phys. Rev. Lett.*, Vol. 21, pp. 1645–1648, Dec 1968.
- [136] S. A. Murthy, D. Krause, Z. L. Li, and L. R. Hunter. New limits on the electron electric dipole moment from cesium. *Phys. Rev. Lett.*, Vol. 63, pp. 965–968, Aug 1989.
- [137] E. D. Commins, S. B. Ross, D. DeMille, and B. C. Regan. Improved experimental limit on the electric dipole moment of the electron. *Phys. Rev. A*, Vol. 50, pp. 2960–2977, Oct 1994.

- [138] B. C. Regan, Eugene D. Commins, Christian J. Schmidt, and David DeMille. New limit on the electron electric dipole moment. *Phys. Rev. Lett.*, Vol. 88, p. 071805, Feb 2002.
- [139] J. J. Hudson, B. E. Sauer, M. R. Tarbutt, and E. A. Hinds. Measurement of the electron electric dipole moment using ybf molecules. *Phys. Rev. Lett.*, Vol. 89, p. 023003, Jun 2002.
- [140] B. J. Heidenreich, O. T. Elliott, N. D. Charney, K. A. Virgien, A. W. Bridges, M. A. McKeon, S. K. Peck, D. Krause, J. E. Gordon, L. R. Hunter, and S. K. Lamoreaux. Limit on the electron electric dipole moment in gadolinium-iron garnet. *Phys. Rev. Lett.*, Vol. 95, p. 253004, Dec 2005.
- [141] J. Baron, W. C. Campbell, D. DeMille, J. M. Doyle, G. Gabrielse, Y. V. Gurevich, P. W. Hess, N. R. Hutzler, E. Kirilov, I. Kozyryev, et al. Order of magnitude smaller limit on the electric dipole moment of the electron. *Science*, Vol. 343, No. 6168, pp. 269–272, 2014.
- [142] M. D. Swallows, T. H. Loftus, W. C. Griffith, B. R. Heckel, E. N. Fortson, and M. V. Romalis. Techniques used to search for a permanent electric dipole moment of the  $^{199}\text{Hg}$  atom and the implications for  $CP$  violation. *Phys. Rev. A*, Vol. 87, p. 012102, Jan 2013.
- [143] V. F. Dmitriev, R. A. Sen'kov. Schiff moment of the mercury nucleus and the proton dipole moment. *Physics of Atomic Nuclei*, Vol. 67, No. 10, pp. 1799–1803, 2004.
- [144] V. F. Dmitriev, R. A. Sen'kov, and N. Auerbach. Effects of core polarization on the nuclear schiff moment. *Phys. Rev. C*, Vol. 71, p. 035501, Mar 2005.
- [145] W. C. Haxton and E. M. Henley. Enhanced  $t$ -nonconserving nuclear moments. *Phys. Rev. Lett.*, Vol. 51, pp. 1937–1940, Nov 1983.
- [146] V. P. Gudkov, Xiao-Gang He, and B. H. J. McKellar.  $Cp$ -odd nucleon potential. *Phys. Rev. C*, Vol. 47, pp. 2365–2368, May 1993.
- [147] I. S. Towner and A. C. Hayes.  $P,t$ -violating nuclear matrix elements in the one-meson exchange approximation. *Phys. Rev. C*, Vol. 49, pp. 2391–2397, May 1994.
- [148] V. A. Dzuba, V. V. Flambaum, J. S. M. Ginges, and M. G. Kozlov. Electric dipole moments of hg, xe, rn, ra, pu, and tlf induced by the nuclear schiff moment and limits on time-reversal violating interactions. *Phys. Rev. A*, Vol. 66, p. 012111, Jul 2002.
- [149] J. de Vries, E. Mereghetti, and A. Walker-Loud. Baryon mass splittings and strong  $CP$  violation in  $su(3)$  chiral perturbation theory. *Phys. Rev. C*, Vol. 92, p. 045201, Oct 2015.
- [150] T. E. Chupp, P. Fierlinger, M. J. Ramsey-Musolf, and J. T. Singh. Electric dipole moments of atoms, molecules, nuclei, and particles. *Reviews of Modern Physics*, Vol. 91, No. 1, p. 015001, 2019.
- [151] L. I. Schiff. Measurability of nuclear electric dipole moments. *Phys. Rev.*, Vol. 132, pp. 2194–2200, Dec 1963.
- [152] I. B. Khriplovich and S. Lamoreaux. *CP violation without strangeness: electric dipole moments of particles, atoms, and molecules*. Springer-Verlag Berlin Heidelberg, 1997.
- [153] V. Spevak, N. Auerbach, and V. V. Flambaum. Enhanced  $t$ -odd,  $p$ -odd electromagnetic moments in reflection asymmetric nuclei. *Phys. Rev. C*, Vol. 56, pp. 1357–1369, Sep 1997.

- [154] J. S. M. Ginges and V. V. Flambaum. Violations of fundamental symmetries in atoms and tests of unification theories of elementary particles. *Physics Reports*, Vol. 397, No. 2, pp. 63–154, 2004.